Corrosion Behavior of Metallic Bio-implant Alloys

by

SHIMA KARIMI
B.A.Sc., The University of British Columbia, 2009

A THESIS SUBMITTED IN PARTIAL FULFILLMENT OF
THE REQUIREMENTS FOR THE DEGREE OF
DOCTOR OF PHILOSOPHY

in

THE FACULTY OF GRADUATE AND POSTDOCTORAL STUDIES

(Materials Engineering)

THE UNIVERSITY OF BRITISH COLUMBIA
(Vancouver)

April 2014

Abstract

The most common metallic biomaterials are 316L, Co-28Cr-6Mo, and Ti-6Al-4V alloys used as prostheses and fixation devices. These materials are biocompatible and have high corrosion resistance. However, metallic biomaterials are not completely inert in the body. The presence of dissolved oxygen, chloride, phosphate, and organic molecules in the body fluids could influence their corrosion behavior.

Protein is one of the components of the human body fluids. Body fluids contain different concentrations of protein and even the protein concentration varies at the implant/tissue interface during the healing period. Some proteins are negatively-charged at a neutral body pH and they react with the positively-charged ions released from metallic samples. The reactions either form an absorbed film on the surface of the samples or produce metal/protein/hydroxylated compounds. The primary objective of my project is to investigate influences of protein on corrosion behavior of three commonly used biomaterials. The hypothesis is that the variation of protein concentration can alter corrosion resistance and ion release of biomaterials. This Study could help to develop implants with a better corrosion performance and minimal ion release. This development could promote the physical and mental health of patients and reduce cost and time of revision surgeries. To pursue this study, bovine serum albumin (BSA) and human serum albumin (HSA) were added to phosphate-buffered saline (PBS) solutions. A combination of electrochemical and non-electrochemical corrosion methods was used to understand the

kinetics of electrochemical reactions, identify the oxide layer growth mechanism and protein adsorption, and detect ion release and surface morphology with and without input of external energy.

The dissolution rates of iron from 316L and cobalt from Co-28Cr-6Mo alloys in the BSA solution were lower than that in the HSA solutions. The surface chemistry of the specimens showed that the adsorption of Na into the Ti-6Al-4V oxide layer depends on the type of protein. In the presence of HSA, sodium (2-methyl-propenoate) was detected whereas Na bound to the sulfhydryl group of bovine serum albumin (BSA) and formed sodium mercaptoacetate. Finally, BSA was a stronger cathodic inhibitor than HSA for 316L and Co-28Cr-6Mo alloys.

Preface

The research presented in this thesis was carried out in the University of British Columbia (UBC) corrosion laboratory in the Department of Materials Engineering under the supervision of Dr. Akram Alfantazi. This research work has been supported by Natural Science and Engineering Research Council of Canada (NSERC). The NSERC support helped us to publish four journal papers and present in four international conferences which are included in this dissertation. I am the primary author of all the published work in which Professor Akram Alfantazi helped me extensively with.

Journal Papers:

1. **S. Karimi** and A.M. Alfantazi, "Ion release and surface oxide composition of AISI 316L, Co 28Cr-6Mo, and Ti-6Al-4V alloys immersed in human serum albumin solutions", Materials Science and Engineering C, (2014) Reference # MSC 4563.
2. **S. Karimi** and A.M. Alfantazi, "Electrochemical Corrosion Behavior of Orthopedic Biomaterials in Presence of Human Serum Albumin", J. Electrochem. Soc., 160 (2013) C206-C214.
3. **S. Karimi**, T. Nickchi, A.M. Alfantazi, "Long-term Corrosion Investigation of AISI 316L, Co–28Cr–6Mo, and Ti–6Al–4V Alloys in Simulated Body Solutions", Appl. Surf. Sci., 258 (2012) 6087–6096.
4. **S. Karimi**, T. Nickchi, A.M. Alfantazi, "Effects of Bovine Serum Albumin on the Corrosion Behavior of AISI 316L, Co-28Cr-6Mo, and Ti-6Al-4V Alloys in Phosphate Buffered Saline Solutions", Corros. Sci., 53 (2011) 3262–3272.

Conference Presentation with Proceeding:

1. **S. Karimi,** A.M. Alfantazi, "The Role of Human Serum Albumin on Corrosion of Orthopedic Biomaterials", Eurocorr 2012, Istanbul, Turkey, Sep 2012.

Conference Presentation:

1. **S. Karimi,** A.M. Alfantazi, "The Electrochemical Corrosion Behavior of AISI 316L, Co-28Cr-6Mo, and Ti-6Al-4V Alloys in Presence of Bovine Serum Albumin in Phosphate Buffered Saline Solutions", NACE Corrosion, Houston, TX, March 2011.

2. **S. Karimi,** A.M. Alfantazi, "The Effect of Bovine Serum Albumin on the Polarization Behavior of Stainless Steel, Cobalt-Chromium, and Titanium Bio-implants Alloys" COM, Vancouver, BC, October 2010.
3. **S. Karimi,** A.M. Alfantazi, "A Comparison Study on the Corrosion Behaviors of Stainless Steel, Cobalt-Chromium, and Titanium Bio-implants Alloys", 22nd Canadian Materials Science Conference, Waterloo, ON, June 2010.

Table of Contents

List of Tables

List of Figures

List of Symbols

A	area of immersed specimen (cm^2)
a	atomic weight ($g\ mol^{-1}$)
B	Tafel constant (26 mV)
C_{ads}	oxide/adsorbed interface capacitance (F)
C_b	barrier layer capacitance (F)
cm	centimeter
C_{ox}	metal/oxide interface capacitance (F)
°C	degree Celsius
E_{corr}	corrosion potential (V vs. Ag/AgCl)
E_{OCP}	Open circuit potential (V vs. Ag/AgCl)
F	Faraday constant ($96500\ C\ mol^{-1}$)
ΔG^0_f	Gibbs free energy off formation of ion at temperature T ($J\ mole^{-1}$)
g	gram
ΔH^0	standard enthalpy of electrochemical activation ($J\ mole^{-1}$)
i_{corr}	corrosion current density ($\mu A\ cm^{-2}$)
i_{pa}	anodic current density($mA\ cm^{-2}$)
K	constant in corrosion rate calculation (8.76×10^4)
L	liter
mg	milligram
mm	millimeter

mm Hg	millimeter of mercury
n	equivalent exchange (equivalent mol^{-1})
n_C	deviation coefficient between real and pure capacitance ($0< n_C <1$)
R	ideal gas constant (8.314 J $mole^{-1}$ K^{-1})
R_{ads}	interfacial resistance at oxide/adsorbed interface ($k\Omega\ cm^2$)
R_{ox}	interfacial resistance at metal/oxide interface ($k\Omega\ cm^2$)
R_b	barrier film resistance ($k\Omega\ cm^2$)
$R_{P\text{-}LPR}$	polarization resistance obtained from LPR curves-the slope of the linear polarization curves ($k\Omega\ cm^2$)
R_p	polarization resistance ($k\Omega\ cm^2$)
R_s	solution resistance ($\Omega\ cm^2$)
T	time of immersion (hour)
W	mass loss (mg)
Y_0	general admittance function ($\mu\Omega^{-1}\ (s)^{n_c}\ cm^{-2}$)
Z_{CPE}	impedance of the constant phase element ($\mu\Omega^{-1}\ (rad)^{n_c}\ cm^{-2}$)
β_{red}	Cathodic Tafel constant (mV)
β_{ox}	anodic Tafel constant (mV)
η	overpotential (V)
μm	micrometer
ρ	density ($g\ cm^{-3}$)
ω	angular frequency ($rad\ s^{-1}$)

List of Acronyms

AAS	atomic absorption spectroscopy
BCC	body-centered cubic
BSA	bovine serum albumin
CPE	constant phase element
EEC	equivalent electrical circuit
EIS	electrochemical impedance spectroscopy
FBS	fetal bovine serum
HCP	hexagonal, close-packed
HSA	human serum albumin
ICP	induced couple plasma
ICP-OES	coupled plasma-optical emission spectroscopy
ICP-MS	inductively coupled plasma-mass spectroscopy
IPL	international plasma labs
OCP	open circuit potential

PAR	Princeton Applied Research
PBS	phosphate buffered saline
PDP	potentiodynamic polarization
QCM	quartz crystal microbalance
QCM-D	quartz crystal microbalance-dissipation monitoring
SCC	stress corrosion cracking
SEM	scanning electron microscopy
SIE	simulated interstitial electrolyte
SUS	simulated uterine solution
TRY	tryptophan
XPS	X-ray photoelectron spectroscopy

Acknowledgements

This dissertation would not have been successful without help, support, and guidance of my research advisor Dr. Akram Alfantazi. I offer my utmost gratitude to him for giving me the honor of working in his group, his enthusiasm, attention to details, and encouragement.

I would like to express my gratitude to Dr. Frank Ko, Dr. Tom Troczynski and Edouard Asselin for reviewing my thesis and thesis proposal and giving me helpful comments.

A special note of gratitude goes to the Materials Engineering Machine Shop staff, especially Mr. Ross McLeod for their technical input.

I would like to thank my fellow lab mates and friends in the Materials Engineering department for sharing ideas and helpful discussion.

The financial support of Natural Science and Engineering Research Council of Canada (NSERC) is gratefully acknowledged.

I would like to give my sincere and heartfelt thanks to my parents for their continuous and consistent support and encouragement to pursue my studies. Finally, I am thankful to my loving husband, Hadi, for his patience, unfailing support, dedication, and unconditional love in the past years. This accomplishment would not have been completed without him.

Dedication

To :

My Loving Parents, My Dear Sisters and Brothers,

& My Loving Husband,

"To all of you, I shall be forever indebted"

Chapter 1: Introduction

Various metallic biomaterials have been introduced since the first fabrication of metallic implants. The primary applications of metallic biomaterials are prostheses and fixation devices in the medical industry. Hard tissues are replaced by prostheses such as total joint replacements and skull plates while damaged or broken bones are stabilized by fixation devices such as nails, screws, nuts, and wires. Replacing damaged joints by metallic bio-implants relieves patient pain and helps them to continue their normal life. The worldwide sales of orthopaedic biomaterials were $14 billion in 2002 with an expected growth rate of 7% to 9% annually (Hallab et al., 2004). AISI 316L, wrought Co-28Cr-6Mo, and Ti-6Al-4V are common biomaterials in today's biomedical industry. These have biocompatible chemical compositions avoiding adverse tissue reactions with high corrosion resistance. The high corrosion resistance of these materials relies on the growth of a passive layer. However, biomaterials are not completely inert in the body.

After replacement surgeries, reactive sites such as unsaturated, chemical bonds are formed on metallic implants from their passive surface (Kasemo & Lausmaa, 1994). Interaction of reactive sites with surrounding tissue may dissociate biomolecules such as protein, along with O_2, H_2, H_2O, and hydrocarbons (Kasemo & Lausmaa, 1994). The biomolecules dissociation is one reason for adverse biological reactions and corrosion of metallic bio-implants. In fact, failure of metallic implants due to corrosion has been reported in several cases. For instance, signs of corrosion attack were observed in 35% of 148 retrieved hip

implants in their head-neck taper connections (J. L. Gilbert et al., 1993). Hip replacement implants generally last 10-20 years with an approximate revision rate of 7% after 10 years of service (Hallab et al., 2004); however, metal-on-metal hip implants designed by Johnson and Johnson recently failed with the rate of 37% within 4.6 years (Nadrich, 2013) which cost approximately 4 Billion dollars. In fact, implant failure significantly impacts the physical and mental health of recipients and brings about economic consequences due to the cost of revision surgeries as well.

In addition to the corrosion of metallic implants, ion release of these devices is a serious concern that threatens patient health. Ion release as a consequence of body fluid interacting with a metal-oxide surface or corrosion product can disturb normal cell behavior and cellular metabolism (Cahoon & Paxton, 2004). Ion release can also cause metal sensitivity and implant failure. Generally, metal sensitivity was estimated to affect 10-15% of the population (Basketter et al., 1993). The most common metal sensitizers are nickel, cobalt, and chromium (Basketter et al., 1993; Blac, 1984; Haudrech et al., 1994; Kanerva et al., 1994; Merritt & Rodrigo, 1996) and, to some extent, titanium (Lalor et al., 1991). All these metals are present in medical grade alloys. Release of chromium and cobalt into the body from CoCrMo metal-on-metal hip implants may cause cellular toxicity, metal hypersensitivity, and chromosomal changes (Cahoon & Paxton, 2004; Howie et al., 1996; Nyrén et al., 1995). Last but not the least, release of ions and corrosion products may cause oxidative damage. In oxidative damage, the oxidation–reduction balances in human bodies are disrupted due to the accumulation of transition metals in toxic doses, especially chromium and nickel. This

disturbance affects redox-sensitive signaling molecules, prevents normal cell signaling and gene expression, and forms metal–organic complexes. These entire disturbances shift the body's pH, leading to toxicity and carcinogenicity (Clark & Williams, 2004; Merritt & Brown, 2004; Sargeant & Goswami, 2007).

In order to improve the performance of metallic implants and prevent revision surgeries, the corrosion and ion release of metallic biomaterials need to be improved. Furthermore, human involvement in sports and industrial activities increases the need for developing promising biomaterials for younger patients and faster recovery from replacement surgeries and cut unnecessary revision surgeries. A better performance and longer lifetime are needed to extend healthcare to millions of patients worldwide. This requires a careful corrosion evaluation of metallic biomaterials to physiological body responses which could alternate corrosion behavior and ion release of metallic implants. This can be implemented by understanding the metal-tissue interactions at the implant surface in realistic body environments. These understandings could be used for the development of biocompatible biomaterials with significantly high corrosion resistance and minimal ion release.

Chapter 2: Literature review

2.1 Metallic biomaterials

A biomaterial is defined as "*a material intended to interface with biological systems to evaluate, treat, augment, or replace any tissue, organ, or function of the body*" in a contextual dictionary of biomaterials science published in 1999 (D. Williams, 1999). Metallic biomaterials have been used as prosthetic devices such as artificial hips, knees, elbows, etc. Metallic orthopaedic implants and artificial joints can replace bone or assist hard tissue functions. The combination of strength, wear resistance, and corrosion resistance of the metallic biomaterials made them unique for orthopedic implants (J. L. Gilbert & Mali, 2012). Briefly, ideal materials should exhibit the following properties (Balamurugan et al., 2008):

- Biocompatibility
- Resistance to corrosion and biological degradation
- Strength to sustain cyclic loading
- Proper modulus to prevent stress shielding

Williams defined biocompatibility as "*the ability of a material to perform with an appropriate host response in a specific application*" (D. Williams, 1989). A biocompatible material does not cause any adverse reactions in human bodies. Adverse body reactions activate immune systems and change the neutral body environment to an acidic system. The pH of the tissue next to a loosened total hip implant was acidic (Konttinen et al., 2001). The drop of the pH could also occur right after surgery and then recover to 7.4 within weeks (Konttinen et al.,

2001). The change of pH could alter the corrosion behavior of metallic biomaterials (Khan et al., 1999; Pourbaix, 1984). Biocompatible materials with high corrosion resistant can keep their integrity while the rate of the ion release of these materials is very low.

Materials with stiffness close to bone and reasonable strength are required to prohibit stress shielding and fatigue failure (Fraker, 1995). Stress shielding is a phenomenon that occurs by removing the stress from bones causing bone resorption and implant failure. The risk of stress shielding can be reduced by applying materials with strength modulus close to the strength of the bone (Balamurugan et al., 2008). Mechanical properties of some biomaterials and bone are shown in Table 2-1 (Hallab et al., 2004). Titanium and titanium alloys have the lowest elastic modulus among metals compared to stainless steel and Co-Cr alloys.

Table 2-1 : Mechanical properties of some biomaterials and cortical bone-redrawn (Hallab et al., 2004)

Orthopedic biomaterials	ASTM designation	Elastic modulus (GPa)	Yield strength (MPa)	Fatigue strength (MPa)	Hardness (Vickers Hardness number)
Cortical bone	Low strain	15.2	114	30-45	
	High strain	40.8	-		
Stainless steel	ASTM F138	190	792	241-820	130-180
Co-Cr alloys	ASTM F75	210-253	448-841	207-950	300-400
	ASTM F90	210	448-1606	586-1220	300-400
	ASTM F562	200-230	300-2000	340-520	8-50(Rockwell)
	ASTM F1537	200-300	960	200-300	41(Rockwell)
Ti alloys	ASTM F67	110	485	300	120-200
	ASTM F136	116	897-1034	620-689	310

Some popular metallic biomaterials along with their chemical compositions are summarized in Table 2-2 (Hallab et al., 2004).

Table 2-2 : Chemical composition of commonly used metallic biomaterials (Hallab et al., 2004)

Alloy	Ni	Co	Cr	Ti	Mo	Al	Fe	Mn	W	C	Si	V
Stainless steel	10-15.5		17-19		2-4		61-68		<2	<0.06	<1.0	
ASTM F75	<2	61-66	27-30		4.5-7		<1.5	<1.0		<0.35	<0.1	
ASTM F90	9-11	46-51	19-20				<0.3	<2.5	14-16	<0.15	<1.0	
ASTM F562	33-37	35	19-21	<1	9-11		<1	<0.15			<0.15	
CP Ti				99			0.2-0.5			<0.1		
Ti-6Al-4V				89-91		5.5-6.5				<0.08		3.5-4.5

2.2 Metallic biomaterial issues in human bodies

Removal of bio-implants from the body because the implant could not meet its intended functions has been considered as a failure (Sivakumar et al., 1995). Although metallic biomaterials have shown good biocompatibility and high corrosion and wear resistance in physiological solutions, failure of metallic implants has been reported (Amel-Farzad et al., 2007; Ellman & Levine, 2011; Fraitzl et al., 2011; Huot Carlson et al., 2012; Kop & Swarts, 2009; Korovessis et al., 2006; Milošev et al., 2006; Paliwal et al., 2010; Sotereanos et al., 2013; Sudhakar, 2005). A survey of failures in stainless steel orthopaedic implants was provided by Sivakumar *et al.* (Sivakumar et al., 1995).

Table 2-3 : Classification of the failed implants based on the reported causes of removal-redrawn (Sivakumar et al., 1995)

Reported cause	Number of implants	Incidence (%)
Fracture	21	42
Corrosion	12	24
Adverse tissue reaction	7	14
Cracks without fracture	4	8
Wear	3	6
Bending without fracture	3	6

In this survey, 50 patients with premature removal of implants were chosen from local hospitals in Madras City, India. The implant failure was classified into the six categories shown in Table 2-3 (Sivakumar et al., 1995). 24% failure of the stainless steel implants was due to corrosion, and ranked second place after fracture failure.

The corrosion of 16 retrieved hip stems with a modular neck taper junction was examined by macroscopic inspection, corrosion testing, and scanning electron microscopy (SEM) to

clarify the corrosion mechanism (Kop & Swarts, 2009). The patient demographics, reasons for removal and extent of corrosion are presented in Table 2-4. In this Table, M and F refer to male and female patients. The corrosion severances were scored from 1 to 4 in which 1 indicates no sign of crevice and fretting corrosion and 4 means higher than 10% of surface-containing corrosion, black debris, pits, etch marks, and several bands of fretting scars (Kop & Swarts, 2009). In the 37.5% of the retrieved implant, significant signs of fretting and crevice corrosion at the neck-stem taper were observed (Kop & Swarts, 2009).

Table 2-4 : Implantation time, reasons for removal and extent of corrosion (Kop & Swarts, 2009)

Patient	Time in Situ (mo)	Reason for Removal as Recorded by Surgeon	Corrosion on Neck*		Fretting on Neck*	
			Stem	Head	Stem	Head
1	49	Pain, loose stem	2	1	1	1
2	7	Pain, loose stem	1	1	1	1
3	0	Dislocation poor position	1	1	1	1
4	4	Pain, loose stem	1	1	1	1
5	3	Pain, dislocation	1	1	1	1
6	4	Pain, loose stem	1	1	1	1
7†	17	Pain, heterotopic ossification	3	1	2	1
8	22	Pain, loosening	3	2	2	1
9	2	Pain, dislocation	1	1	1	1
10	0.2	Dislocation poor position	1	1	1	1
11	1	Pain, infection	1	1	1	1
12	60	Pain, infection	3	1	3	1
13	2	Joint instability	1	1	1	1
14†	50	Pain, dislocation	4	3	4	4
15	4	Loose/mobile neck	1	1	1	1
16	36	Pain, dislocation	4	2	3	1

Metallic implants are at risk of slow diffusion of metal ions through the passive film, transpassive dissolution under high oxidizing conditions, and local breakdown of passive films as a consequence of pitting or crevice corrosion (Bundy, 1994). The corrosion

resistances of 316L stainless steel, cobalt alloy, and Ti-6Al-4V alloys were evaluated (Gurappa, 2002) in Hank's solution at 37°C and a pH of 7.4 (Figure 2-1).

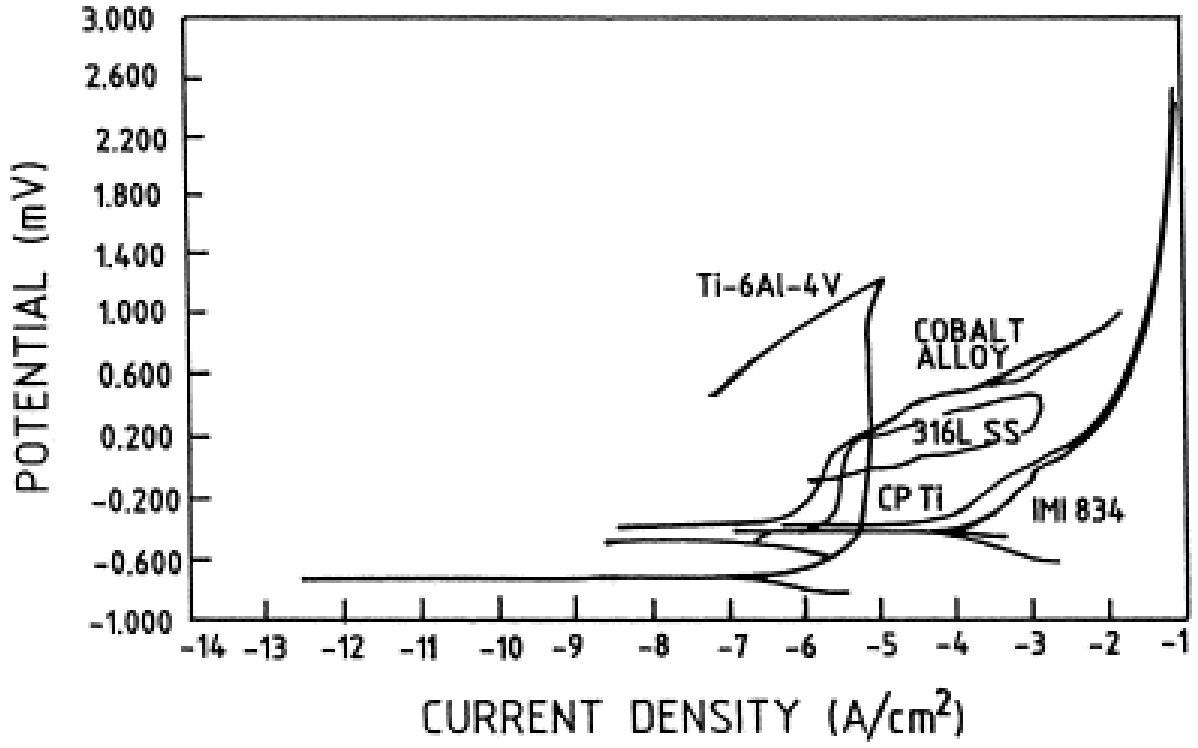

Figure 2-1 : Cyclic polarization plots of 316L, Co-Ni-Cr-Mo, pure Ti and Ti-6Al-4V alloys in de-aerated Hank's solution at 37°C (Gurappa, 2002)

A hysteresis loop for 316L stainless shows that 316L is susceptible to pitting and crevice corrosion while titanium and cobalt alloys have good pitting and crevice corrosion resistance (Gurappa, 2002) in the selected medium. This result confirms the work done by Scales *et al.* (Scales et al., 1961). They reported corrosion of plates, screws, and femoral nail-plates of stainless steel and CoCrMo alloys separately or in conjunction with each other from 109 patients (Scales et al., 1961). Stainless steel implants were corroded mainly at the

conjunction sites, whereas no corrosion evidence was observed for CoCrMo implants. However, exertion of the mechanical load could change corrosion behavior of CoCrMo and cause stress corrosion cracking (SCC), corrosion fatigue, and fretting corrosion. Failure of two femoral stainless steel compression plates and one femoral nail-plate, one CP titanium oral maxillo-facial plate for jaw reconstruction, and several Nitinol wires were reported. In this study, the cause of CP titanium plate failure was localised corrosion and intergranular cracking whereas Nitinol wires failed due to the pitting corrosion during service (Azevedo & Hippert, 2002). In a recent investigation, the fatigue failure of titanium total hip arthroplasty was due to the combined effects of crevice and fretting corrosion, metal-on-metal articulation, etc. (Ellman & Levine, 2011). Corrosion fatigue mitigation with respect to structural and surface an aspect of metallic implants has been reviewed (Antunes & de Oliveira, Mara Cristina Lopes, 2012). A 20–60 times increase in the corrosion rate was demonstrated in a tribocorrosion study of wrought high carbon CoCrMo, wrought low carbon CoCrMo, and 316L alloys in 0.36% NaCl and 50% bovine calf serum solutions (Yan et al., 2007). This increase is attributed to the friction force that constantly removes passive film and accelerates the rate of ion release. Yan *et al.* also concluded that the presence of protein increases the metal ion release in static environments but decreases ion release in sliding by systems because bovine serum lubricates the counter bodies (Yan et al., 2007).

Clinical and radiographic evaluations were done on the 640 metal-on-metal total hip replacements over a mean of 7.1 years (Milošev et al., 2006). 5.3% of the implants were retrieved while six of them were subjected to abrasive wear (Milošev et al., 2006). The wear

of the implant releases small particles and ions into the surrounding tissues. The increase of ion concentration is harmful for the body. In a study, retrieval surgeries of 6.5% CoCrMo hip implants with metal-on-metal articulation were reported (Korovessis et al., 2006). The main cause of implant failure was aseptic loosening and septic failure which resulted in the release of cobalt (Samelko et al., 2013). The release of chromium and cobalt into the body could be harmful because they could cause cellular toxicity, metal hypersensitivity, and chromosomal changes (Korovessis et al., 2006; Samelko et al., 2013; Walter et al., 2008).

Walter *et al.* tested 29 patients after hip implant surgery (Walter et al., 2008). They recorded the level of chromium and cobalt in their serum, plasma, blood, and urine. Chromium mostly was presented in the serum and plasma whereas the minimal chromium levels were found within the red blood cells. Cobalt, same as Chromium, mostly was found in the serum and plasma. The level of cobalt is lower than the level of chromium in the red blood cells (Walter et al., 2008). Rae studied the effect of the ion solubility in the body fluids and the level of toxicity (Rae, 1981). It was demonstrated that cultures of fibroblasts were poisoned by cobalt and vanadium, but were not affected by nickel, chromium, titanium, or aluminum under the same conditions. In his study, cobalt from the Co–Cr alloy, nickel from stainless steel and vanadium from the titanium alloy were the most harmful components in surgical alloys (Rae, 1981).

Clinical use of Ti-6Al-4V alloy is controversial. Although corrosion resistance and breakdown potential of titanium alloys in the body is usually higher than stainless steel and CoCrMo

alloys in vitro corrosion testing (Gurappa, 2002), failure of nine Ti-6Al-4V hip implants placed in the tissue for an average time of 33.5 months has been observed (Agins et al., 1988). A histological examination of tissues adjacent to failed implants indicated that toxic ions were liberated into the surrounding tissues (Agins et al., 1988). Hallab *et al.* specified that the accumulation of ions such as vanadium and aluminium could cause long term health problems such as peripheral neuropathy, osteomalacia, and Alzheimer's disease (Solar et al., 2004). In contrast, Dobbs and Scales indicated that the clinical use of Ti-6Al-4V alloys as biomaterials are safe for the human body (Dobbs & Scales, 1983). The review of the failure of metallic implants indicates that there is still room for improvement of metallic implants performance especially corrosion and ion release of orthopedic biomaterials.

From the author's point of view, one of the issues associated with corrosion studies of biomaterials is a selection of test environments and conditions due to the complexity of the body environment and response to the implant. For instance, oxidation-reduction potentials of metallic implants vary by time of implantation because oxide layer growth is a function of time (Nilner and Holland, 1985). Several in vitro corrosion studies have been conducted to investigate factors affecting corrosion behavior of metallic bio-implants (Alves et al., 2009; Ask et al., 1989; Hodgson et al., 2002; Hodgson et al., 2004; Miloev & Strehblow, 2003; Caron et al., 1997; Shih et al., 2004; Sodhi et al., 1991) in which researchers employed various test environments and conditions. These environments and conditions were selected based on the body environment and response to metal/tissue interfaces. Some of these factors are described in the following section.

2.3 Body environment and metal-tissue interface

The human body environment contains corrosive solutions at 37°C regulated homeostatically (Kruger, 1979). For example, serum and interstitial fluid in the human body contain 113 and 117 mg L^{-1} chloride ions, respectively (Balamurugan et al., 2008). In addition to chloride ions, body fluids include Ca^{+2}, Mg^{+2}, PO_3^{-3}, SO_2^{-4} as well as organic acid anions. Phospholipids, cholesterols, natural fats, proteins, glucose, and amino acids are some complex compounds which are present in the human body in smaller amounts. In Table 2-5 compositions of selected components of three body fluids are presented (Kuhn et al., 1986).

Table 2-5 : Compositions of interstitial and synovial fluids along with serum-redrawn (Kuhn et al., 1986)

Component	Interstitial Fluid (mg L^{-1})	Synovial Fluid (mg L^{-1})	Serum (mg L^{-1})
Sodium	3280	3127	3265
Potassium	156	156	156
Calcium	100	60	100
Magnesium	24	-	24
Chloride	4042	3811	3581
Bicarbonate	1892	1880	1648
Phosphate	96	96	96
Sulfate	48	48	48
Organic Acids	245	-	210
Protein	4144	15000	66300

Body fluids also contain gases such as oxygen and carbon dioxide. The concentrations of these gaseous species in various body fluids are shown in Table 2-6 (Bundy, 2008). Oxygen, which has an essential role in body functions, is a cathodic reactant in the corrosion of

implants. Variation of the partial pressure of oxygen (changes from 2.67 x 10^2 to 1.33 × 10^4 Pa (Black, 1992)) may develop differential aeration cells. Concentration of oxygen in the human body is also significantly lower than the oxygen concentration in air which delays the surface oxide film formation and increases the amount of ion release of implants (Hanawa, 2004). In addition, the stability of the implant's passive films is influenced by a pH change which is regulated by carbon dioxide (Bundy, 2008).

Table 2-6 : Concentrations and partial pressure of the gaseous species in various fluids in contact with surgical implants-redrawn (Bundy, 2008)

Gas component	Arterial blood	Venous blood	Interstitial fluid
O_2	100 mm Hg	40 mm Hg	2-40 mm Hg
Dissolved O_2	3 mL/L	1.2 mL/L	-
O_2 combined with hemoglobin	200 mL/L	154 mL/L	-
CO_2	15-19 mm Hg	17-20 mm Hg	46 mm Hg

Body pH regulates homeostatically and depends on the function of tissue varying from 6.8 to 7.78 (Bundy, 2008). However, human body pH drops to 5.4 (Frateur et al., 2006) at the inflammatory process. It is also possible that the pH changes over some areas of implants after long-term service. In this case, pH alternation creates potential and current gradients which can initiate the mitigation of local corrosion attacks (Popa et al., 2003).

In the human body fluid, the total concentration of organics is more than 80 g L^{-1} including mainly proteins along with other substances such as fatty acids, glucose, cholesterol, lactate, and urea (Bundy, 2008; Kannan et al., 2002). Protein-surface and cell-surface interactions

could lead to success or failure of the implant (Kasemo & Lausmaa, 1994). These interactions form micro- and sub-micrometer-sized metal products that could cause an inflammatory response and appearance of foreign body giant cells (Balamurugan et al., 2008). Electrical currents oscillation results from the body response which could alter homeostatic body environments such as pH and partial pressure of oxygen.

When an implant is placed inside a human body, a thermodynamic driving force will build up at the interface between implants and tissue to lower the surface energy (Kasemo & Lausmaa, 1994). As a result, reactions of various kinds occur and proceed until the lowest thermodynamics state or a kinetic barrier layer develops at the interface. The basic reaction is the oxidation of metals which may result in the release of ions or formation of metal oxide, metal chlorides, organometallic compounds, etc. (Hallab et al., 2004). Kasemo and Gold (Kasemo & Gold, 1999) studied the implant-tissue interface events. The first interaction of an ideal clean implant oxide surface is with water molecules. The result of this interaction is a build-up of a water mono- or bilayer. Water may dissociate to hydroxylated (OH^- terminated) or stay intact, mainly depending on the surface activities of the implant. If water-surface interactions form weak bonds, the implant surface will turn hydrophobic (Kasemo & Gold, 1999) causing natural ions, e.g. Na^+ and Cl^-, to incorporate into the water over-layers as hydrated ions.

Biomolecules in the bioliquids then adsorb to the layer of ions and water (Kasemo & Gold, 1999). One of main components of biomolecules is protein. Protein readily coats an implant

surface (Bundy, 2008) due to the laws of mass transport, presence of attractive van der Waals forces, and electrostatic interactions. Cations released from metallic implant favors the adsorption of negatively-charged species such as protein, chloride, and phosphates. The interaction of protein and cations at the interface creates an adsorbed layer of protein, which can reduce the interaction between the barrier film and the solution. Colloidal organometallic complexes are also formed at the oxide layer/ corrosive solution interface (Cahoon & Paxton, 2004). These complexes can change the pH of albumin solutions and may enhance the rate of metal dissolution and corrosion rate (Clark & Williams, 2004; Merritt & Brown, 2004). Metal dissolution rate may also vary by alternation of protein concentration in the body fluid during the healing period at the implant tissue interface. In Figure 2-2, the remodelling process of tissue at the interface zone with the implant in the first 10 years after implantation is illustrated (Kasemo & Lausmaa, 1994). As it is shown, space filled with biofluid is formed after implantation which mostly contains protein. The gap between the implant and the native tissue gradually decreases by the adsorption of protein to the oxide surface. Change of protein concentration in biofluid can have an effect on the metal dissolution rate and corrosion behavior of metallic bio-implants.

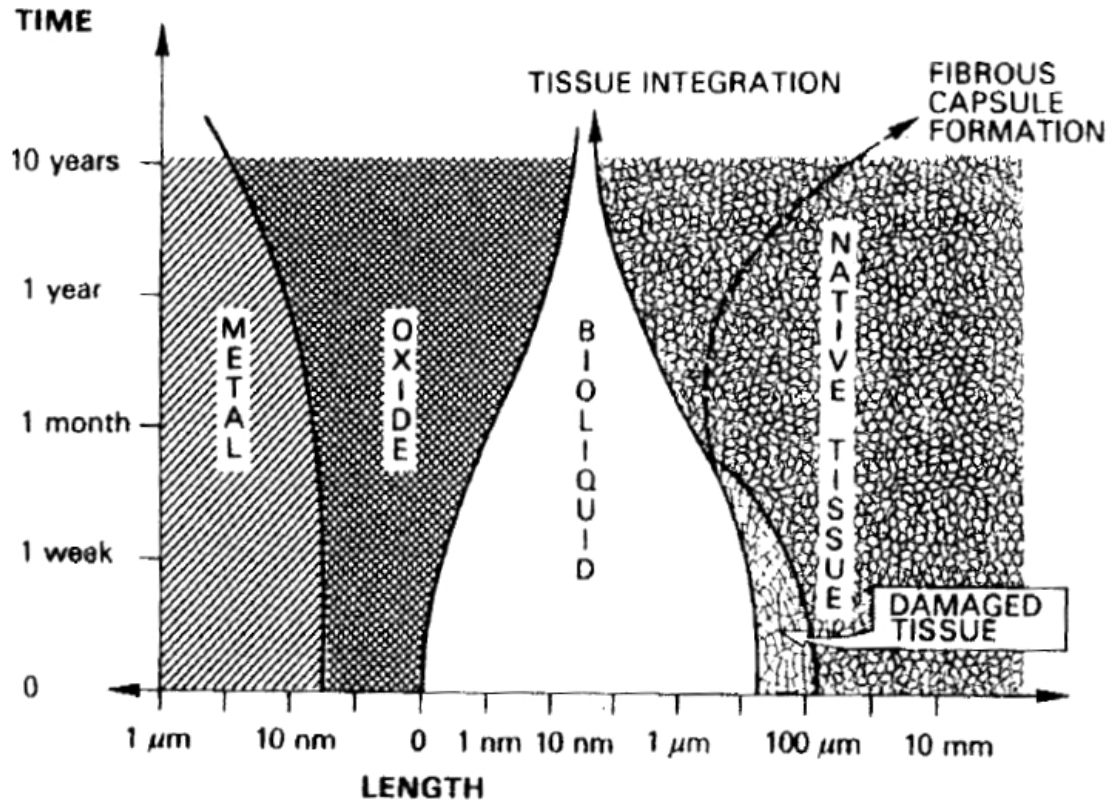

Figure 2-2 : Remodelling process of tissue generation close to implant (Kasemo & Lausmaa, 1994)

Nobel materials such as gold and silver have little or no driving force for corrosion whereas the high corrosion resistance of stainless steel, Co-Cr, Ti, and Ti alloys relies on the development of passive film. This film acts as a kinetic barrier film to impede corrosion. The passive film is, in fact, very dynamic in the biological environment and their passivity depends on the implant-tissue interaction reactions. Protein is one of the body fluid components that readily interacts with surgical implants. The protein adsorption onto the surgical implant is influenced by the substrate electrochemical state (Gettens & Gilbert, 2008). The influences of several factors on electrochemical and surface characterizations of

biomaterials in the presence of protein have been investigated. Some of the electrochemical corrosion studies were briefly reviewed.

2.4 Effect of protein on electrochemical corrosion behavior of bio-implants

The interaction of protein with the metallic surface depends on several factors such as substrate nature, immersion time, proteins type, pH, and temperature. Several studies have been conducted to investigate the effect of these factors on the corrosion behavior of metallic bio-implants in the presence of proteins (Cheng & Roscoe, 2005; Fukuzaki et al., 1995; Jackson et al., 2000; Khan et al., 1999; Muñoz & Mischler, 2007; Tang et al., 2006; Yan et al., 2007).

The surface characterization of metallic biomaterials in the presence of protein in various solutions has been studied. 316L in the presence of dissolved salts of NaCl, $MgCl_2$, and $CaCl_2$ with 0 and 20 mg L^{-1} BSA were also studied (Zanna et al., 2006). The XPS analysis results showed that the adsorption of protein is independent of Na^+ but the presence of Ca^{2+} and Mg^{2+} increases the BSA adsorption on 316L. The passive film composition formed on orthopedic stainless steel was analyzed by Milosev and Strehblow (Milošev & Strehblow, 2000) at different oxidation potentials. The XPS analysis showed that the passive film established on orthopedic stainless steel contains Cr and Fe and small amounts of Ni and Mo where their chemical composition depends on oxidation potential. For instance, the passive layer is depleted of iron and enriched in chromium and nickel at high oxidation potential (Milošev & Strehblow, 2000). The adsorption of BSA on pure chromium and molybdenum in

0.1 M phosphate buffer (Na_2HPO_4 + NaH_2PO_4) solution was characterized by Pradier *et al.* (Pradier et al., 2003) by XPS. BSA adsorption is initially rapid and reaches a plateau for a greater BSA concentration and immersion period. The Cr surface contains the oxide Cr_2O_3 and the hydroxide Cr $(OH)_3$, and Mo surface is covered with a thin layer of MoO_2 oxide and a small amount of hydroxide (Pradier et al., 2003). The amount of adsorbed phosphate on Cr is higher than Mo in BSA and PBS solutions. The authors addressed these differences by different levels of hydroxylation and charges of metallic samples. The level of hydroxylation and charge of metallic samples depends on pH solutions. For example, the TiO_2 surface is negatively charged in a pH range of 5.15 to 7.15 (Wassell & Embery, 1996) and has amphoteric hydroxyl groups (Boehm, 1971), which means both acidic and basic OH- groups exist on its surface.

The effect of pH and temperature on electrochemical corrosion behaviors of different biomaterials has also been investigated. For instance, Wassell and Embery (Wassell & Embery, 1996) studied the adsorption of BSA on titanium powder in solutions containing calcium and phosphate ions as a function of pH. BSA adsorption decreases with increasing pH on the surface of titanium. The reason for this is that both the titanium surface and BSA are negatively charged at a pH range of 5.15 to 7.15, whereas at pH= 4, the titanium powder surface charge is positive. The chance of formation of attractive forces, therefore, increases when pH decreases (Wassell & Embery, 1996). The electrochemical corrosion behavior of high-carbon CoCrMo alloy in solutions of 0.14 M NaCl and BSA (5, 20, 50, and 500 mg L^{-1}) in a temperature range of 298 to 333 K were evaluated (Valero Vidal et al., 2010). When BSA

concentration was 0 to 20 mg L^{-1}, change of temperature did not affect the corrosion current density of the CoCrMo alloy; however, an increase of temperature increased corrosion current density at a BSA concentration greater than 20 mg L^{-1}. The Valero team considered two overlapped time constants from the impedance spectra in Figure 2-3. The first time constant corresponded to the oxide resistance/capacitance of the inner layer and the second was related to the outer layer resistance and double layer capacitance. Therefore, the semicircle diameter indicates the charge transfer resistance. Charge transfer resistance depends on BSA concentrations and temperature variations. The author also mentioned that protein can modify the nature of the CoCrMo passive film at open-circuit potential (OCP) due to the high affinity of protein to adsorb to the surface via chemisorption (Valero Vidal et al., 2010). BSA, as a protein simulator, has been used in many electrochemical corrosion studies.

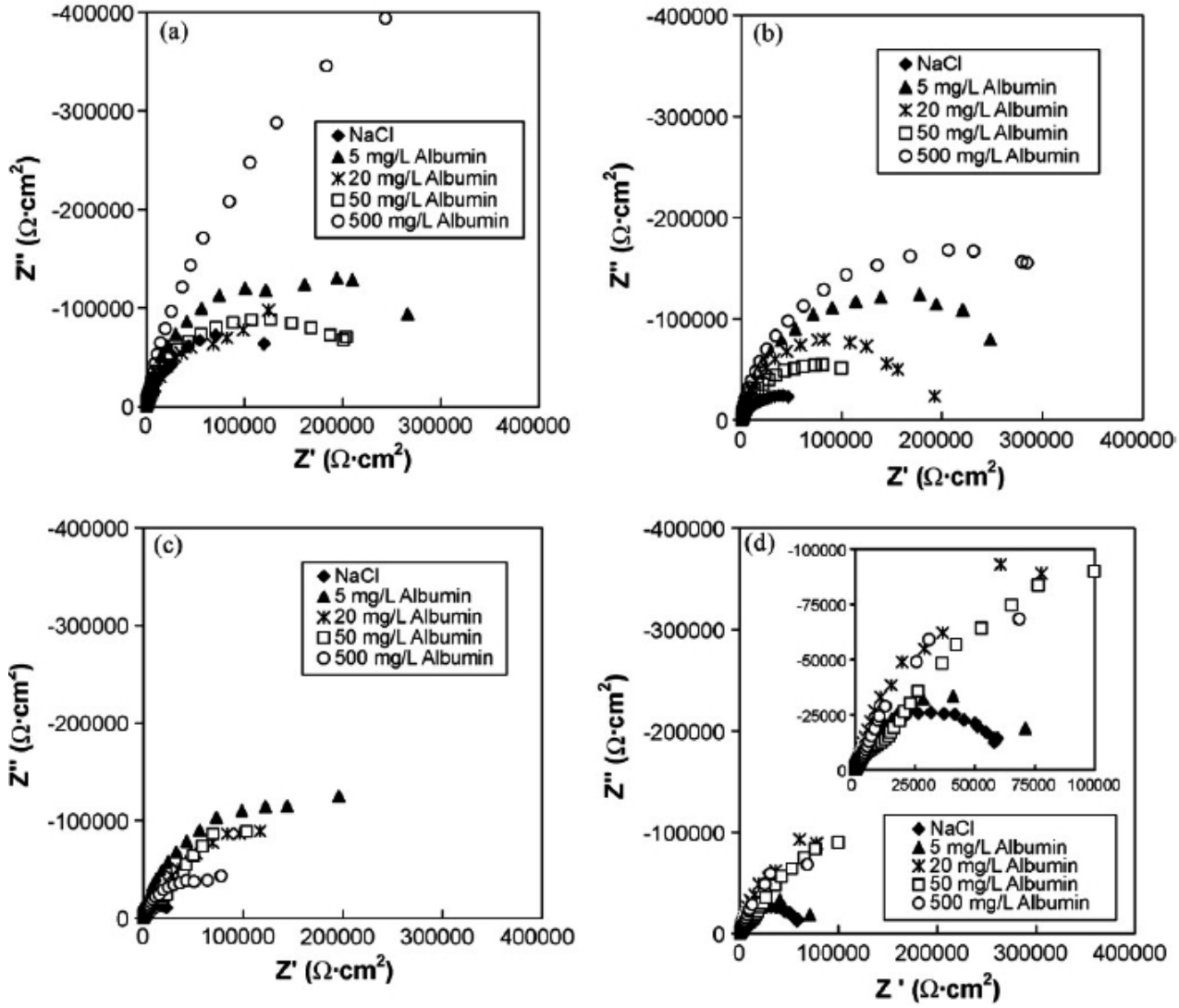

Figure 2-3 : Nyquist diagrams of CoCrMo alloy in 0.14M NaCl solution with several BSA additions at different temperatures (a) 298, (b) 313, (c) 323, and (d) 333 K (Valero Vidal et al., 2010)

The effect of immersion time on corrosion behavior of CP Ti, Ti-6Al-4V, Ti6Al17Nb and CoCrMo alloys in the presence of 0.1 M sodium sulphate and fetal bovine serum was studied

by Contu *et al.* (Contu et al., 2002). The impedance spectra of the samples in fetal serum bovine are illustrated in Figure 2-4.

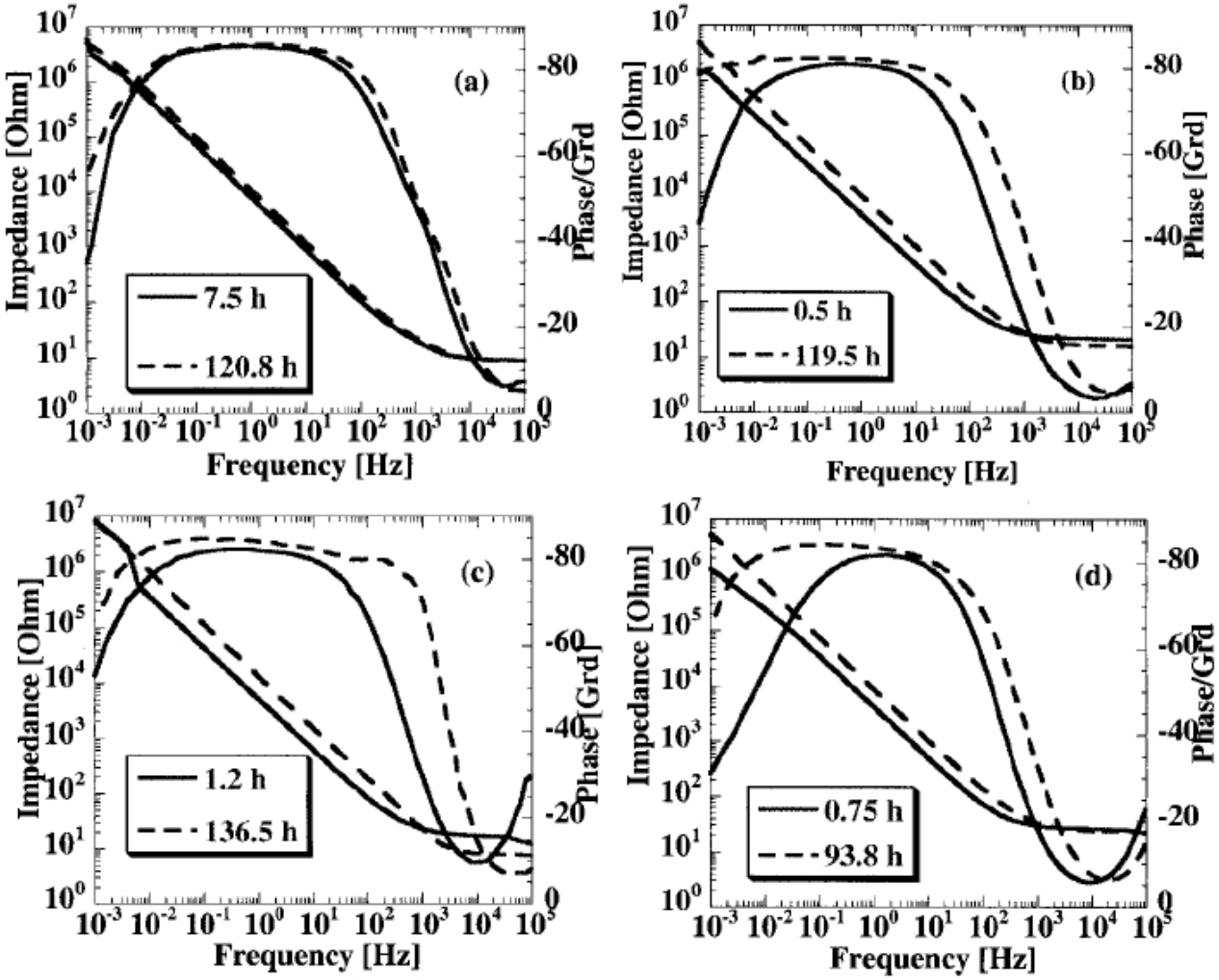

Figure 2-4 : Effect of the immersion time on the impedance spectra (Bode plot) of mechanically polished samples. (a) CP Ti, (b) Ti-6Al-4V, (c) Ti-6Al-7Nb, and (d) CoCrMo alloys immersed in bovine serum (Contu et al., 2002)

The results indicated that the polarization resistance of all samples have higher values at longer immersion times and the presence of protein lowers the polarization resistance. In

addition, the lowest polarization resistance was obtained for CoCrMo alloy right after its exposure to the solution (Contu et al., 2002). The electrochemical behavior of 316L and CoCrMo was investigated (Valero Vidal & Muñoz, 2008) in four synthetic solutions of 0.14 M NaCl, 0.14 M NaCl + 0.5 g L^{-1} albumin, PBS (0.14 M NaCl, 1 mM KH_2PO_4, 3 mM KCl, Na_2HPO_4) and PBS + 0.5 g L^{-1} albumin after immersion periods of 1 and 24 hours. 316L passive film formation was independent of immersion time while the interface behavior of the CoCrMo improved at the longer immersion time.

The presence of protein could also affect the corrosion resistance of biomaterials. Burstein & Liu (Burstein & Liu, 2007) investigated the nucleation of corrosion pits on 316L and commercially-pure titanium microelectrodes in Ringer's physiological solution at 37°C. They concluded that the presence of serum facilitates the nucleation of pits on 316L and titanium. However, the pit nucleation is more sensitive to the presence of serum on the stainless steel than pure titanium. Vidal and Munoz stated that the passive layer of the CoCrMo alloy is more homogeneous and thicker than the AISI 316L passive films by comparing charge transfer resistance and capacitance of CoCrMo and 316L alloys (Valero Vidal & Muñoz, 2008). The charge transfer resistance of both alloys increased in the phosphate-containing solutions because of a blocking effect of phosphate ions on the passive film. The polarization curves (Valero Vidal & Muñoz, 2008) of 316L in these solutions are shown in Figure 2-5. The breakdown potential of 316L in the PBS solution is higher than in the NaCl solution (Sousa & Barbosa, 1991; Valero Vidal & Muñoz, 2008). The reason for this is that HPO_4^{2-} and $H_2PO_4^{2-}$ are able to adsorb to the positively-charged surface of 316L and form a passive layer to delay

pitting initiation (Valero Vidal & Muñoz, 2008). The alloy's microstructure could affect the corrosion behavior of the samples. For example, the passive film of the annealed Nb is more protective than that of as-cast and cold-rolled samples (Wang & Alfantazi, 2013).

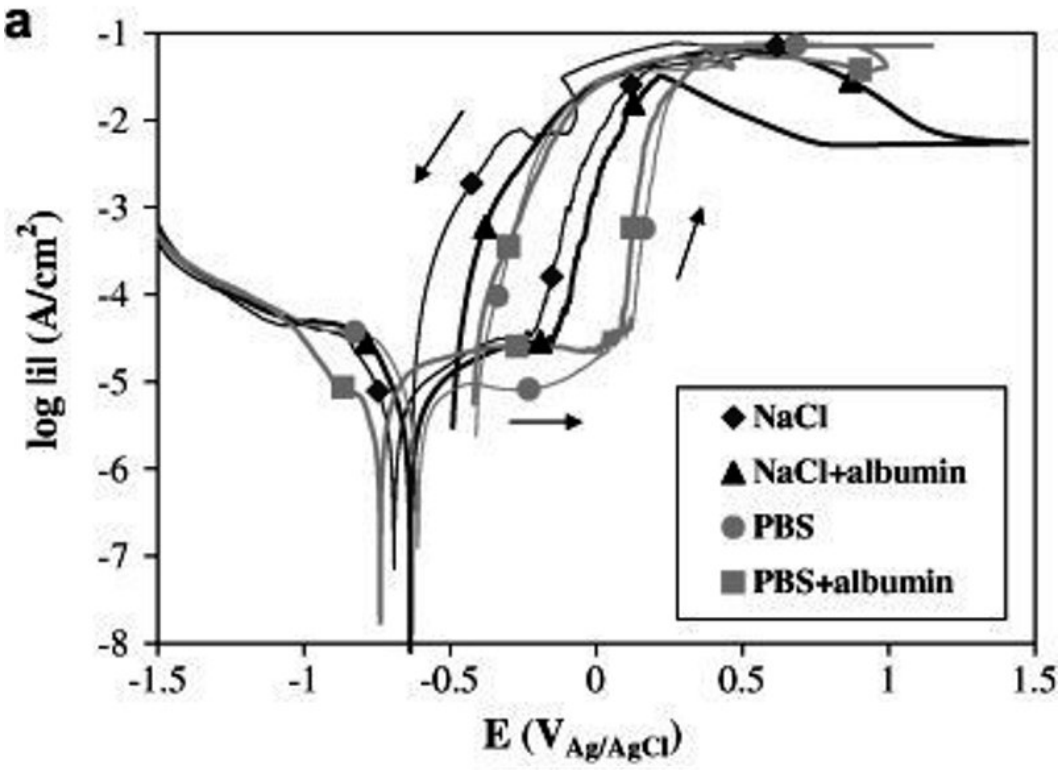

Figure 2-5 : Potentiodynamic curves of AISI 316L in NaCl and PBS solutions at 37°C and pH 7.4 (Valero Vidal & Muñoz, 2008)

Protein type can also influence the corrosion behavior of metallic biomaterials. Corrosion potential (E_{corr}) of 316L and CoCrMo decreased in solutions of PBS with albumin compared to E_{corr} in PBS solutions without albumin (Valero Vidal & Muñoz, 2008). This behavior can be related to inhabitant behavior of phosphate and albumin. Phosphates and albumin act as anodic (Hanawa et al., 2001) and cathodic (Hiromoto et al., 2005) inhibitors on CoCrMo alloy surfaces, respectively. Ouerd *et al.* (Ouerd et al., 2008) investigated the influence of

phosphate ions and calf serum solutions on the corrosive behavior of CoCrMo alloy. They indicated that the active surface of CoCrMo is mainly blocked by phosphate ions whereas no significant change was observed by the addition of calf serum. On the other hand, Omanovic and Roscoe (Omanovic & Roscoe, 1999) demonstrated that the addition of BSA up to 1.5 mg L^{-1} to the electrolyte increases the corrosion rate at the open circuit potential. Lori and Hanawa (Lori & Hanawa, 2001) studied the adsorption of glycine, the simplest amino acid, on gold and titanium surfaces in Hank's solutions. In their study, the variations of mass and open circuit potential and mass and current were measured by a quartz crystal microbalance (QCM). The results showed that the adsorption of glycine and stabilizing time on the gold and titanium surfaces is enhanced by increasing the glycine concentration. Furthermore, titanium is able to adsorb glycine more than gold due to the interaction of the passive layer (TiO_2) with glycine. The adsorption behavior of 0 and 1 g L^{-1} human serum albumin (HSA) in 0.1 M phosphate buffer was investigated by Electrochemical Impedance Spectroscopy (EIS) on a glassy carbon electrode (Marie de Ficquelmont-Loïzos et al., 1997). This research indicated that HSA could inhibit reduction reactions such as hydrogen evolution reaction. Therefore, the type of protein and its concentration can change the corrosion behavior of biomaterials. In this research study, the focus is mostly on corrosion of common biomaterials in the presence of BSA and HSA. A list of electrochemical corrosion study in presence of BSA and HSA is provided in Table 2-7 and Table 2-8.

Table 2-7 : List of electrochemical corrosion studies in presence of BSA along with the experimental techniques, materials, background solution, protein and concentrations, and pH range

#	Journal's title	Experimental technique	Materials' type	Background sol.	Protein	Protein conc.	PH
1	Electrochemical studies on the influence of proteins on the corrosion of implant alloy (R. L. Williams et al., 1988)	PD in static and fretting modes	316L, Ti, Ti-6Al-4V	0.9% NaCl	Bovine calf serum	10%	7.4
2	Electrochemistry of AISI 316L stainless steel in calcium phosphate and protein solutions(Sousa & Barbosa, 1991)	PD, PS, Galvanostatic	316L	0.9% NaCl	BSA	10%	7.4
3	Influence of low dissolved oxygen concentration in body fluid on corrosion fatigue behaviors of implant metals (Morita et al., 1992)	Fatigue test	316L	0.9% NaCl	Bovine calf serum	10%	6.7& 5.4
4	Corrosion resistance of titanium CP in saline physiological solutions with calcium phosphate and proteins (Sousa & Barbosa, 1993)	PD, EIS, Galvanostatic	Ti	0.15M NaCl+ 1 mM $CaCl_2$	BSA	10%	7.4
5	Adsorption of protein onto stainless-steel surfaces (Fukuzaki et al., 1995)	Zeta potential was measured by the streaming potential method	nonporous stainless-steel particles	10^{-3} M KNO_3	BSA and Gelatin	0.2-7 g L^{-1}	3.2-8
6	Adsorption of bovine serum albumin on to titanium powder (Wassell & Embery, 1996)	Microelectrophoresis	Ti powder	0.02 M sodium acetate	BSA	0.1-10 g L^{-1}	5.15-7.15
7	The corrosion behavior of Ti-6Al-4V, Ti-6Al-7Nb and Ti-13Nb-13Zr in protein solutions (Khan et al., 1999)	Cyclic polarization	Ti-6Al-4V, Ti-6Al-7Nb & Ti-13Nb-13Zr	PBS	Bovine calf serum & BSA	0.1, 1, 1 g L^{-1}	5, 7.4, 9
8	Electrochemical studies of the adsorption behavior of bovine serum albumin on stainless steel (Jackson et al., 2000)	OCP, PD, EIS	304L	KH_2PO_4 & NaOH (0.05M)	BSA	1.5 mg L^{-1}	7.0
9	Interactions between calcium, phosphate, and albumin on the surface of titanium (Lima et al., 2001)	PD, chronoamperometric, XRD, EDS, XPS (X-ray photoelectron spectroscopy)	Pure Ti deposited by calcium phosphate	HBSS	BSA	0 and 4 g L^{-1}	7.2
10	Electrochemical studies on the stability and corrosion resistance of titanium-based implant materials (Aziz-Kerrzo et al., 2001)	Cyclic polarization, PD, EIS	Ti, Ti-6Al-4V & Ti-45Ni	PBS	-	-	7.4
11	Electrochemical characterization of passive films on Ti alloys under simulated biological conditions (Hodgson et al., 2002)	EIS and photoelectrochemical analysis	Ti, Ti-6Al-4V & Ti6Al17Nb	0.14M NaCl, 1& 10 mM KH_2PO_4, 2.5 & 10 mM CaCl2	-	-	7.4
12	Characterization of implant materials in fetal bovine serum and sodium sulfate by electrochemical impedance spectroscopy I (Contu et al., 2002)	EIS	cp Ti, wrought Ti-6Al-4V, wrought Ti-6Al-7Nb, and cast CoCrMo	0.1M sodium sulfate	fetal bovine serum	0.1 g L^{-1}	7-7.3

Table 2-7: (Cont'd) List of electrochemical corrosion studies in presence of BSA along with the experimental techniques, materials, background solution, protein and concentrations, and pH range

#	Journal's title	Experimental technique	Materials' type	Background sol.	Protein	Protein conc.	PH
13	Characterization of different materials for corrosion resistance under simulated body fluid conditions (Gurappa, 2002)	OCP, cyclic polarization, EIS	316L, CoNiCrMo, Ti, Ti-6Al-4V	Hank's solution	-	-	7.4
14	The composition of the surface passive film formed on CoCrMo alloy in simulated physiological solution (Miloev & Strehblow, 2003)	PD, XPS	CoCrMo	Hank's solution+ 50m M tri-sodium citrate dihydrate	-	-	7.5
15	Characterization of implant materials in fetal bovine serum and sodium sulfate by electrochemical impedance spectroscopy. II. Coarsely sandblasted samples (Contu et al., 2003)	EIS	sandblasted samples of cp Ti, wrought Ti-6Al-4V, wrought Ti-6Al-7Nb, and cast CoCrMo	0.1M sodium sulfate	fetal bovine serum	0.1 g L^{-1}	7-7.3
16	Passive and transpassive behavior of CoCrMo in simulated biological solutions (Hodgson et al., 2004)	PD,EIS,CV, Induced coupled plasma-mass spectroscopy (ICP-MS), XPS	CoCrMo	0.14 M NaCl or a simulated body fluid	-	-	7.4
17	Adsorption characteristics of bovine serum albumin and its peptide fragments on a stainless steel surface (Sakiyama et al., 2004)	FT-IR spectroscopy	316L particles	100 mM KNO_3, HNO_3, KOH	BSA	0.2 g L^{-1}	3, 7 & 10.5
18	Effect of surface oxide properties on corrosion resistance of 316L stainless steel for biomedical applications (Shih et al., 2004)	PD, XPS, TEM, AES	316L	Ringer's solution	-	-	7.4
19	Serum effect on the electrochemical behavior of titanium, Ti-6Al-4V and Ti6Al17Nb alloys in sulphuric acid and sodium hydroxide (Contu et al., 2004)	PD & EIS	Ti, Ti-6Al-4V & Ti6Al17Nb	2M sulphuric acid & 2M sodium hydroxide	Bovine serum	0, 1, 4.8, 20 vol.%	NA
20	Corrosion behavior of CoCrMo implant alloy during fretting in bovine serum (Contu et al., 2005)	OCP(t=800 s), PD	CoCrMo	Buffer Citrate (pH=4), KH_2PO_4/$NaHPO_4$(pH=7), 2M NaOH	Bovine calf serum	17.5 vol.%	4 & 7
21	Corrosion behavior and surface characterization of titanium in solution containing fluoride and albumin (Takemoto et al., 2005)	LPR, PD,XPS	Ti	sodium chloride sodium fluoride (containing 2.0 g/l fluoride)	BSA	0.1 and 1 g L^{-1}	5
22	Microstructure and corrosion behavior in biological environments of the new forged low-Ni CoCrMo alloys (Hiromoto et al., 2005)	XPS, XRD, PD	low-Ni Co–29Cr–(6, 8)Mo, Co–29Cr–6Mo–1Ni	0.14 M NaCl, Hanks' sol., and E-MEM	fetal bovine serum(just for (E-MEM)	10 vol%	5.5, 7.3, 8.3

Table 2-7: (Cont'd) List of electrochemical corrosion studies in presence of BSA along with the experimental techniques, materials, background solution, protein and concentrations, and pH range

#	Journal's title	Experimental technique	Materials' type	Background sol.	Protein	Protein conc.	PH
23	Corrosion behavior of titanium in the presence of calcium phosphate and serum proteins (Cheng & Roscoe, 2005)	OCP, PD, EIS	Cp Ti	PBS	BSA & fibrinogen	0.05 g L^{-1}	7.4
24	Electrochemical impedance spectroscopy study of Ti-6Al-4V alloy in artificial saliva fluoride and/or bovine albumin (Cosman et al., 2005)	EIS	Ti-6Al-4V	Modified Fusayama artificial saliva	BSA	0.01,0.1, 0.2, 0.5 %	5
25	Comparison of metal release from various metallic biomaterials in vitro (Okazaki & Gotoh, 2005)	Ion release by an immersion test for 7 days	316L,Co–Cr–Mo, Ti, Ti–6Al–4V, Ti–6Al–7Nb & Ti–15Zr–4Nb–4Ta	α-medium, PBS, 0.9% NaCl, artificial saliva,1 mass% lactic acid and 0.01 mass% HCl	calf serum		
26	In vitro corrosion study by EIS of an equiatomic NiTi alloy and an implant quality AISI 316 stainless steel (Rondelli et al., 2005)	EIS	NiTi, 316L	PBS & MEM	fetal calf serum & fibroblast cell	10%	-
27	Influence of bovine serum albumin in sulphuric acid aqueous solution on the corrosion and the passivation of an iron-chromium alloy (Frateur et al., 2006)	PD, EIS, PM-IRRAS, XPS	Fe–17Cr	0.05M H2SO4 solution	BSA	10 or 20mg L^{-1}	1.3
28	Electrochemical study of Type 304 and 316L stainless steels in simulated body fluids and cell cultures (Tang et al., 2006)	OCP, PD, LPR	304 and 316L	Hank's solution	fetal bovine serum	10%	-
29	Biotribocorrosion of CoCrMo orthopedic implant materials-Assessing the formation and effect of the biofilm (Yan et al., 2007)	PD, Gravimetric analysis & Current vs. Time(PS), XPS	316L, High carbon CoCrMo & low carbon CoCrMo	In either 0.36% NaCl or 50% serum	Bovine calf serum	50%	7.2-7.8
30	Reactivity of Titanium in Physiological Medium (Ouerd et al., 2007)	Ocp, PD, CV, EIS	Ti	PBS & water	Bovine calf serum	21%	7 & 8
31	interactive effects of albumin and phosphate ions on the corrosion (Muñoz & Mischler, 2007)	PD & EIS	Wrought Co-28Cr-6Mo	PBS & 0.14M NaCl	Albumin	0.5 g L^{-1}	7.4
32	Nucleation of corrosion pits in Ringer's solution containing bovine serum (Burstein & Liu, 2007)	Measured I vs time	316L and Ti	Ringer's solution	BSA	0.1 wt% and 0.4 wt%	7.4
33	Electrochemical characterization of biomedical alloys for surgical implants in simulated body fluids (Valero Vidal & Muñoz, 2008)	PD, PS & EIS	316L & CoCrMo	PBS & 0.14M NaCl	Albumin	0.5 g L^{-1}	7.4
34	Reactivity of CoCrMo alloy in physiological medium: Electrochemical characterization of the metal/protein interface (Ouerd et al., 2008)	EIS, Linear voltammetry polarization	CoCrMo	0.1Mphosphate buffer	Fetal bovine serum	1.9 g L^{-1}	7.4

Table 2-7: (Cont'd) List of electrochemical corrosion studies in presence of BSA along with the experimental techniques, materials, background solution, protein and concentrations, and pH range

#	Journal's title	Experimental technique	Materials' type	Background sol.	Protein	Protein conc.	PH
35	Electrochemical characterization of AISI 316L stainless steel in contact with simulated body fluid under infection conditions (López et al., 2008)	Cyclic polarization, EIS	316L	Netrual and acidis sbf	-	-	7.24 & 4
36	Effects of pH on the electrochemical behavior of titanium alloys for implant applications (Souza et al., 2009)	Cyclic polarization, PD, EIS	Ti-6Al-4 V& Ti-13Nb-13Zr	Ringer's solution	-	-	5.5 and 7
37	Adsorption of bovine serum albumin on CoCrMo surface: Effect of temperature and protein concentration (Valero Vidal et al., 2010)	PD, EIS	CoCrMo	0.14M NaCl	BSA	5,20,50, and 500 mg L^{-1}	7.4
38	Study of the adsorption process of bovine serum albumin on passivated surfaces of CoCrMo biomedical alloy (Vidal & Muñoz, 2010)	PD, EIS	High carbon CoCrMo	PBS	BSA	100 mg L^{-1}	7.4
39	Influence of the sliding velocity and the applied potential on the corrosion and wear behavior of HC CoCrMo biomedical alloy in simulated body fluids (Igual Muñoz & Casabán Julián, 2010)	Tribocorrosion tests (OCP, PD, I /time)	CoCrMo	PBS	BSA	0.5 g L^{-1}	7.4
40	Electrochemical behavior of TiO_2 nanotube on titanium in artificial saliva containing bovine serum albumin (C. Liu et al., 2012)	PD,EIS	polished Ti and TiO_2 nanotube	Artificial saliva	BSA	5g L^{-1}	-
41	Study of the biotribocorrosion behavior of titanium biomedical alloys in simulated body fluids by electrochemical techniques (Dimah et al., 2012)	PD and PS under sliding conditions	Ti-Grade 2, Ti-6Al-4V and Ti-6Al-4V-ELI	PBS	BSA	0.5 g L^{-1}	7.4
42	Influence of albumin and inorganic ions on electrochemical corrosion behavior of plasma electrolytic oxidation coated magnesium for surgical implants (Wan et al., 2013)	PD,EIS, XPS	pure magnesium	0.9 wt.% NaCl and PBS	BSA	1 g L^{-1}	7.4
43	Effect of protein adsorption on the corrosion behavior of 70Cu–30Ni alloy in artificial seawater (Torres Bautista et al., 2013)	EIS, XPS and ToF-SIMS	70Cu–30Ni (wt.%)	artificial seawater	BSA	0 and 20 mg L^{-1}	8.0

Table 2-8 : List of electrochemical corrosion studies in presence of HSA along with the experimental techniques, materials, background solution, protein and concentrations, and pH range

#	Journal's title	Experimental technique	Materials' type	Background sol.	Protein	Protein conc.	PH
1	Long-time and short-time investigation of the electrode interface through electrochemical impedance measurements. Application to adsorption of human serum albumin onto glassy carbon rotating disc electrode (Marie de Ficquelmont-Loïzos et al., 1997)	EIS	Glassy carbon rotating disc electrode	0.1M phosphate buffer in the presence of equimolar (5×10^{-4} M) ferricyanide + ferrocyanide ions as steady-state indicator	HSA	1 g cm^{-3}	7.4
2	Enhanced Performance of an Affinity Biosensor Interface based on Mixed Self-Assembled monolayers of thiols on Gold (Frederix et al., 2003)	contact angle measurements, cyclic voltammetry, FTIR	Gold	6 m$MK_3Fe(CN)_6$ solution with 1 M KCl (for cyclic voltammetry)	HSA	-	&.4
3	The effect of galvanic coupling between modern fracture fixation constructs in physiologically relevant solutions: the role of serum proteins on the corrosion of Ti-6Al-4V and 316L alloys (Grebner & Hansen, 2008)	OCP,EIS, galvanic current measurements	316L and Ti-6Al-4V	Hanks Balanced Salt Solution	Albumin and fibrinogen	4.7% (w/v) albumin and 0.36% (w/v) fibrinogen	7.4
4	The behavior of pure titanium in albumin solution (Ionitaa et al., 2008)	immersed for 10 days, FTIR, UV-VIS-NIR spectrometer	pure titanium	PBS	human body plasma	2wt%	7.4
5	Corrosion behavior of copper in the presence of proteins (Cao et al., 2011)	OCP, PD, EIS	Copper	simulated uterine solution (SUS)	HSA, gamma-globulin and hemoglobin	0.5 g L^{-1}	7

A glance at the Table 2-7and Table 2-8 reveals that relatively a few electrochemical corrosion studies are conducted in HSA solutions compared to BSA.

2.5 Immersion corrosion studies of metallic biomaterials in simulated biological environments

In addition to electrochemical corrosion tests, immersion corrosion studies were conducted to investigate the ion release and surface morphology of biomaterials in the presence of protein. In this approach, surface reactions in a simulated biological environment can be determined from identifying the surface oxide composition and detecting ion released into the simulated body environment.

Okazaki and Gotoh (Okazaki & Gotoh, 2005) studied the metal release of 316L, CoCrMo casting alloy, pure Ti, Ti–6Al–4V, V-free Ti–6Al–7Nb and Ti–15Zr–4Nb–4Ta alloys immersed in various solutions of α-medium, PBS, calf serum, 0.9% NaCl, artificial saliva, 1.2% L-cysteine, 1% lactic acid and 0.01% HCl for a seven-day static immersion test. The concentration of metals was determined by inductively coupled plasma-mass (ICP-MS) and graphite furnace atomic absorption spectroscopy (AAS). The release of metal relative to the solution pH was reported and discussed by Okazaki and Gotoh (Okazaki & Gotoh, 2005). Metal release from CoCrMo (ASTM F-75) and Ti implant alloys (Ti-6Al-4V: ASTM F136, and commercially pure Ti, cpTi: ASTM F67) in 4 mL of serum under a constant rocking motion at 0.25 Hz for 1 week was measured by Hallab *et al.* (Hallab et al., 2003). The obtained results are shown in Figure 2-6. Chromium dissolution from the CoCrMo alloy steadily increased

over the course of 4 days. However, the titanium dissolution rate was relatively fast within the first hour and then levelled off for the next 100 hours.

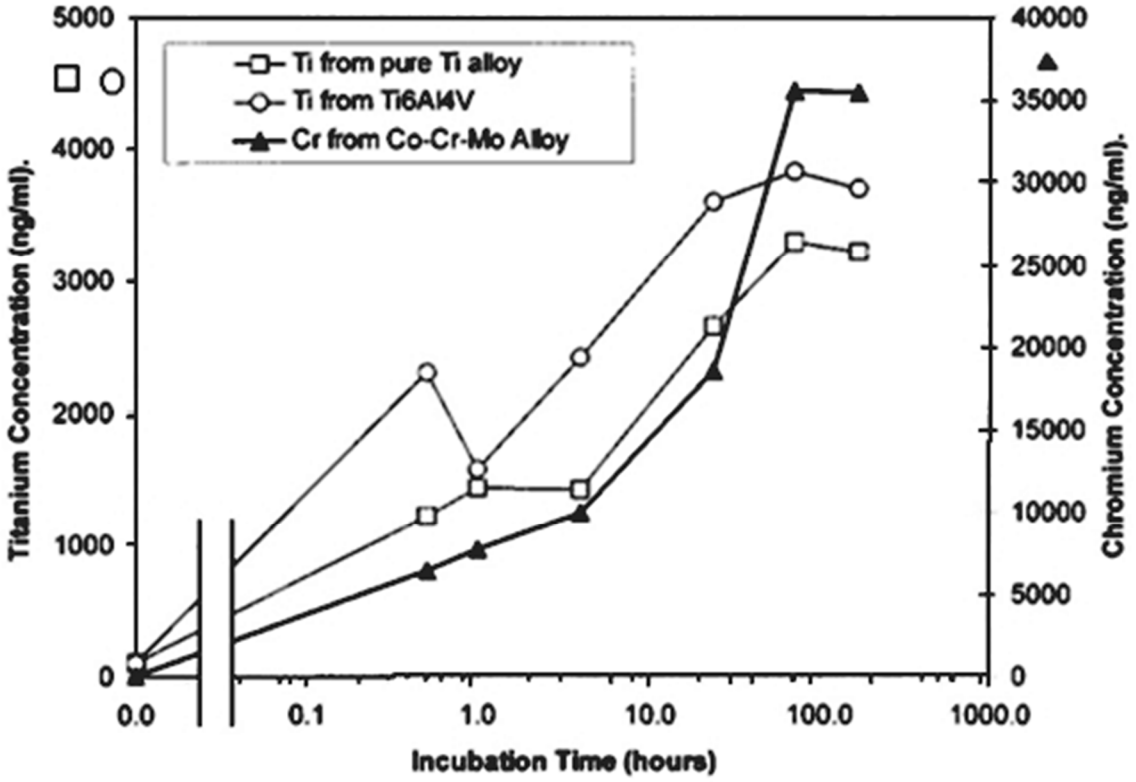

Figure 2-6 : The amounts of Ti (ng mL^{-1} or parts per billion, ppb) released into serum from CP Ti and Ti-6Al-4V beads (on the left) and the amount of Cr released into serum from Co-based alloy (on the right); Data are expressed as an average of nine samples (Hallab et al., 2003)

A comparison between the presented results from this study and our static immersion test results showed that the amount of Cr release in this study is significantly higher than Cr release obtained in our work. This can be related to the fact that the samples were free of load in our study; therefore, the passive layer did not abrade to release Cr. Yan *et al*. stated

that the presence of protein increased the metal ion release in static environments but decreased ion release in sliding systems because bovine serum lubricated the counter bodies (Yan et al., 2007). Protein concentration could also change the corrosion behavior and ion release of metallic biomaterials (Huang, 2003; Valero Vidal et al., 2010; Wang & Alfantazi, 2013; Wang et al., 2012).

In a 5-day immersion corrosion study, the composition of the oxide layer of a high carbon CoCr alloy was compared in several simulated biological fluids such as human serum, fetal bovine serum (FBS), synovial fluid, and PBS (Lewis et al., 2006). The low deposition of calcium phosphate led to the release of cobalt and chromium migrated from the bulk materials (Lewis et al., 2006; Lewis et al., 2005). Dissolution of cobalt from the Co-36.7Cr-4.6Mo alloy and the deposition of calcium and phosphate were also informed in Hanks' solution and Eagle's MEM containing 10% FBS over a 7-day immersion test (Hanawa et al., 2001). The presence of Ca^{2+} and Mg^{2+} increased the BSA adsorption on 316L, whereas the adsorption of protein was independent of Na^{+} (Marcus & Maurice, 2006). Therefore, calcium deposition can affect protein adsorption and ion dissolution from metallic biomaterials. The ion release of 316L and high carbon CoCr powders was also measured by atomic absorption spectroscopy (AAS) up to five days of incubation in human serum (Woodman et al., 1984). The predominant form of the corrosion product was organometallic complexes. These complexes form either at the metal-solution interface or in the solution. For instance, chromium and nickel interactions with protein were at the interface and cobalt bonded to serum in the solution (Woodman et al., 1984).

Table 2-9 and Table 2-10 enlist the immersion corrosion studies in the presence of BSA and HSA. Similar to electrochemical corrosion studies, the number of immersion corrosion studies in the presence of BSA is higher than those in HSA solutions. Overall, the immersion corrosion studies on metallic implants have not been widely investigated as the electrochemical corrosion investigations.

Table 2-9 : List of immersion corrosion studies in presence of BSA along with the experimental techniques, materials, background solution, protein and concentrations, and pH range

#	Journal's title	Experimental technique	Materials' type	Background sol.	Protein	Protein conc.	PH
1	Passive dissolution of titanium in biological environments (Healy & Ducheyne, 1996)	Static immersion test for 10-200 days	Titanium fibers (0.05mm)	Simulated interstitial electrolye (SIE)	Human serum	60% serum and 40% SIE	7.5
2	Adsorption of bovine serum albumin on to titanium powder (Wassell & Embery, 1996)	Microelectrophoresis	Ti powder	0.02M sodium acetate	BSA	0.1-10 g L^{-1}	5.15-7.15
3	Ion release from NiTi orthodontic wires in artificial saliva with various acidities (Huang et al., 2003)	Static immersion test for 1-28 days, AAS	NiTi	Modofoed Fusayama artificial saliva	-		2.5-6.25
4	Comparison of metal release from various metallic biomaterials in vitro (Okazaki & Gotoh, 2005)	Ion release by an immersion test for 7 days	316L,Co–Cr–Mo, Ti grade 2, Ti–6Al–4V, Ti–6Al–7Nb & Ti–15Zr–4Nb–4Ta	α-medium,PBS, calf serum, 0.9% NaCl, artificial saliva,1.2 mass% l-cysteine,1 mass% lactic acid and 0.01 mass% HCl	calf serum		
6	Electrochemical study of Type 304 and 316L stainless steels in simulated body fluids and cell cultures (Tang et al., 2006)	OCP, PD, LPR	304 and 316L	Hank's solution & MEM	fetal bovine serum	10%	-
7	Degradation behavior of metallic biomaterials for degradable stent (Fiset et al., 2007)	PD, static (168 days) and dynamic immersion	Mg, pure Fe, Fe-35Mn	Hank's solution	-		7.4
8	Corrosion resistance measurements of dental alloys, are they correlated? (Al-Hity et al., 2007)	A 7-day immersion test, ICP-AES, LPR	Alloys of gold and palladium, Co-Cr and Ni-Cr alloys	Fusayama	-		2.3
9	metal release from stainless steel, CoCrMo and Ni-Ti alloys in vascular implant (Okazaki & Gotoh, 2008)	A 7-day immersion test, XPS, ICP-MS	316L, (0.12C) and (0.06C) Co-Cr-Mo-Ni-Fe, Ti-Ni alloys		Fetal bovine serum, Calf serum	0.27 g L^{-1}, and 100%	
10	The behavior of pure titanium in albumin solution (Ionitaa et al., 2008)	immersed for 10 days, FTIR, UV-VIS-NIR spectrometer	pure titanium	PBS	BSA	10 wt%	7.4
11	Corrosion behavior of NiTi alloy in fetal serum (Hang et al., 2010)	OCP, EIS, SEM, XPS, ICP (immersed for 200 hours)	NiTi	Fetal bovine serum, PBS	Fetal bovine serum	100%	7.4

Table 2-9: (Cont'd) List of immersion corrosion studies in presence of BSA along with the experimental techniques, materials, background solution, protein and concentrations, and pH range

#	Journal's title	Experimental technique	Materials' type	Background sol.	Protein	Protein conc.	PH
12	Effects of alloying elements (Mn, Co, Al, W, Sn, B, C and S) on biodegradability and in vitro biocompatibility of pure iron (B. Liu & Zheng, 2011)	Static (3, 10, 30, 90, 180 days) and dynamic immersion tests, ICP-AES	Pure Fe, Fe-(Mn, Co, Al, W, B, C, S)	Hank's solution	-		2.3 and 5.3
13	Influence of albumin and inorganic ions on electrochemical corrosion behavior of plasma electrolytic oxidation coated magnesium for surgical implants (Wan et al., 2013)	Immersed for 14 days, SEM and equipped energy dispersive X-ray spectroscopy (EDX)	Pure magnesium	0.9 wt.% NaCl and PBS	BSA	1 g L^{-1}	7.4
14	Growth of calcium phosphates on magnesium substrates for corrosion control in biomedical applications via immersion techniques (Shadanbaz et al., 2013)	Immersed for 7,21, and 28 days, SEM, EDX, weight loss measurements	Pure magnesium coated with CaP	physiological buffers, Earles balanced salt solution, minimum essential media, and minimum essential media	BSA	40 g L^{-1} to mimic blood plasma level	7.4

Table 2-10 : List of immersion corrosion studies in presence of HSA along with the experimental techniques, materials, background solution, protein and concentrations, and pH range

#	Journal's title	Experimental technique	Materials' type	Background sol.	Protein	Protein conc.	Immersion period	PH
1	Isolation of serum protein organometallic corrosion products from 316LSS and HS-21 in vitro and in vivo (Woodman et al., 1984)	Gel chromatography on cross-linked dextran (G-200) & AAS	316L and HS-21		HSA		5 days	
2	Adsorption of human serum albumin (HSA) onto colloidal TiO2 particles, Part I (Oliva et al., 2003)	Electrophoretic mobility measurements	Titanium dioxide (TiO_2)	different concentrations of NaCl (1×10^{-3} or 1×10^{-1} M)	HSA	0.24 g L^{-1}	5 and 12 hours	range 3.7–8.0
3	Interfacial kinetics of titanium- and cobalt-based implant alloys in human serum: Metal release and biofilm formation (Hallab et al., 2003)	AAS	0.5 mL of spherical particles of CoCrMo, Ti-6Al-4V, cpTi		HSA		0, 0.5, 2, 8, 24, 72, and 168 hours.	-
4	The Entrapment of Corrosion Products from CoCr Implant Alloys in the Deposits of Calcium Phosphate: A Comparison of Serum, Synovial Fluid, Albumin, EDTA, and Water (Lewis et al., 2006)	XPS and Time-of-Flight Secondary Ion Mass Spectroscopy (ToF-SIMS)	CoCrMo alloy		HSA		1, 6, and 24 h and 5 days	7.4-7.8

In many corrosion studies, BSA has been used instead of HSA to investigate the effect of protein in simulated human body environments. In this thesis, we are interested in determining the corrosion behavior of 316L, CoCrMo and Ti-6Al-4V alloys in BSA and HSA solutions.

2.6 Bovine serum albumin versus human serum albumin

BSA and HSA are homologous proteins because of similar positions of cystine; however, HSA and BSA contain 585 and 583 amino acid residues, respectively (Hirayama et al., 1990). In addition, BSA has two tryptophan moieties (Trp 135 and Trp 214) located in subdomains IA and IIA, whereas HSA contains one tryptophan (Trp 214) in subdomain IIA (Carter et al., 1994). These structural differences can influence the affinities of human and animal serum for binding to chemicals; for example, HSA has a higher affinity to bind to $Cr_2O_7^{2-}$ compared to BSA (Zhang et al., 2011). The difference of BSA and HSA adsorption on negatively charged hydrophilic chromium metal has been studied by Lundin *et al.* (Lundin et al., 2011). The protein adsorption is measured by employing quartz crystal microbalance-dissipation monitoring (QCM-D) in PBS solutions (Figure 2-7). Relatively stable plateaus were obtained for BSA and HSA which indicated that the structure of these proteins did not change after adsorption. In addition, low adsorption due to a strong protein-surface binding was reported for BSA and HSA (Lundin et al., 2011). However, the amount of BSA adsorbed on the surface of chromium is different from that of HSA depending on exposure time. The isoelectric point of BSA and HSA are 4.2-4.8 (Moriyama et al., 1996; Lee & Ruckenstein, 1988) and 5.2 -6.6

(Moriyama et al., 1996), respectively. This could possibly result in different electrochemical corrosion behaviors of metallic biomaterials in HSA compared to electrochemical corrosion behaviors of those materials in BSA solutions.

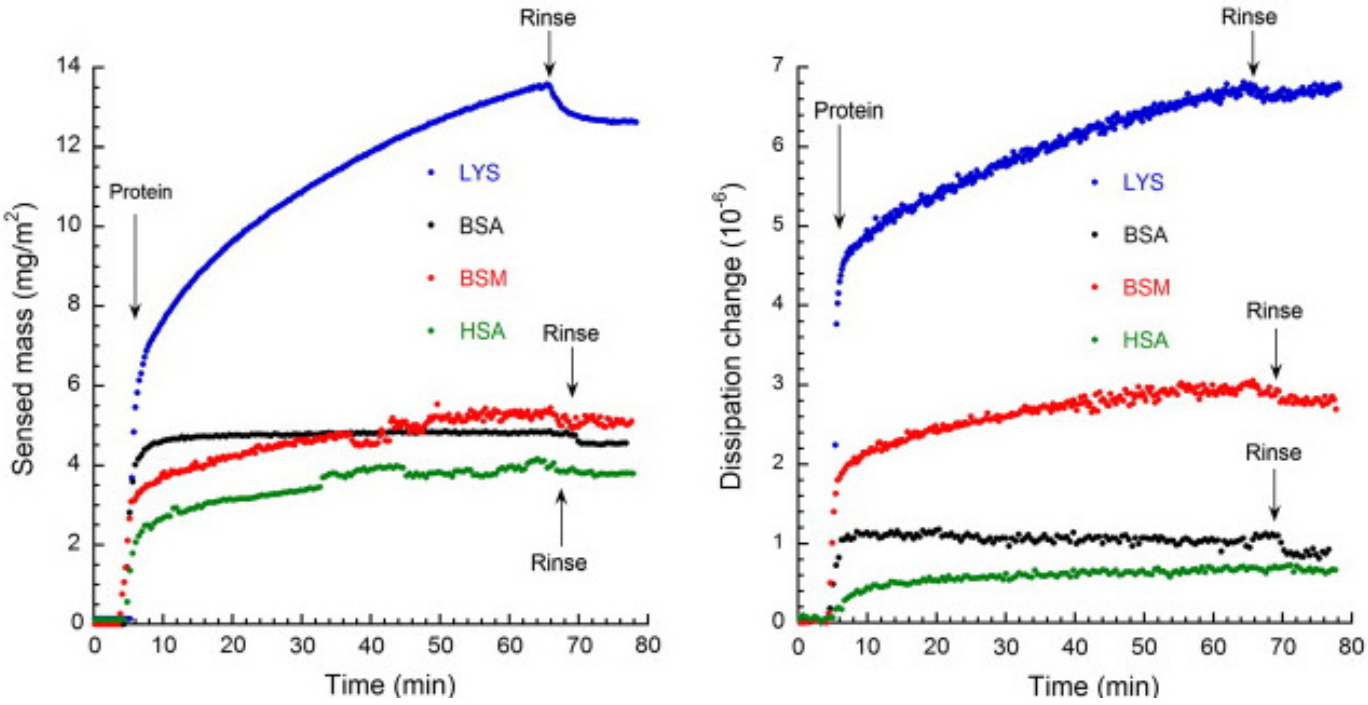

Figure 2-7 : The QCM sensed mass, according to Voigt (left), and change in energy dissipation (right) for LYS, BSA, HSA, and BSM adsorbed on chromium metal QCM surfaces from 1 g/L protein solutions in a PBS buffer at a pH of 7.4 (Lundin et al., 2011)

In a study done by Zhao *et al.* (Zhao et al., 2007), the interaction of BSA and HSA with Camptothecin, an anti-cancer drug have been compared by using the cyclic voltammetry method on a pyrolytic graphite electrode. The cathodic peak observed in Camptothecin solutions was diminished upon addition of HSA while this drop was not observed in the

solution containing BSA. The camptothecin peak current versus the addition of different volumes of HSA/BSA in the solutions is shown in Figure 2-8.

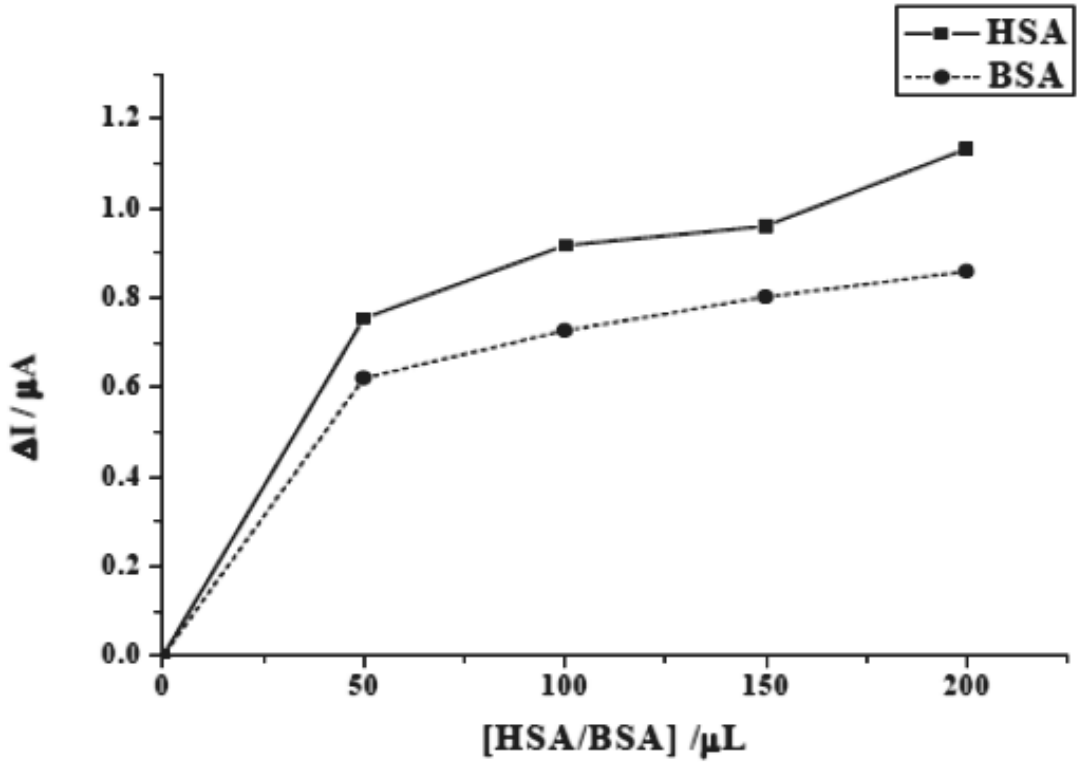

Figure 2-8 : Plot of the decrease of the camptothecin peak current versus the addition of different volume of HSA/BSA in the solutions (Zhao et al., 2007)

The author concluded that the interaction of HSA with Camptothecin forms a non-electrochemical complex which blocks electron transfer between the working electrode and the solution whereas this behavior was not observed for BSA.

2.7 Summary

The last 20 years of corrosion studies involving metallic biomaterials have been reviewed to indicate the novelty of this research study (Table 2-7, Table 2-8, Table 2-9 and Table 2-10). To the best of our knowledge, HSA has been used in only five electrochemical corrosion studies (Table 2-8), and only four immersion corrosion studies (Table 2-10). Some of these studies guided us to make a better plan for our research. For instance, the corrosion behavior of Ti-6Al-4V in PBS solutions containing 0.1 and 1 g L^{-1} bovine calf serum and BSA has been investigated by cyclic polarization tests (Khan et al., 1999). Inspired by this study, we employed other techniques, such as EIS and LPR, to understand BSA and HSA adsorption and oxide layer growth mechanism and to measure an instantaneous corrosion rate. These techniques were used in other studies in which the background solutions, the concentration of human serum, and the working electrodes were different. The examples of these studies are the adsorption behavior of human serum in 0.1M phosphate buffer in the presence of equimolar (5 × 10−4 M) ferricyanide + ferrocyanide ions on glassy carbon investigated by EIS in 0 and 1 g L^{-1} human serum (Marie de Ficquelmont-Loïzos et al., 1997) or the electrochemical corrosion study of copper in simulated uterine and human serum (0.5 g L^{-1}) (Cao et al., 2011).

The potentiodynamic polarization (PDP) and EIS measurements have been conducted to study the adsorption of BSA on CoCrMo surface in 0.14M NaCl having BSA concentrations of 5, 20, 50, and 500 mg L^{-1} (Valero Vidal et al., 2010). In our study, the presence of phosphate

in the PBS solutions helped us to investigate the effect of phosphate ions on the corrosion behavior of the selected alloys. The most important inorganic constituents of biological hard tissues are calcium and phosphate. The precipitation of phosphate on the samples' surface could alter the oxide layer composition and corrosion behavior of the specimen. In most of the corrosion studies of biomaterials, the concentration of protein is limited to a low concentration of BSA and HSA (e.g. 1 g L^{-1}). However, a wide range of protein concentrations is selected to provide a more realistic environment of a human body which has been suggested by Kuhn *et al.* (Kuhn et al., 1986). The protein concentration is defined according to the protein contents of human's interstitial fluid (Kuhn et al., 1986) in our study.

Furthermore, the purpose of many recent static immersion corrosion studies has mostly been focused on examining the surface morphology of the metallic biomaterials. Weight loss of biomaterials has been rarely identified by static immersion corrosion tests in the presence of protein. Ion release of metallic biomaterials is also investigated in a few research studies. Among these studies is Okazaki and Gotoh's measured ion release of various biomaterials. Their approach (Okazaki & Gotoh, 2005) is similar to our planned method but differs in the test duration, protein type and background solutions. The ion release of 316L and HS-21 (Woodman et al., 1984) and high carbon CoCr (Lewis et al., 2006) alloys were also analyzed by AAS up to five days of incubation in human serum. In our static immersion tests, the specimens were immersed in PBS solutions containing 0 to 4 g L^{-1} BSA or HSA for 7, 14, and 22 weeks. The extended time periods enable us to provide a more reliable data because corrosion is not a linear function of time. The amount of ion released into the PBS-BSA and

PBS-HSA solutions was measured by ICP-OES analysis for a better accuracy. Finally, these results were combined with the surface chemical composition analysis for different BSA or HSA concentrations which have not been analyzed in other studies.

Chapter 3: Objectives

Human body is a dynamic environment that contains organic and inorganic substances such as proteins, sodium, calcium, chloride, and phosphate. Presence of these inorganic and organic substances in *In-Vitro* corrosion study is necessary to generate a more realistic human body environment. Researchers added animal serum albumin (e.g. BSA) to Hank's, Ringer's, and PBS solutions to investigate the effect of organic and inorganic elements in *In-Vitro* corrosion studies (Table 2-7 and Table 2-8). Albumin is the most abundant element of blood plasma which binds to hormones, fatty acids, drugs and metal ions (Carter & Ho 1994; Carter et al. 1994). In fact, bovine and human albumins have N-terminal sequences which could bind to positively charged ions release from metallic biomaterials (Bal et al. 1998). This interaction could change corrosion behaviour of metallic biomaterials.

Although corrosion behaviour of metallic biomaterials has been investigated in bovine serum albumin solutions, to the best of our knowledge, HSA has been used in only a few corrosion studies (Table 2-7, Table 2-8, Table 2-9 and Table 2-10). A study on corrosion behavior of metallic biomaterials in the presence of HSA was purposed after carefully investigated the previous corrosion studies. This research study includes:

- Corrosion resistance evaluation of metallic biomaterials in presence of phosphate ions and various BSA and HSA concentrations in a wide range (0-4 g L^{-1})
- Presence of human serum albumin in electrochemical and immersion corrosion studies of different biomaterials

- Weight loss measurement, ion release and surface composition analysis of metallic biomaterials after long-term immersion (~5 months) experiments

PBS has been selected as a background solution because it contains phosphate. Phosphate could precipitate on the samples' surface, alter the oxide layer composition, and affect the corrosion behavior of the specimen. One of the most important inorganic constituents of biological hard tissues is phosphate.

Our literature review shows that most researchers have experimented protein concentrations of up to 1 g L^{-1}. Kuhn *et al.* (Kuhn et al., 1986) has suggested that less than 6 g L^{-1} protein concentration is required in vitro corrosion studies to properly simulate a realistic body fluid. A variety of ranges of HSA concentrations in PBS solutions (0, 0.2, 0.4, 1.2, 2, and 4 g L^{-1}) is also used. Immediately after surgery, the gap between the implant and the native tissue fills with biofluids which contain protein (Kasemo & Lausmaa, 1994). The clearance between the implant and tissue gradually shrinks by the adsorption of protein and growth of the oxide layer. This will change the protein concentrations of the biofluids. This physiological body response may alter the metal dissolution rate and the corrosion behavior of metallic bio-implants.

This research work involves electrochemical and non-electrochemical corrosion experiments to investigate cathodic and anodic behavior, protein adsorption, oxide layer growth, ion release, surface morphology and chemistry and weight loss of the selected alloys. Therefore the objectives of this research study are:

- To have a better understanding of the role of protein on corrosion behaviour of metallic biomaterials
- To investigate the effect of a human body's physiological response (protein concentration alternations after surgeries) on corrosion of the selected materials
- To investigate the long-term effect of human protein concentration variations on weight loss, ion release, and surface composition of the biomaterials
- To compare corrosion behaviour of common biomaterials in simulated human protein environments with simulated animal protein environments

In this research study, we found that the metal dissolution rate of alloying elements from Ti-6Al-4V alloy is independent of alloying composition in which vanadium dissolution rate was almost the same as titanium. The presence of BSA and HSA increased the stability of the 316L and Co-28Cr-6Mo passive film. However, BSA and HSA reduced the barrier layer stability of the Ti-6Al-4V in a certain concentration range. In addition, type of protein could influence on the surface composition of metallic biomaterials. For example, the 316L contained Fe_2O_3, MoO_2, and MoO_3 in HSA solutions. They were absent in surface composition of 316L formed in BSA solutions. Finally, BSA is a stronger cathodic inhibitor than HSA on surface of 316L and CoCrMo alloys; therefore, rate of release of iron and cobalt are faster in presence of HSA.

The outcome of this study could be used to explain severe evidence of corrosion and ion release of metallic implants observed in vivo studies, modify the performance of metallic implants and also to introduce new materials which could stand the inevitable body

responses after surgery. For instance, new titanium base alloy with a biocompatible element such as niobium instead of vanadium is suggested because vanadium release is detrimental to the human body. This may increase the life time of the orthopedic implants and reduce the cost of necessitates revision surgeries.

Chapter 4: Approach and methodology

The aim of these experiments is to compare the corrosion behavior of three metallic bio-implants in the presence of various BSA and HSA concentrations with advanced electrochemical and immersion corrosion tests. The advanced electrochemical techniques employed in this study are OCP, PDP, EIS, LPR, and cyclic voltammetry measurements. In addition to electrochemical corrosion experiments, long term static immersion corrosion was conducted to measure weight loss, analyze oxide chemical composition by XPS and detect the amount of the ion released by ICP-optical emission spectroscopy (OES). The details of the procedure for electrochemical and immersion corrosion experiments in BSA and HSA solutions are described below.

4.1 Materials

4.1.1 Chemical composition

The samples were prepared from solid rods of 316L (Goodfellow Cambridge Limited), Co-28Cr-6Mo (ATI Allvac Limited) and Ti-6Al-4V (Goodfellow Cambridge Limited) with diameters of 1, 2.5, and 1.2 cm, respectively. The chemical composition of 316L, Co-28Cr-6Mo, and Ti-6Al-4V is specified in the ASTM standards F139, F1537, and F1472, respectively. In addition, the sample's chemical compositions were determined by sending them to international plasma labs (IPL) to be analyzed by ICP-MS. The chemical compositions of 316L, CoCrMo, and Ti-6Al-4V alloys defined in ASTMs and measured by ICP-MS are summarized in Table 4-1.

Table 4-1 : Chemical composition of 316L, Co-28Cr-6Mo, and Ti-6Al-4V from ASTM standards and by ICP-MS analysis

		Composition (wt %)									
		C	Fe	Cr	Ni	Mo	Mg	Co	Ti	Al	V
316L	ASTM	0.03 Max	Bulk	17-19	13-15	2.3-3	2.0 Max				
	ICP	0.03	65	18	13	2.9					
Co-28Cr-6Mo	ASTM	0.05-0.35	0.75 Max	26-30	1 Max	5-7		Bulk			
	ICP	0.06	0.81	26		5.4		67.8			
Ti-6Al-4V	ASTM	0.08 Max	0.30 Max						Bulk	5.5-6.8	3.5-4.5
	ICP	0	0.33						90	6.0	4.0

The amount of iron detected by ICP analysis on the composition of Co-28Cr-6Mo and Ti-6Al-4V alloys is slightly higher than the ASTM standard. The accuracy of Fe isotopic analyses depends on some parameters including incomplete separation of Fe from matrix elements and the presence of direct isobars from $^{54}Cr^{+}$ on $^{54}Fe^{+}$ and $^{58}Ni^{+}$ on $^{58}Fe^{+}$ (Dauphas et al., 2009). This small deviation is negligible since both Cr and Ni are present in the chemical composition of Co-28Cr-6Mo and Ti-4Al-4V alloys.

4.1.2 Metallography

Discs of 316L, Co-28Cr-6Mo, and Ti-6Al-4V alloys were mechanically polished with 6 and 1 μm alumina powder. The polished samples were ultrasonically cleaned in a soap solution for 5 minutes and in deionized water for 5 minutes, rinsed with ethanol, and dried in hot air. The microstructure of 316L was revealed (Figure 4-1) by etching the specimen in a glyceregia reagent (3 parts glycerine, 2 parts 37% hydrochloric acid (HCl), 1 part 68% nitric acid (HNO_3)).

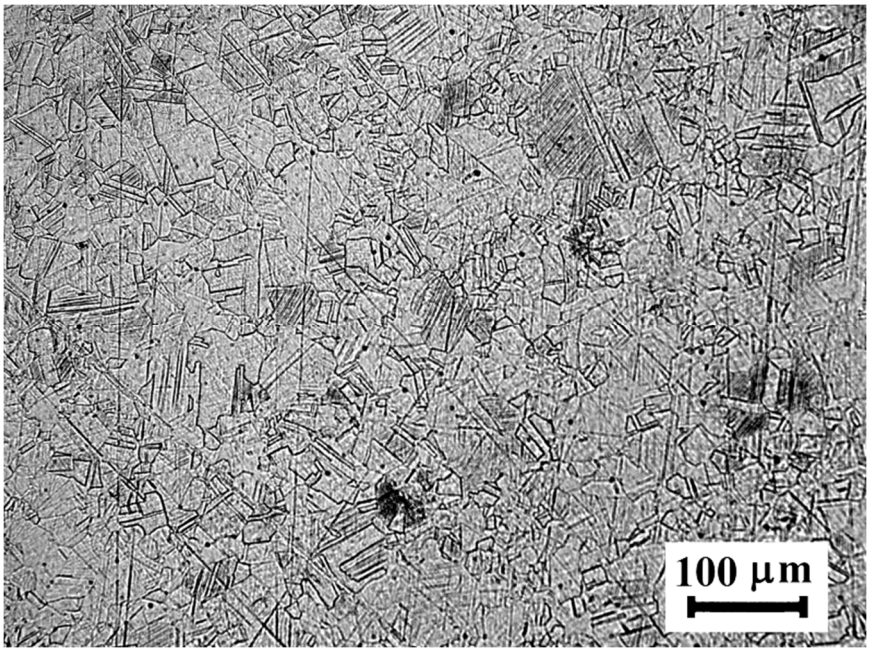

Figure 4-1 : An optical microstructure of 316L etched in glyceregia reagent

The grain size of the 316L was measured by the linear intersection method. The detail of this method is provided in (M.R. Louthan, 1986). The measured average grain size was 12 µm. Austenite and a small amount of ferrite was observed which was consistent with the Fraker *et al.* study (Fraker, 1987). Chromium carbide was not seen at grain boundaries, indicating that the alloy is not susceptible to grain-boundary attack.

The wrought Co-28Cr-6Mo sample was etched in a solution of 20 mL 37% hydrochloric acid (HCl) and 1 mL 30% vol. hydrogen peroxide (H_2O_2). The optical microstructure of Co-28Cr-6Mo is illustrated in Figure 4-2.

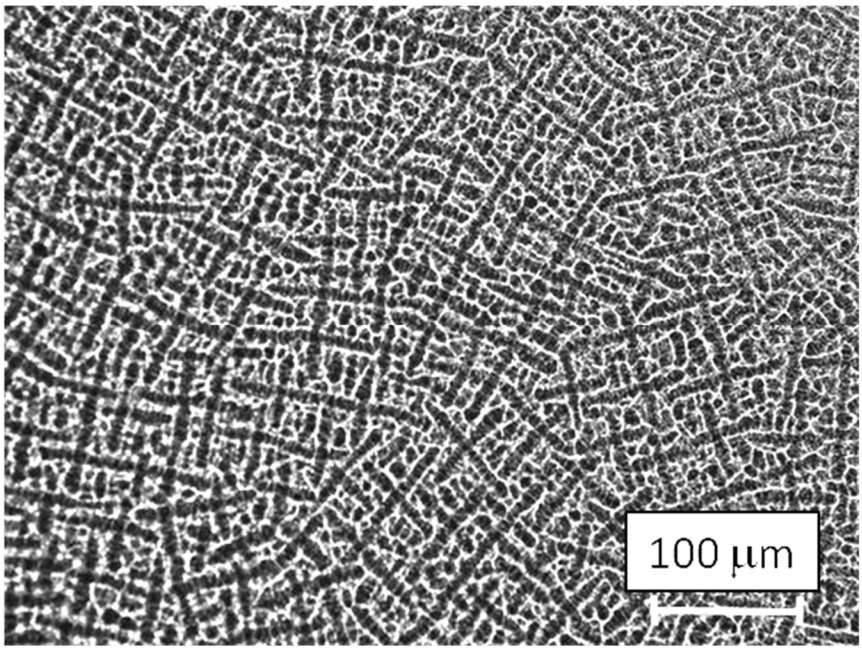

Figure 4-2 : An optical microstructure of Co-28Cr-6Mo etched with 40 mL hydrochloric acid (HCl) and 2 mL Hydrogen peroxide (H_2O_2)

The optical microstructure of this alloy contains the interdendritic primary $M_{23}C_6$ carbides (chromium-rich) in a face-centered cubic (FCC) CoCrMo solid-solution matrix (Klarstrom et al., 2004). The formation of this phase in the structure of Co-28Cr-6Mo depends on the carbon content, alloy composition, and the thermal processing conditions (Mineta et al., 2010).

In Figure 4-3, an SEM image from the surface structure of Ti-6Al-4V is illustrated. The alloy was etched in a solution of 100 mL water, 2 mL 69% nitric acid (HNO_3), and 1 mL 49% hydrofluoric acid (HF).

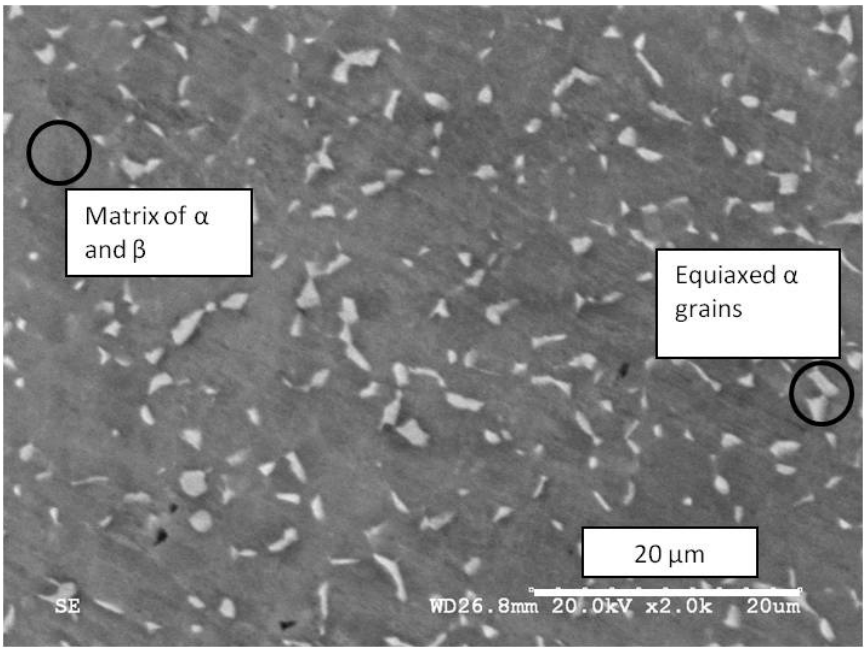

Figure 4-3 : An optical microstructure of Ti-6Al-4V etched with 100 mL water, 2 mL nitric acid (HNO_3), and 1 mL hydrofluoric acid (HF)

The elongated alpha grains (bright) in a matrix of transformed beta phase were observed. The alpha phase has a hexagonal close-packed (HCP) structure and the beta phase has a body-centered cubic (BCC) structure. Aluminium and oxygen are alpha stabilizers, while chromium, vanadium, and iron are beta stabilizers (Fraker, 1995).

4.1.3 Sample preparation for electrochemical corrosion tests

The rods of 316L, CoCrMo, and Ti-6Al-4V were cut into 4 mm thick discs by electromechanical cutting wire in the UBC Materials Engineering department machine shop. To make an electrical connection, a copper wire was bound to a disc by employing a conductive silver epoxy. The discs were then mounted in a cold-curing epoxy resin (LECO), mechanically polished with 6 µm alumina powder, and ultrasonically cleaned for 2 minutes

in a soap solution and in deionized water for 5 minutes. Finally, the samples were rinsed with ethanol, and dried in hot air before conducting electrochemical corrosion experiments.

4.1.4 Sample preparation for immersion corrosion experiments

135 Plates of 316L, Co-28Cr-6Mo, and Ti-6Al-4V alloys, 45 plates from each alloy, with dimensions of 20 X 40 X 1 mm^3 were cut from sheets of 316L and Ti-6Al-4V alloys and a rod of Co-28Cr-6Mo. A one-millimeter-diameter hole was drilled at the top center of the width of the plates as illustrated in Figure 4-4.

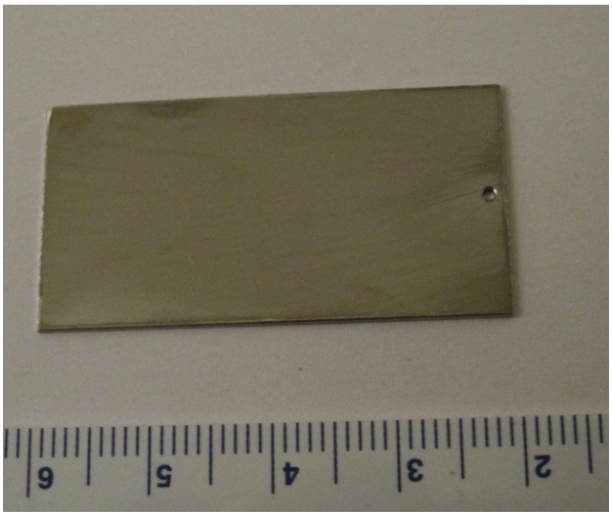

Figure 4-4 : A plate of 316L for a static immersion test

The samples were mechanically polished with 6 μm alumina powder, and ultrasonically cleaned in a soap solution, deionized water, and ethanol each for 5 minutes. Finally, the samples were dried in hot air. The samples' weight were measured by a SCIENTECH ZSA 120 scale and recorded before immersing the samples in the solutions.

4.2 Electrolyte

The corrosion behavior of 316L, Co-28Cr-6Mo, and Ti-6Al-4V alloys was evaluated in solutions of PBS, as a background solution, containing various concentrations of BSA and HSA. BSA and HSA concentrations used in this study varied from 0 to 4 g L^{-1}. The range of the protein concentration in PBS solutions was chosen based on the protein concentration of human interstitial fluid (Kuhn et al., 1986). The pH of the electrolytes was 7.4-7.8 at 37°C and the tests were conducted in aerated environments, except for the cyclic voltammetry experiments.

4.2.1 Phosphate buffered saline

The chemical composition of the PBS solution is selected from ASTM standards (F2129) and is indicated in Table 4-2. PBS solutions were prepared by carefully weighing the chemical powders in a weight boat, pouring them into an empty 1-liter volumetric flask, and diluting it by deionized water until the water meniscus reached the mark on the flask.

Table 4-2 : Chemical composition of PBS solution

Chemical	Composition (g L^{-1})
NaCl	8.00
KCl	0.200
Na_2HPO_4	1.15
KH_2PO_4	0.200

Simulated boilogical fluid of PBS was chosen because it contains phosphate ions. One of the most important minerals of biological hard tissues is phosphate. The generation of new bone

requires the presence of phosphate (Penido & Alon, 2012). Therefore, phosphate could have a role in the corrosion behavior of metallic implants. For example, phosphate can precipitate on the samples' surface and can alter the oxide layer composition (Hodgson et al., 2004).

4.2.2 Bovine serum albumin

The last updated molecular weight of bovine serum albumin is reported 66,430 gr mol^{-1} (Hirayama et al., 1990; Laurell et al., 1975). BSA is a single polypeptide chain consisting of about 583 amino acid residues. It contains 17 disulfide bridges and 1 sulfhydryl group at the pH range of 5-7 (Hirayama et al., 1990; Laurell et al., 1975). Further structural and chemical information is provided in (Carter & Ho, 1994; Weijers, 1977).

BSA was provided as lyophilized powder (≥98% agarose gel electrophoresis) from Sigma-Aldrich Inc.. The selected BSA concentrations used in this study were 0.2, 0.4, 1.2, 2, and 4 g L^{-1}. The solutions of PBS and BSA were made by weighing BSA powder, adding it to an empty 1-liter volumetric flask along with PBS chemicals, and diluting it by ionized water until the water meniscus reached the mark on the flask.

4.2.3 Human serum albumin

One of the major soluble protein constituents of the circulatory system is HSA, which is involved in many physiological functions. It is also in charge of controlling colloidal osmotic blood pressure and mineral transportation in regulatory processes (Herve et al., 1994). HSA has 585 amino acids where its amino acids sequence includes 17 disulphide bridges, one free sulfhydryl (SH^-), and a single tryptophan ($C_{11}H_{12}N_2O_2$) (Carter & Ho, 1994; Carter et al., 1994;

He & Carter, 1992). The primary structure of HSA contains three homologous domains (named I, II, and III) and each domain has two separate helical subdomains (named A and B) (Fasano et al., 2005). The only tryptophan of HSA is located in subdomain IIA which is a hydrophobic fold (Moriyama et al., 1996).

BSA and HSA are homologous proteins because of similar position of cystine; however, HSA and BSA contain 585 and 583 amino acid residues, respectively (Hirayama et al., 1990). In addition, BSA has two tryptophan moieties ($C_{11}H_{12}N_2O_2$) located in subdomains IA and IIA whereas HSA contains one tryptophan in subdomain IIA (Carter et al., 1994). These structural differences can influence the affinities of human and animal serum for binding to chemicals; for example, HSA has a higher affinity to bind to $Cr_2O_7^{2-}$ compared to BSA (Zhang et al., 2011).

HSA was provided from Sigma-Aldrich. The selected HSA concentrations used in this study were similar to the BSA concentrations (0.2, 0.4, 1.2, 2, and 4 g L^{-1}). The HSA-PBS solutions were prepared by weighing HSA powder and the chemical component of PBS in weight boats, filling it to an empty 1-liter volumetric flask, and diluting it by deionized water until the water meniscus reached the mark on the flask. The range of the protein concentration in PBS solutions was chosen based on the protein concentration of human interstitial fluid (Kuhn et al., 1986). The pH of the PBS-HAS solution was 7.4 and the addition of protein did not change the solutions pH considerably.

4.3 Electrochemical corrosion study

Electrochemical measurements were performed with Princeton Applied Research (PAR) VersaStat 4 potentiostat/galvanostat. This device is capable of measuring direct and alternating current. The electrochemical corrosion tests were carried out using a conventional three-electrode electrochemical cell. The samples were placed in a water-jacketed cell as a working electrode. The water-jacketed cell was connected to a heater (Cole-Parmer) to maintain a temperature of 37°C. A graphite rod and an Ag/AgCl ($[Cl^-]$ = 4 M) electrode was used as a counter electrode and a reference electrode, respectively. Each electrochemical corrosion test was repeated at least three times. The reproducibility of the results are shown in Figure 7-2, Figure 7-5, Figure 7-7, and Figure 7-10. The parameters that were applied for (I) OCP, (II) PD, (III) EIS, (IV) LPR, (V) potentiostatic polarization, and (VI) cyclic voltammetry experiments are described below:

I. OCP measurements were carried out for one hour in order to monitor the potential-time behavior of the electrodes in PBS solutions with various BSA and HSA concentrations.
II. PDP tests were conducted in a potential range of -0.25 V vs. OCP to 1 V vs. Ag/AgCl (in BSA solutions) and 0.6 V vs. Ag/AgCl (in HSA solution) with a scan rate of 0.167 mV s^{-1} after immersing the samples in solutions for one hour.
III. The corrosion mechanism of the passive film/electrolyte interface was investigated by EIS. The measurements were performed with the amplitude of 10 mV at OCP in the frequency range of 0.01 to 10,000 Hz and a sampling rate

of 10 points per decade. In this frequency range, we were able to obtain stable EIS results.

IV. Polarization resistance of the samples was measured at ±50 mV vs. OCP with a potential sweep rate of 0.167 mV s^{-1} after immersing the specimens in the electrolyte for 1 hour before starting the test.

V. A potentiostatic polarization experiment was conducted to prepare CoCrMo specimens for XPS analysis. The potentials and protein concentration were chosen based on the potentiodynamic polarization results.

VI. Cyclic voltammetry experiments were conducted to investigate the adsorption behavior of protein on the surface of samples. Prior to starting the cyclic voltammetry tests, the PBS solution was purged by argon (Praxair Product Inc.) for 1 hour to carry out the measurements in de-aerated solutions. The protein solution was prepared in a separated cell which was connected to the electrochemical corrosion cell to maintain similar environmental conditions (temperature and oxygen content of the solutions) between the two cells and to add the protein solution to the PBS solution without exposing the solutions to the outside environment of the cells. The protein solutions were added to the PBS solutions right after measuring the response of the electrode in protein-free solutions. The solution pH slightly dropped to 7.2 after purging. In protein-free solutions, a large potential region (-1.5 to 2 V vs. Ag/AgCl) was examined to find current responses of the process occurring at the electrode

surfaces where the responses were reproducible with continuous cycling. Since the responses depend on the electrode materials, these potential regions were determined at (V vs. Ag/AgCl) -1.1 to -0.1 for 316L, at -1.4 to 0 for CoCrMo, and at -1.3 to -0.5 for Ti-6Al-4V alloys. The formation of oxide layers on 316L, CoCrMo, and Ti-6Al-4V alloys were determined in the anodic region where the current peak gradually decreased in each subsequent cycle implying the growth of oxide layers. This gradual change of charge became stable and reproducible after a prolonged cyclization of the electrodes. To ensure high reproducibility of the electrodes surface, 200 cycles with a scan rate of 300 mV S^{-1} were employed before the addition of protein. The same scan rate was applied after the addition of protein. The protein concentration of 4 g L^{-1} HSA and BSA was chosen based on the OCP difference of the specimen in the aerated PBS-BSA and PBS-HSA solutions with protein-free solutions. The OCP difference reached to the highest values when protein concentration was 4 g L^{-1}. The OCP of 316L, Co-28Cr-6Mo, and Ti-6Al-4V alloys in either PBS-BSA or PBS-HSA are shown in Figure 5-1.

The long term effect of protein on the corrosion behavior of 316L, Co-28Cr-6Mo, and Ti-6Al-4V alloys was evaluated by static immersion corrosion tests. Immersion tests were performed to identify the real time corrosion rates, ion release, and surface oxide layer compositions of the selected materials.

Each plate was hung by fluorocarbon plastic strings in one beaker and fully immersed in 200 mL of PBS solution containing protein concentrations of 0, 0.2, 0.4, 2, and 4 g L^{-1}. The beakers and samples were cleaned according to ASTM standard D5245-92. All the beakers were then placed inside a 37 °C water bath where the temperature was monitored by water circulator Haake C1 with accuracy of 0.1 °C. The specimens were kept in the water bath for 8, 14, and 22 weeks. Three sets of experiments were performed for each protein concentration. In order to measure corrosion rates, the samples were weighed with a SCIENTECH ZSA 120 scale with an accuracy of 0.1 mg after completing the immersion experiment.

4.4 Solution characterization

The plates were removed from the solution container at the end of each immersion time. Solutions were then stirred thoroughly and a 50 mL-solution was stored in sterilized polypropylene test tubes and the rest was kept as back-up solutions. The protein content of the solution was digested prior to the ICP-OES analysis. The detailed acid digestion procedure is explained in section 4.4.1. The ICP-OES analysis was accomplished by VARIAN 725-ES to detect the amount of metal release from the specimens after the immersion tests. The ICP-OES analyzer was calibrated by multi-element ICP-AES & MS standard (SCP SCIENCE, 100 μg mL^{-1}). The standard solution was diluted to six different concentrations by digested BSA/HSA and PBS solutions to establish working curves for instrument calibration. Therefore, concentrations were given directly by the instrument computer program (ICP Expert II).

4.4.1 Protein digestion procedure

The protein content of the solution needs to be digested prior to the ICP-OES analysis because protein can precipitate under high pressure and temperature, which confines the detection limit of the system. The immersed solutions were heated on a hot plate in a beaker cleaned according to ASTM D5245-92. Heating continued until the solution volume decreased to nearly 1 mL and then 6 mL nitric acid (environmental grade, provided from Anachemia Science) was added. Again, the solution was evaporated under high temperature to 1 mL and 6 mL of hydrogen peroxide (*Trace*SELECT ≥ 30% RT) was added. When the solution's temperatures cooled down, deionized water was added up to the initial volume (50 mL).

4.5 Surface characterization

The surface oxide composition of CoCrMo alloys were studied in two potentials by using the potentiostatic polarization technique. Before the potentiostatic polarization test, the samples were polished using 6 μm diamond paste, ultrasonically cleaned in a soap solution and deionized water for 5 minutes, then rinsed once again with deionized water and dried in hot air. Three samples were prepared for XPS analysis. Two samples of CoCrMo were polarized for 2 hours at 0.007 and 0.250 V vs. Ag/AgCl in PBS solutions not containing BSA at 37 °C. The last CoCrMo sample was polarized for 2 hours at 0.250 V vs. Ag/AgCl in PBS solutions containing 4 g L^{-1} BSA at 37 °C. The long term effect of protein on chemical composition of oxide layers of 316L, CoCrMo and Ti-6Al-4V alloys after the immersion corrosion experiment was also studied by XPS analysis. To achieve this goal, specimens

immersed in 0, 0.2, and 4 g L^{-1} protein for 22 weeks. They were then gently rinsed by deionized water and dried in hot air. The samples were then placed inside a desiccator before XPS analysis. The XPS analysis results are presented in section 6.3 and 8.3.

The chemical composition of the oxide layer was analyzed by a Leybold MAX200 XPS spectrometer, using a monochromatic Mg Kα X-ray source and pass energies of 192 and 48 eV for survey and narrow scans, respectively. The reported binding energy is relative to the Fermi level. No sputtering or charge neutralization will be applied before starting the XPS analysis to keep the surface unattached. All samples were tested at a take-off angle of 90 ° with respect to the surface normal.

Chapter 5: Electrochemical corrosion of 316L, Co-28Cr-6Mo, and Ti-6Al-4V in phosphate-buffered saline solutions and in the presence of BSA

One of the goals of this study is to assess the corrosion performance of the 316L, CoCrMo and Ti-6Al-4V alloys in the presence of protein. Rapidly after implantation, proteins adsorb into the implants' surface right after the interaction of ions and small molecules from blood components (Kasemo & Lausmaa, 1986; Kasemo & Gold, 1999). The adsorption of proteins, known as active components of the blood, influences the surface free energy of the implant (Albrektsson et al., 1983; Kasemo & Gold, 1999; Rudee & Price, 1985). Proteins are negatively charged and metal ions are positively charged in the body's pH of 7.4. The interactions of metal ions with proteins generate colloidal organometallic complexes. These complexes could disturb local chemical equilibrium, reduce activation energy, and enhance the corrosion rate (Omanovic & Roscoe, 1999; Woodman et al., 1984). Therefore, protein adsorption could affect the electrochemical corrosion behavior of metallic biomaterials.

This study has been conducted in different protein concentrations employing advanced electrochemical corrosion techniques to investigate the kinetic of electrochemical reactions at implant-tissue interface as a function of protein concentrations. As a first step, the corrosion performance of 316L, Co-28Cr-6Mo, and Ti-6Al-4V alloys was evaluated in PBS solutions having different concentrations of animal serum albumin (BSA). The goals of *in-vitro* electrochemical experiments are to determine critical potentials and study corrosion phenomena in a short time and in a less aggressive environment.

5.1 OCP measurements

The final OCP values as a function of BSA concentration helps in interpreting the interactions of BSA with the passive film. Therefore, the steady-state OCP values after one hour of immersion in the PBS solutions as a function of BSA concentrations are displayed in Figure 5-1.

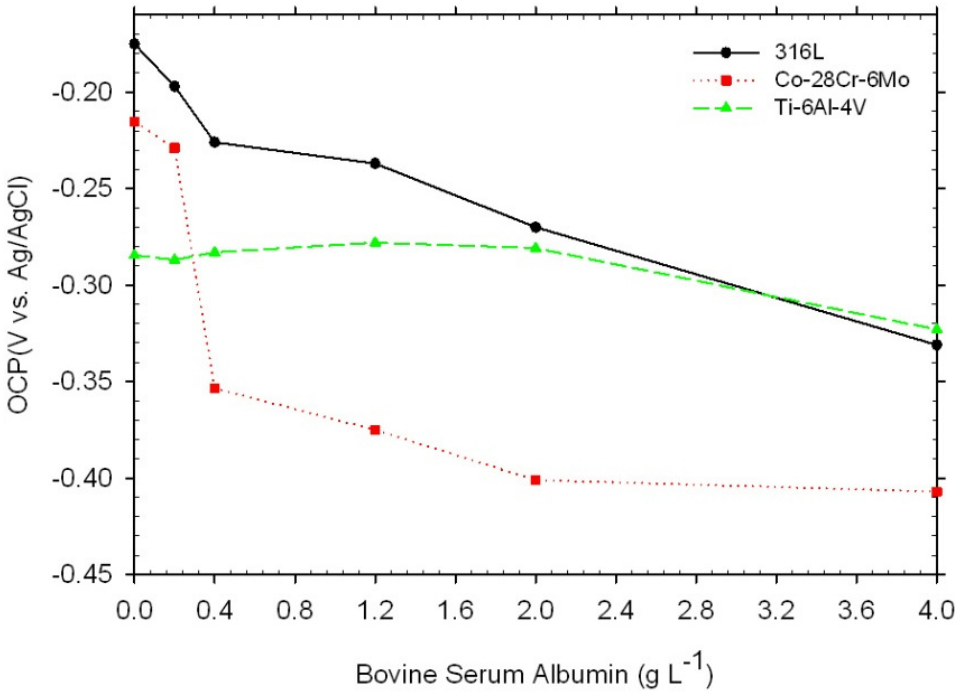

Figure 5-1 : Variation of OCP as a function of BSA concentration in aerated PBS solutions at 37°C and a pH of 7.4

It is shown that 316L became more active when BSA concentration increased. This can be explained by the presence of both phosphate and BSA, which decreased the potential of 316L. Vidal and Muñoz (Valero Vidal & Muñoz, 2008) also showed that when a BSA

concentration of 0.5 g L^{-1} was added to a PBS solution at 37 °C, the corrosion potential of 316L decreased. This shows that BSA interactions with the passive film resulted in lower OCP values. The other possibility could be the BSA inhibitive action on cathodic reactions, i.e. oxygen reduction and hydrogen evolution reactions. BSA is expected to block the cathodic sites on the sample and thus decrease the exchange current density of cathodic reactions (Tang et al., 2006). Therefore, BSA could act as a cathodic inhibitor at higher concentrations.

The OCP of the Co-28Cr-6Mo samples dropped as the BSA concentration was increased to 2 g L^{-1} and then reached a plateau at the concentration of 4 g L^{-1}. Hiromoto *et al.* investigated the corrosion behavior of CoCr alloys in Hank's solution, saline solution, and cell culture medium. They stated that the OCP values of Co-28Cr-6Mo alloy decreases due to cobalt dissolution processes and increases due to protein adsorption on the surface (Hiromoto et al., 2005). Therefore, the observed trend in OCP values can be explained by considering the competition between metal dissolution and formation of a diffusion barrier. At the lower concentrations, the dissolution processes are dominant, which causes the OCP to drop, while at higher concentrations, the dissolution and adsorption processes occur simultaneously and thus a plateau is observed.

The OCP of Ti-6Al-4V alloy was relatively constant in the PBS solutions with and without BSA, except for the BSA concentration of 4 g L^{-1}. Wassel and Embery showed that the number of segments per unit area of the sorbent surface is high at low BSA concentrations (Wassell & Embery, 1996). At low concentrations, slow structural rearrangements with sufficient

time and space are provided for the adsorbed protein to accommodate the surface, whereas at high BSA concentrations, protein collision is fast which reduces the time or room for achieving the optimized interactions between BSA and the oxide layer (Wassell & Embery, 1996). Therefore, the BSA binding is loose at 4 g L^{-1} BSA which results in the activation of the Ti-6Al-4V surface.

5.2 Potentiodynamic study

Figure 5-2 illustrates the potentiodynamic polarization behavior of 316L in a solution of PBS with different BSA concentrations at 37°C in aerated conditions.

The cathodic polarization branch shifted to a lower potential value when BSA concentration was increased. Tang *et al.* stated that the cathodic polarization behavior corresponds to the oxygen reduction, and BSA inhibits the oxygen reduction reaction by decreasing the number of active sites on the metal for reduction reactions (Tang et al., 2006). Furthermore, Stankovich and Bard studied the reduction of BSA in pH of 7.4 by cyclic voltammetry at the hanging mercury drop electrode (Stankovich & Bard, 1978). They reported that BSA is reduced at a potential range of -0.455 to -0.655 V vs. Ag/AgCl and current range of 3.7 to 7.5 μA cm^{-2} in BSA concentration of 1.38 g L^{-1}. It can then be concluded that one of the cathodic reactions within this potential range is a reduction of BSA. Therefore, the cathodic branch is likely the sum of the current from both the oxygen and BSA reduction reactions.

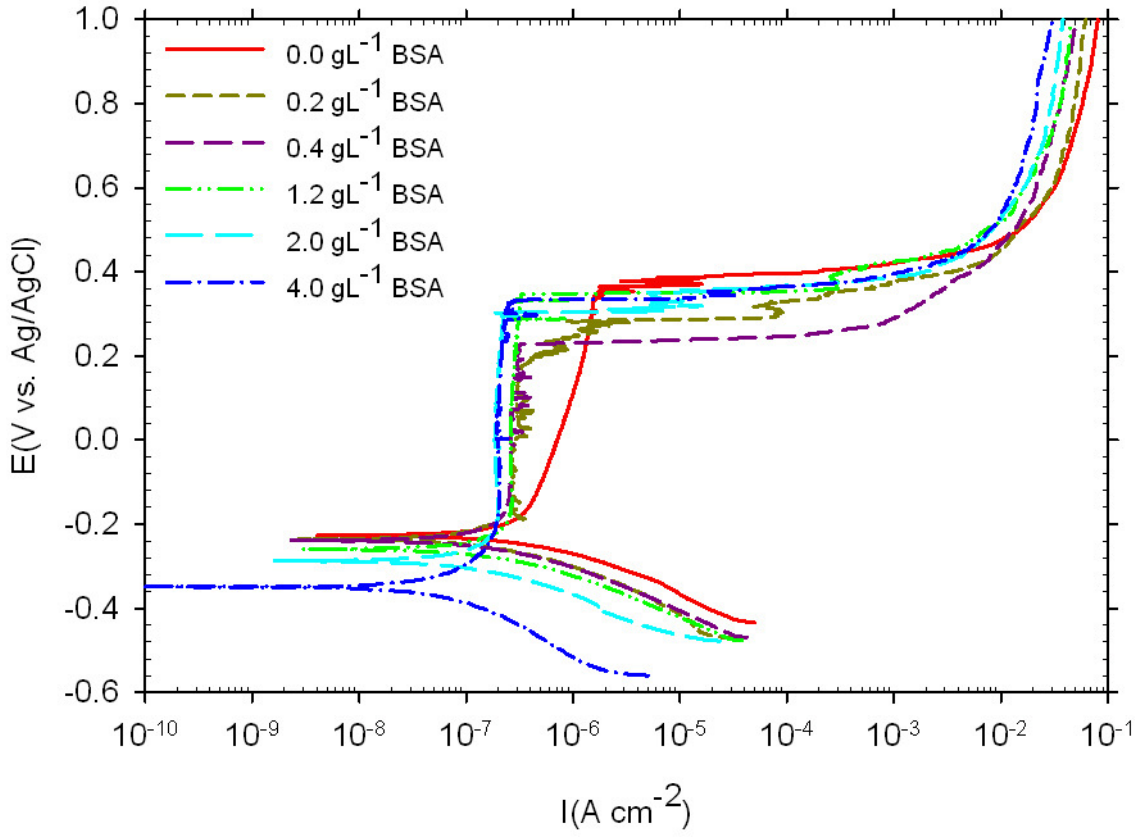

Figure 5-2 : Potentiodynamic polarization curves of 316L in PBS solutions with various BSA concentrations (0 to 4 g L-1) from -0.25 V vs. OCP to 1 V vs. Ag/AgCl with a scan rate of 0.167 mV s^{-1} in aerated conditions at 37°C and a 7.4 pH

A distinct change in the anodic polarization of 316L was observed when BSA was added to PBS. The anodic polarization branch which corresponds to the metal dissolution and passive film formation became more stable in the presence of BSA. This means that the interaction of proteins, dissolved ions, and passive layer can enhance the stability of the oxide layer in the PBS solutions in certain potential ranges. The passive layer on 316L constitutes a high amount of chromium and iron and a low amount of nickel and molybdenum oxides and

hydroxides (Bastidas et al., 2002; Kocijan et al., 2007; Milošev & Strehblow, 2000; Olsson & Landolt, 2003; Shih et al., 2004). Svare *et al.* stated that BSA has little or no effect on the anodic dissolution of nickel (Svare et al., 1970). In the serum or saline solution, Merritt *et al.* (Merritt et al., 1983) showed that nickel does not exist in the 316L passive layer. Thus, the interaction of BSA with molybdenum, iron, and chromium should be considered. Molybdenum increases the corrosion resistance of 316L by decreasing the number of active sites (Bastidas et al., 2002; Clayton & Lu, 1986). In a study done by Zanna *et al.*, the XPS data revealed that the 316L surface is depleted in Mo^{6+} because of the preferential interaction of BSA and Mo^{6+} (Zanna et al., 2006). BSA adsorbs on the 316L surface and remains chemically intact (Zanna et al., 2006) which could enhance the stability of passive film in BSA solutions. Considering the iron and chromium on the surface, Omanovic and Roscoe (Omanovic & Roscoe, 1999) stated that BSA increases chromium and the iron dissolution rate of stainless steel when BSA concentration is 1.5 mg L^{-1} in a PBS solution. Hence, the change of passive layer properties could be related to the interaction of BSA with iron and chromium in addition to molybdenum. We also observed that the passive film current did not change at concentrations greater than 0.4 g L^{-1}. Omanovic and Roscoe showed that metal dissolution becomes independent of the BSA concentration at concentrations more than 0.5 mg L^{-1} (Omanovic & Roscoe, 1999). The lowest breakdown potential for 316L was observed when BSA concentration was 0.2 g L^{-1}. The breakdown potentials reached 346 mV vs. Ag/AgCl at BSA concentration of 1.2 g L^{-1}. The breakdown potential and the corrosion potential (E_{corr}) of the metallic samples are reported in Table 5-1.

The potentiodynamic polarization curves for the Co-28Cr-6Mo samples in aerated conditions are shown in Figure 5-3. The cathodic and anodic branches moved to lower potentials when the BSA concentration was increased to 0.4 g L^{-1}. Vidal and Muñoz indicated that albumin is known as a cathodic inhibitor on CoCrMo alloys and that phosphates act as an anodic inhibitor (Valero Vidal & Muñoz, 2008). Based on their findings, the shifting in E_{corr} values can be related to the dominant action of BSA as the inhibitor.

Table 5-1 : Corrosion potential (E_{corr}) and breakdown potential of 316L, Co-28Cr-6Mo, and Ti-6Al-4V in aerated PBS solutions at 37°C and pH = 7.4 having various concentrations of BSA obtained from potentiodynamic polarization measurements

BSA (g L^{-1})	E_{corr} (mV vs. Ag/AgCl)			Breakdown Potential (mV vs. Ag/AgCl)		
	316L	Co-28Cr-6Mo	Ti-6Al-4V	316L	Co-28Cr-6Mo	Ti-6Al-4V
0	-227±0.03	-209±0.02	-244±0.02	355±0.1	62.5±0.1	-
0.2	-235±0.03	-208±0.04	-328±0.04	177±0.1	60.5±0.1	-
0.4	-239±0.03	-398±0.03	-279±0.02	228±0.1	362±0.1	-
1.2	-259±0.02	-381±0.01	-278±0.03	346±0.1	325±0.1	-
2	-287± 0.04	-423±0.02	-254±0.04	350±0.1	330±0.1	-
4	-349±0.03	-379±0.03	-325±0.02	326±0.1	346±0.1	-

Two passive regions (from -0.07 to 0.2 V vs. Ag/AgCl and from 0.4 to 0.5 V vs. Ag/AgCl) at BSA concentrations of less than 0.2 g L^{-1} and one passive region (from -0.2 to 0.3 V vs. Ag/AgCl) at BSA concentrations of greater than 0.4 g L^{-1} were observed for the Co-28Cr-6Mo alloy. In addition, the potentiodynamic polarization curves consisted of shoulders at

potentials close to 0.6 V vs. Ag/AgCl. This behavior likely corresponds to the phosphate-chromium complex formation and dissolution (Muñoz & Mischler, 2007). The phosphate-metal complex formation has been observed in the case of 316L and Ti alloys (Miloev et al., 2000; Sousa & Barbosa, 1991). The final transpassive region started at 0.55 V vs. Ag/AgCl. In this region, the oxidation of chromium (III) to chromium (IV) could occur (Hodgson et al., 2004), which activates the surface and causes transpassive dissolution of the passive surface (Virtanen et al., 2008).

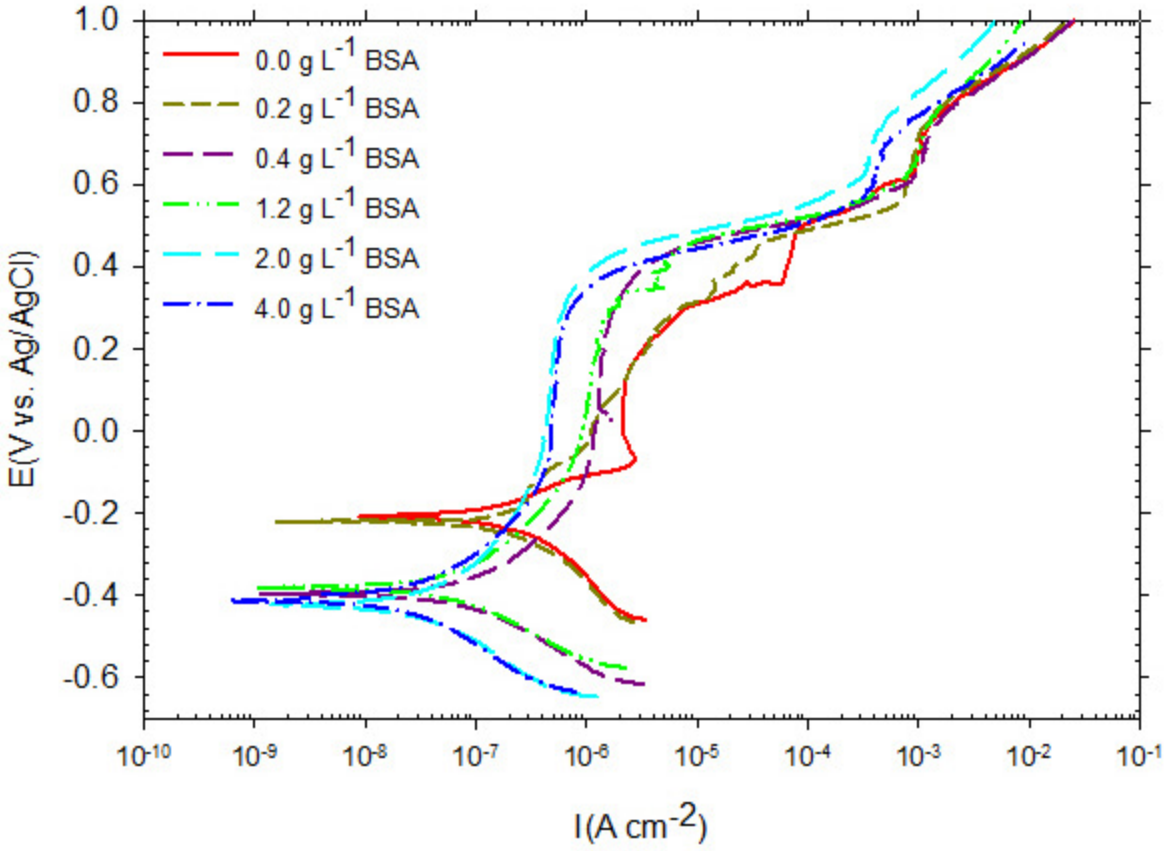

Figure 5-3 : Potentiodynamic polarization curves of Co-28Cr-6Mo in PBS solutions with various BSA concentrations (0 to 4 g L^{-1}) from -0.25 V vs. OCP to 1 V vs. Ag/AgCl with a scan rate of 0.167 mV s^{-1} in aerated conditions at 37°C and a 7.4 pH

The passive layer of Co-28Cr-6Mo became more stable in the PBS solution containing 0.4 g L^{-1} BSA because the passive region current density was decreased and metal dissolution at the transpassive region (0.3 to 0.5 V vs. Ag/AgCl) was eliminated at BSA concentrations of 0.4 to 4 g L^{-1}. Furthermore, the passive current density of Co-28Cr-6Mo decreased by increasing BSA concentration. These observations can be related to the formation of an adsorbed film on Co-28Cr-6Mo at BSA concentrations higher than 0.4 g L^{-1}. The adsorbed film is also dependent on the BSA concentrations in the PBS solutions.

The observed passive behavior of Co–28Cr–6Mo alloy at low and high BSA concentrations was further studied by XPS analysis to investigate the effect of potential and protein on passive behavior of this alloy. The compositions of Co–28Cr–6Mo oxide layer in at. % at potentials of 0.007 and 0.25 V vs. Ag/AgCl in PBS solutions with 0 and 4 g L^{-1} BSA are summarized in Table 5-2 and the overall survey scans are presented in Figure 5-4.

Table 5-2 : Composition of Co–28Cr–6Mo surface oxide film by XPS at 0.007 and 0.25 V vs. Ag/AgCl in PBS solutions containing 0 and 4 g L^{-1} BSA at 37°C and a pH of 7.4

		Concentration (at.%)								
BSA g L^{-1}	Potential V vs. Ag/AgCl	Co	Cr	Mo	O	C	Na	P	Cl	N
0	0.007	0.00	2.97	0.7	40.23	36.25	5.60	7.34	6.01	
0	0.250	1.16	5.05	1.82	48.54	35.43	1.70	3.45	2.97	
4	0.007	1.73	3.23	1.12	42.05	42.33	1.19	0.96	1.31	6.08

The XPS analysis revealed that cobalt existed in the PBS solution at 0.25 V vs. Ag/AgCl potential whereas at a lower potential, cobalt was not detected on the Co–28Cr–6Mo oxide layer. It is reported that Co–28Cr–6Mo alloys are able to form a spontaneous oxide layer with a main contribution of Cr_2O_3 and a small amount of Co- and Mo-oxides (Miloev et al., 2000). This passive layer composition depends on external parameters such as potential and passivation time (Miloev et al., 2000). Hodgson *et al.* indicated that the dissolution of the CoCrMo alloying element is proportional to the chemical composition of the CoCrMo alloy up to breakdown potential (Hodgson et al., 2004). Therefore, the difference in the passive current is likely because of cobalt oxidation at higher potentials. It was also observed in a detailed scan of molybdenum that it converts from a metallic to an oxide state. This supports the Miloev *et al.* observation that the predominant oxides are Cr_2O_3 and Cr $(OH)_3$ at lower potentials and Co (CoO) and Mo (MoO_3) oxides at higher potentials(Miloev et al., 2000).

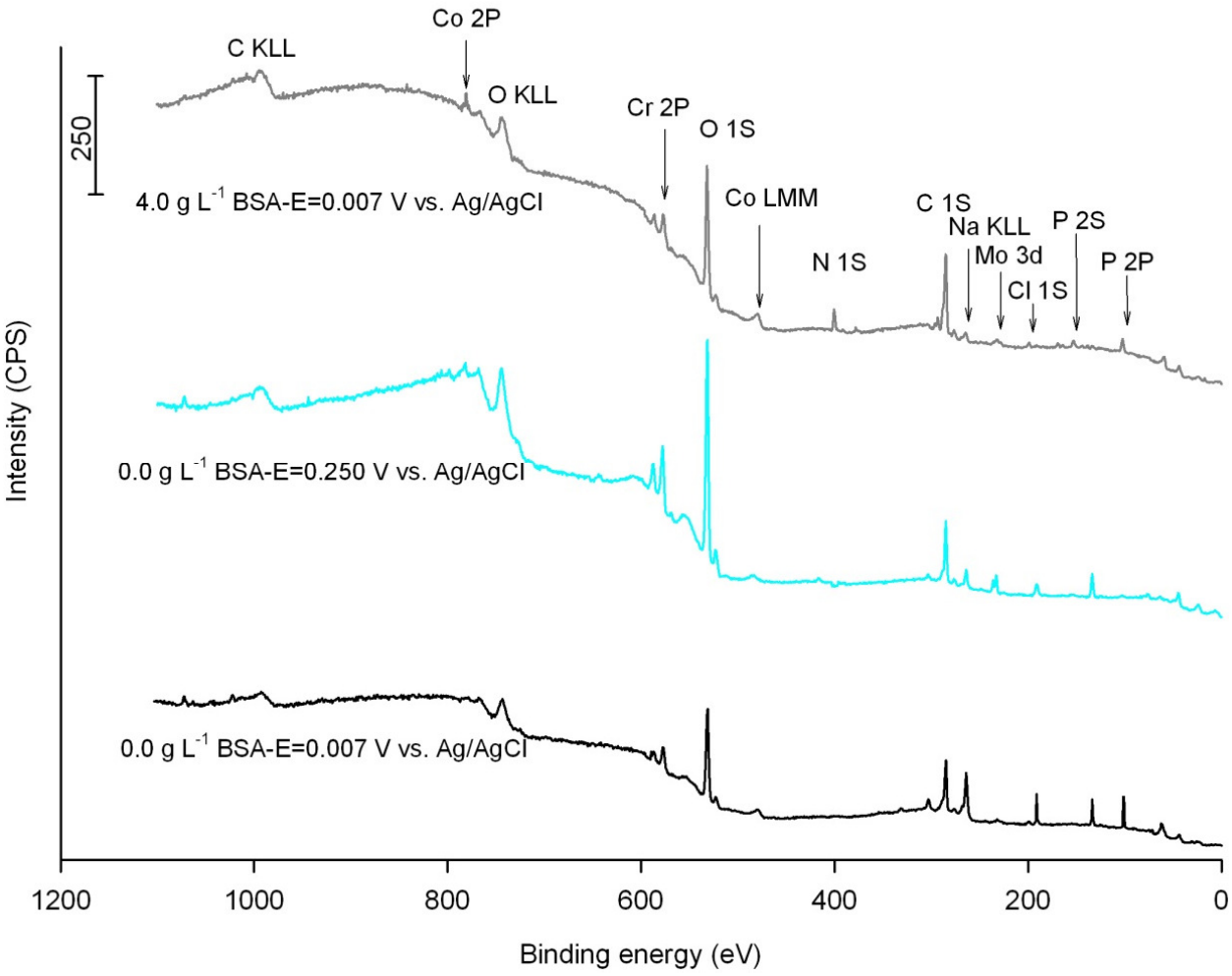

Figure 5-4 : XPS spectra of Co–28Cr–6Mo alloy at 0.007 V vs. Ag/AgCl in PBS solutions with 0 and 4 g L−1 BSA and at 0.25 V vs. Ag/AgCl in PBS solutions without BSA

Figure 5-5 shows the polarization behavior of Ti-6Al-4V alloy in solutions of PBS containing different concentrations of BSA. The cathodic polarization behaviors of the Ti-6Al-4V samples were similar to electrolyte with different BSA concentrations meaning that the cathodic behavior is due to oxygen evolution.

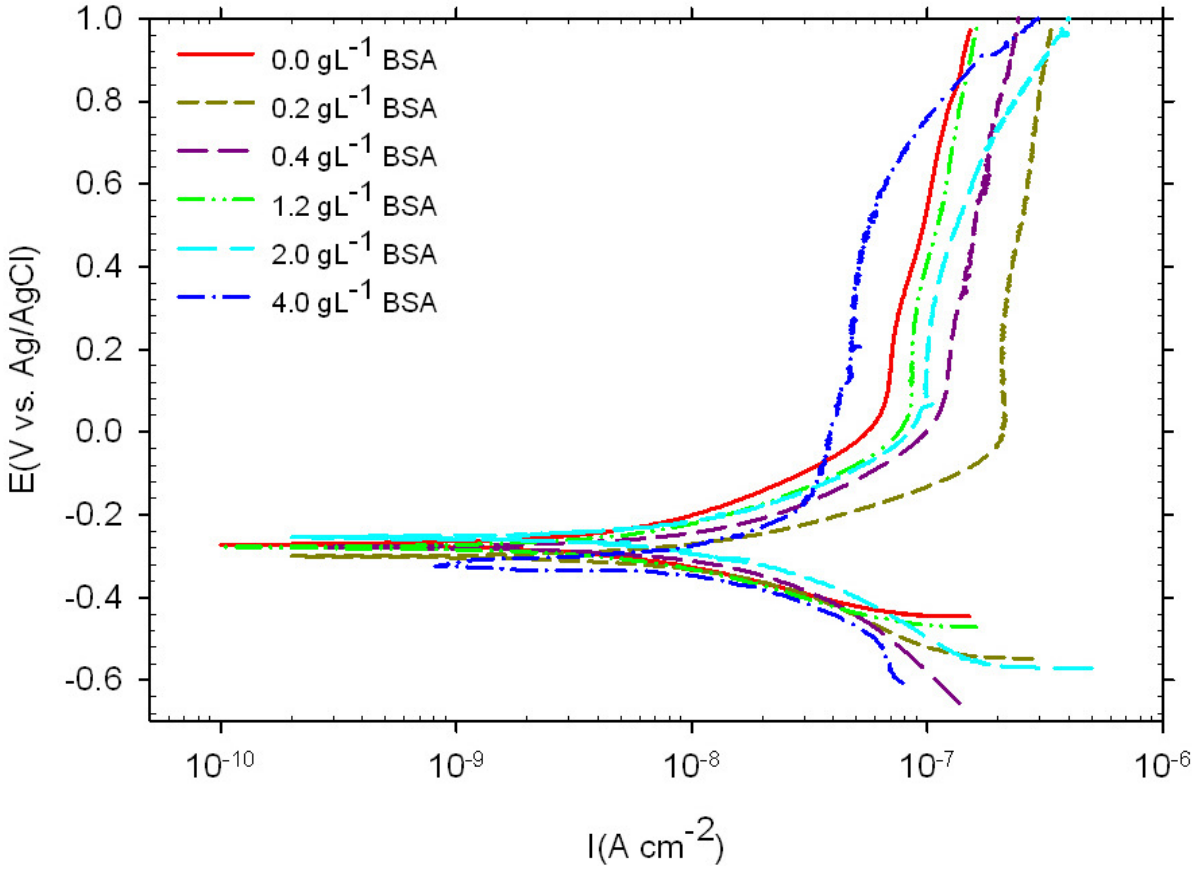

Figure 5-5 : Potentiodynamic polarization curves of Ti-6Al-4V in PBS solution with various BSA concentrations (0 to 4 g L^{-1}) from -0.25 V vs. OCP to 1 V vs. Ag/AgCl with a scan rate of 0.167 mV s^{-1} in aerated conditions at 37°C and a 7.4 pH

A breakdown potential was not detected for the Ti-6Al-4V samples up to 1 V vs. Ag/AgCl. The breakdown potential and the corrosion potential (E_{corr}) of the metallic samples are reported in Table 5-1.

The stability of the titanium alloys passive layer could be evaluated by considering the interaction of the outer passive layer and the solution. Ti–6Al–4V alloy has two metal-oxide interfaces. The inner interface contains TiO_2, TiO, and Ti_2O_3 and the outer layer is enriched

with Al_2O_3 (Khan et al., 1999; Kuhn et al., 1986; Miloev et al., 2000; Pourbaix, 1984). Chemisorption of water on the surface of TiO_2 produces two types of surface hydroxyl groups which can be distinguished by their coordination with Ti^{4+} ions (Boehm, 1971). These hydroxyl groups on the surface of TiO_2 are amphoteric (Boehm, 1971). Singly and doubly coordinations of these bonds postulated to be basic and acidic, respectively (Boehm, 1971). The reactions (i) and (ii) (Wassell & Embery, 1996) show proton dissociation on the surface of TiO_2.

Protonated base: $Ti\text{-}OH_2^+ \leftrightarrow Ti\text{-}OH + H^+$ 5-1

Acidic hydroxyl groups: $-OH \leftrightarrow O^- + H^+$ 5-2

Phosphate ions ($H_2PO_4^-$, HPO_4^{2-}) are able to bind to titanium ions in exchange reactions with the basic hydroxyl groups (Wassell & Embery, 1996). The adsorption of BSA on titanium has shown that the chemical adsorption of BSA onto the TiO_2 depends on the number of surface hydroxyl groups and values of the polar components of the total surface energy (Desroches et al., 2007; Feng et al., 2002).

Addition of BSA decreased passive current density of Ti-6Al-4V alloy significantly. The passive current density of the Ti-6Al-4V alloy decreased when BSA concentration was increased from 0.2 to 4 g L^{-1}. When BSA concentration was 4 g L^{-1}, the passive current density was less than the passive current density in the solution without BSA. This is evidence that a BSA concentration higher than 4 g L^{-1} is required to increase stability of the oxide layer or to

produce an adsorb layer. Sunny and Sharma studied the oxide layer growth and protein adsorption in a protein mixture (Sunny & Sharma, 1991). They indicated that the rate of protein adsorption is increased by the growth of the oxide layer on the surface of titanium and the Ti-6Al-4V alloy because the oxide layer enhances the hydrophobicity of the alloy surface (Sharma & Sunny, 1986). This result can be used to explain the decrease in the passive current density of Ti-6Al-4V alloy by the addition of BSA to the PBS solutions.

In general, the passive layer of Ti-6Al-4V alloy was formed at a lower current density (about 10^{-7} A cm^{-2}) compared to 316L (about 7×10^{-7} A cm^{-2}) and Co-28Cr-6Mo (about 10^{-6} A cm^{-2}) alloys. These results show that the passive layer of the Ti-6Al-4V alloy is more protective than the passive layers of 316L and Co-28Cr-6Mo Alloys. In addition, less ion release is expected from the Ti alloy than the Co-28Cr-6Mo and 316L.

5.3 Electrochemical impedance spectroscopy

In Figure 5-6, the Bode and Bode phase diagrams for 316L, Co-28Cr-6Mo, and Ti-6Al-4V alloys in PBS solutions containing different BSA concentrations at 37°C are provided. The absolute impedance data was independent of frequency from 10^4 down to 10^3 Hz. This frequency range showed a resistive behavior corresponding to the solution resistance between the working and the reference electrode.

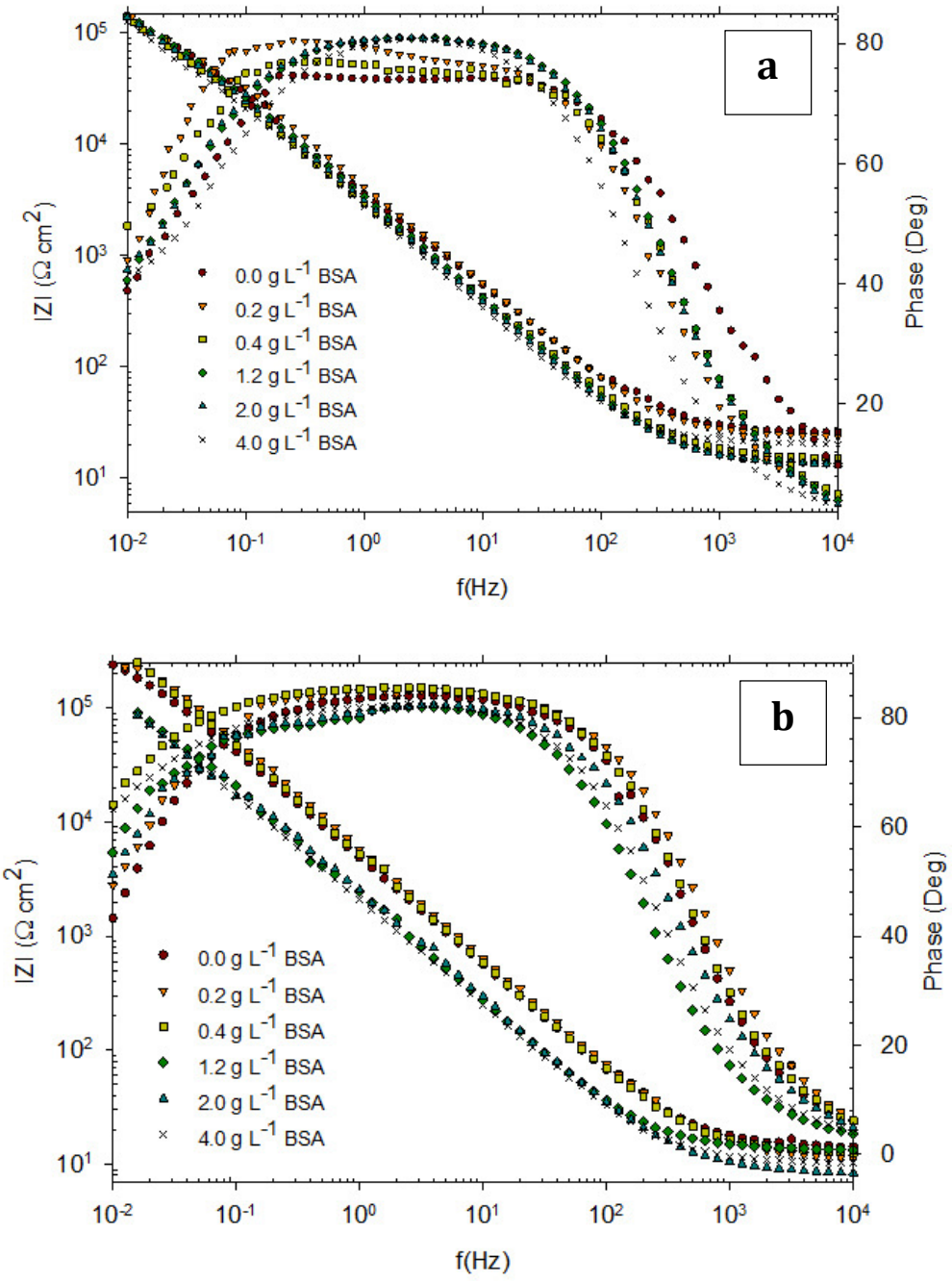

Figure 5-6 : Bode and Bode phase plots of the (a) 316L, (b) Co-28Cr-6MO, and (c) Ti-6Al-4V alloys after 1 hour of immersion at OCP in aerated PBS solutions at 37 °C and pH = 7.4 with various concentrations of BSA

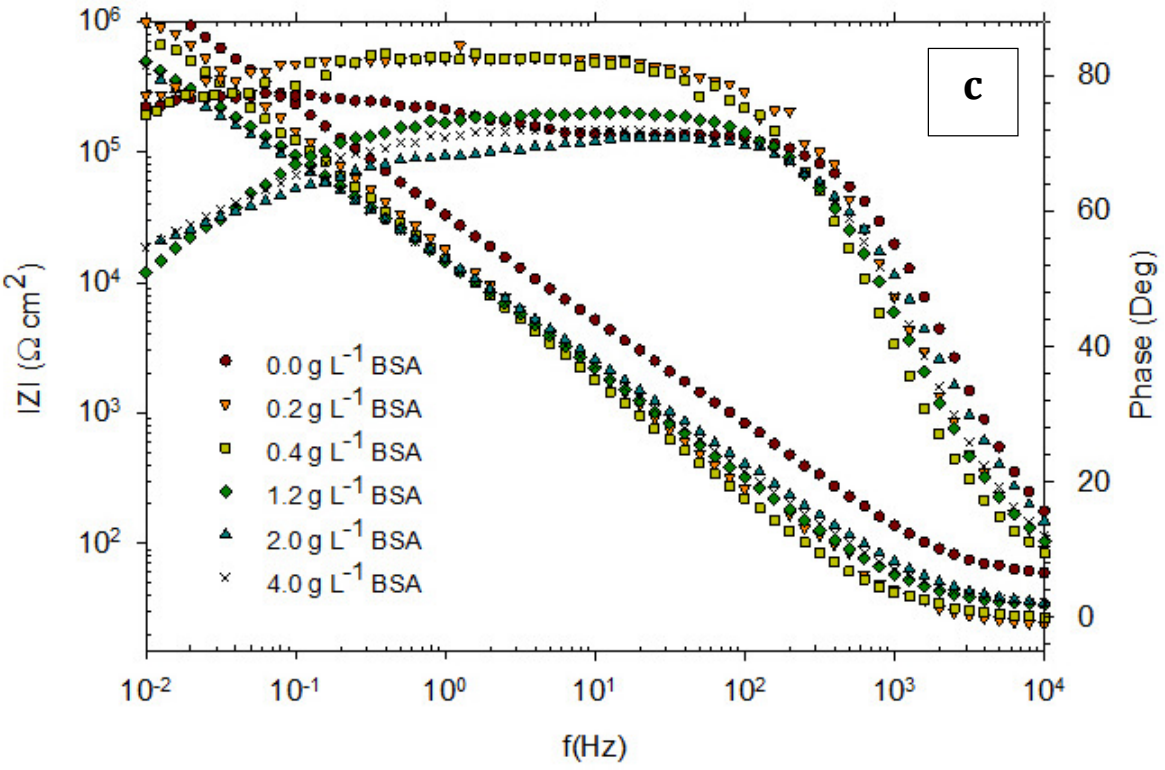

Figure 5-6: (Cont'd) Bode and Bode phase plots of the (a) 316L, (b) Co-28Cr-6MO, and (c) Ti-6Al-4V alloys after 1 hour of immersion at OCP in aerated PBS solutions at 37 °C and pH = 7.4 with various concentrations of BSA

The phase values reached their maximum values (~80°) for 316L and Co-28Cr-6Mo alloys at a frequency range of 20 to 0.2 Hz whereas the phase angle of Ti-6Al-4V impedance reached its maximum value (~80°) at a frequency range of 80 to 0.1 Hz. In these frequency ranges, the metallic samples showed capacitive behaviours. In addition, the passive behaviour of the metallic samples was observed at these frequency ranges because the phase angle values were independent of frequency while the absolute impedance values were increasing.

The absolute impedance increased and the phase angle shifted to the lower values by decreasing the frequency from 0.2 to 0.01 Hz for 316L and Co-28Cr-6Mo alloys and from 0.1 to 0.01 Hz for the Ti-6Al-4V samples. The impedance curves of the 316L samples tested in PBS solutions with and without BSA showed similar behaviors. The absolute impedance magnitude decreased when BSA was added to PBS solutions for Ti-6Al-4V alloys. Furthermore, the impedance values for Co-28Cr-6Mo alloys declined at BSA concentration higher than 1.2 g L^{-1}. A typical Nyquist diagram for 316L, Co-28Cr-6Mo, and Ti-6Al-4V alloys in PBS solutions containing different BSA concentrations at 37°C is shown in Figure 5-7.

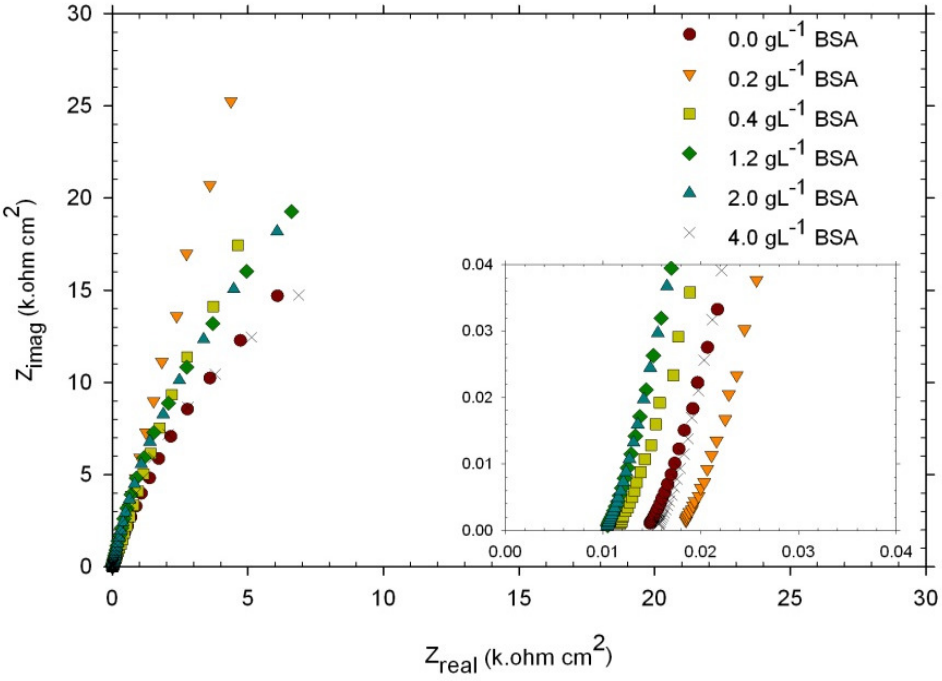

Figure 5-7 : Nyquist diagrams of (a)316L, (b)Co-28Cr-6Mo, and (c)Ti-6Al-4V alloys after 1 hour of immersion at OCP in aerated PBS solution at 37°C and pH = 7.4 with various BSA concentrations

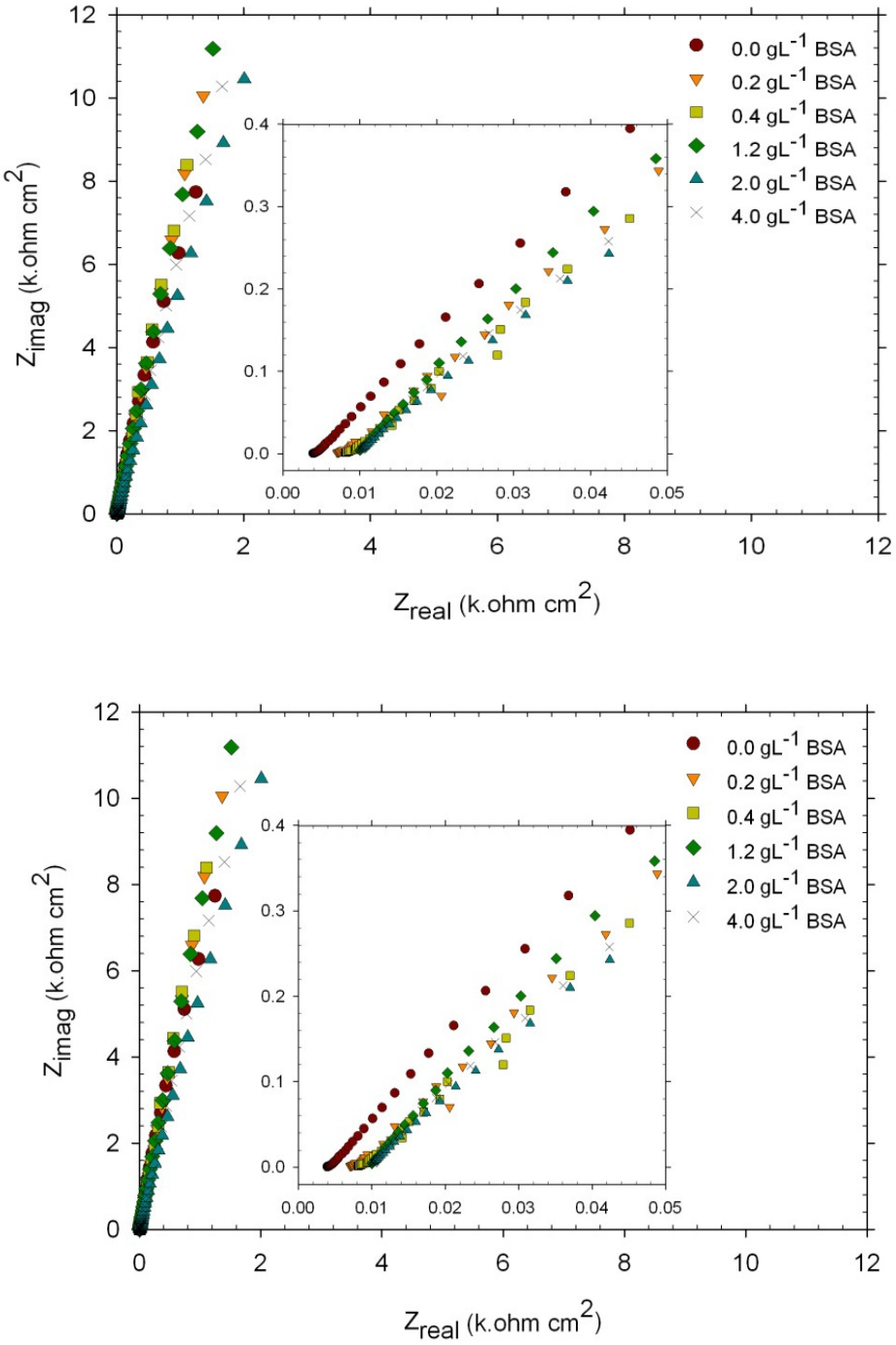

Figure 5-7 : (Cont'd) Nyquist diagrams of (a)316L, (b)Co-28Cr-6Mo, and (c)Ti-6Al-4V alloys after 1 hour of immersion at OCP in aerated PBS solution at 37°C and pH = 7.4 with various BSA concentrations

The impedance can be characterized by a large semicircle capacitive loop and the Nyquist curves showed a one-time constant. Therefore, a simple Randles equivalent circuit (R_S (R_b C_b)) was used Figure 5-8. In this circuit, R_S is designated as the solution resistance between the working and the reference electrode and R_b and C_b are the resistance and capacitance of the barrier layer. Constant phase element (CPE) is used instead of pure capacitor to consider the non-uniform current distribution due to surface roughness and non-homogeneities related to BSA adsorption (López et al., 2008; Omanovic & Roscoe, 1999; Valero Vidal & Muñoz, 2008). The impedance of a constant phase element (Equation 5-3) is defined as follows:

$$Z_{CPE} = \frac{1}{(j\omega)^{n_C} Y_0} \qquad 5\text{-}3$$

Where the exponent n_C is a coefficient related to deviation between real capacitance and pure capacitance, Y_0 is the general admittance function, and ω represents the angular frequency. The magnitude of the electrical circuit parameters were simulated by ZSimpWin software package.

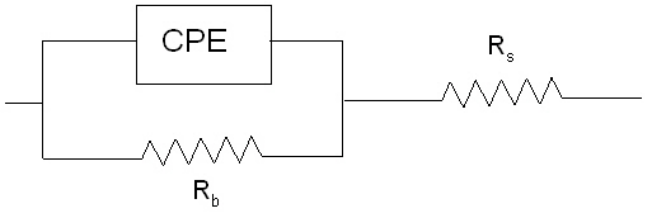

Figure 5-8 : Equivalent Randle electrical circuit

The magnitude of the electrical circuit components along with the chi-square value (χ^2) are reported in Table 5-3. The typical χ^2 values were less than 4×10^{-3} indicating a satisfactory fit.

Table 5-3 : EIS equivalent Randle circuit parameters of 316L, Co-28Cr-6Mo, and Ti-6Al-4V alloys after 1 hour immersion in aerated PBS solutions with various BSA concentrations at 37°C, pH = 7.4 and OCP potential

specimen	BSA	R_s	R_b	Y_0	n_C	$\chi^2\times10^{-4}$
	g L^{-1}	Ω cm^2	kΩ cm^2	μΩ^{-1} s^n cm^{-2}		
316L	0	15.0	81.7	88.3	0.87	2.47
	0.2	18.6	99.8	59.7	0.88	4.93
	0.4	11.7	101.2	66.9	0.86	6.41
	1.2	10.8	114.2	71.9	0.91	4.48
	2	10.7	114.8	77.4	0.91	4.58
	4	16.1	53.9	86.2	0.91	5.28
Co-28Cr-6Mo	0	13.4	76.7	30.3	0.93	5.97
	0.2	9.25	69.2	49.0	0.82	21
	0.4	13.3	104.7	53.6	0.95	17.2
	1.2	16.8	132.9	65.8	0.92	6.72
	2	10.7	251.4	65.7	0.92	13.4
	4	12.8	671.7	72.8	0.92	6.67
Ti-4Al-4V	0	4.1	180.6	102.8	0.93	5.87
	0.2	7.1	268.9	35.5	0.90	37.6
	0.4	8.3	310.0	41.9	0.91	9.75
	1.2	9.4	282.5	46.2	0.85	4.5
	2	9.1	271.1	46.7	0.81	1.33
	4	9.2	269.1	49	0.82	1.10

The variation of solution resistance values can be related to the dissolution of ions from the alloy surface (decreasing Rs) or protein adsorption (Valero Vidal & Muñoz, 2008). The polarization resistance increased when the BSA concentration was greater than 0.4 g L^{-1} except for 316L at BSA concentration of 4 g L^{-1}. This means that the addition of BSA to PBS solutions increased the thickness of the barrier layer. This outcome confirms the results obtained from potentiodynamic polarization measurements.

5.4 Linear polarization resistance

The LPR graphs of samples at BSA concentrations of 0, 1.2, and 4 g L^{-1} are presented in Figure 5-9. The results show that the Ti-6Al-4V alloy has the lowest corrosion rate followed by Co-28Cr-6Mo and 316L alloys, respectively. The addition of BSA to the solution did not influence the corrosion rates for Ti-6Al-4V.

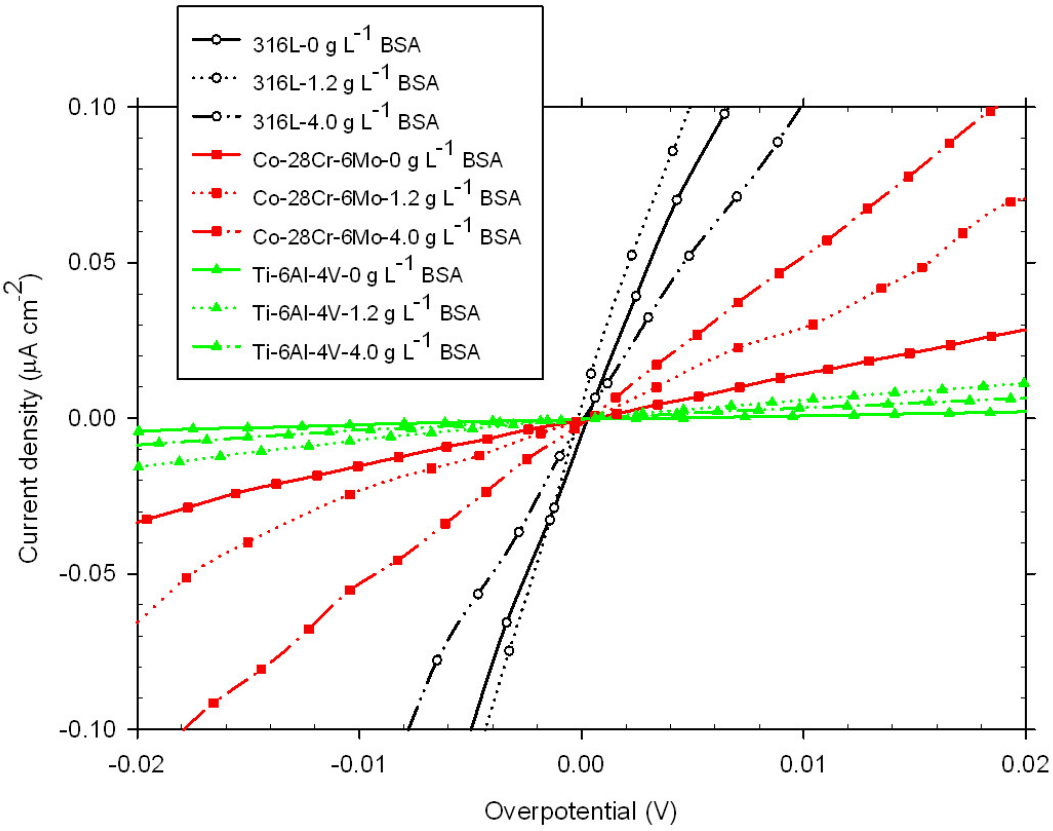

Figure 5-9 : Linear polarization curves for 316L, Co-28Cr-6Mo, and Ti-6Al-4V alloys after 1 hour of immersion at OCP in aerated PBS solution at 37°C and pH = 7.4 with BSA concentration of 0, 1.2, and 4.0 g L^{-1}

5.5 Corrosion rate calculations

The values of corrosion current density (i_{corr}) of alloys were calculated by considering their polarization resistance (R_p) and using equations 5-4 and 5-5 (Stansbury & Buchanan, 2000). The polarization resistance was obtained from the electrical circuit model (R_b) and the slope of the linear polarization curves ($R_{P\text{-}LPR}$).

$$i_{corr} = \frac{B}{R_p} \quad 5\text{-}4$$

$$B = \frac{1}{2.3\,(\frac{1}{\beta_{ox}} + \frac{1}{\beta_{red}})} \quad 5\text{-}5$$

The cathodic and anodic Tafel slope values were approximated. The normal values of $\beta_{red,X}$ and $\beta_{ox,M}$ vary from 60 mV to infinity and from 60 mV to 120 mV, respectively (Stansbury & Buchanan, 2000). Therefore, using equation 5-5, the value of B is between 13 mV to 52 mV. The values of i_{corr} and the corrosion rate of the metallic samples by LPR and EIS measurements are summarized in Table 5-4. This Table also contains the atomic weight (a) of the metallic samples in g mol^{-1}, the corrosion current density (i_{corr}) in μA cm^{-2}, the number of equivalent exchange (n), and the density (ρ) in g cm^{-3}. These variables along with Faraday's constant (F) in coulombs mol^{-1} were used in equation 5-6 to find the corrosion rate of the metallic samples in PBS solutions.

$$Corrosion\ rate\ (\mu m\ per\ Year) = 3.1536 \times 10^5\ \frac{a\ i_{corr}}{nF\ \rho} \quad 5\text{-}6$$

Table 5-4 : Atomic weight (a), density (ρ), and number of exchange atoms (n) along with corrosion current density (i_{corr}) and corrosion rate of 316L, Co-28Cr-6Mo, and Ti-6Al-4V alloys obtained from EIS and LPR data

specimen	BSA	a	ρ	n	i_{corr} (EIS)	Corrosion rate (EIS)	i_{corr} (LPR)	Corrosion rate (LPR)
	g L^{-1}	g mol^{-1}	g cm^{-3}	equivalent mol^{-1}	µA cm^{-2}	µm $year^{-1}$	µA cm^{-2}	µm $year^{-1}$
316L	0	56.30	7.85	3	0.40±0.2	3.1±1.9	0.67±0.1	5.2±1.2
	0.2				0.33±0.02	2.5±1.5	0.70±0.3	5.5±2.2
	0.4				0.32±0.04	2.5±1.5	0.68±0.5	5.3±4.0
	1.2				0.28±0.2	2.2±1.3	0.43±0.3	3.3±2.1
	2				0.28±0.2	2.2±1.3	0.36±0.07	2.8±0.6
	4				0.60±0.4	4.7±2.8	0.45±0.2	3.5±1.2
Co-28Cr-6Mo	0	58.61	8.09	3	0.42±0.02	3.4±2.0	0.12±0.05	0.9±0.4
	0.2				0.47±0.02	3.7±2.2	0.19±0.02	1.5±0.2
	0.4				0.31±0.02	2.4±1.5	0.22±0.06	1.7±0.4
	1.2				0.24±0.2	1.9±1.2	0.12±0.01	0.9±0.1
	2				0.13±0.08	1.0±0.6	0.43±0.2	3.4±1.6
	4				0.05±0.03	0.4±0.2	0.20±0.04	1.6±0.3
Ti-6Al-4V	0	46.65	4.37	4	0.18±0.1	1.6±1.3	0.01±0.004	0.1±0.03
	0.2				0.12±0.07	1.1±0.8	0.02±0.003	0.1±0.03
	0.4				0.10±0.06	0.9±0.7	0.01±0.003	0.1±0.02
	1.2				0.12±0.7	1.0±0.8	0.02±0.006	0.2±0.05
	2				0.12±0.7	1.1±0.8	0.01±0.003	0.1±0.02
	4				0.12±0.7	1.1±0.8	0.02±0.003	0.1±0.02

The corrosion rates calculated for Ti-6Al-4V alloy by LPR are nearly one order of magnitude smaller than the corrosion rate calculated by EIS. This, in the authors' view, shows that low frequency processes likely took place in the metal/solution interfaces that were not detected at frequencies as low as 0.01 Hz. Therefore, a simple Randles circuit, which was used for $R_{P\text{-}EIS}$ calculation, neglects those processes and thus overestimates the corrosion rate. Nonetheless, since no other features are observed in the EIS spectra, a Randles circuit was used. There was no distinct trend between the corrosion rates and BSA concentrations. However, Ti-6Al-4V alloy had the lowest corrosion rate compared to 316L and Co-28Cr-6Mo alloys.

5.6 Summary

The alloys 316L stainless steel, wrought Co-28Cr-6Mo and Ti-6Al-4V were tested in aerated solutions of PBS and BSA at simulated body conditions by OCP, potentiodynamic polarization measurements, EIS, and LPR. The following conclusions were drawn:

- OCP values of all the samples shifted towards more cathodic potentials by increasing BSA concentrations. The decrease in OCP values were observed at low BSA concentrations for Co-28Cr-6Mo alloy and at high BSA concentrations for Ti-6Al-4V alloy.
- The presence of BSA had a significant effect on the passive behavior of Co-28Cr-6Mo alloy when BSA concentrations were greater than 0.4 g L^{-1}.
- Ti-6Al-4V alloy had the highest breakdown potential in the solution of PBS and BSA. The passive layer formed on the surface of the Ti-6Al-4V alloy was more intact than 316L and Co-28Cr-6Mo.
- The presence of BSA increased the stability of the 316L and Co-28Cr-6Mo passive film. However, BSA in a concentration range of 0.2 to 2 g L^{-1} reduced the barrier layer stability of the Ti-6Al-4V samples.
- No distinct trend was found for the effect of protein concentration on the corrosion rate of 316L, Co-28Cr-6Mo, or the Ti-6Al-4V alloys.

Chapter 6: Long term corrosion behavior of 316L, CoCrMo and Ti-6Al-4V alloys in the presence of BSA

One of the main requirements of the metallic implants is to have high corrosion resistance in the human body environment. The presence of a passive layer on the surface of bio-implant alloys significantly increases their corrosion resistance; however, they are not completely inert in the body. Interactions between body fluids and the surface oxide layer may cause ion release. If the level of the ion released from the implant exceeds the normal level, the implant will have harmful effects on patient health. The long term corrosion study of metallic implants helped us to investigate the effect of immersion time on the mass loss, surface composition, and ion release.

In the previous chapter, the instantaneous corrosion behavior of 316L, wrought Co-28Cr-6Mo, and Ti-6Al-4V alloys at various BSA concentrations were studied. In this chapter, a long term static immersion corrosion behavior of the selected biomaterials was investigated in aerated PBS solutions with various BSA concentrations at 37°C for up to 22 weeks. Surface and solution composition of these alloys were analyzed by XPS and ICP-OES measurements. The goal was to detect the ions and the amount of them released from the selected biomaterials and to predict the interaction of biomaterials with simulated biological fluids.

6.1 Weight loss and corrosion rate

The weight loss of the AISI 316L, Co-28Cr-6Mo, and Ti-6Al-4V alloys up to the 22-week immersion tests as a function of BSA concentrations are presented in Figure 6-1, Figure 6-2, and Figure 6-3, respectively. The points refer to the average weight loss and an error bar is the standard deviation of the three measurements.

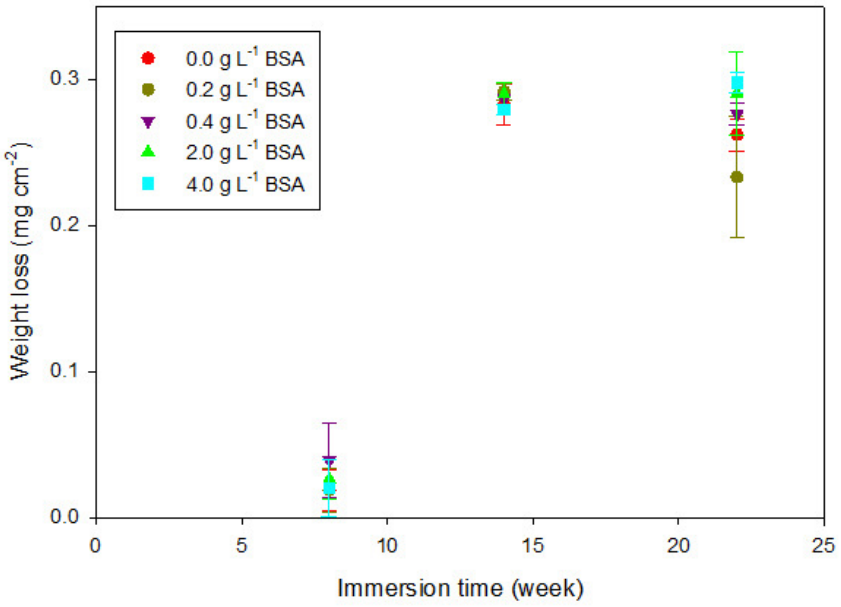

Figure 6-1 : Weight changes of the 316L after 8, 14, and 22 weeks immersion in PBS solutions with various BSA concentrations (0 to 4 g L^{-1}) at 37°C

The highest weight loss was observed for samples incubated for 14 weeks. After 14 weeks, a small weight gain was generally observed which could be related to the growth of the oxide layer or precipitation of previously dissolved ions. Koike and Fujii (Koike & Fujii, 2001) also reported weight gain of pure titanium when it was immersed in physiological saline solution

due to Ti dissolution and the formation of TiO_2. Protein concentration levels did not show a significant effect on the degradation of the 316L, Co-28Cr-6Mo and Ti-6Al-4V alloys. In all the given conditions, the weight loss of stainless steel was higher than the other alloys.

The surfaces of all the samples were examined using both optical and scanning electron microscopes (Hitachi S-3000N). No sign of localized corrosion was observed on any specimens. Therefore, the weight loss data was used to calculate the corrosion rates by Equation 6-1 (ASTM G31-72 , 2004). The calculated results of this work and the previous study are presented in Table 6-1.

$$\text{Corrosion rate } (\mu\text{m year}^{-1}) = \frac{K \times W}{A \times T \times \rho} \qquad 6\text{-}1$$

where K is a constant (8.76×10^4), T is time of exposure (in hours), A is area of immersed specimen (in cm^2), W is mass loss (in mg), and ρ is density (in g cm^{-3}).

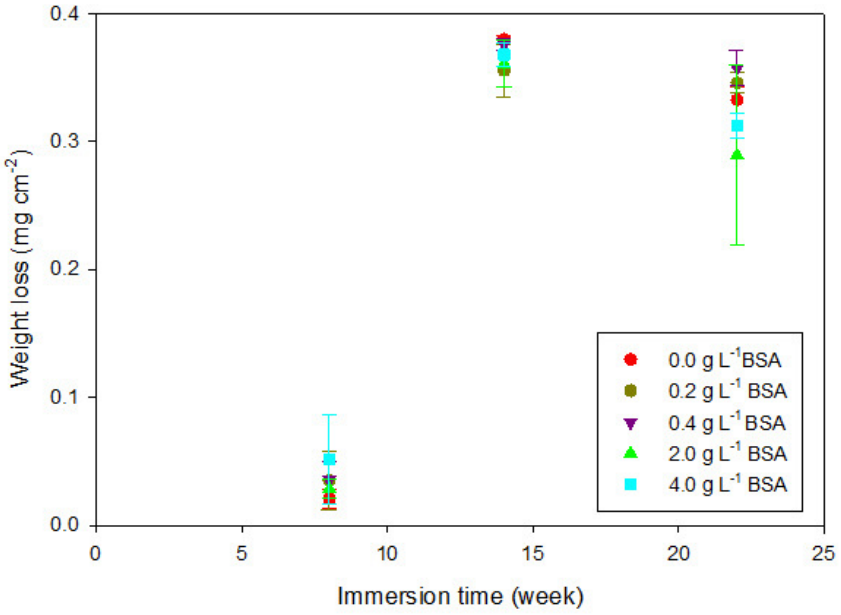

Figure 6-2 : Weight changes of the Co-28Cr-6Mo after 8, 14, and 22 weeks immersion in PBS solutions with various BSA concentrations (0 to 4 g L^{-1})) at 37°C

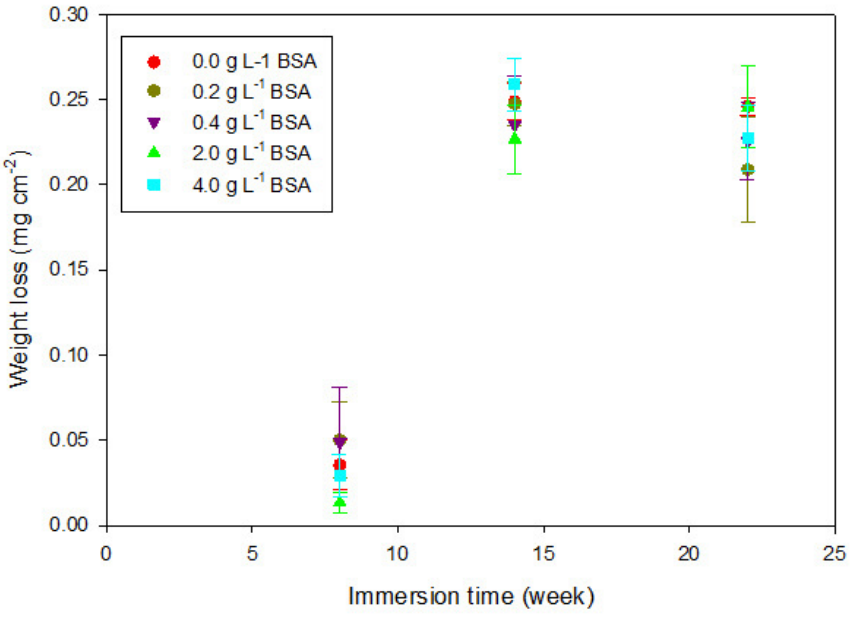

Figure 6-3 : Weight changes of Ti-6Al-4V after 8, 14, and 22 weeks immersion in PBS solutions with various BSA concentrations (0 to 4 g L^{-1}) at 37°C

Table 6-1 : Corrosion rate of 316L, Co-28Cr-6Mo, and Ti-6Al-4V alloys after 22 weeks of exposure to the solutions of PBS with various BSA concentrations (0 to 4 g L^{-1}) at 37 °C and corrosion rates from EIS measurement

	BSA Concentration (g L^{-1})	Density (g cm^{-3})	Corrosion Rate (μm $year^{-1}$)	
			From immersion test	From EIS
316L	0	7.8521	1.3 ± 0.1	3.1 ± 1.9
	0.2		0.8 ± 0.7	2.5 ± 1.5
	0.4		1.4 ± 0.0	2.5 ± 1.5
	2		1.4 ± 0.1	2.2 ± 1.3
	4		1.8 ± 0.6	4.7 ± 2.8
Co-28Cr-6Mo	0	8.0860	1.6 ± 0.1	3.4 ± 2.0
	0.2		1.6 ± 0.0	3.7 ± 2.2
	0.4		1.7 ± 0.1	2.4 ± 1.5
	2		1.4 ± 0.3	1.0 ± 0.6
	4		1.0 ± 0.9	0.4 ± 0.2
Ti-6Al-4V	0	4.3693	2.2 ± 0.0	1.6 ± 1.3
	0.2		1.8 ± 0.3	1.1 ± 0.8
	0.4		2.0 ± 0.2	0.9 ± 0.7
	2		2.2 ± 0.2	1.1 ± 0.8
	4		2.0 ± 0.2	1.1 ± 0.8

A comparison of the calculated corrosion rates with the previously calculated corrosion rates (Karimi et al., 2011) obtained from EIS measurement data indicates that the values are comparable for the 316L and Co-28Cr-6Mo, and Ti-6Al-4V alloys.

6.2 Solution characterization

The quantity of metal released from 316L into solution is summarized in Figure 6-4. Also, the converted analytical detection limits of the studied ions are calculated as: Fe, Ni, Cr 0.0625 mg cm^{-2}, and Mo 0.125 mg cm^{-2}. All the measured Fe concentrations were far beyond

the detection limit and the amount of Fe released increased by increasing the BSA concentration in PBS solutions (Figure 6-4a). This trend was observed in all three immersion times. Therefore, the immersion time did not alter the effect of the BSA concentration on the iron release rate. However, the iron release rate increased up to 14 weeks and then decreased at 22 weeks with each BSA concentration. Comparisons of the iron release with the weight loss results showed that weight loss and iron release follow the same trend. This is possibly due to the precipitation of dissolved iron over a long period of time. The amount of Fe release is considerably higher than that of the other elements. The high dissolution rate of Fe compared to other 316L alloy's components in PBS solution is also reported by Okazaki and Gotoh (Okazaki & Gotoh, 2005). This can be explained by the high concentration of iron in stainless steel (Hansen et al., 1994) and the chemical structure of the passive layer. The 316L passive layer contains high amounts of chromium and iron (Olsson & Landolt, 2003; Shih et al., 2004). The passive layer of stainless steel has enriched an inner Cr oxide and an outer Fe oxide layer where the Fe oxide is not compactly bound to the surface (Omanovic & Roscoe, 1999). Therefore, the iron dissolution rate is higher than other alloying elements in 316L. The nickel release constantly increased over time and long-term precipitation of Ni is unlikely (Figure 6-4b). This observation is based on results from the 14 and 22 week tests in those Ni concentration measurements at 8 weeks were lower than the detection limit. Chromium showed the lowest quantity of the ion released from 316L (Figure 6-4c). In fact, the measurements at 8 weeks were below the detection limit and were only slightly higher at 14 and 22 weeks. The quantity of the Ni release is higher than Chromium.

Chromium precipitates on the surface and forms a passive layer whereas Ni dissolves into the solution. Merritt *et al.* showed that the passive layer of 316L is depleted of nickel when it is immersed in serum or saline solution (Merritt et al., 1983). It seems that after an initial Cr release, the chromium dissolution stops as the values at 14 and 22 weeks are nearly the same.

The BSA did not seem to interact appreciably with chromium as chromium concentration was not significantly different at varying BSA levels. Ni and Cr concentration of 15 patients' blood serum was measured before and for six months after a hip replacement surgery (Blac et al., 1983). The study showed that Cr levels initially rose and then diminished. However, the increase in Ni levels continued even six months after the surgery. The behavior of Mo (Figure 6-4d) was also similar to Cr in terms of the effect of BSA and exposure time. A very low dissolution rate of Cr and Mo was also detected in the PBS solution after seven days of immersion by ICP-mass spectroscopy with 0.05 ng ml^{-1} detection limit (Okazaki & Gotoh, 2005) .

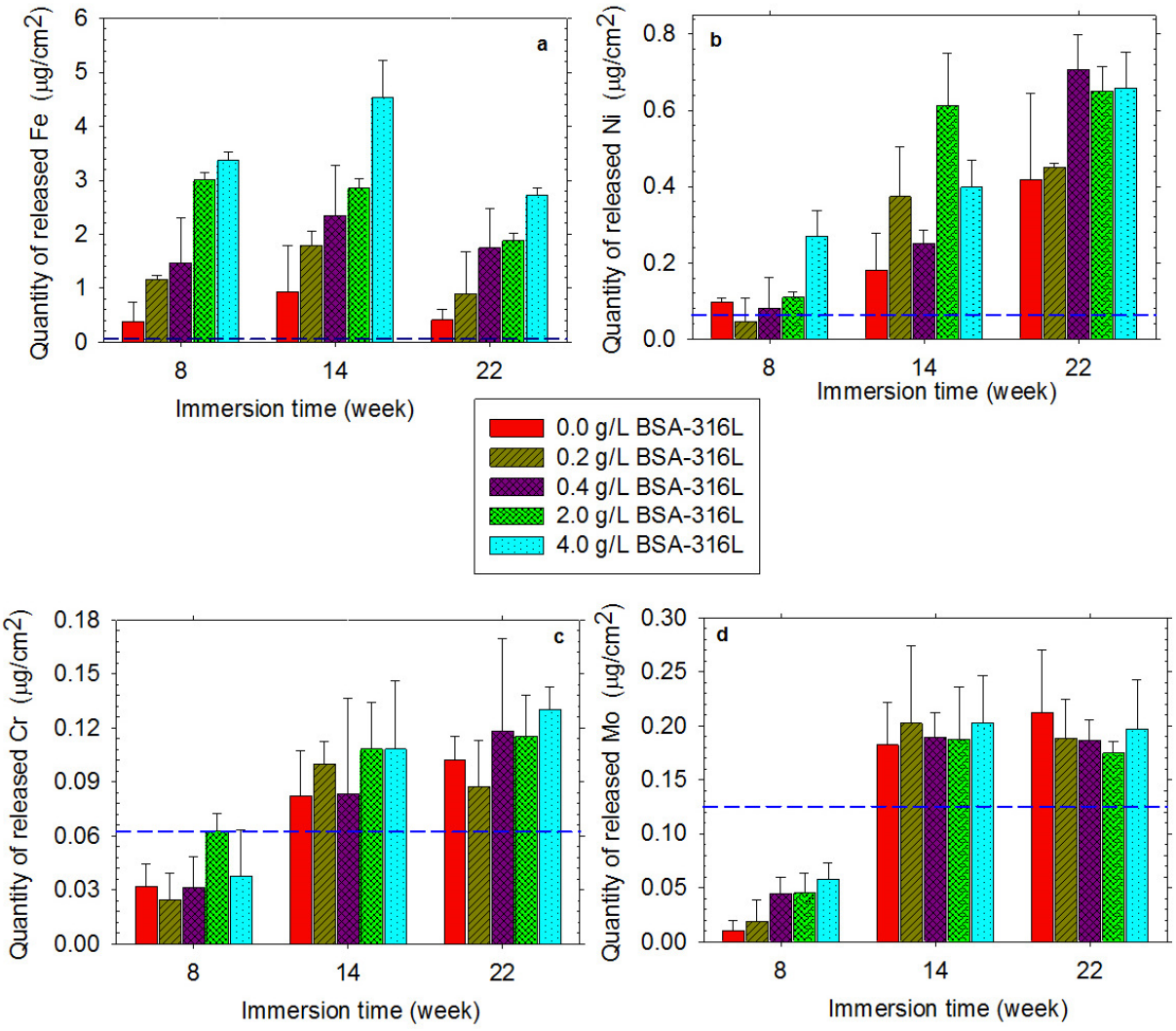

Figure 6-4 : The amount of released a) Fe, b) Ni, c) Cr, d) Mo from 316L into PBS solutions with various BSA concentrations (0 to 4 g L^{-1}) at 37 °C after 8, 14 and 22 weeks. The dash line shows the converted analytical detection limit

Figure 6-5 shows the quantity of Co, Cr, and Mo released for Co-28Cr-6Mo samples. The converted detection limit for Co and Cr is 0.0625 mg cm^{-2}, and the detection limit of Mo is 0.125 mg cm^{-2}. The detected amount of Co was above the detection limit (Figure 6-5a). The

Co release had the highest dissolution rate within 14 weeks of the immersion test and then the amount of Co released diminished. This refers to Co precipitation on the surface of the Co-28Cr-6Mo alloy during a longer time period. Co release was faster than Mo and Cr which can be explained by a higher concentration of Co than other alloying elements. Researchers have also shown that the Co release from the Co-28Cr-6Mo alloys is faster than other alloying components (Lin & Bumgardner, 2004; Okazaki & Gotoh, 2005). The formation of Cr oxide is thermodynamically more favorable than Co oxides/hydroxides based on the Gibb's free energy of formation ($\Delta_f G°$ Co_3O_4=-774 kJ mol^{-1}, $\Delta_f G°$ Co $(OH)_2$= -454.4 kJ mol^{-1}, $\Delta_f G°$ CoO=-214 kJ mol^{-1} and $\Delta_f G°$ Cr_2O_3=-1058.1 kJ mol^{-1} (Speight, 2005)). The ΔG for dissolution reaction of Cr_2O_3 to CrO_4^{2-} and $Cr_2O_7^{2-}$ is more positive than the ΔG for dissolution reaction of Co oxides/hydroxides to Co^{2+}. As a result, the Cr dissolution rate is slower than the Co dissolution rate. The detected amount of Cr released for the Co-28Cr-6Mo alloys is below the detection limit at 8 weeks and slightly increased over time (Figure 6-5b). The Cr release increased over time in the absence of BSA which means that BSA prevented a high Cr release rate during longer immersion times. Mo release of the CoCrMo alloy was higher than the detection limit for 14 and 22 weeks (Figure 6-5c). The addition of BSA to the PBS solution increased the Mo release at 14 weeks. However, this trend was reversed at 22 weeks. Consequently, the Mo dissolution rate is slower at longer exposure times and precipitates on the surface. Interestingly, the XPS result (Table 6-2) showed that the surface Mo concentration of CoCrMo increased at 4 g L^{-1} BSA solutions which could refer to the precipitation of dissolved Mo. In addition, the obtained results from ion release of CoCrMo

alloy supports the results of weight loss in which the amount of Co, Cr, and Mo released decreased after 22 weeks of the immersion test.

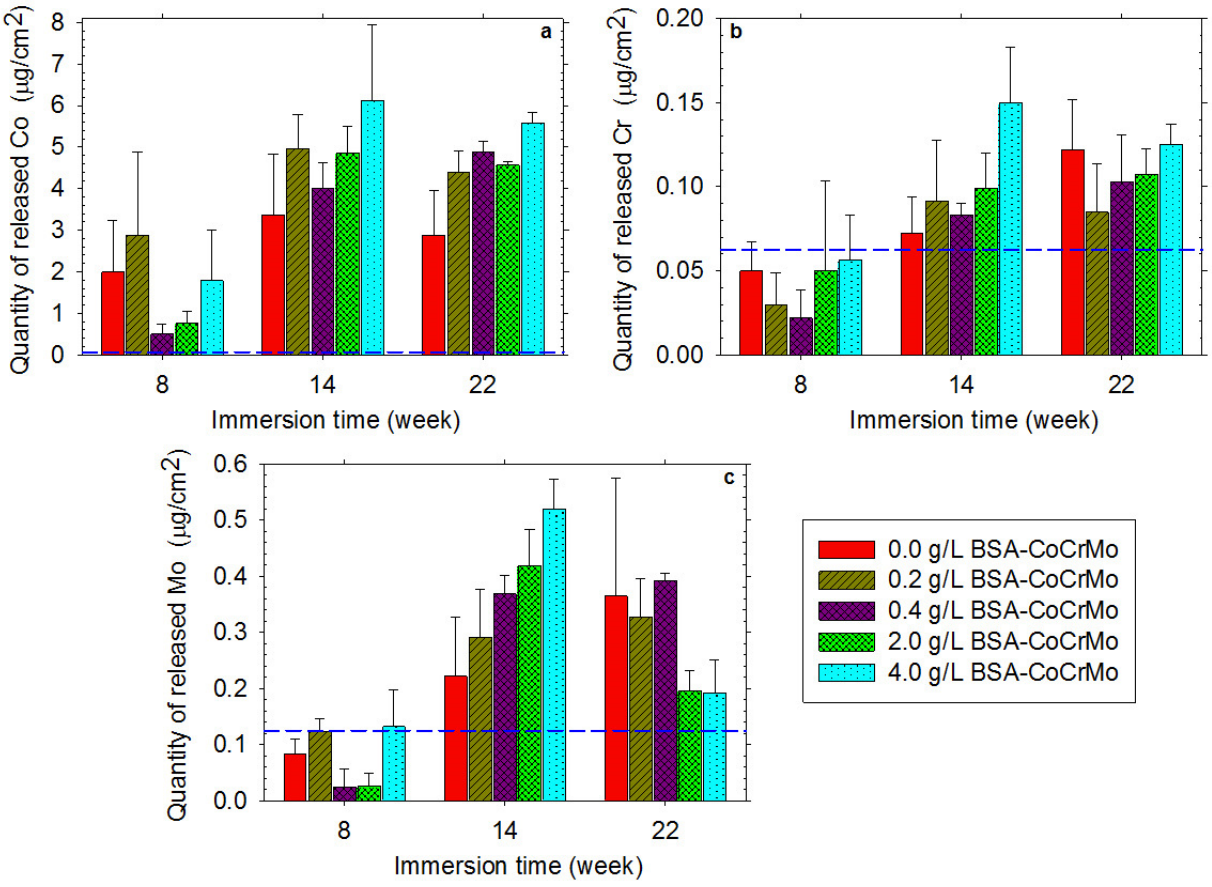

Figure 6-5 : The amount of released a) Co, b) Cr, and c) Mo from Co-28Cr-6Mo into PBS solutiions with various BSA concentrations (0 to 4 g L^{-1}) at 37°C after 8, 14, and 22 weeks. The dash line shows the converted analytical detection limit

The quantities of released Ti and V for the Ti-6Al-4V alloy are presented in Figure 6-6a and b. The major ion released from Ti-6Al-4V alloy is titanium. The detection limit of titanium and vanadium is 0.0625 mg cm^{-2}, as is shown in Figure 6-6. Titanium concentration was much lower than the detection limit when the BSA concentration was lower than 4 g L^{-1} (Figure 6-6a). On the other hand, titanium released into the solution considerably increased

at longer exposure times (from 4 to 8 weeks). However, increasing the exposure time to 22 weeks did not increase the titanium release and the Ti release stopped after 14 weeks. Ion release of NiTi wires in artificial saliva at a 6.25 pH was investigated by Huang *et al.* (Huang et al., 2003). In their study, the amount of Ti release increased up to 14 days and then stopped with longer immersion periods. The highest Ti dissolution is reached in a shorter period of immersion testing compared to our results which could be related to the different test environment.

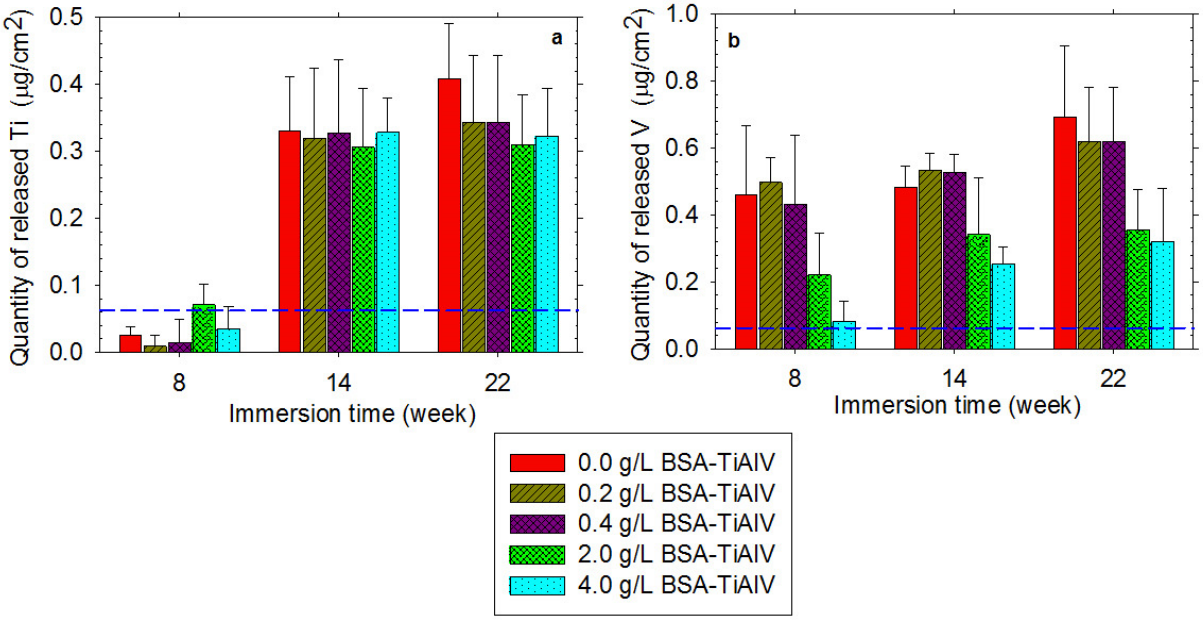

Figure 6-6 : The amount of released a) Ti, and b) V from Ti-6Al-4V into PBS solutiions with various BSA concentrations (0 to 4 g L^{-1}) at 37°C after 8, 14, and 22 weeks. The dash line shows the converted analytical detection limit

In addition, variation of BSA did not significantly affect the release of Ti at 14 and 22 week exposure periods. However, BSA impeded the vanadium release at all the exposure times (Figure 6-6b). Vanadium release was also time dependent in that vanadium concentration increased with longer exposure periods. Al released from the Ti-6Al-4V alloy was not detected by the ICP-OES method.

6.3 Surface characterization

The survey spectra of passivated 316L, Co-28Cr-6Mo, and Ti-6Al-4V samples after 22 weeks of exposure to PBS and BSA solutions are shown in Figure 6-7, Figure 6-8, Figure 6-9. The general features of the spectra are peaks of carbon (C 1s) and oxygen (O 1s) which are observed on all the samples, while nitrogen (N 1s) was only detected for samples immersed in solutions containing BSA. BSA has peptides of CO–NH, carboxyl (–COOH) and amino ($-NH_2$) groups (Frateur et al., 2006; Takemoto et al., 2005). Therefore, N 1s and a part of the C 1s peaks refer to a presence of BSA. Carbon contamination is unavoidable in XPS studies; therefore, a part of the C 1s peaks possibly corresponds to carbon contamination.

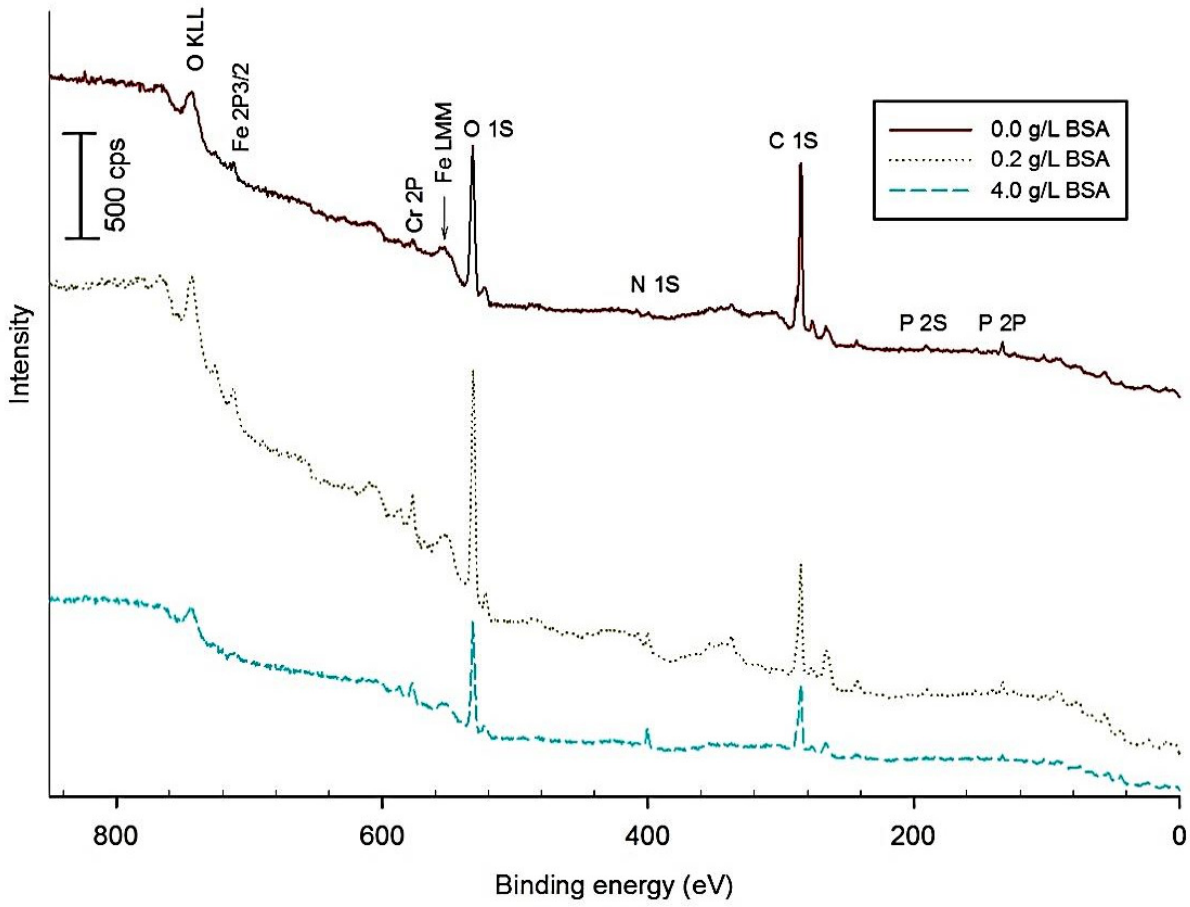

Figure 6-7 : XPS Survey scan of 316L after 22 weeks of exposure in solutions of PBS with BSA concentrations of 0, 0.2, and 4 g L^{-1} at 37 °C

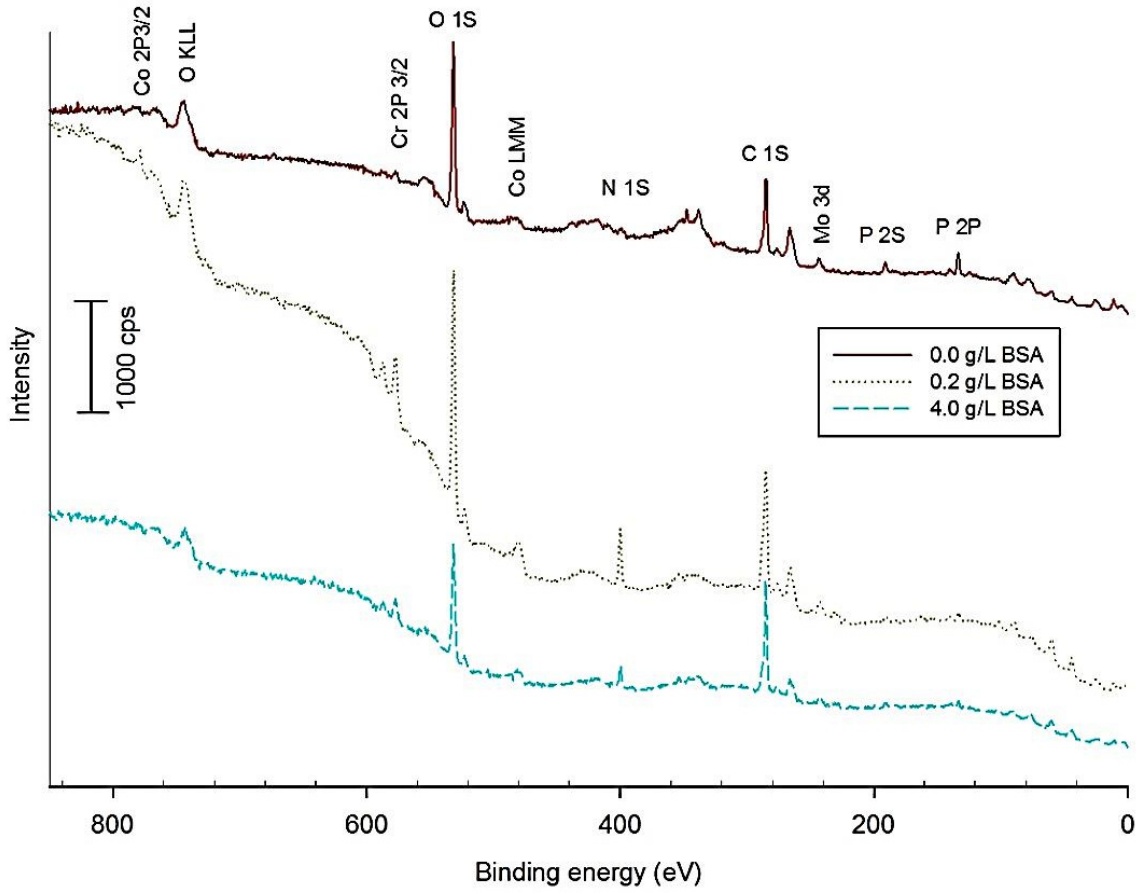

Figure 6-8 : XPS Survey scan of Co-28Cr-6Mo after 22 weeks of exposure in solutions of PBS with BSA concentrations of 0, 0.2, and 4 g L^{-1} at 37 °C

In addition to peaks of C 1s, O 1s, and N 1s, iron and chromium for 316L (Figure 6-7), chromium, molybdenum, and cobalt for Co-28Cr-6Mo (Figure 6-8), and titanium for Ti-6Al-4V (Figure 6-9) alloys were identified.

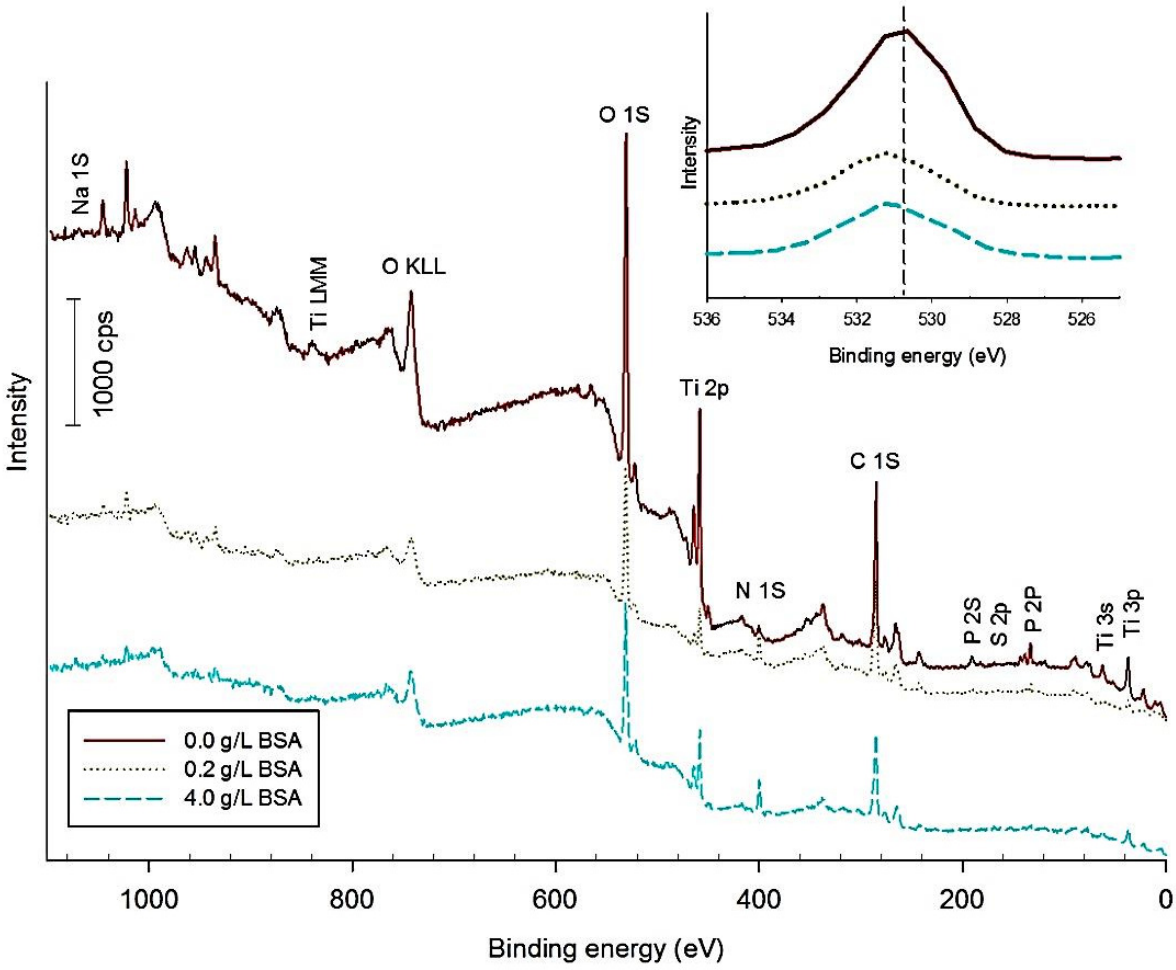

Figure 6-9 : XPS Survey scan of Ti-6Al-4V after 22 weeks of exposure in solutions of PBS with BSA concentrations of 0, 0.2, and 4 g L^{-1} at 37 °C

The surface concentrations of these elements in at.% are summarized in Table 6-2. In addition, the ratios of Cr/Fe in the 316L and Cr/Co in the Co-28Cr-6Mo surface oxide films along with the ratio of Ti in the oxide layer to the bulk chemical composition of Ti-6Al-4V are calculated and reported in Table 6-2.

Table 6-2 : Surface film composition of 316L, Co-28Cr-6Mo, and Ti-6Al-4V alloys after 22 weeks exposure to the solutions of PBS with BSA concentrations of 0, 0.2, and 4 g L^{-1} at 37 °C; the ratios of Cr/Fe in the 316L and Cr/Co in the Co-28Cr-6Mo surface oxide films along with the ratio of Ti in the oxide layer to the bulk chemical composition of Ti-6Al-4V

Sample	BSA g L^{-1}	Atomic concentration (at. %)							Ratio						
		Fe	Cr	Co	Mo	Ti	N	O	P	Na	S	C	Cr/Fe	Cr/ Co	Ti/ Bulk
		2p	2p	2p	3d	2p	1s	1s	2p	1s	2p	1s			
316L	0	1.3	1.0	-		-	0	50.0	3.5	-	-	65.2	0.77	-	-
	0.2	2.7	3.0	-	-	-	4.4	41.9	2.6	-	-	45.5	1.09	-	-
	4	1.4	2.1	-	-	-	7.4	34.2	1.3	-	-	53.5	1.45	-	-
Co-28Cr-6Mo	0	-	1.3	-	0.2	-	0	44.6	6.1	-	-	47.9	-	-	-
	0.2	-	3.4	0.9	0.3	-	9.2	32.6	1.9	-	-	51.6	-	3.92	-
	4	-	2.8	0.8	0.5	-	7.7	29.2	1.6	-	-	57.4	-	3.24	-
Ti-6Al-4V	0	-	-	-	-	7.7	-	46.7	2.7	0.2	-	42.6	-	-	0.24
	0.2	-	-	-	-	3.0	9.3	32.0	1.7	0.5	1.2	52.3	-	-	0.11
	4	-	-	-	-	4.6	9.0	36.0	1.7	0.9	1.0	44.2	-	-	0.16

The surface analysis using XPS data showed that by increasing the BSA concentration, both the oxygen and phosphorous content of the 316L surface decreased while the nitrogen content increased. Phosphorous was present in the background PBS solution. The decrease in phosphorous and oxygen can be related to a blockage of the 316L surface by BSA. Nitrogen concentration, as an indication of BSA adsorption, increased. Thus, this refers to adsorption of BSA and more adsorption of BSA at higher concentrations as well as the blockage of the surface from the background solution. The iron and chromium content of the 316L specimens increased up to the BSA concentration of 0.2 g L^{-1} and then decreased at 4 g L^{-1}. Therefore, the higher the amount of BSA that adsorbs onto the 316L alloy, the less the

amount of iron and chromium that precipitates on the alloy's surface. This statement can be supported by referring to a study done by Omanovic and Roscoe (Omanovic & Roscoe, 1999). Their study showed that BSA adsorption caused an increase in metal dissolution at open circuit potential and was accompanied by the transfer of charge. They proposed that the adsorption of BSA on stainless steel involves the interaction of negatively-charged carboxylate groups of the proteins with the stainless steel surface. The Cr/Fe ratio of the 316L oxide layer is less than one but this ratio is considerably higher in the alloy composition. This ratio has a higher value in PBS solution containing BSA which indicates the affinity of iron to react with BSA to form a dissolvable compound. The higher dissolution of iron in a higher BSA concentration can support this interpretation. In addition, the passive layers that form in the presence of protein are thicker (Sousa & Barbosa, 1991), likely due to the growth of chromium oxides.

The addition of BSA decreased the surface phosphorous and oxygen concentration of the Co-28Cr-6Mo alloy because BSA could form a negatively-charged barrier film (Lewis et al., 2005) blocking oxygen and phosphorous from the surface. The maximum nitrogen was observed on the surface of the Co-28Cr-6Mo alloy at a BSA concentration of 0.2 g L^{-1} where oxygen and phosphorous concentrations on the surface were greater than those in the presence of 4 g L^{-1} BSA. In addition, cobalt and chromium had higher concentrations when the Co-28Cr-6Mo samples were immersed in 0.2 g L^{-1} BSA solutions. The reaction of positively-charged ions with negatively charged albumin can produce an adsorbed film (Valero Vidal & Muñoz, 2008) or metal/protein/hydroxylated compounds (Khan et al., 1999). In the solution with

low BSA concentration, formation of an adsorbed layer of BSA can cause growth of the oxide layer which results in an increase in cobalt and chromium surface concentrations. However, the formation of the compounds increased which could interrupt the development of the adsorbed layer in the solution with a high BSA concentration. Therefore, lower amounts of cobalt, chromium, and nitrogen were detected on the surface of Co-28Cr-6Mo alloy in the high BSA concentration. In contrast to cobalt and chromium, the Mo content of CoCrMo increased at a higher BSA concentration. It seems that Mo forms stable organometallic compounds which precipitate on the surface rather than dissolving into the solution. The calculated Cr/Co ratio (Table 6-2) indicates that the chromium precipitation is about 3.5 times faster than cobalt, which confirms the thermodynamic stability of Cr oxides compared to Co oxides. The Cr/Co ratio decreased in high BSA concentrations because protein has a lower affinity for cobalt than for chromium (Lewis et al., 2005). Therefore, the dissolution rate of Cr increased in the presence of the high BSA concentration. The absence of Co in the solution without BSA also confirms the affinity of protein to Co.

The phosphorous content of the Ti-6Al-4V alloys decreased when they were immersed in PBS and BSA solution. The phosphorous content did not change by changing BSA concentrations while the maximum nitrogen concentration of the Ti-6Al-4V alloys was observed at 0.2 g L^{-1} BSA. The higher adsorption of BSA at low BSA concentrations is similar to the adsorption of BSA on the Co-28Cr-6Mo alloy surface, which was discussed previously. The surface content of Ti-6Al-4V became enriched by oxygen and titanium at higher BSA concentrations. Therefore, the growth of the oxide layer is faster in PBS solutions with high

BSA concentrations. In addition, BSA can block the terminal oxygen atoms of the Ti-6Al-4V passive layer with electrolytes (Contu et al., 2002), which impede the charge transfer responsible for the dissolution of the passive film. Sodium was also found on the surface of the Ti-6Al-4V alloys in the presence of BSA whereas this element was not detected on the surface of Co-28Cr-6Mo and 316L alloys (Table 6-2). Takemoto *et al.* also reported the adsorption of sodium on the surface of titanium in an albumin solution (Takemoto et al., 2005). It seems that the presence of BSA leads to the adsorption of sodium on the Ti surface because it has a higher concentration in a solution containing 4 g L^{-1} BSA. The ratio of the titanium in the surface oxide film to its bulk concentration is reported in Table 6-2. The highest ratio was obtained for the samples immersed in solutions without BSA where no nitrogen and a low amount of carbon and sodium were adsorbed on the passive layer. It is assumed that the surface oxide film has two layers based on the study done by Hiromoto *et al.* (Hiromoto et al., 2004). The inner oxide layer contains oxygen, cationic titanium, and anions from the solution whereas the outer layer includes carbon, nitrogen, and adsorbed biomolecules. Therefore, the inner oxide layer is enriched with titanium as it was the only alloy component present in the oxide surface along with small amounts of sodium and phosphorus.

In the solution without BSA, an oxygen peak was detected at about 530 eV corresponding to a metal-oxygen bond (Lin & Bumgardner, 2004). For example, the oxygen peak of the Ti-6Al-4V alloy was detected at 530.8 eV showing the formation of TiO and TiO_2 (Lin & Bumgardner, 2004; Milosev et al., 2000). Oxygen peaks were shifted to higher binding energy levels (e.g

531.2 eV) in solutions containing BSA. This binding energy is attributed to oxygen bonds in organic compounds (Lin & Bumgardner, 2004) that indicate adsorption of BSA on the surface of the bio-implant alloys. The shift in the oxygen peak energy levels were also observed in this study and the oxygen peak on titanium is separately presented in the inset of Figure 6-9. The O 1s peaks were deconvoluted into two sub-peaks with binding energies of 530.8 and 532.2 eV. Figure 6-10 presents O 1s peak deconvolution of the Ti-6Al-4V alloy exposed to BSA solutions.

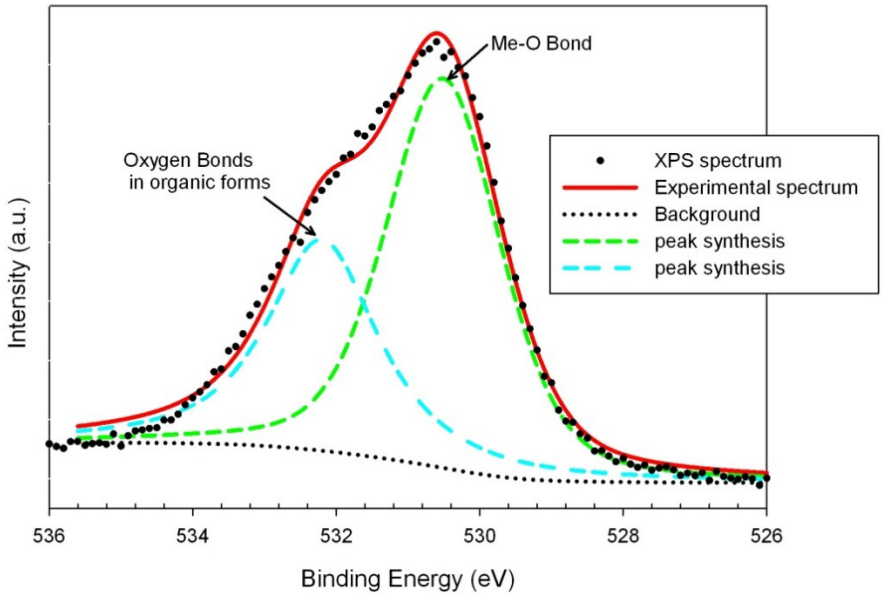

Figure 6-10 : Measured high resolution spectra of O 1s of the Ti-6Al-4V alloy after 22 weeks of exposure in PBS solutions with 4 g L^{-1} BSA concentration at 37 °C along with the peak doublets

The software XPSPEAK was used for curve fitting and the Shirley method was employed for background subtraction of all the peaks deconvolution. The high resolution spectra of Fe and Cr peaks of 316L are shown in Figure 6-11 and Figure 6-12. The Cr peak was decomposed into two peaks originating from Cr^{3+} $2p_{1/2}$ and $2p_{3/2}$ with binding energies of 576.4 and 585.4

eV, respectively. Similar findings are noted here by Hiromoto *et al.* (Hiromoto et al., 2005) and Hanawa *et al.* (Hanawa et al., 2001). In addition, XPS results revealed the presence of Fe on the oxide layer of 316L. The Fe peak refers to the binding energy of 710.3 eV corresponding to Fe^{3+} $2p_{3/2}$. Bastidas *et al.* (Bastidas et al., 2002) also found the existence of iron oxide at a binding energy of 710.3 eV on stainless steel surfaces.

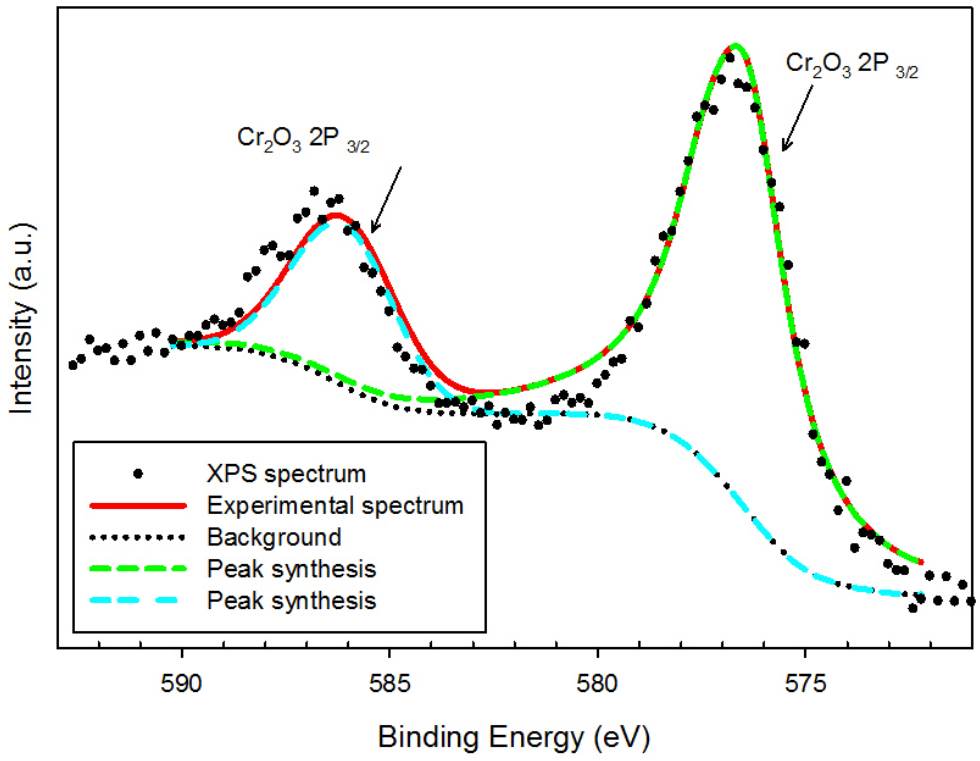

Figure 6-11 : Measured high resolution spectra of Cr 2p of the 316L sample after 22 weeks of exposure in PBS solutions with 4 g L^{-1} BSA concentration at 37 °C along with the peak doublets

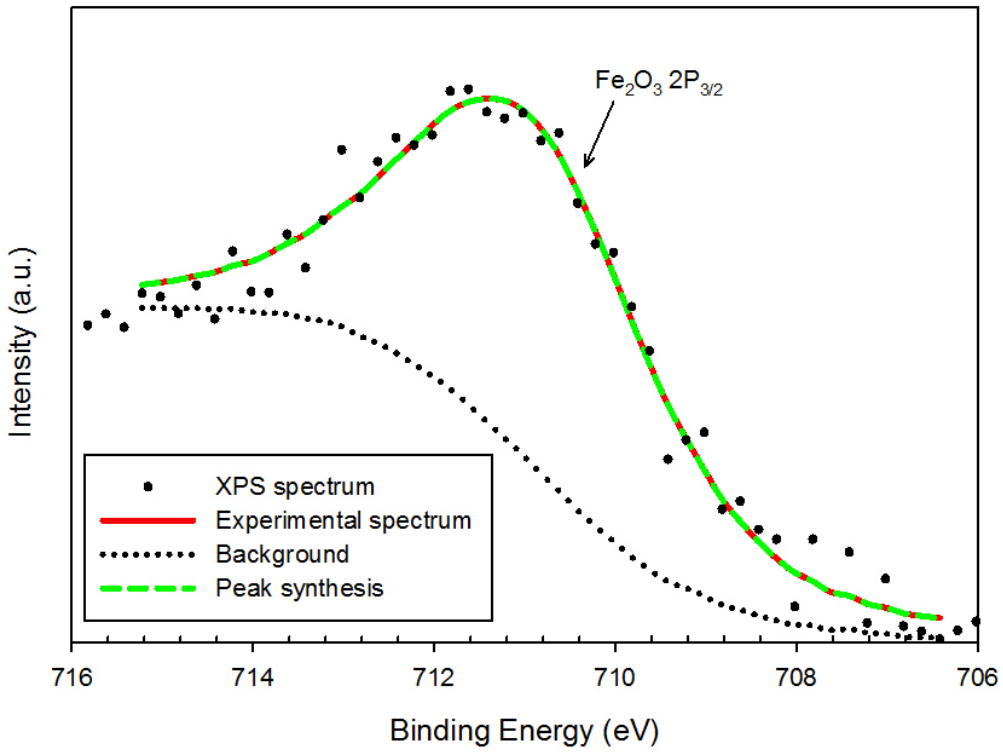

Figure 6-12 : Measured high resolution spectra of Fe 2p of the 316L sample after 22 weeks of exposure in PBS solutions with 4 g L^{-1} BSA concentration at 37 °C along with the peak doublets

Figure 6-13, Figure 6-14 and Figure 6-15 show the high resolution spectra of Co, Cr, and Mo peaks detected on the Co-28Cr-6Mo surface.

The Co peak was deconvoluted to two doublets at binding energies of 778 and 780.9 eV corresponding to the presence of Co^{o} $2p_{3/2}$ and Co^{2+} $2p_{3/2}$.

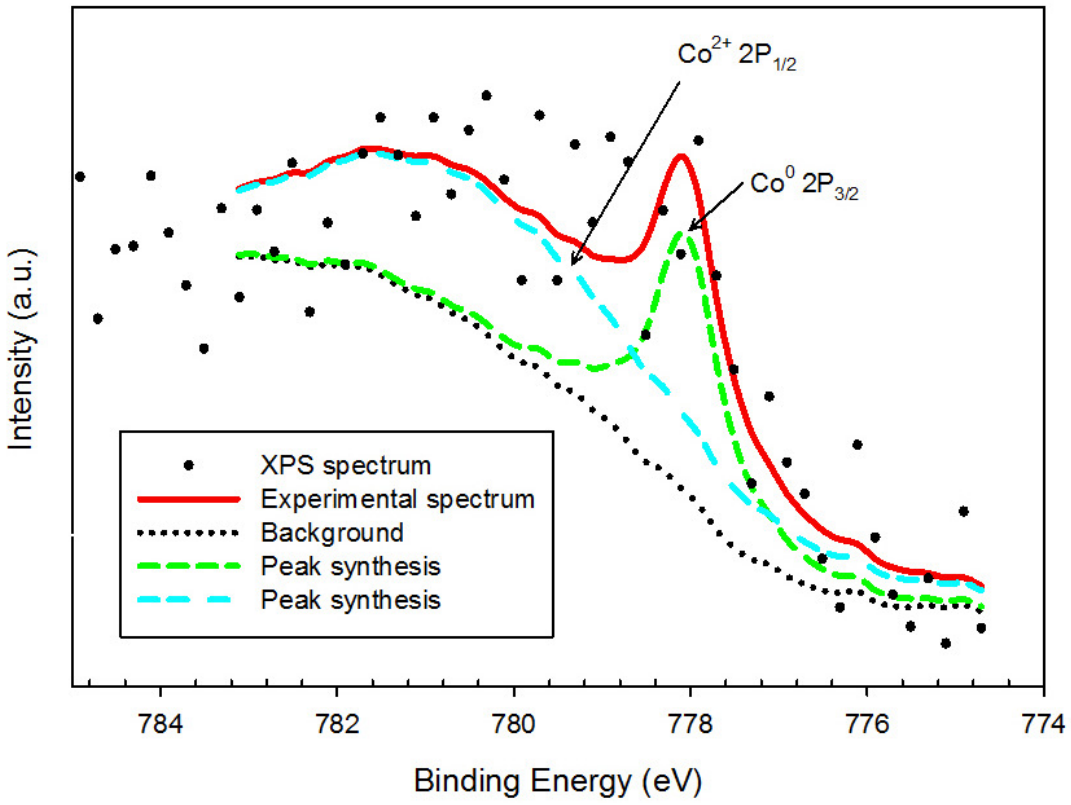

Figure 6-13 : Measured high resolution spectra of Co 2p of the Co-28Cr-6Mo sample after 22 weeks of exposure in PBS solutions with 4 g L^{-1} BSA concentration at 37 °C along with the peak doublets

The XPS spectrum of molybdenum was decomposed to three doublet peaks of Mo^{o} $3d_{5/2}$ at 227.6 eV, Mo^{o} $3d_{3/2}$ at 231.2 eV and Mo^{6+} $3d_{5/2}$ at 235.5 eV (Figure 6-14).

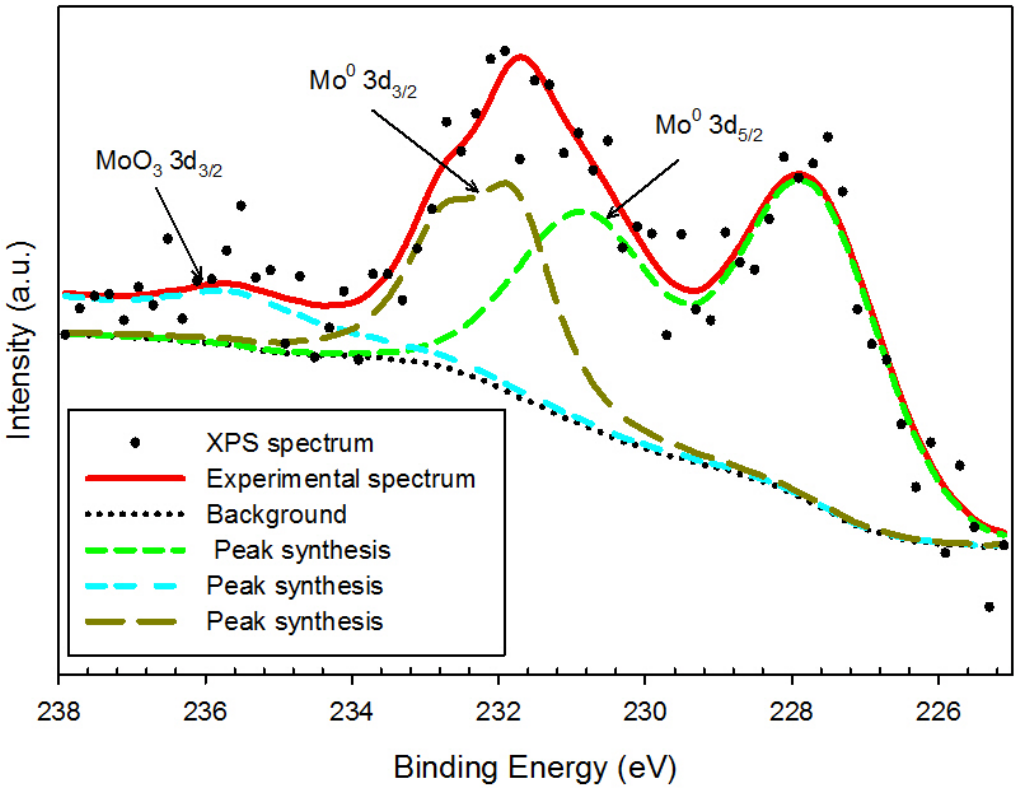

Figure 6-14 : Measured high resolution spectra of Mo 3d of the Co-28Cr-6Mo sample after 22 weeks of exposure in PBS solutions with 4 g L^{-1} BSA concentration at 37 °C along with the peak doublets

The deconvolution of a high resolution Cr peak for the CoCrMo alloy is similar to 316L (Figure 6-11). Hodgson *et al.* (Hodgson et al., 2004) and Hanawa *et al.* (Hanawa et al., 2001) also reported the presence of oxides of Co, Cr, and Mo on the surface of the CoCrMo alloy.

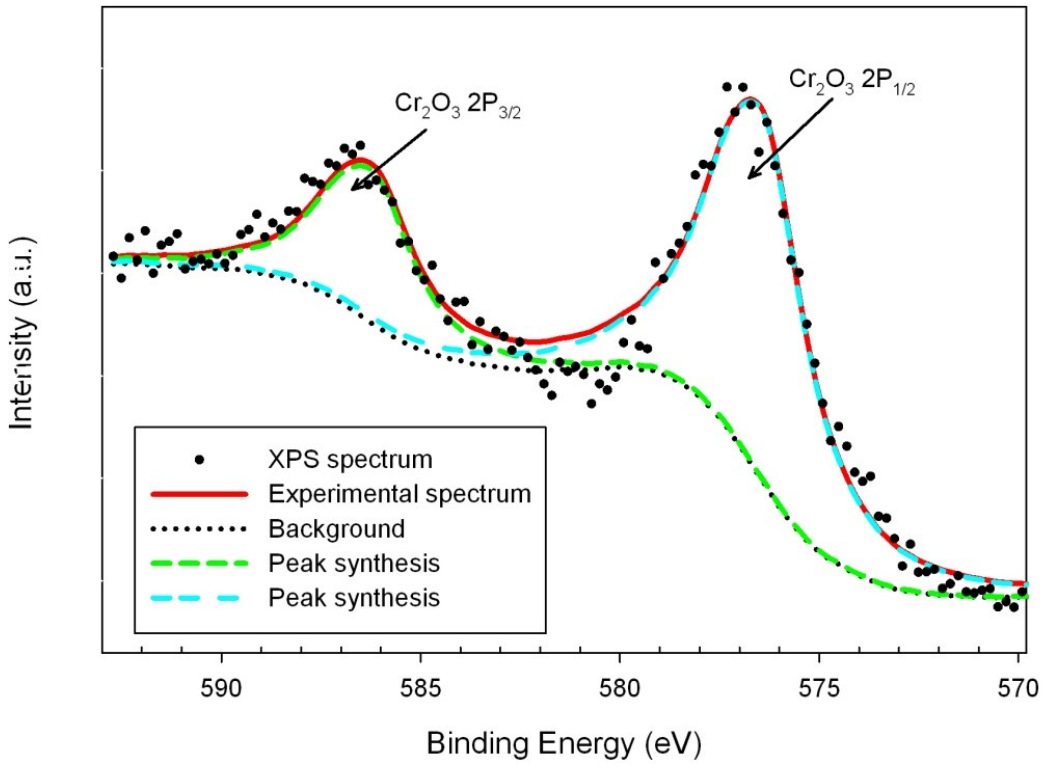

Figure 6-15 : Measured high resolution spectra of Cr 2p of the Co-28Cr-6Mo sample after 22 weeks of exposure in PBS solutions with 4 g L^{-1} BSA concentration at 37 °C along with the peak doublets

A high resolution Ti spectrum for the Ti-6Al-4V alloy is illustrated in Figure 6-16. The peak was attributed to Ti^{4+} $2p_{1/2}$ at binding energy of 464.2 eV and to Ti^{4+} $2p_{3/2}$ at binding energy of 458.4 eV. The TiO_2 peak was observed as Ti $2p_{3/2}$ by Sleigh *et al.* (Sleigh et al., 1996) and illustrated as two Ti $2p_{1/2}$ and Ti $2p_{3/2}$ peaks by Healy and Ducheyne (Healy & Ducheyne, 1992).

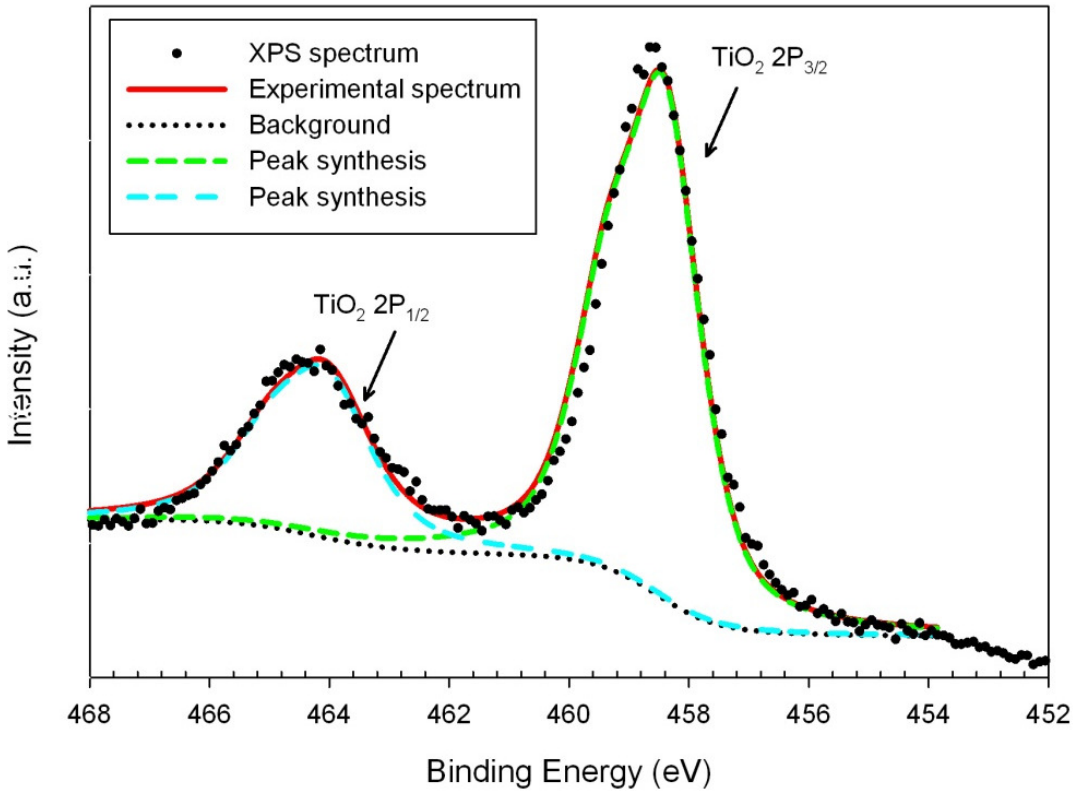

Figure 6-16 : Measured high resolution spectra of Ti 2p of the Ti-6Al-4V sample after 22 weeks of exposure to PBS solutions with 4 g L^{-1} BSA concentration at 37 °C along with the peak doublets

6.4 Summary

The experimental results have led us to the following conclusions:

- Weight loss of the specimens was observed up to 14 weeks exposure in the solution. However, weight of the samples increased slightly after 14 weeks due to the precipitation of dissolved ions.

- Corrosion rates of the samples were calculated from mass loss. They are consistent with the corrosion rate calculated from EIS data in our previous work (Karimi et al., 2011) .
- Fe dissolution of the 316L was rapid up to 14 weeks immersion in PBS and BSA solutions followed by a decrease in the amount of Fe released. Similar behavior was determined for the Co dissolution from the CoCrMo alloy that confirms the results of weight loss.
- Vanadium released from Ti-6Al-4V alloy is dependent on time and, although it has lower alloying composition than Ti, its dissolution rate is almost the same as titanium. The variation of BSA concentration did not significantly affect the Ti release and the dissolution was halted after 14 weeks of immersion.
- The XPS results showed that the main element of the oxide layer on CoCrMo and 316L is Cr. This is congruent with the ICP-OES results in which Cr has the lowest dissolution rate compared to the other alloying elements of the 316L and CoCrMo alloys.

Chapter 7: Electrochemical corrosion behavior of orthopedic biomaterials in the presence of human serum albumin

Relatively few studies related to the effect of protein concentration variations in a wide concentration range have been presented. Within these few studies, the electrochemical corrosion performance of the common metallic biomaterials was mostly investigated in the presence of animal serum albumin (e.g. BSA) but not human serum albumin (HSA). Using HSA instead of animal serum will help us to simulate a more realistic body environment as well as to investigate the effect of protein type on corrosion behavior of the metallic biomaterials. Therefore, the effect of HSA in a concentration range of 0 to 4 g L^{-1} in phosphate-buffered saline (PBS) on the electrochemical corrosion behavior of AISI 316L, wrought Co-28Cr-6Mo and Ti-6Al-4V was investigated by advanced electrochemical corrosion experiments (OCP, PDP, EIS, and LPR). In addition to the electrochemical techniques used earlier, a cyclic voltammetry experiment was performed to compare the kinetics of the electrode reaction in PBS-BSA and PBS-HSA solutions.

7.1 OCP measurements

In Figure 7-1, the OCP variation of 316, Co-28Cr-6Mo and Ti-6Al-4V alloys obtained after one hour of immersion of the samples in the PBS solutions containing various HSA concentrations are shown. In addition, the OCPs of those alloys in PBS-BSA solutions are included in Figure 7-1 which were measured from our previous work (Karimi et al., 2011). In these figures, the error bars are indicative of the calculated standard deviations based on

the 3-times replication of the OCP experiment. The reproducibility of OCP of 316L in PBS solutions having 0.2 g L^{-1} HAS is presented in Figure 7-2.

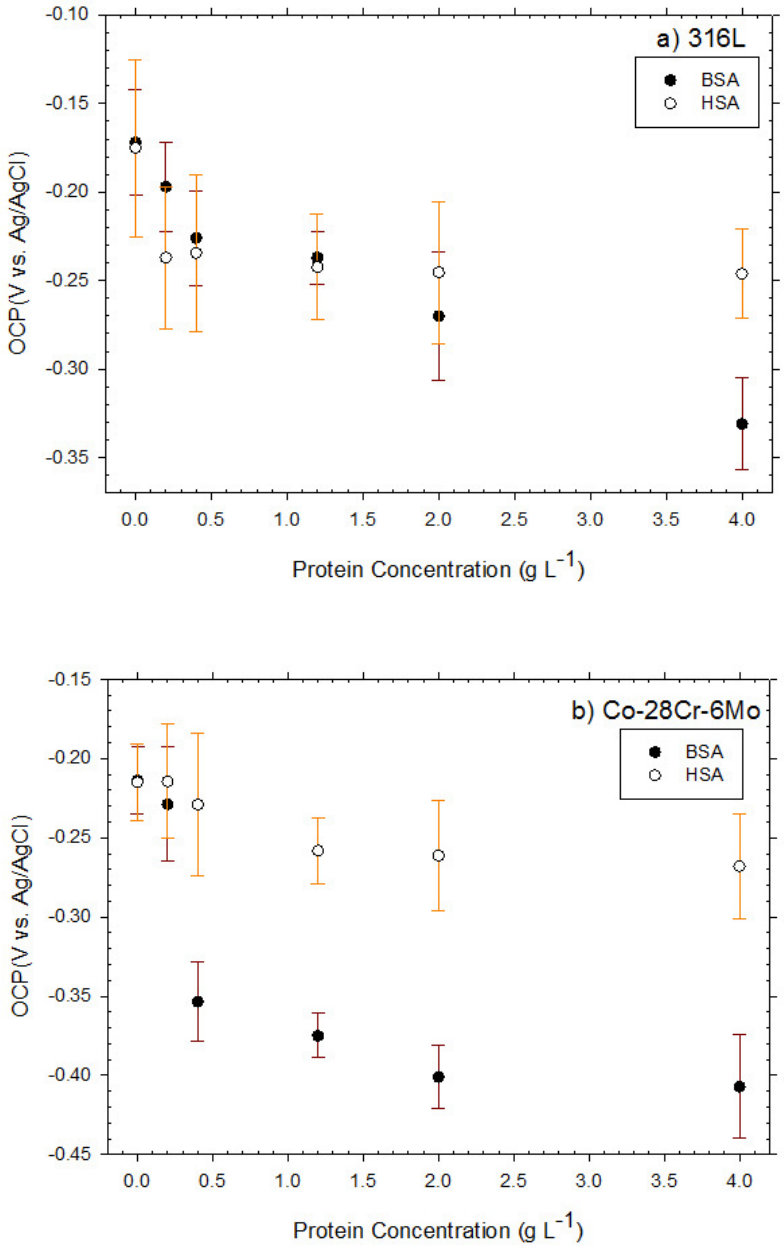

Figure 7-1 : Measured OCPs of a) 316L, b) Co-28Cr-6Mo and c) Ti-6Al-4V alloys as a function of HSA and BSA concentrations after one hour immersion in aerated PBS-HSA and PBS-BSA solutions at 37°C and a pH of 7.4

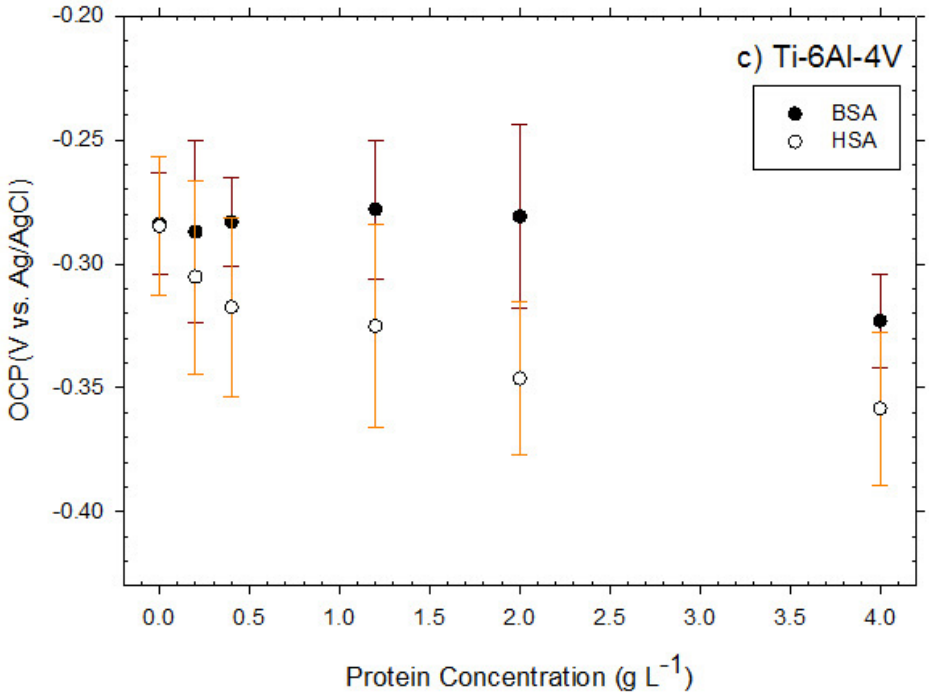

Figure 7-1 : (Cont'd) Measured OCPs of a) 316L, b) Co-28Cr-6Mo and c) Ti-6Al-4V alloys as a function of HSA and BSA concentrations after one hour immersion in aerated PBS-HSA and PBS-BSA solutions at 37°C and a pH of 7.4

The corrosion potential of all the alloys shifted to a lower value when either HSA or BSA was added to the PBS solutions. This observation was also reported by Valero Vidal & Muñoz (Valero Vidal & Muñoz, 2008) for 316L and CoCrMo and by Wang *et al*. (Wang et al., 2012) for Nb in PBS and albumin solutions. HSA, similar to BSA, could have an inhibitive action on cathodic reactions, i.e. hydrogen evolution reactions, by blocking the active sites on the samples (Karimi et al., 2011; Tang et al., 2006; Valero Vidal & Muñoz, 2008).

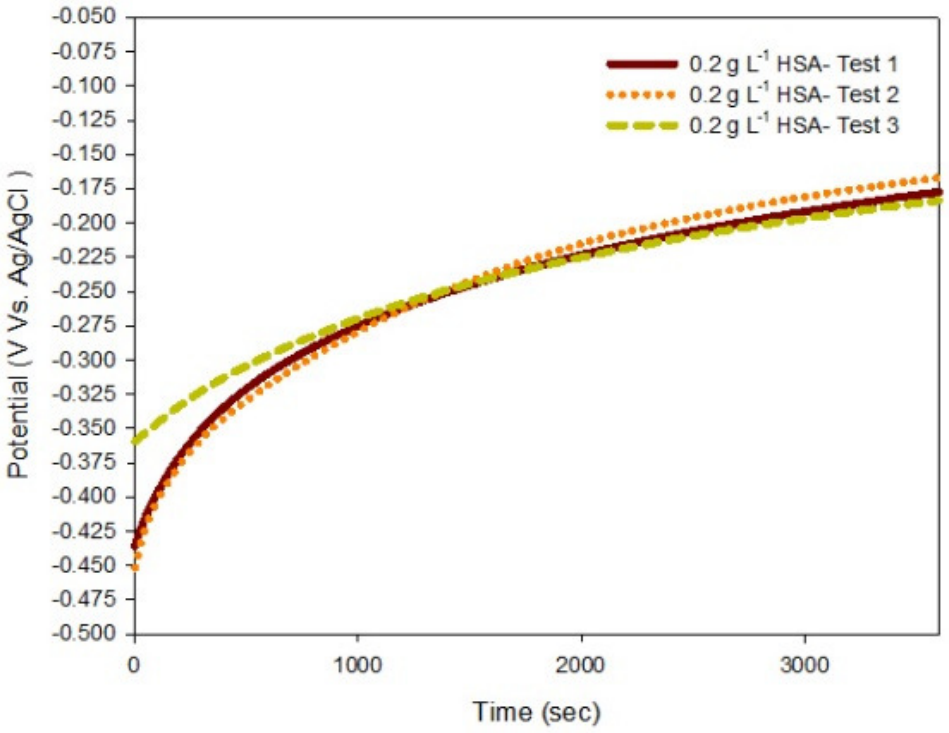

Figure 7-2 : Reproducible OCP values of 316L alloys within one hour immersion in aerated PBS with 0.2 g L^{-1} HSA solutions at 37°C and a pH of 7.4

Although the addition of HSA dropped the OCP of 316L, the increase of HSA concentrations from 0.2 to 4 g L^{-1} did not change the OCP of 316L. The stainless steel OCP drop of 20-30 mV was also determined by Omanovic and Roscoe (Omanovic & Roscoe, 1999) for a PBS solution containing 1.5 mg L^{-1} BSA. The shift of OCP in the presence of HSA could result from the changes in the iron dissolution and hydrogen evolution rates. The rate of iron dissolution from 316L is the fastest among other alloying elements in the PBS and protein solution (Karimi et al., 2012). The outer part of the passive layer mostly contains iron oxides and hydroxides (Omanovic & Roscoe, 1999) and human serum albumin has a high affinity to bind

to iron (Porath & Olin, 1983). Therefore, the presence of HSA could change iron dissolution and hydrogen evolution.

The OCP values of Co-28Cr-6Mo alloy in the presence of 0 and 0.2 g L^{-1} were almost equal (Figure 7-1 b). The increase of the HSA concentration from 0.2 to 1.2 g L^{-1} decreased the OCP of the Co-28Cr-6Mo alloy. The OCP then reached a fairly steady value for HSA concentrations higher than 1.2 g L^{-1}. The dissolution of cobalt from the CoCrMo alloy in the presence of protein could reduce the OCP as has been reported by other researchers (Clark & Williams, 2004; Hiromoto et al., 2005; Kragh-Hansen et al., 2002). Cobalt can bind to the N-terminus of HSA (Bar-Or et al., 2008; Liang et al., 2001) or other binding sites of HSA (Mothes & Faller, 2007). Therefore, cobalt dissolution from the Co-28Cr-6Mo alloy could lead to the drop of OCP at low HSA concentrations (up to the HSA concentration of 1.2 g L^{-1}) where the rate of cobalt dissolution is likely faster than protein adsorption. At the higher HSA concentrations, the OCP reached a steady value where protein adsorption and cobalt dissolution occurred simultaneously.

The OCP of Ti-6Al-4V alloys slightly decreased when the HSA concentrations were increased (Figure 7-1 c). In the neutral solutions, both the HSA and Ti-6Al-4V surface are negatively charged (Oliva et al., 2003). Therefore, the protein adsorption is most likely dependent on hydration effects (Ellingsen, 1991; Klinger et al., 1997; Wassell & Embery, 1996). The oxide layer of Ti-6Al-4V alloys is hydrophobic (Sunny & Sharma, 1991) which accelerates protein

adsorption by the replacement of HSA with water molecules. This could shift the OCP of the Ti-6Al-4V alloy to a lower potential in the presence of HSA.

7.2 Cyclic voltammetry

The pre-treatment of the electrode with continuous cycling made the electrode surface inert; therefore, the potential drop across the oxide film could be neglected. The selected potential regions were around the OCP of the specimens where the peaks were stable. In de-aerated PBS solutions, the measured OCPs of 316L, CoCrMo, and Ti-6Al-4V alloys were about -0.41, -0.45, and -0.63 V vs. Ag/AgCl, respectively. The cyclic voltammogram of 316L, CoCrMo, and Ti-6Al-4V alloys are shown in Figure 7-3 a, b, and c. Baselines (dotted lines) used to determine the anodic current peak (i_{pa}) are also illustrated in these Figures.

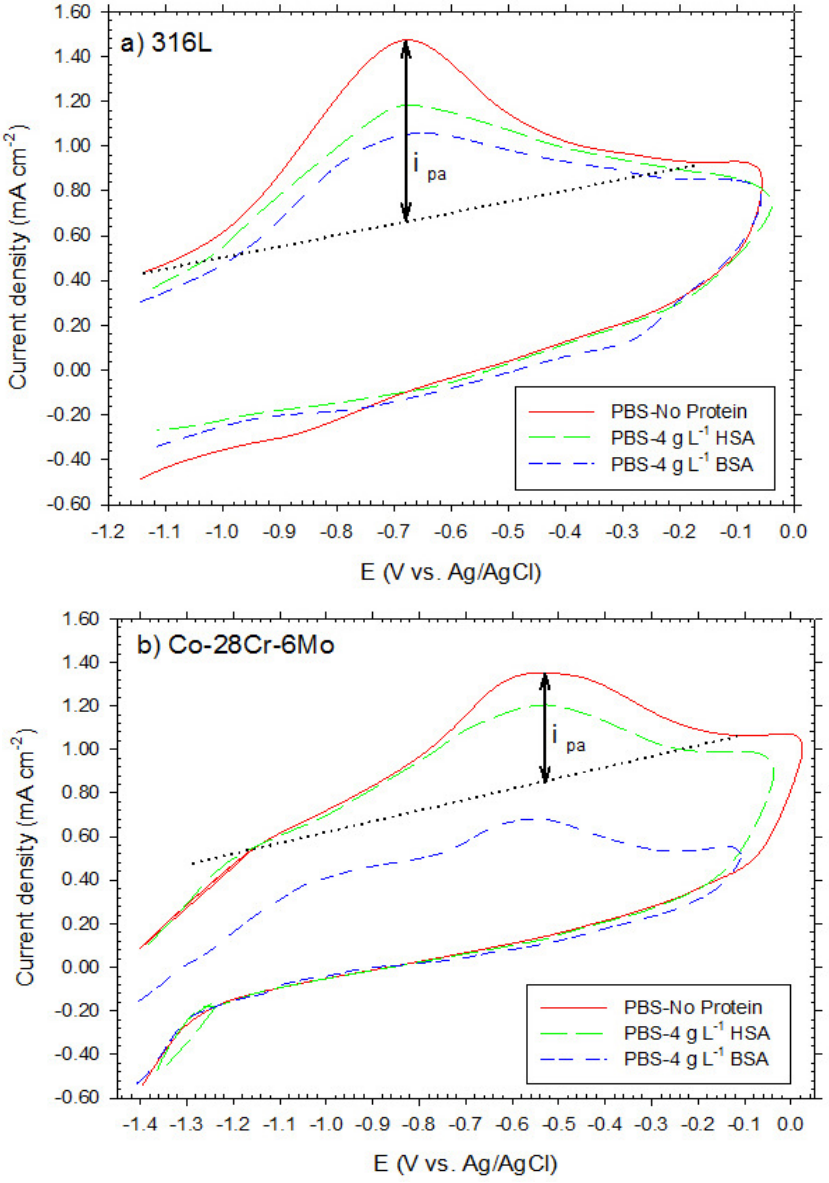

Figure 7-3: Cyclic voltammograms of a) 316L, b) Co-28Cr-6Mo, and c) Ti-6Al-4V alloys in deaerated PBS solutions containing either 4 g L^{-1} HSA or BSA at 37°C and a pH of 7.2

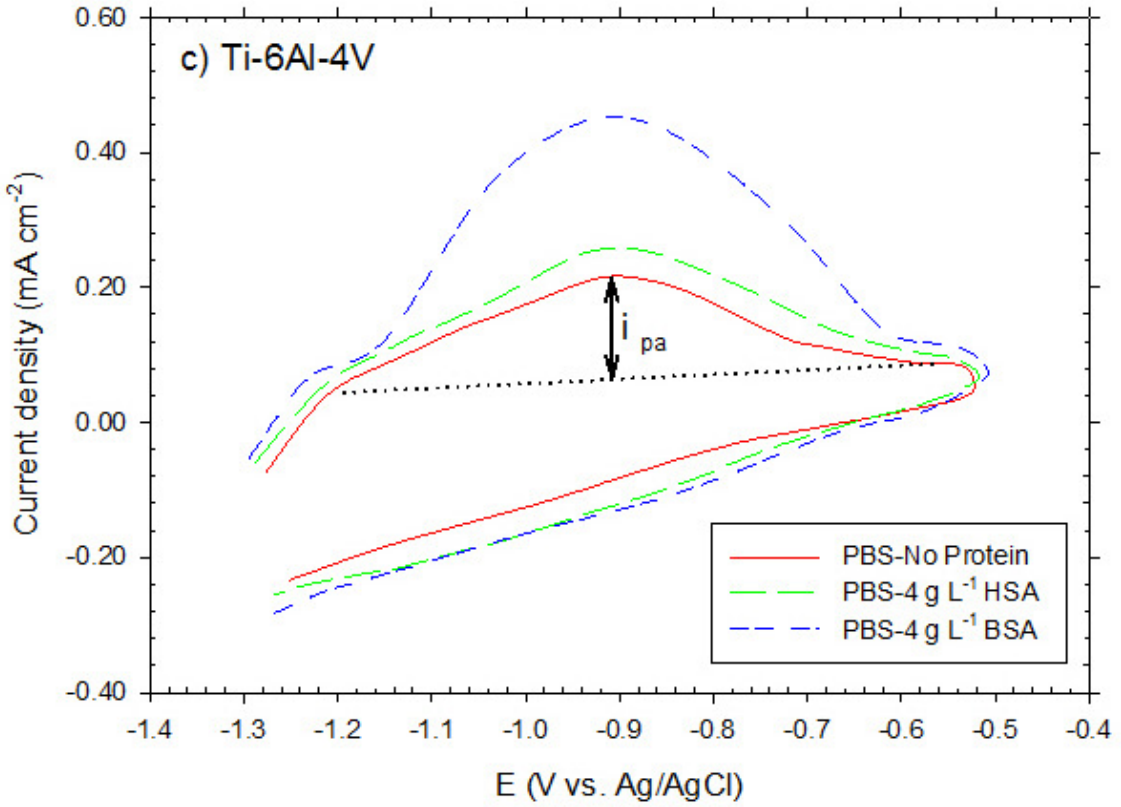

Figure 7-3: (Cont'd) Cyclic voltammograms of a) 316L, b) Co-28Cr-6Mo, and c) Ti-6Al-4V alloys in deaerated PBS solutions containing either 4 g L^{-1} HSA or BSA at 37°C and a pH of 7.2

A peak was discovered with the i_{pa} value of 0.8 mA cm^{-2} and potential of -0.68 V vs. Ag/AgCl for 316L electrode in only PBS solutions (Figure 7-3 a-solid line). This peak could be attributed to the oxidation of iron (Equation 7-1).

$$Fe \leftrightarrow Fe^{2+} + 2e \qquad 7\text{-}1$$

The iron dissolution from the outer oxide layer of 316L in this potential range has also been determined by other researchers (Ramasubramanian et al., 1985; Sato et al., 1970). Iron ions

can diffuse from the steel-oxide interface enriching the oxide-solution interface with iron oxides (Omanovic & Roscoe, 1999; Ramasubramanian et al., 1985). Referring to these observations, the current anodic peak of the 316L electrode could result from the iron dissolution of the outer passive film exposed to the solutions.

The CoCrMo alloy in the PBS solution was observed at -0.5 V vs. Ag/AgCl where i_{pa} value was 0.54 mA cm^{-2} (Figure 7-3b-solid line). Metikos-Hukovic *et al*. (Metikos-Hukovic et al., 2003) determined a similar current peak from the cyclic response of the CoCrMo alloy in Hanks solution and assigned it to the electroformation of Co (II) oxide/hydroxide at the pre-existing Cr_2O_3 layer. From our recent work, the main species that dissolves from Co-28Cr-6Mo is cobalt (Karimi et al., 2012) and the amount of cobalt is higher in the outer part of the passive film (Hodgson et al., 2004). The observed i_{pa} can be then ascribed to the oxidation of cobalt (Equation 7-2).

$$Co \leftrightarrow Co^{2+} + 2e \qquad 7\text{-}2$$

The cyclic voltammogram of Ti-6Al-4V alloy in PBS solution is depicted in Figure 7-3c (solid line). The anodic peak potential and i_{pa} were -0.9 V vs. Ag/AgCl and 0.14 mA cm^{-2}, respectively. The interaction of TiO_2 with solution could form basic (Equation 7-3) and acidic (Equation 7-4) hydroxyl groups (Boehm, 1971; Wassell & Embery, 1996).

$$Ti - OH_2^+ \leftrightarrow Ti - OH + H^+ \qquad 7\text{-}3$$

$$-OH \leftrightarrow O^- + H^+ \qquad 7\text{-}4$$

Hydrogen produced in Reaction 3 and 4 can adsorb onto the surface (Oshida, 2006). The detected anodic peak of Ti-6Al-4V electrode could point to the oxidation of adsorbed hydrogen (Equation 7-5).

$$H^+ + e^- \leftrightarrow H_{ADS} \qquad 7\text{-}5$$

This peak was also evidenced at this potential for the TiO-containing species (Bonilla & Zinola, 1998; Jackson et al., 2000).

In returning to the cathodic scan, no cathodic peak was found for the specimens (Figure 7-3a, b, and c) in the presence or absence of proteins. The reduction potential of BSA was measured at a potential region of -0.45 to -0.65 V vs. Ag/AgCl on a mercury drop electrode in a PBS solution having 1.38 g L^{-1} BSA (Stankovich & Bard, 1978), which was not detected in the studied potential regions on the selected electrodes.

Although the addition of protein into PBS solutions did not change the shapes of the voltammogram, the resulting currents were affected by the addition of BSA and HSA (Figure 7-3a, b, and c-dashed lines). In the presence of protein, the i_{pa} value of 316L and CoCrMo alloys decreased while the i_{pa} of Ti-6Al-4V alloy increased. This is indicative of the protein interaction with these alloys. In our previously published papers (Karimi et al., 2012), the X-ray photoelectron spectroscopy (XPS) analysis of 316L and CoCrMo showed that the amount of iron and cobalt increased in the presence of protein. Therefore, the decrease of the i_{pa} of 316L and CoCrMo implies that the protein inhibition action slowed down the dissolution rate of iron from 316L and cobalt from the CoCrMo alloy. In a study of the titanium response to

the presence of BSA (Jackson et al., 2000), the increase of the i_{pa} in the presence of protein was addressed by "external donation of hydrogen atoms" via the protonated amino groups which could lead to protein adsorption. This can be explained by the following proposed reaction (Equation 7-6) (Oliva et al., 2003):

$$\mathrm{Ti-OH + R-NH_3^+ \rightarrow Ti-OH_2^+ : NH_2-R} \qquad 7\text{-}6$$

As a result, HSA and BSA can adsorb on 316L, CoCrMo, and Ti-6Al-4V alloys, however, the surface coverage of BSA and HSA is not similar because the i_{pa} of each alloy immersed in PBS-HSA solutions is different from that in PBS-BSA solutions. BSA and HSA are homologous proteins having a similar sequence and conformation, however, HSA and BSA contain 585 and 583 amino acid residues, respectively (Bell & Brenner, 1982; Brown, 1975; Carter & Ho, 1994; Carter et al., 1994; He & Carter, 1992; Hirayama et al., 1990; Moriyama et al., 1996). In addition, BSA has two tryptophan moieties (Trp 135 and Trp 214) located in subdomains IA and IIA, whereas HSA contains one tryptophan (Trp 214) in subdomain IIA (Carter & Ho, 1994; Carter et al., 1994; Moriyama et al., 1996). The positions of tryptophan residues in the three-dimensional structures of HSA and BSA have been depicted (Hamdani et al., 2009). Trp 212 and Trp 214 are located in a hydrophobic fold (Moriyama et al., 1996), and the second tryptophan of BSA (Trp 134) is on the surface of the molecules (Peterman & Laidler, 1980). These structural differences could influence the affinities of human and animal serum to adsorb on the alloy's surface. For example, the adsorption of BSA and HSA has been studied

on the surface of stainless steel (Lundin et al., 2011) where the authors concluded that the amount of adsorbed BSA is higher than HSA. Similarly to this work, our cyclic voltammetry results showed that the BSA adsorption is greater than HSA adsorption because the lowest i_{pa} value was detected in the solution of PBS-BSA for 316L and Co-28Cr-6Mo alloys. This means that the dissolution of iron for 316L and cobalt from Co-28Cr-6Mo alloy decreased. In the case of the Ti-6Al-4V alloy, the highest i_{pa} (Figure 7-3c) was measured in the PBS-BSA solution meaning that the rate of external donation of hydrogen atoms and, as a result, BSA coverage was greater than HSA coverage.

7.3 Electrochemical polarization measurements

The potentiodynamic polarization of 316L in solutions of PBS having six different HSA concentrations is presented in Figure 7-4. The increase of the HSA concentration slightly moved the cathodic branch to lower potentials in which the cathodic polarization behavior corresponds to oxygen reduction (Tang et al., 2006) or protein adsorption (Stankovich & Bard, 1978). The potentiodynamic polarization measurements were repeated at least 3 times to ensure the reproducibility of the data. The reproducible result for 316L samples in 0.4 g L^{-1} HAS is shown in Figure 7-5.

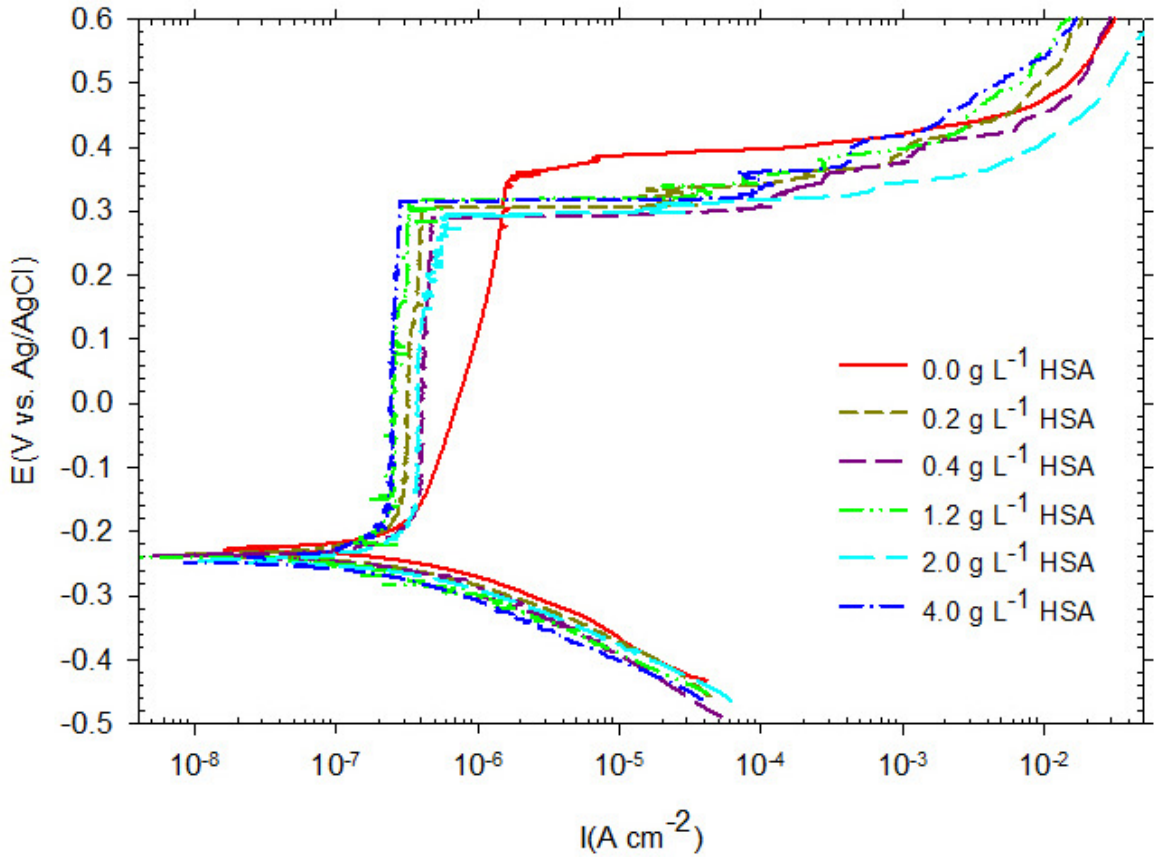

Figure 7-4 : : Potentiodynamic polarization curves of 316L in aerated PBS solutions containing various HSA concentrations (0-4 g L^{-1}) from -0.25 V vs. OCP to 0.6 V vs. Ag/AgCl with a scan rate of 0.167 mV s^{-1} at 37°C and a pH of 7.4

The addition of HSA to PBS solutions also changed the anodic polarization behavior of 316L. The current density of the passive region slightly increased as potentials were increased in HSA-free solutions, whereas the current densities in the passive region remained constant in the presence of HSA up to the breakdown potential. This observation can be related to the surface coverage of 316L by HSA. The main components of the 316L passive layer are chromium and iron along with small amounts of nickel and molybdenum oxides and hydroxides (Bastidas et al., 2002; Kocijan et al., 2007; Shih et al., 2004). The spontaneous

adsorption of protein onto the 316L passive layer has been determined by a highly negative Gibbs energy of adsorption (Desroches et al., 2007). The cyclic voltammetry results also confirmed the adsorption of HSA on the 316L passive film which could slow down the dissolution of iron. An XPS study (Karimi et al., 2012) also found that the iron content of 316L increases in the presence of protein. The shift of the 316L passive current density to lower values in HSA solutions could be another indication of the blockage of the 316L surface by a HSA adsorbed film.

Figure 7-6 shows the PDP polarization behavior of the Co-28Cr-6Mo alloy in PBS and HSA solutions. The corrosion potential of the Co-28Cr-6Mo alloy decreased upon the addition of HSA, indicating that HSA can act as a cathodic inhibitor. Valero Vidal & Muñoz stated that HSA has a dominant cathodic inhabitation action over other anions, such as phosphates ions, which are known as anodic inhibitors (Valero Vidal & Muñoz, 2008).

HSA adsorption can change the anodic behavior of the Co-28Cr-6Mo alloy by the deceleration of the oxidation reactions (e.g. cobalt dissolution) at the anodic region. The XPS study of the Co-28Cr-6Mo alloy showed that Co-28Cr-6Mo alloys form oxide layers with a main contribution of Cr_2O_3 and small amount of Co- and Mo-oxides (Karimi et al., 2011; Miloev et al., 2000). This passive layer does not act as an absolute barrier and Cr^{3+}, Co^{2+}, and Mo^{3+} release into the solution (Karimi et al., 2012; Lewis et al., 2005) due to the oxidation of the base metals. Protein has a high affinity to bind to the dissolved chromium and cobalt (Lewis et al., 2005). An XPS study found that the oxide layer of Co-28Cr-6Mo alloys contains higher

amounts of cobalt in protein solutions (Karimi et al., 2012) pointing to the blocking of cobalt dissolution by HSA. Furthermore, the blocking action of HSA from corrosive substances is more effective at higher HSA concentrations which can be related to the proportionality of chromium binding to protein concentrations. Chromium binding to protein is greater at higher protein concentrations (Yang & Black, 1994) because protein can accelerate the formation of chromium-protein complexes to block Co-28Cr-6Mo film from corrosive substances.

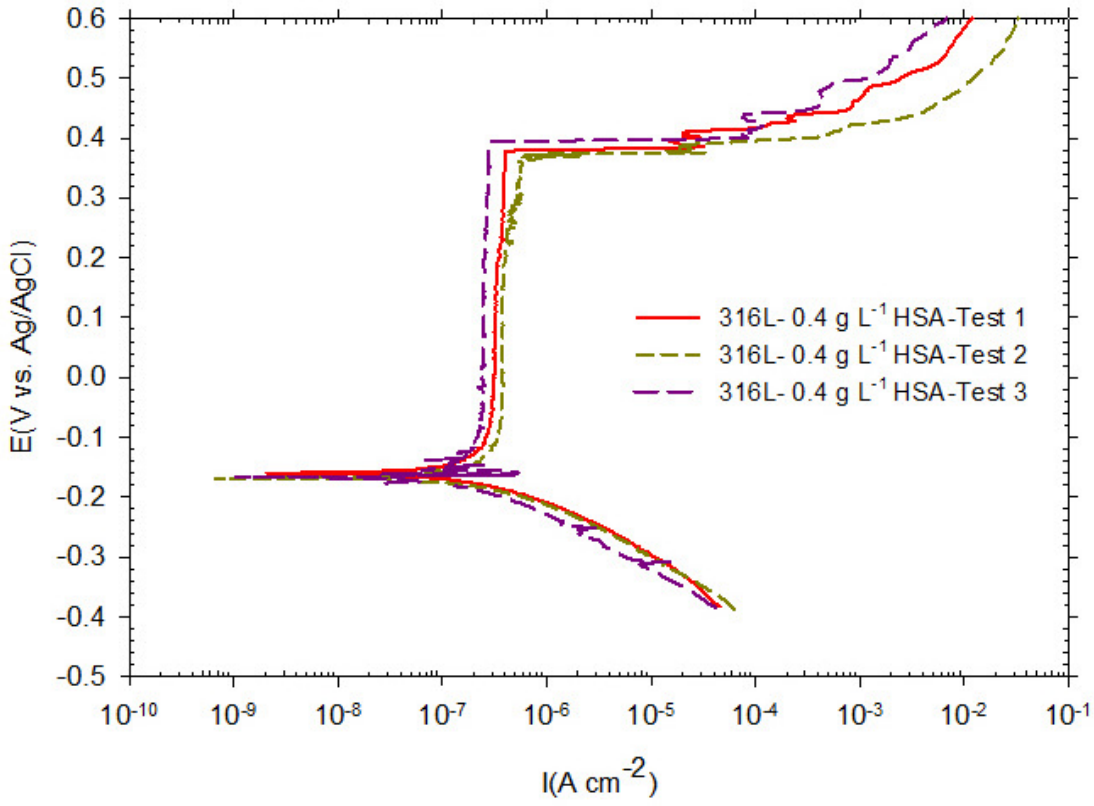

Figure 7-5: Reproducibility of potentiodynamic polarization data of 316L in aerated PBS solutions containing 0.4 g L^{-1} HSA from -0.25 V vs. OCP to 0.6 V vs. Ag/AgCl with a scan rate of 0.167 mV s-1 at 37°C and a pH of 7.4

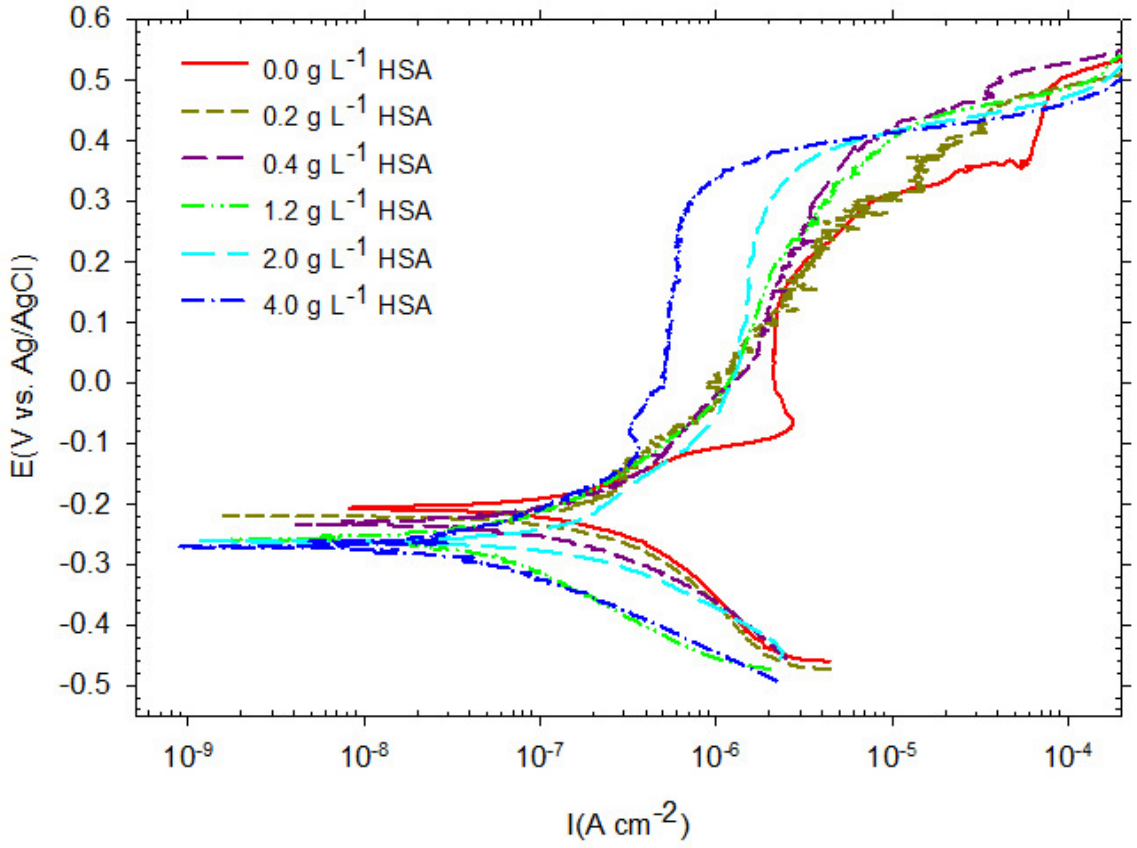

Figure 7-6 : Potentiodynamic polarization curves of Co-28Cr-6Mo in aerated PBS solutions containing various HSA concentrations (0-4 g L^{-1}) from -0.25 V vs. OCP to 0.6 V vs. Ag/AgCl with a scan rate of 0.167 mV s^{-1} at 37°C and a pH of 7.4

The polarization behavior of the Ti-6Al-4V alloys in PBS and HSA solutions are shown in Figure 5. The cathodic branches of the Ti-6Al-4V alloy in PBS solutions of 0 to 1.2 g L^{-1} HSA showed similar behaviors.

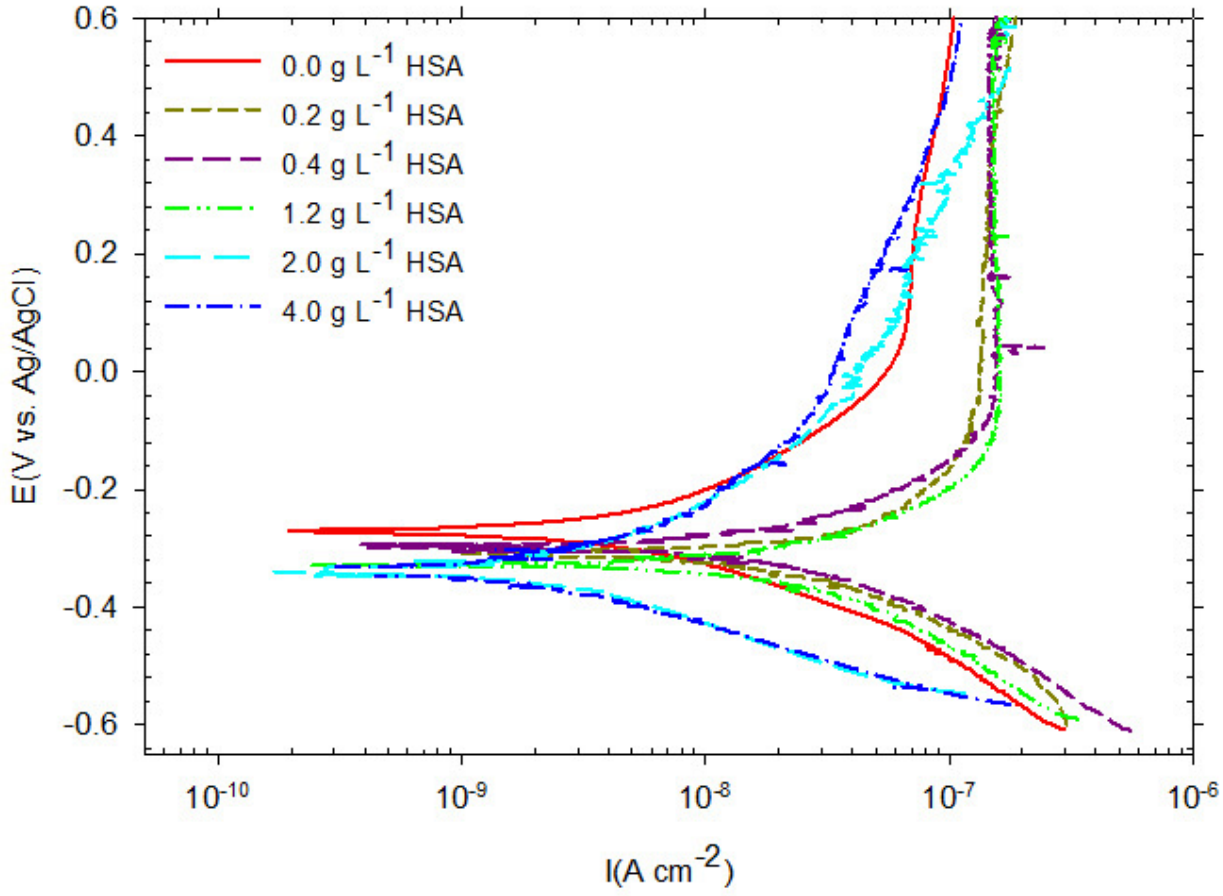

Figure 7-7 : Potentiodynamic polarization curves of Ti-6Al-4V in aerated PBS solutions containing various HSA concentrations (0-4 g L^{-1}) from -0.25 V vs. OCP to 0.6 V vs. Ag/AgCl with a scan rate of 0.167 mV s^{-1} at 37°C and a pH of 7.4

The cathodic branches shifted to lower potentials and the corrosion current densities decreased when HSA concentrations were increased to 2 and 4 g L^{-1}. It means that HSA could act as an adsorption inhibitor to form chemisorbed bonds with the metal's surface and block cathodic sites at HSA concentrations of more than 2 g L^{-1}. The highest passive current density for the Ti-6Al-4V samples was determined in PBS solutions with 0.2 to 1.2 g L^{-1} HSA. In the

pH of 7.4, one of the major HSA functional groups is $R\text{-}COO^-$ (Oliva et al., 2003; SINGH et al., 2009) and the main components of the passive layer are Ti-OH and Ti_2O^- (Boehm, 1971; Khan et al., 1996; Kuhn et al., 1986; Miloev & Strehblow, 2003; Oliva et al., 2003). The interaction of those could lead to Equation 7-6 and 7-7 (Oliva et al., 2003) indicating the consumption of a surface hydroxyl group of the oxide layer and the formation of an adsorbed layer of protein.

$$Ti - OH + R - COO^- \rightarrow Ti - OH \ldots .^- \ OOC - R \qquad 7\text{-}7$$

The growth of a stable film on Ti-6Al-4V alloy is affected in the presence of protein (Feng et al., 2002; Sharma & Sunny, 1986). In PBS solutions of 0.2 to 1.2 g L^{-1} HSA, protein consumed surface hydroxyl groups in order to adsorb onto the oxide layer. In the HSA solutions of 2 and 4 g L^{-1}, the increase of the protein concentration increased the amount of protonated amino groups which, in turn, decreased the passive current density and increased the film's stability.

In Figure 7-8 a, b, and c, the polarization behavior of the selected alloys in aerated PBS solutions having either HSA or BSA is compared. The details of the polarization results in the presence of various BSA concentrations are described (Karimi et al., 2011).

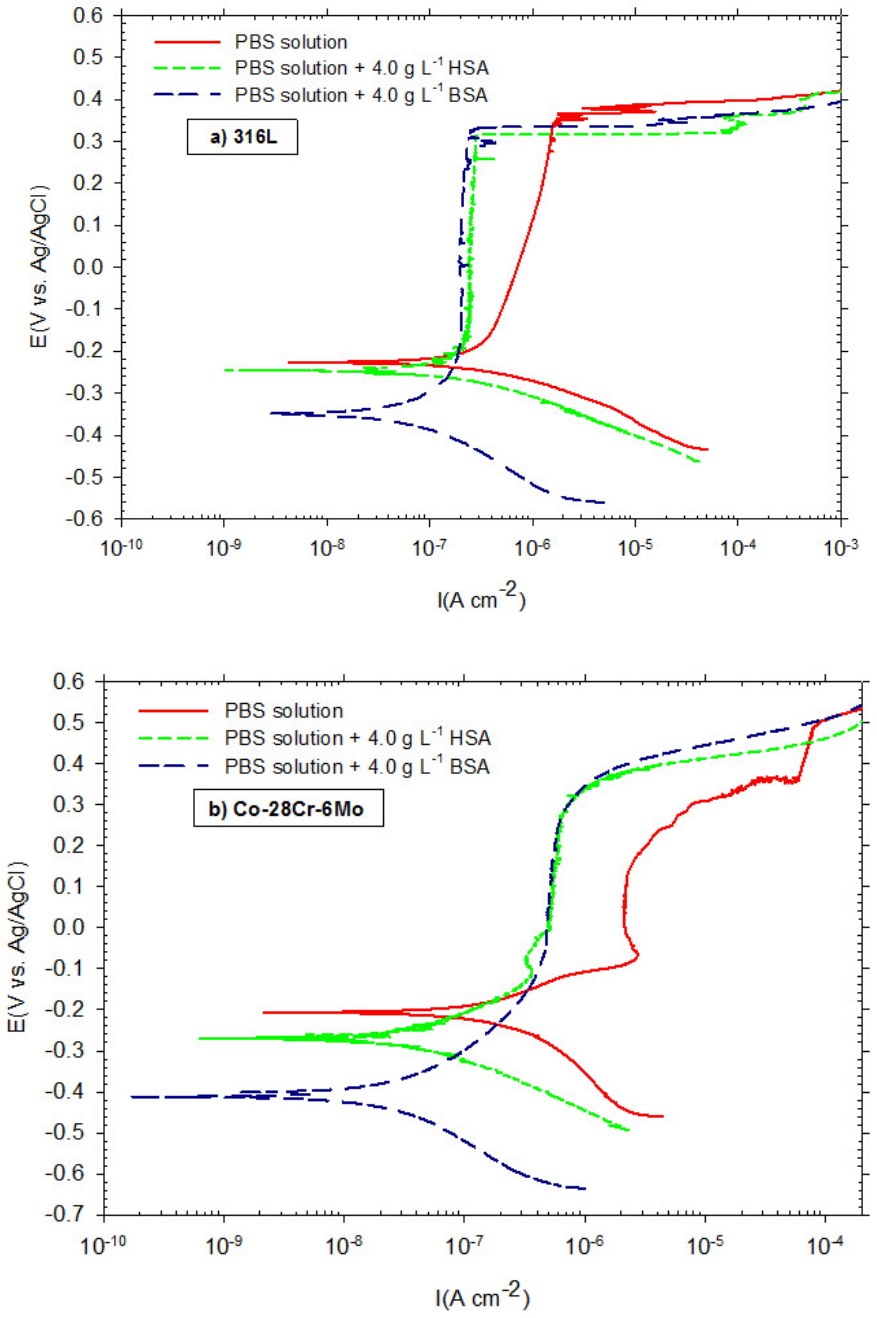

Figure 7-8 : Potentiodynamic polarization curves of a) 316L, b) Co-28Cr-6Mo and c) Ti-6Al-4V alloys in aerated PBS solutions containing either 4 g L^{-1} HSA or BSA with a scan rate of 0.167 mV s^{-1} at 37°C and a pH of 7.4

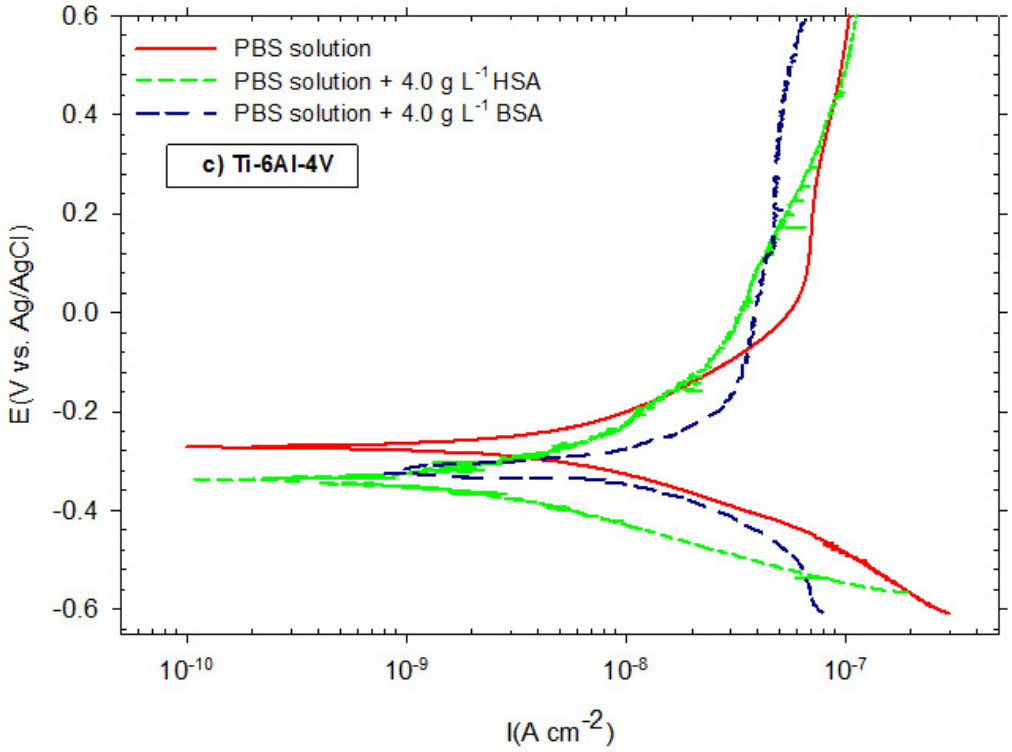

Figure 7-8: (Cont'd) Potentiodynamic polarization curves of a) 316L, b) Co-28Cr-6Mo and c) Ti-6Al-4V alloys in aerated PBS solutions containing either 4 g L^{-1} HSA or BSA with a scan rate of 0.167 mV s^{-1} at 37°C and a pH of 7.4

The corrosion potential of both the 316L and Co-28Cr-6Mo alloys decreased in the BSA solutions. In addition, the corrosion potentials of 316L and Co-28Cr-6Mo alloys in PBS-BSA solutions were lower than that in PBS-HSA solutions. This can be related to the blocking action of BSA and HSA in which BSA may act as a stronger cathodic inhibitor than HSA at high concentrations. This observation confirms the cyclic voltammetry results in which the drop of the current peak of 316L and Co-28Cr-6Mo alloys were larger in the PBS-BSA

solutions compared to that in the PBS-HSA solutions, indicating lower dissolution of iron and cobalt from 316L and Co-28Cr-6Mo alloys.

316L and Co-28Cr-6Mo alloys (Figure 7-8a and b) showed similar passive behaviors in solutions of BSA and HSA in the passive region. However, these similarities were not observed for Ti-6Al-4V alloys (Figure 7-8c) which could be addressed by adsorption behavior of BSA and HSA on the passive layers of these alloys. The chemical compositions of the 316L and Co-28Cr-6Mo passive layers, which mostly contain chromium oxides/hydroxides, are comparable, whereas the passive layer of the Ti-6Al-4V alloy is primarily titanium oxides/hydroxides. In addition, the cyclic voltammetry and polarization results implied that the mechanism of protein adsorption onto the Ti-6Al-4V alloy is different from that onto 316L and the Co-28Cr-6Mo alloys. To further investigate the characterization of the interface and surface process, EIS measurements were made.

7.4 Electrochemical impedance spectroscopy

The Bode magnitude and Bode phase diagrams (Figure 7-9a, b, and c) are provided for 316L, Co-28Cr-6Mo, and Ti-6Al-4V alloys in solutions of PBS with various HSA concentrations (0 to 4 g L^{-1}). The reproducibility of EIS measurements for 316L in PBS-HSA solutions after 3 times measurements are presented in Figure 7-10.

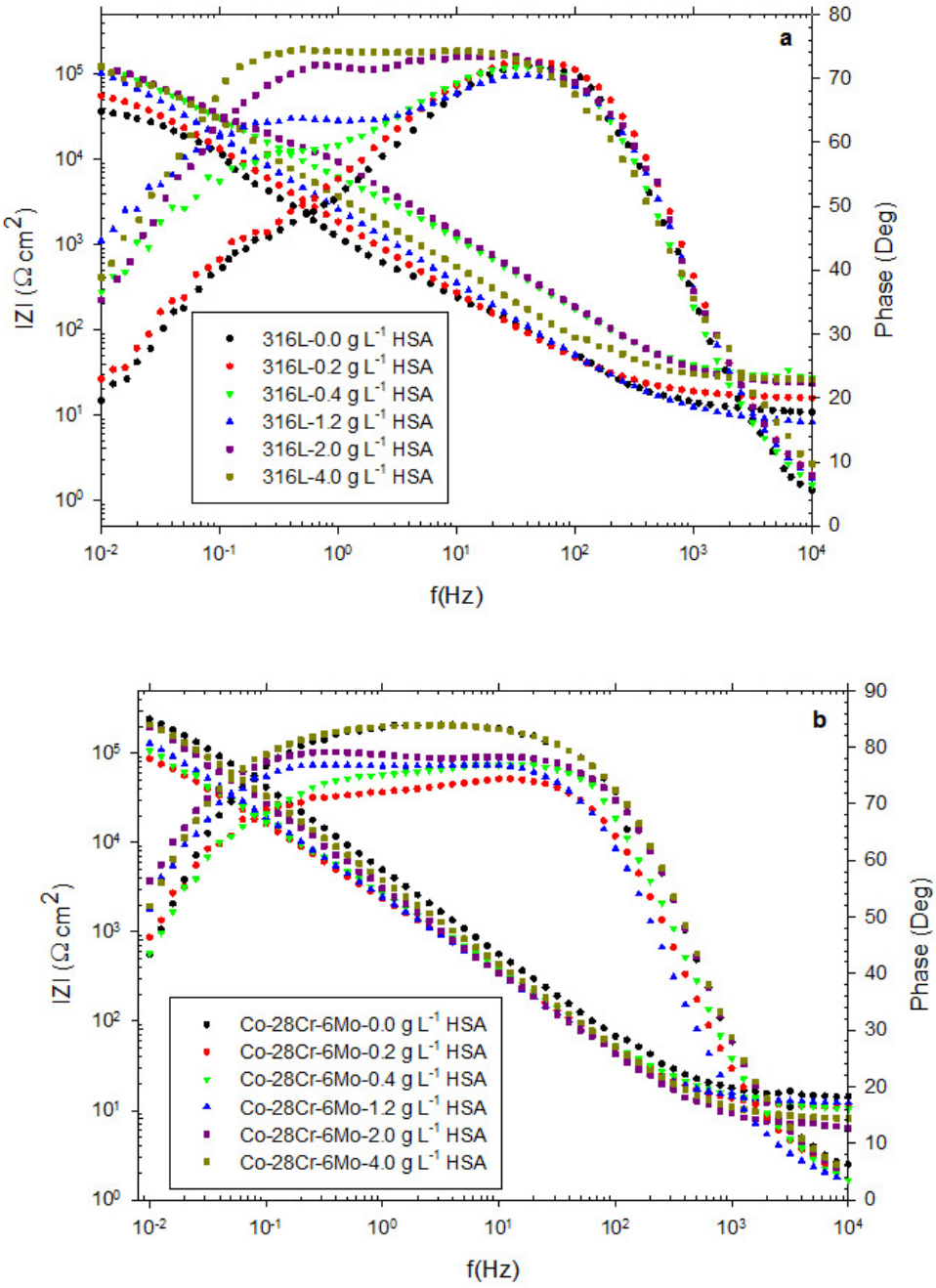

Figure 7-9: Bode magnitude and Bode phase plots of the a) 316L , b) Co-28Cr-6Mo, and c) Ti-6Al-4V alloys after 1 hour immersion at OCP in aereted PBS solutions at 37 °C and pH = 7.4 with various concentrations of HSA

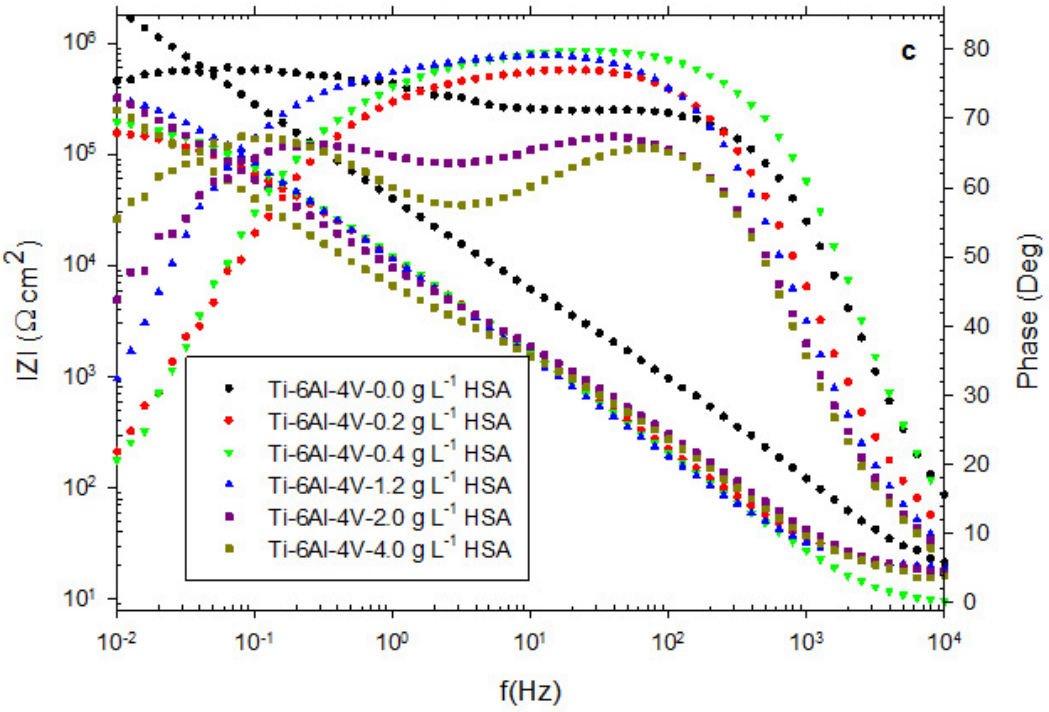

Figure 7-9: (Cont'd) Bode magnitude and Bode phase plots of the a) 316L , b) Co-28Cr-6Mo, and c) Ti-6Al-4V alloys after 1 hour immersion at OCP in aereted PBS solutions at 37 °C and pH = 7.4 with various concentrations of HSA

The presence of two distinct capacitive behaviors can be detected from the Bode phase diagrams of 316L in Figure 7-9a. The overlapping time constants are clearly separated up to the HSA concentration of 4 g L^{-1}. The variation of HSA concentrations did not affect the phase shift responses at high-frequency ranges. However, the phase angle responses shift to lower magnitudes at low frequencies. HSA adsorption initiates at low frequencies while the changes of the passive layer mechanism can be observed at high frequencies. This means that protein concentration alternation has a significant effect on the protein adsorption mechanism but not on oxide layer growth.

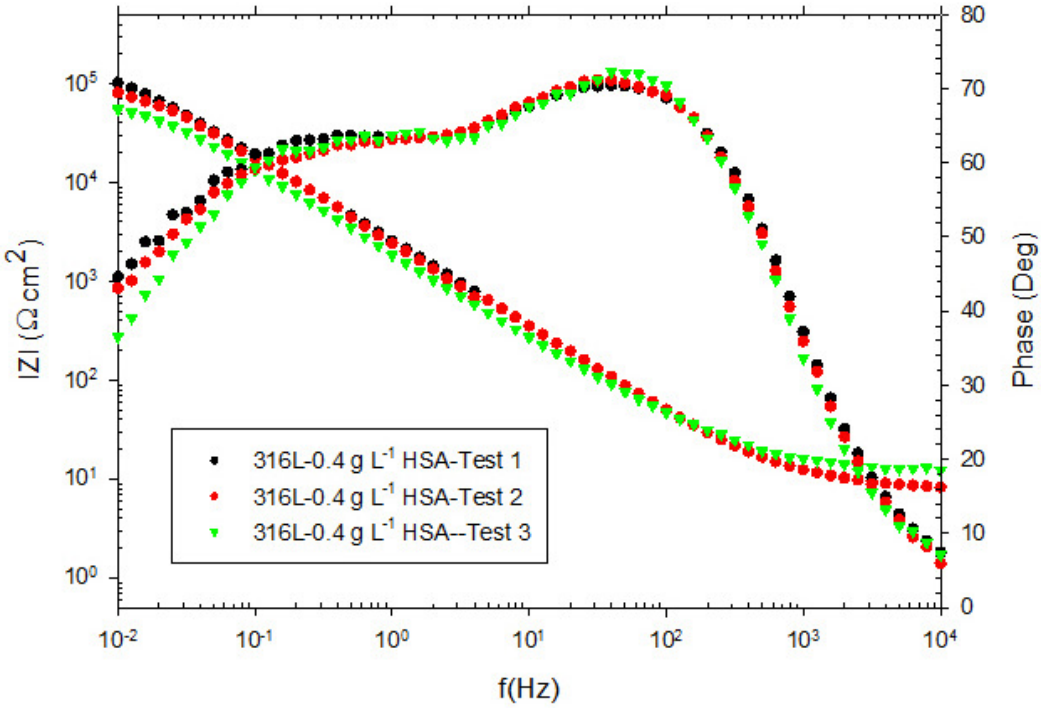

Figure 7-10: Bode magnitude and Bode phase plots of the 316L after 1 hour immersion at OCP in aereted PBS solutions at 37 °C and pH = 7.4 with 4 g L^{-1} HSA

The Co-28Cr-6Mo alloy showed two time constants as can be identified from the Bode phase diagrams in Figure 7-9b. The appearance of the two time constants was less notable than those on 316L. The small difference in the RC-element between the two existing time constants can be explained by high affinity of HSA to bind to cobalt which could lead to the formation of cobalt-HSA complexes (Kragh-Hansen et al., 2002). Increasing HSA concentration shifted the phase angle responses of Co-28Cr-6Mo alloy to greater magnitudes (from 70° to 80°) at the medium-frequency range indicating that the protein concentration can impact the capacitive behavior of the Co-28Cr-6Mo alloy. The existence of two time constants can be found from the Bode phase diagram of the Ti-6Al-4V alloy presented in

Figure 7-9c. The appearance of two time constants was obvious when the HSA concentration is 2 and 4 g L^{-1}.

The Bode diagrams of 316L and CoCrMo showed similar trends over the studied frequency range for various HSA concentrations. This was also measured for the Ti-6Al-4V alloy except the absolute impedance data of Ti-6Al-4V alloy shifted to lower magnitudes in the presence of HSA. Ti-6Al-4V showed the highest absolute impedance compared to 316L and Co-28Cr-6Mo alloys at low frequencies meaning the oxide and adsorbed protein layer of Ti-6Al-4V alloy is more compact than the 316L and CoCrMo alloys.

The observed two overlapping time constants have been modeled to the equivalent electrical circuit (EEC) shown in Figure 7-11. This model has been employed (Alves et al., 2009; Casabán Julián & Igual Muñoz, 2011; Vasilescu et al., 2011) for the formation of a bilayer passive layer at the alloys/passive films/solution interface.

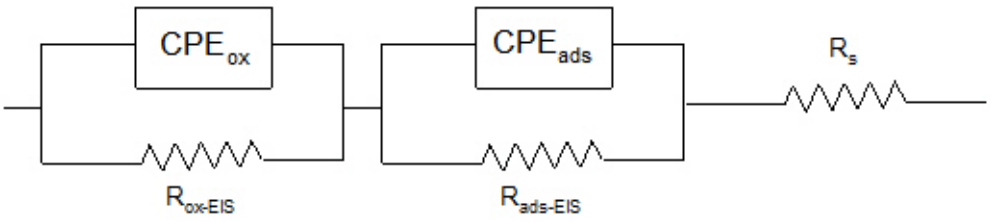

Figure 7-11 : Equivalent electrical circuit (EEC)

The time constants were attributed to the metal/oxide film (R_{ox} and C_{ox}) and to the oxide/adsorbed layer (R_{ads} and C_{ads}), while R_s was assigned for solution resistance between the working and reference electrode. A constant phase angle element (CPE) was employed because of a non-uniform current distribution resulting from surface roughness and HSA adsorption (Lopez et al., 2003; Omanovic & Roscoe, 1999; Valero Vidal & Muñoz, 2008; Valero Vidal & Muñoz, 2008). The impedance of a constant phase element is defined as follows (Equation 7-8):

$$Z_{CPE} = ((j\omega)^{n_C} Y_0)^{-1} \qquad 7\text{-}8$$

where the exponent n_C is a coefficient, Y_0 is the general admittance function, and ω represents the angular frequency.

In the Table 7-1, magnitudes of the electrical circuit parameters were found from experimental data by a ZSimpWin software package. The chi-square value of less than 10^{-3} was achieved for these parameters.

Table 7-1 : EIS equivalent circuit parameters of 316L, Co-28Cr-6Mo, and Ti-6Al-4V alloys after 1 hour immersion in aerated PBS solutions with various HSA concentrations at 37°C, pH = 7.4, and OCP potential

	HSA Concentration ($g\ L^{-1}$)	R_s ($\Omega\ cm^2$)	Adsorb layer			Oxide layer		
			Y_o ($\mu\Omega^{-1}\ S^n\ cm^{-2}$)	n_C	R_{ads} ($k\Omega\ cm^2$)	Y_o ($\mu\Omega^{-1}\ S^n\ cm^{-2}$)	n_C	R_{ox} ($k\Omega\ cm^2$)
316L	0.00	10	580	0.68	1.0	152	0.80	37.80
	0.20	15	522	0.68	1.3	148	0.80	62.10
	0.40	15	448	0.71	2.3	148	0.82	161.3
	1.2	11	447	0.74	2.5	138	0.87	164.6
	2.0	15	424	0.78	3.0	110	0.88	168.0
	4.0	15	420	0.78	3.1	91.0	0.86	165.0
Co-28Cr-6Mo	0.00	15	95.0	0.93	0.2	362	0.86	105.1
	0.20	15	92.0	0.88	0.1	320	0.85	106.5
	0.40	11	91.0	0.85	0.2	392	0.85	139.6
	1.2	8.0	64.0	0.91	0.3	333	0.85	328.8
	2.0	8.0	65.0	0.93	0.3	342	0.85	338.6
	4.0	8.0	47.0	0.94	0.3	350	0.85	325.4
Ti-6Al-4V	0.00	15	38.0	0.78	1.7	90.0	0.82	600.6
	0.20	17	45.0	0.78	0.10	230	0.87	173.9
	0.40	19	45.0	0.79	0.20	220	0.91	193.6
	1.2	19	38.0	0.87	1.3	176	0.89	376.1
	2.0	18	29.0	0.84	1.5	124	0.84	473.3
	4.0	16	28.0	0.84	1.5	87.0	0.83	560.3

The result of the electrical circuit parameters indicates that the impedance magnitude of the adsorbed layer decreased and the resistance of the adsorbed layers (R_{ads}) increased for 316L, Co-28Cr-6Mo, and Ti-6Al-4V alloys for HSA concentrations of 0.2 to 4 g L^{-1}. This shows that

the surface coverage of the adsorbed protein on these alloys increased by increasing the HSA concentrations. This can be related to the formation of iron-protein complexes on 316L and chromium-protein and cobalt-protein complexes on Co-28Cr-6Mo. For Ti-6Al-4V alloys, this result confirmed the high surface coverage of HSA at high protein concentrations due to the consumption of the surface hydroxyl group of the oxide layer by protein.

7.5 Linear polarization resistance

Figure 7-12 shows a typical LPR graph of 316L, Co-28Cr-6Mo, and Ti-6Al-4V alloys in PBS solutions having HSA concentrations of 0, 0.4, and 4 g L^{-1} at 37°C. The results show that the Ti-6Al-4V alloy has the lowest corrosion rate followed by Co-28Cr-6Mo and 316L alloys. However, no particular trend was found between the HSA concentrations and polarization resistance of the selected alloys. Each measurement were repeated 3 times. Figure 7-13 is as an example of these measurements.

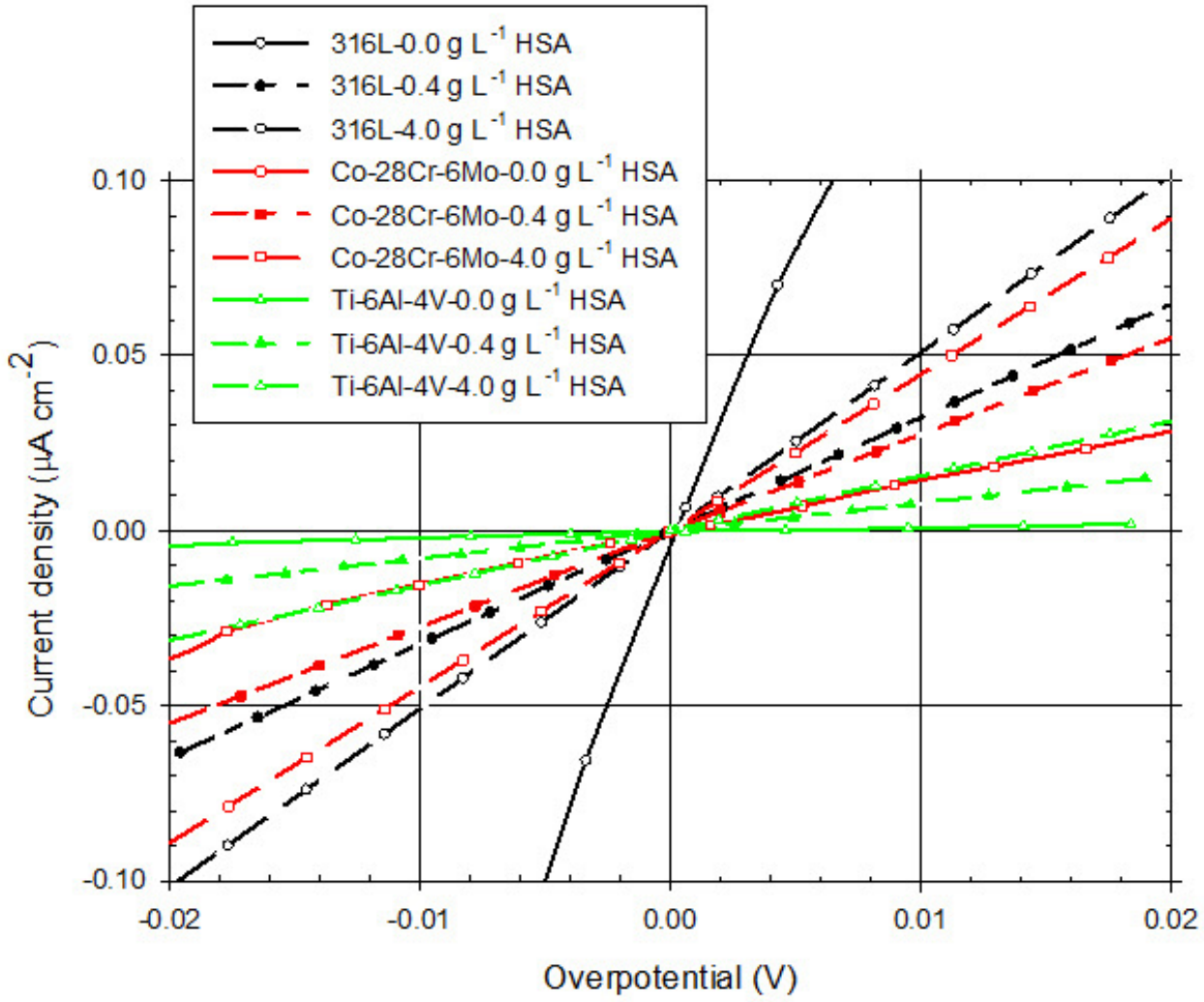

Figure 7-12 : Linear polarization curves for 316L, Co-28Cr-6Mo, and Ti-6Al-4V alloys after 1 hour of immersion at OCP in aerated PBS solutions at 37 °C and pH = 7.4 with HSA concentrations of 0, 0.4, and 4.0 g L^{-1}

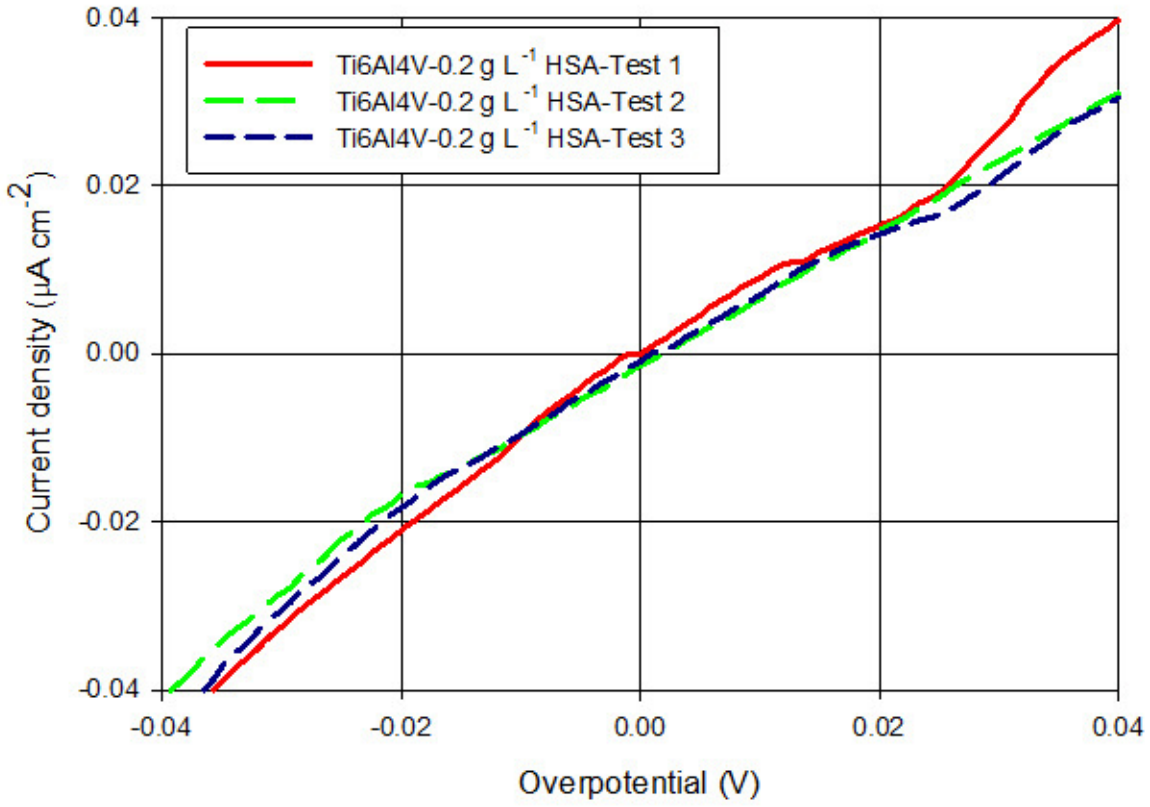

Figure 7-13: Linear polarization curves for Ti-6Al-4V alloys after 1 hour of immersion at OCP in aerated PBS solutions at 37 °C and pH = 7.4 with 0.2 g L^{-1} HSA

7.6 Corrosion rate calculation

Equations 5-4 and 5-5 (Stansbury & Buchanan, 2000) were used to calculate the corrosion current density (i_{corr}) of 316L, Co-28Cr-6Mo, and Ti-6Al-4V alloys in solutions of PBS and HSA.

where R_p is polarization resistance and β_{red} and β_{ox} are cathodic and anodic Tafel slopes. Two R_p values were calculated, $R_{P\text{-}EIS}$ and $R_{P\text{-}LPR}$. $R_{P\text{-}EIS}$ was the summation of R_{ox} and R_{ads}

determined from the EIS Data. $R_{P\text{-}LPR}$ was found from the slope of the linear polarization curves (Figure 7-12). Approximate values for the β_{red} and β_{ox} were used. The value of $\beta_{red,X}$ lies between 60 mV and infinity and the value of $\beta_{ox,M}$ is normally from 60 mV to 120 mV (Stansbury & Buchanan, 2000). The confinement of $\beta_{red,X}$ and $\beta_{ox,M}$ values limits B to a value between 13 and 52 mV. The corrosion rates were then calculated by placing the i_{corr} values from LPR and EIS measurements into Equation5-6. The values of a, n, and ρ along with the corrosion rates for the metallic samples are summarized in Table 7-2.

The standard deviation (SD) of corrosion rates were also calculated based on the 3-time replication of LPR and EIS tests for each HSA concentration. The calculated corrosion rates by LPR were one order of magnitude lower than the measurements by EIS. Therefore, the HSA concentration changes did not significantly affect the corrosion rates of the 316L, Co-28Cr-6Mo, and Ti–6Al–4V alloys.

Table 7-2 : Atomic weight (a), density(ρ), and number of exchange atoms (n) along with corrosion current density (i_{corr}) and corrosion rate of 316L, Co-28Cr-6Mo, and Ti-6Al-4V alloys obtained from EIS and LPR data

specimen	HSA	a	ρ	n	Corrosion rate ± SD (EIS)	Corrosion rate ± SD (LPR)
	g L^{-1}	g mol^{-1}	g cm^{-3}	equivalent mol^{-1}	μm $year^{-1}$	μm $year^{-1}$
316L	0	56.3	7.9	3	6.5±2.9	3.3±0.43
	0.2				4.0±2.4	1.3±0.17
	0.4				1.6±0.93	1.1±0.13
	1.2				1.5±0.91	1.1±0.14
	2				1.5±0.89	1.2±0.15
	4				1.5±0.92	1.5±0.19
Co-28Cr-6Mo	0	58.6	8.1	3	2.4±1.5	1.1±0.12
	0.2				2.4±1.4	0.70±0.090
	0.4				1.8±1.1	0.90±0.07
	1.2				0.90±0.47	0.70±0.09
	2				0.80±0.45	0.90±0.11
	4				0.80±0.47	0.60±0.14
Ti-6Al-4V	0	46.7	4.4	4	0.50±0.38	0.1±0.01
	0.2				1.6±1.3	0.2±0.02
	0.4				1.5±1.2	0.2±0.03
	1.2				0.60±0.60	0.2±0.02
	2				0.60±0.48	0.4±0.05
	4				0.50±0.40	0.1±0.09

7.7 Summary

The following conclusions are drawn by conducting electrochemical corrosion experiments on alloys of 316L stainless steel, wrought Co-28Cr-6Mo, and Ti-6Al-4V in aerated solutions of PBS and HSA:

- The OCP value of the selected alloys dropped with the addition of HSA to the PBS solution.
- One anodic peak was determined for each alloy in PBS solution. The anodic current peak of 316L and Co-28Cr-6Mo resulted from the oxidation of iron and cobalt, whereas the anodic current peak of Ti-6Al-4V alloy was due to the oxidation of the adsorbed hydrogen. The shape of these voltammograms was similar in the presence of proteins; however, the i_{pa} values of 316L and CoCrMo alloys decreased and that of the Ti-6Al-4V alloy increased with the addition of BSA and HSA. These pointed to the formation of an adsorbed layer of protein which could lower the dissolution of iron from 316L and cobalt from the Co-28Cr-6Mo. The dissolution rates of these ions in the BSA solution were lower than that in the HSA solutions.
- The passive behavior/potential of 316L and Co-28Cr-6Mo alloys in solutions of HSA and BSA were similar. However, BSA was a stronger cathodic inhibitor than HSA for 316L and Co-28Cr-6Mo alloys.
- The presence of HSA can enhance the stability of the 316L, Co-28Cr-6Mo, and Ti-6Al-4V passive layers by the blocking of the ions dissolution. For example, the increase of

the HSA concentration to 2 and 4 g L^{-1} increased the stability of the Ti-6Al-4V film. In addition, surface coverage of HSA increased by increasing HSA concentrations. Therefore, the HSA surface coverage is proportional to the HSA concentrations.

Chapter 8: Ion release and surface oxide composition of AISI 316L, Co 28Cr-6Mo, and Ti-6Al-4V alloys immersed in human serum albumin solutions

Weight loss and ion release have been rarely identified by long-term static immersion corrosion tests. In this section, the long-term weight loss, ion release, and surface composition of AISI 316L, the Co-28Cr-6Mo, and Ti-6Al-4V alloys were investigated in a simulated body environment. The samples were immersed in PBS with various HSA concentrations. The presence of HSA helped us to evaluate the corrosion behavior of metallic biomaterials in a more realistic human body environment. HSA is the main component of the human circulatory system which can bind to a variety of ligands. The study of the selected biomaterials in the presence of two proteins created this opportunity to compare the effect of protein in the corrosion behavior of 316L, CoCrMo, and Ti-6Al-4Al alloys. This goal was achieved by following the same procedure used to evaluate corrosion behavior of these alloys in the presence of BSA. Hence, the analysis of the released ions was performed by ICP-OES and the surface chemistry of the specimens was determined by XPS for 8, 14, and 22 weeks. The XPS analysis of Co-28Cr-6Mo alloy showed that the affinity of HSA is different from the affinity of BSA to bind to Mo. This was also observed for Na adsorption on the surface of the Ti-6Al-4V alloy. More results of these experiments are reported in the following.

8.1 Weight loss and corrosion rate

The weight loss of the AISI 316L, Co-28Cr-6Mo, and Ti-6Al-4V alloys immersed in the PBS solutions containing various HSA concentrations over 8, 14, and 22-weeks is shown in Figure 8-1, Figure 8-2, Figure 8-3. The error bars indicate the standard deviation of the weight loss of the three measurements. The immersed samples lost weight significantly within 8 to 14 weeks. Hanawa (Hanawa, 2004) stated that the surface of metallic biomaterials undergoes a repeating process of partial dissolution and precipitation in aqueous solutions. Depending on the rates of partial dissolution and precipitation, either ion releases or oxide layer grows (Hanawa, 2004).

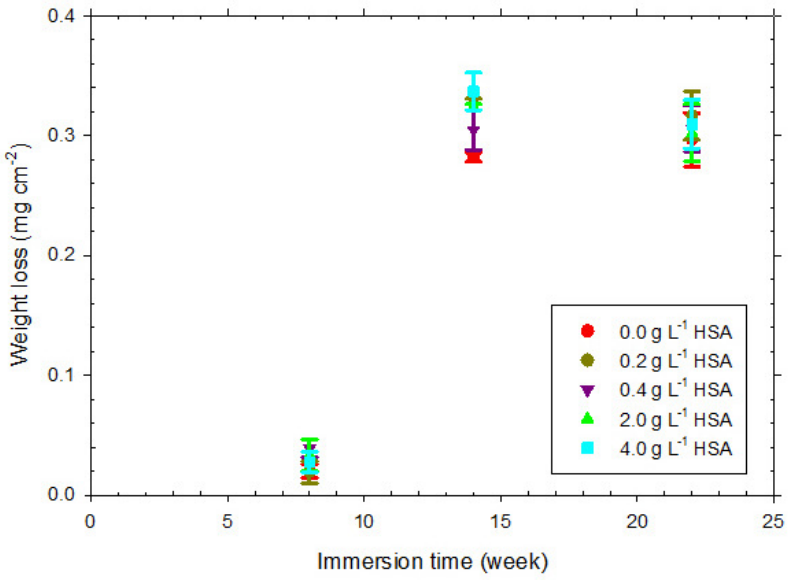

Figure 8-1 : Weight changes of the 316L after 8, 14, and 22 weeks immersion in PBS solutions with various HSA concentrations (0 to 4 g L^{-1}) at 37 °C

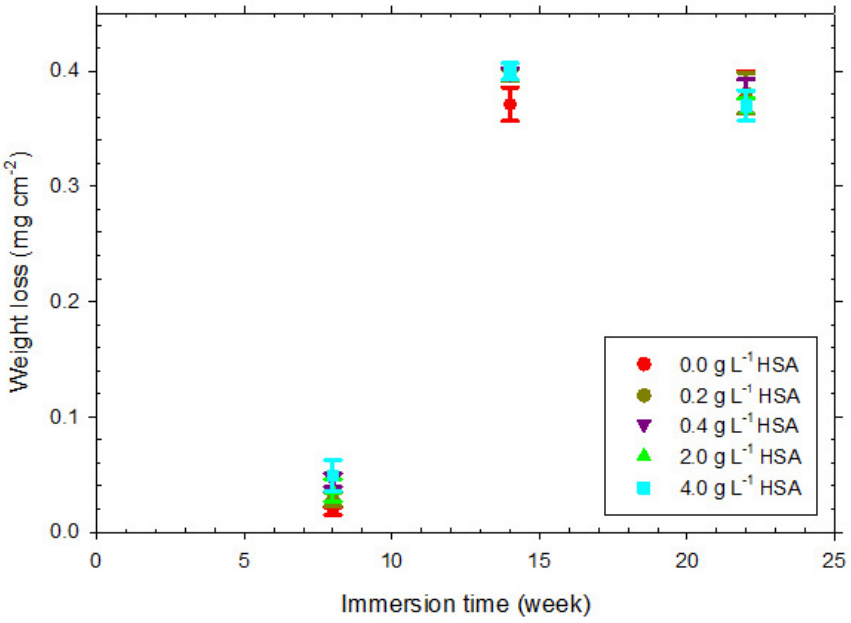

Figure 8-2 : Weight changes of the Co-28Cr-6Mo after 8, 14, and 22 weeks immersion in PBS solutions with various HSA concentrations (0 to 4 g L^{-1}) at 37 °C

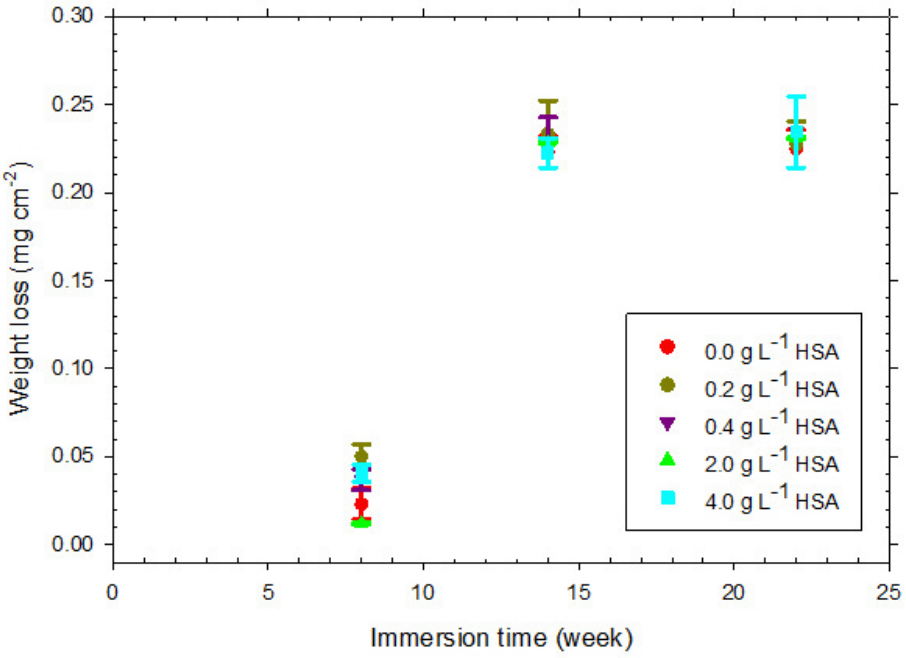

Figure 8-3 : Weight changes of Ti-6Al-4V after 8, 14, and 22 weeks immersion in PBS solutions with various HSA concentrations (0 to 4 g L^{-1}) at 37 °C

After 14 weeks of incubation, the rate of precipitation is faster than dissolution. Therefore, the weight of the samples slightly increased over 14 to 22 weeks of immersion referring to the growth of the oxide layer. Koike and Fujii (Koike & Fujii, 2001) also reported weight gain of pure Ti when it was immersed in a physiological saline solution due to Ti dissolution and the formation of TiO_2.

The weight change results did not show a trend with HSA concentration variations, especially for the Co-28Cr-6Mo alloy. It was assumed that the immersed samples were corroded uniformly because no sign of localized corrosion was observed by optical and scanning electron microscopy (Hitachi S-3000N). Therefore, the corrosion rates of the samples were calculated Equation 6-1 (ASTM G31-72 (ASTM Standard, 2004)). In this Equation, K is a constant (8.76×10^4), T is time of exposure (in hours), A is the area of the immersed specimen (in cm^2), W is mass loss (in mg) and D is density (in g cm^{-3}). The corrosion rates of samples after 22 weeks of immersion and those obtained from electrochemical corrosion results (EIS) in HSA solutions (Karimi & Alfantazi, 2013) can be compared by referring to Table 8-1, where the corrosion rates calculated from immersion and EIS tests are comparable for the selected alloys (Karimi & Alfantazi, 2013).

Table 8-1 : Corrosion rates of 316L, Co-28Cr-6Mo, and Ti-6Al-4V alloys after 22 weeks of exposure to the PBS solutions with various HSA concentrations (0 to 4 g L^{-1}) at 37 °C and previously calculated corrosion rates from EIS measurement

	BSA Concentration (g L^{-1})	Density (g cm^{-3})	Corrosion Rate ± SD (μm $year^{-1}$)	
			immersion	EIS
316L	0	7.8	1.5±0.03	6.5±2.9
	0.20		1.6±0.05	4.0±2.4
	0.40		1.5±0.01	1.6±0.93
	2.0		1.5±0.02	1.5±0.89
	4.0		1.5±0.08	1.5±0.92
Co-28Cr-6Mo	0	8.1	1.8±0.09	2.4±1.5
	0.20		1.8±0.03	2.4±1.4
	0.40		1.8±0.05	1.8±1.1
	2.0		1.8±0.04	0.80±0.45
	4.0		1.8±0.03	0.80±0.47
Ti-6Al-4V	0	4.4	1.9±0.06	0.50±0.38
	0.20		2.0±0.02	1.6±1.3
	0.40		2.1±0.07	1.5±1.2
	2.0		2.0±0.07	0.60±0.48
	4.0		2.1±0.04	0.50±0.40

8.2 Solution characterization

ICP-OES analysis was used to measure the amount of released ions for 316L, Co-28Cr-6Mo, and Ti-6Al-4V alloys in the PBS-HSA solutions after 8, 14, and 22 weeks of immersion. The results are presented in Figure 8-4, Figure 8-5, and Figure 8-6. In these Figures, the error bars shows the calculated standard deviation of ICP-OES measurements from three solutions. The horizontal lines refer to the converted analytical detection limits of the studied ions. The released ions were higher than the detection limit except for Cr release

from 316L and Mo release from Co-28Cr-6Mo in the absence of HSA over 8 weeks of immersion. The amount of released Fe, Cr, Ni, and Mo from 316L is presented Figure 8-4 a, b, c, and d.

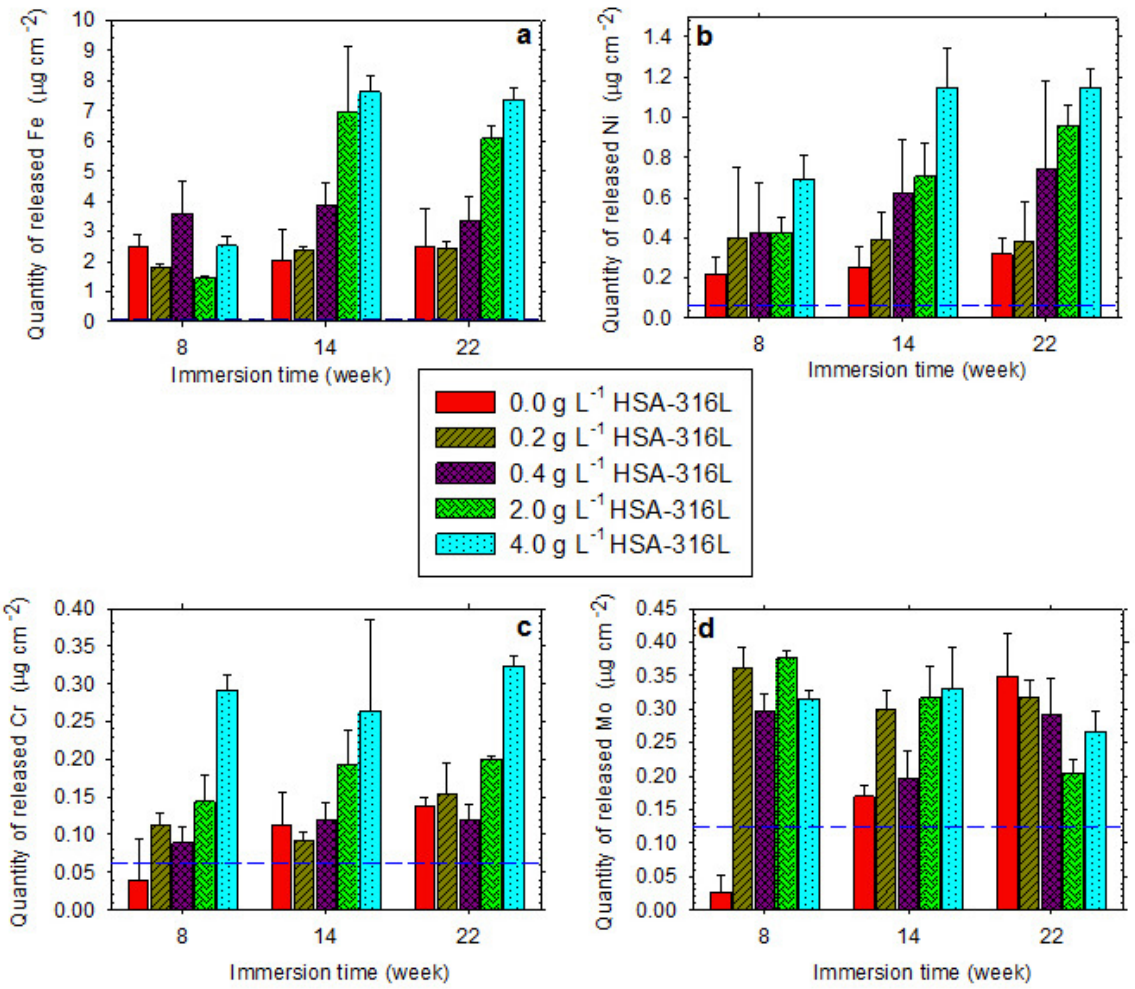

Figure 8-4 : The amount of released a) Fe, b) Ni, c) Cr, d) Mo from 316L into PBS solutions with various HSA concentrations (0 to 4 g L^{-1}) at 37 °C after 8, 14, and 22 weeks. The dash line shows the converted analytical detection limit

The amount of Fe release (Figure 8-4a) was the highest among the other 316L elements as it is the main alloy's component. High dissolution rate of Fe from stainless steel in a PBS solution was also found by Okazaki and Gotoh (Okazaki & Gotoh, 2005). The outer passive layer of the stainless steel enriches by Fe oxide while it is loosely bounded to the underlay surface (Olsson & Landolt, 2003; Omanovic & Roscoe, 1999; Shih et al., 2004). This could explain the high rate of Fe released from 316L. Fe dissolution was increased in the presence of HSA and the increase of HSA concentration also accelerated the rate of Fe release after 14 and 22 weeks (Figure 8-4 a). HSA has a high-affinity Fe^{3+} binding site located in subdomain IB (Fasano et al., 2005). This binding could produce water soluble Fe-albumin complexes such as methaemalbumin (Adams & Berman, 1980). The amount of the Fe release of 316L in a period of 8 to 14 weeks was faster compared to that between 14 and 22 weeks (Figure 8-4 a). This may indicate the Fe precipitation on 316L causing weight gain of 316L after 14 weeks. In addition, precipitation of Fe oxides and hydrated Fe oxides were found in the histological human tissue samples close to stainless steel joint implants (Winter, 1974). The 316L Ni release was ranked second after Fe release (Figure 8-4 b). The amount of dissolved Ni was elevated over incubation periods. HSA has a high affinity to bind to Ni through N-terminal binding sites (Laussac & Sarker, 1984). Release of Ni into the human body is hazardous because the interaction between Ni and biomolecules has a greater possibility than the reaction of Ni with water molecules (Hanawa, 2004). Ni depletion and Cr enrichment of the 316L surface oxide layer in simulated biological fluid were also determined (Hanawa et al., 2002). The release of Cr and Mo (Figure 8-4 c and d) were slow

compared with the Fe release from 316L. No correlation was found between Cr and Mo dissolutions as a function of the HSA concentration.

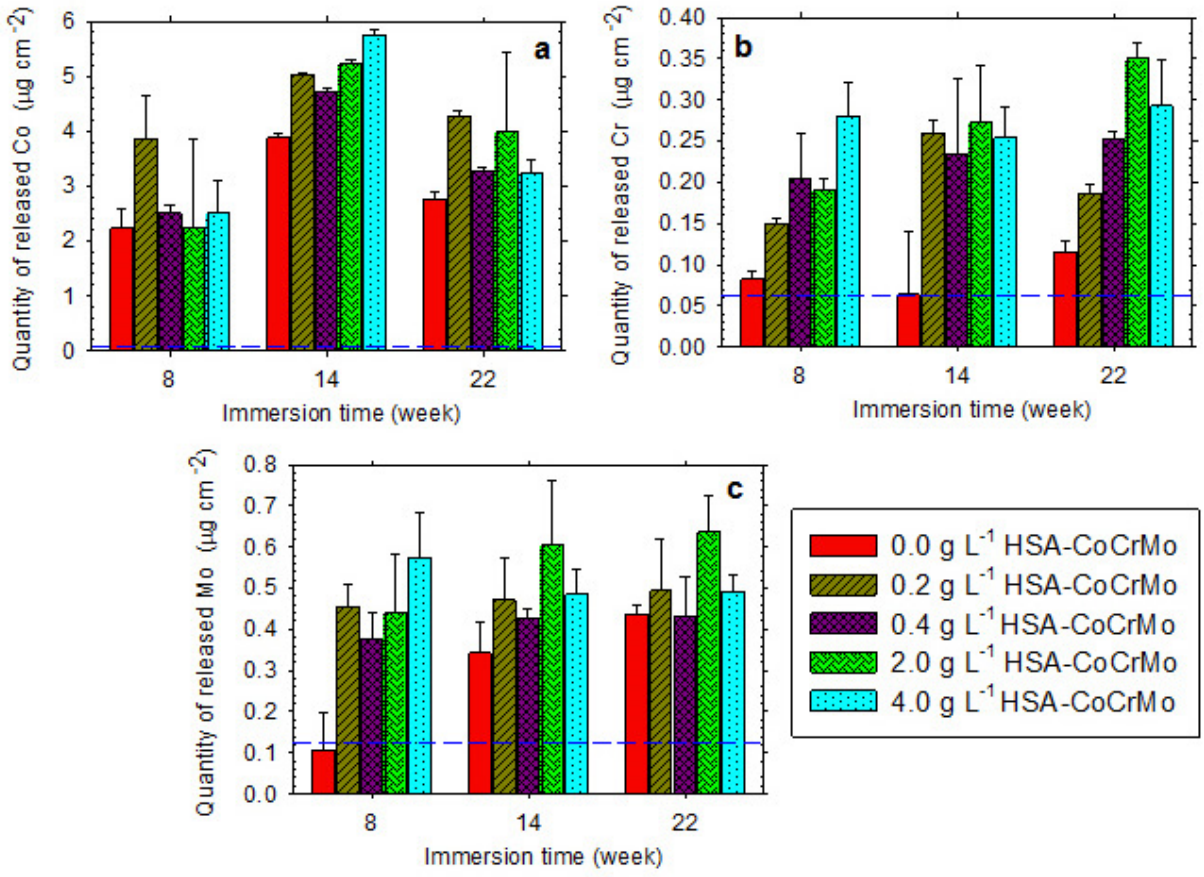

Figure 8-5 : The amount of released a) Co, b) Cr, and c) Mo from Co-28Cr-6Mo into PBS solutions with various HSA concentrations (0 to 4 g L^{-1}) at 37 °C after 8, 14, and 22 weeks. The dash line shows the converted analytical detection limit

Concentrations of Co, Cr, and Mo in the PBS-HSA solutions after 8, 14, and 22 weeks of immersion of Co-28Cr-6Mo alloys are presented in Figure 8-5a, b, and c. Co is the major component of the Co-28Cr-6Mo alloy and it showed the highest dissolution rate among other alloying elements of CoCrMo samples. The major component of the oxide layer of Co-28Cr-

6Mo and 316L alloy is Cr oxides (Hodgson et al., 2004; Ouerd et al., 2008). The Gibb's free energy of formation of CoO (-214 KJ mol^{-1}) and Fe_2O_3 (-724.2 KJ mol^{-1}) are higher than that of Cr_2O_3 (-1058.1 KJ mol^{-1}) (Speight, 2005). This could explain the faster Co and Fe dissolution rates than the Cr dissolution rate from CoCrMo and 316L alloys (Figure 8-4 a, b, Figure 8-5a, and Figure 8-5b). The dissolution rate of cobalt, similar to Fe release from 316L, was decremented after 14 weeks (Figure 8-5a) which could also refer to precipitation of Co complex leading to the weight gain of Co-28Cr-6Mo alloy after 14 weeks. There was no certain relationship between the HSA concentrations and Co release of this alloy over three immersion periods. HSA is known as a physiological carrier of Co^{2+} ions which could bind to Co from carboxylate and N-terminal binding sites (Mothes & Faller, 2007; Sokołowska et al., 2009). The increase of blood Co concentration after hip replacement surgeries has been indicated in clinical studies (Brodner et al., 2003; Cobb & Schmalzreid, 2006; Lhotka et al., 2003; Schaffer et al., 1999). The blood Co concentrations in seven female patients prior to and after total hip replacement surgeries were measured (Milošev et al., 2005). The implants were made of a Co–28Cr–6Mo femoral head and Co–28Cr–6Mo inlay acetabular component. The level of Co in an average period of 60 ± 20 months increased from a mean value of 0.10 μg L^{-1} to 0.35 μg L^{-1}. The increase of Co concentration could cause tissue necrosis (Cobb & Schmalzreid, 2006), chromosomal damage, and carcinogenesis (Granchi et al., 2000; Savarino et al., 2003). Mo dissolution from CoCrMo alloys increased over a period of 22 weeks in no HSA solutions (Figure 8-5c). Mo dissolution increased over a period of 22 weeks in no HSA solutions. In the presence of HSA, Mo release was rapid after 8 and 14 weeks;

however, it did not significantly vary after 14 incubation weeks. The following Mo oxide reaction (Equation 8-1) in protein solutions is suggested by Martin *et al*. (Martin et al., 2013).

$$MoO_2 + 2H_2O \rightleftharpoons MoO_4^{-2} + 4H^+ + 2e- \quad 8\text{-}1$$

The initial dominant event is ion exchange at the metal-solution interface followed by thermodynamic equilibrium of the surface protein adsorption and desorption events (Lowenberg et al., 1994). When a stable adsorbed protein layer is formed, the ion exchange event slows down or stops (Lowenberg et al., 1994). Therefore, proteins could increase the dissolution rate of the Mo oxides to some extent; however, Mo leaching was impeded by the development of a stable and complete covering HSA layer.

Release of Ti and V were detected from Ti-6Al-4V alloys in the PBS solutions with 0-4 g L^{-1} HSA (Figure 8-6a and Figure 8-6b).

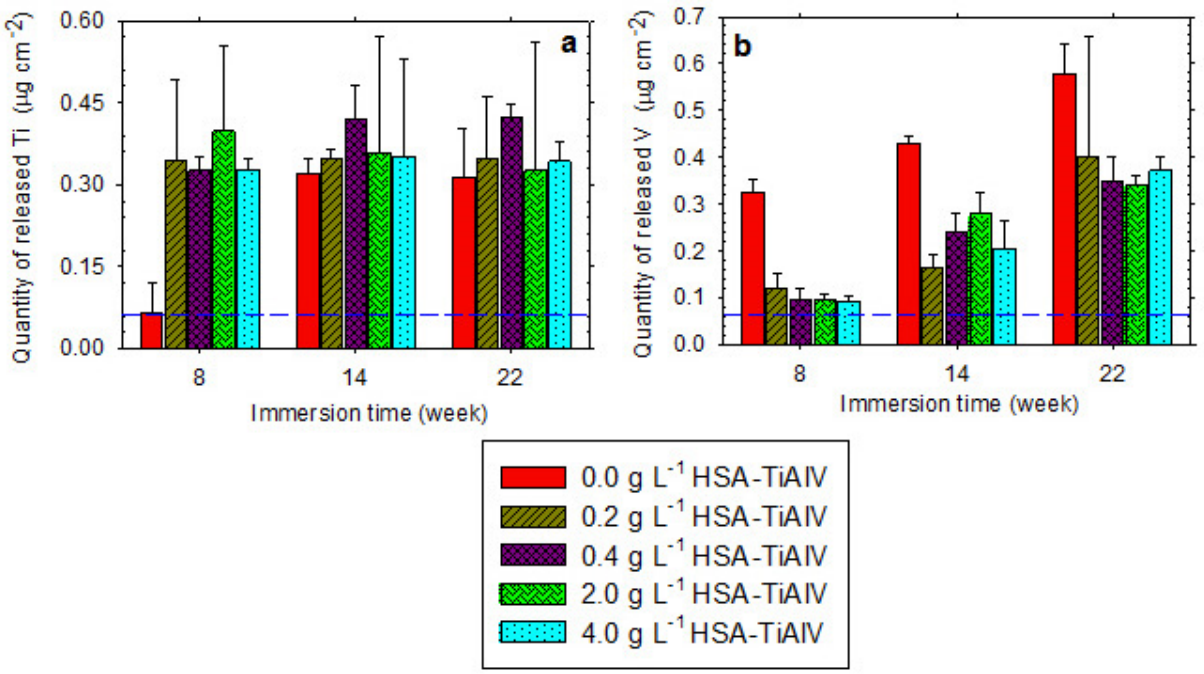

Figure 8-6 : The amount of released a) Ti and b) V from Ti-6Al-4V into PBS solutions with various HSA concentrations (0 to 4 g L^{-1}) at 37 °C after 8, 14, and 22 weeks. The dash line shows the converted analytical detection limit

In only PBS solutions, the rate of Ti release was elevated after 14 weeks of immersion and it did not expressively change after a longer immersion period. In an in-vivo study, the release of Ti was monitored by inserting Ti fibers into the tibia of rabbits for 12 months (Bianco et al. 1997). Ti was released in the surrounding tissues and the level of Ti in serum and urine did not change significantly. Hanawa demonstrated the formation of precipitation of phosphate or Ti phosphate with time on the surface of Ti-6Al-4V (Hanawa, 2004). The deposition of these species could reduce the rate of Ti release. The formation of phosphate

precipitates is more likely in the PBS solutions, which is discussed further with the XPS results. Therefore, phosphate precipitates can decrease Ti dissolution. The rate of Ti release became larger in presence of HSA. HSA may cause the dissolution of the phosphate precipitates and Ti species as is proposed by Equation 8-2 (Ducheyne et al., 1992).

$$Ti^{4+}\text{ (in the oxide)}.\ HPO_4^{2-}\text{ (ads)} \rightarrow TiHPO_4^{2-}\text{ (aq)} \qquad 8\text{-}2$$

The addition of HSA to the PBS solutions also decreased the V dissolution rate (Figure 8-6b). Strong and loose bindings between HSA and Vanadyl cations (VO^{2+}) (Purcell et al., 2001) as well as between NH_3^+ and VO_3^- (Nechay et al., 1986) have been reported. Vanadium leaching was increased by extending the immersion period. Hence, precipitation of protein-V complexes is unlikely although the rate of V release slowed down in the PBS-HSA solutions due to growth of the adsorbed layer.

8.3 Surface characterization

The oxide layer composition of the specimens over 22 weeks of exposure to PBS solutions with 0, 0.2, and 4 g L^{-1} HSA were analyzed by XPS. In the survey scans, peaks of carbon (C 1s), nitrogen (N 1s), oxygen (O 1s), and phosphorous (2s and 2p) were detected for 316L (Figure 8-7), Co-28Cr-6Mo (Figure 8-8), and Ti-6Al-4V (Figure 8-9). A part of the measured carbon content of the passive layer belongs to contamination which is almost unavoidable in XPS analysis. Carbon could also be attributed to amino acids sequence of HSA such as cycteine ($C_3H_7NO_2S$) and a single tryptophan ($C_{11}H_{12}N_2O_2$) (Carter & Ho, 1994; He & Carter, 1992).

The carbon concentration was then normalized by the elimination of the contaminated carbon concentrations measured in the absence of HSA. The oxide compositions (at. %) of each specimen in the PBS solutions of 0, 0.2, and 4 g L^{-1} HSA are reported in Table 8-2. The oxide composition of the specimens contained nitrogen when the samples were immersed in solutions only containing HSA (Figure 8-7, Figure 8-8, Figure 8-9 and Table 8-2).

.

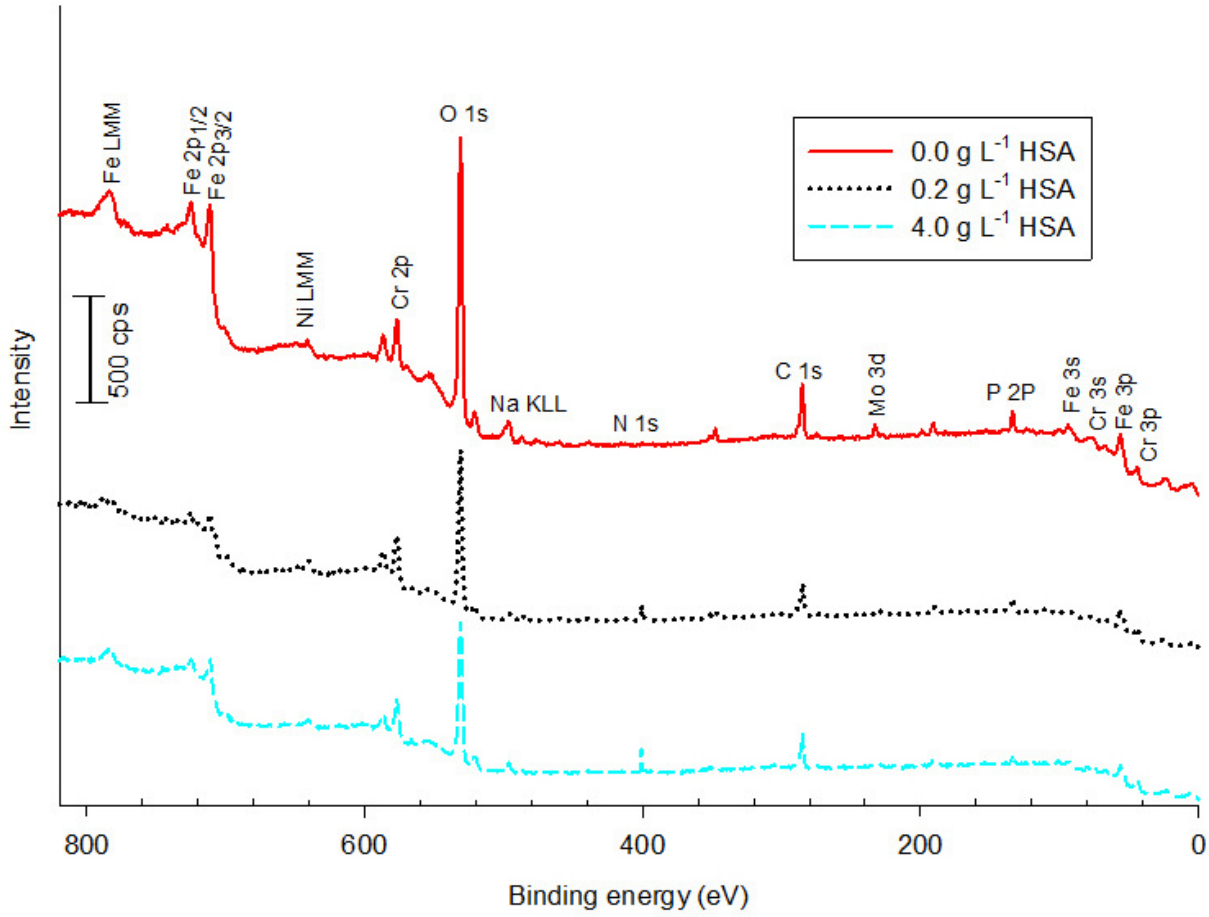

Figure 8-7 : XPS Survey scan of 316L after 22 weeks of exposure in solutions of PBS with HSA concentrations of 0, 0.2, and 4 g L^{-1} at 37 °C

Table 8-2 : Surface film composition of 316L, Co-28Cr-6Mo, and Ti-6Al-4V alloys after 22 weeks exposure to the solutions of PBS with HSA concentrations of 0, 0.2, and 4 g L^{-1} at 37 °C

Sample	HSA	Atomic concentration (at %)										
		C	Fe	Cr	Co	Mo	Ti	N	O	P	Na	Ni
	(g L^{-1})	1s	2p	2p	2p	3d	2p	1s	1s	2p	1s	2p
316L	0.0	0.0	7.4	5.7		0.50			79	7.3		
	0.2	0.54	7.8	9.2		0.52		0.80	73	6.6	1.1	0.73
	4.0	5.3	4.4	7.2		0.60		2.2	73	5.0	1.1	1.3
Co-28Cr-6Mo	0.0	0.0		15		1.0		0.0	78	5.7		
	0.2	7.7		15	5.1	0.70		1.5	64	5.5		
	4.0	14		8.2	2.5	0.40		7.1	62	5.5		
Ti-6Al-4V	0.0	0.0					13	0.0	76	4.2	6.7	
	0.2	18					8.6	10	58	1.9	2.9	
	4.0	6.8					15	8.4	65	1.6	3.0	

Along with the presence of carbon, the detection of nitrogen in the oxide composition indicates HSA adsorption. The nitrogen and carbon contents of the 316L and Co-28Cr-6Mo passive layer were also elevated in the high HSA concentration solutions. This implies a dependency of the HSA adsorption to the HSA concentrations. This observation was reverse for Ti-6Al-4V alloy in which the adsorption of protein decreased by the increase of HSA concentrations.

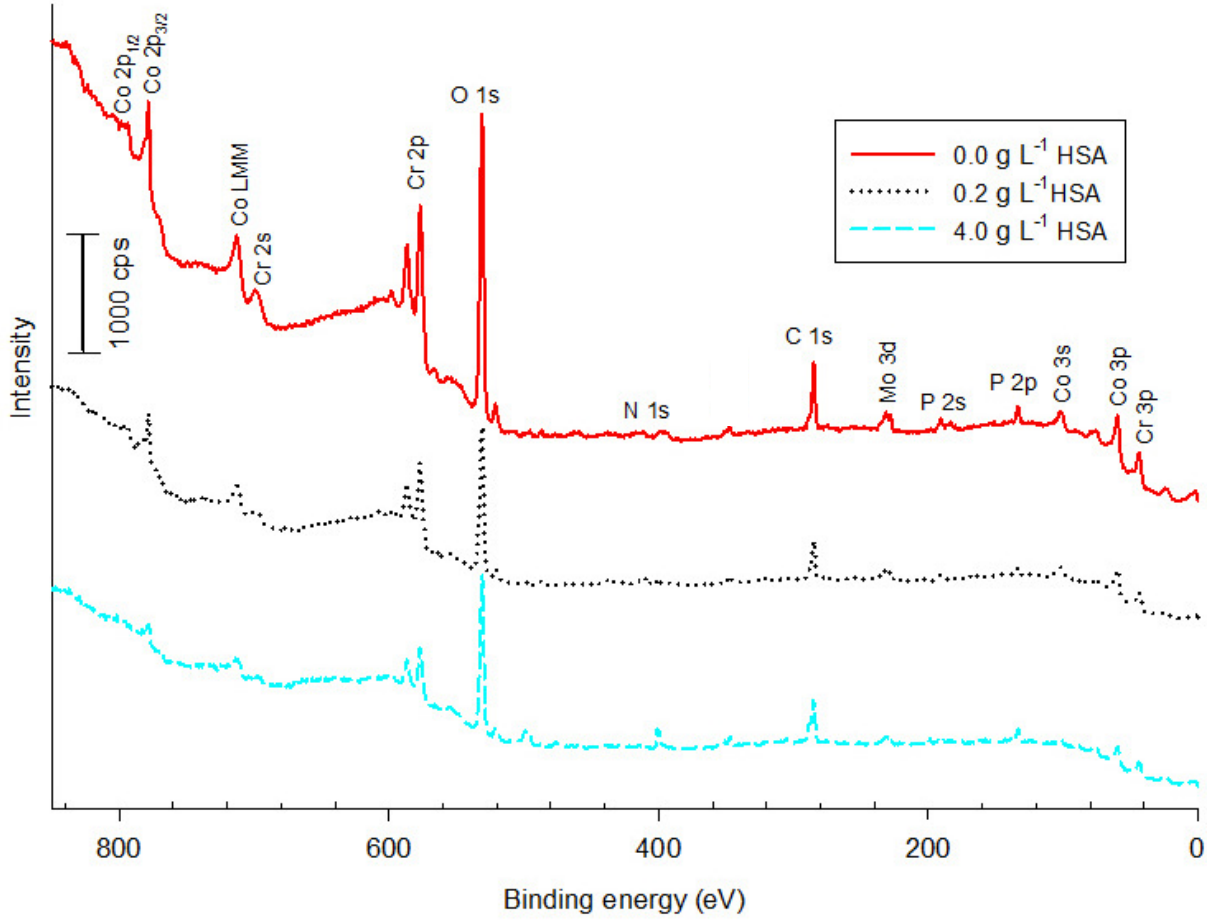

Figure 8-8 : XPS Survey scan of Co-28Cr-6Mo after 22 weeks of exposure in solutions of PBS with HSA concentrations of 0, 0.2, and 4 g L^{-1} at 37 °C

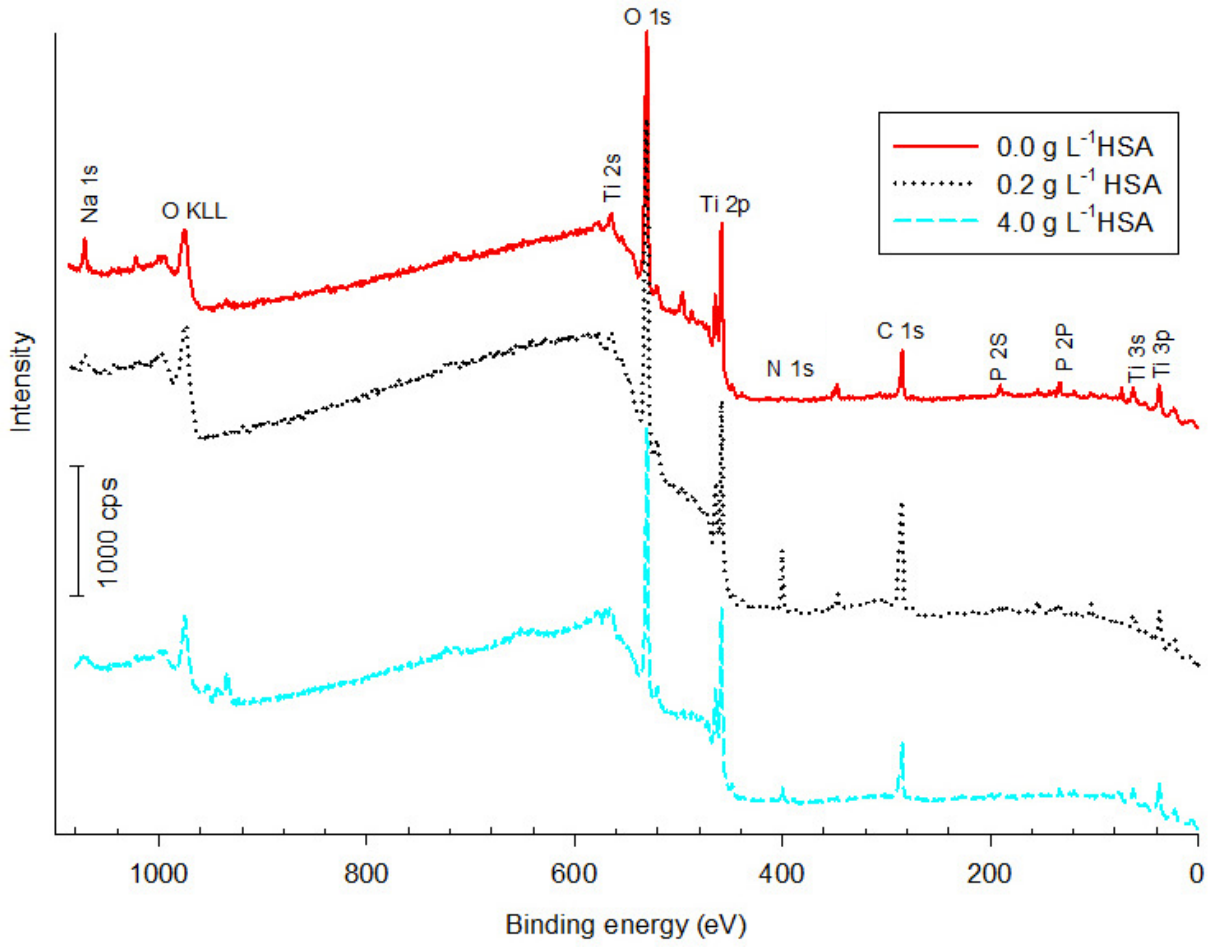

Figure 8-9 : XPS Survey scan of Ti-6Al-4V after 22 weeks of exposure in solutions of PBS with HSA concentrations of 0, 0.2, and 4 g L^{-1} at 37 °C

The amount of the detected oxygen and phosphorous were decremented in solution with HSA compared to those formed in the absence of HSA. This observation was also reported for the similar alloys immersed in BSA solutions (Karimi et al., 2012). It seems that protein can impede phosphorous adsorption because protein adsorption forms a negatively-charged barrier film (such as $R\text{-}COO^-$) at a pH of 6-8 (Kragh-Hansen et al., 2002; Lewis et al., 2005)

which could repel anions of phosphorous and oxygen. The detected oxygen is assumed to be oxy-hydroxides coming from the surface oxide. The oxygen can exist on the specimen's surface through bonds with metals and organic compounds (Karimi et al., 2012; Lin & Bumgardner, 2004). The decrease of the detected oxygen in HSA solutions could refer to the thinning of the passive layer. The released Fe from 316L and the Ti dissolution from Ti-6Al-4V alloys in HSA solutions were identified by ICP analysis (Figure 8-4a and Figure 8-6a). In addition to carbon, nitrogen, oxygen, and phosphorous, the spectra of Fe, Cr, Mo, Na, and Ni for 316L (Figure 8-7), Cr, Co, and Mo for Co-28Cr-6Mo alloy (Figure 8-8), and Ti and Na for Ti-6Al-4V were identified (Figure 8-9).

The iron and chromium content of the 316L reached the highest value when 316L was immersed in 0.2 g L^{-1} HSA solutions (Table 8-2). The chromium peak was deconvoluted to two sub peaks of Cr_2O_3 $2p_{1/2}$ and $2p_{3/2}$ with binding energies of 576.4 and 585.4 eV, respectively (Figure 8-10). The presence of Cr_2O_3 on 316L in simulated biological environments was also detected (Hanawa et al., 2001; Hiromoto et al., 2005; Karimi et al., 2012; Lori & Hanawa, 2001).

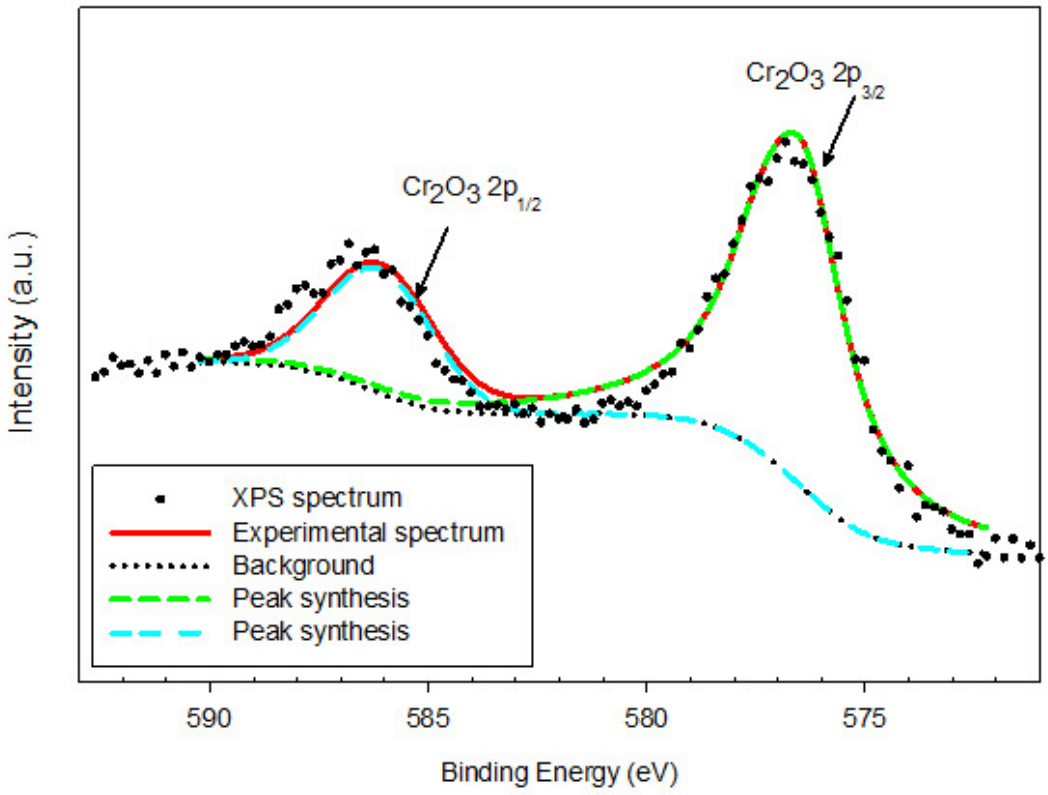

Figure 8-10 : Measured high resolution spectra of Cr 2p of the 316L after 22 weeks of exposure in PBS solutions with 4 g L^{-1} HSA concentration at 37 °C along with the peak doublets

The deconvolution of the Fe spectra of 316L in 0, 0.2, and 4 g L^{-1} HSA solutions are shown in Figure 8-11 a, b, and c. In the 4 g L^{-1} HSA solution, the Fe peak was decomposed into four doublets (Figure 8-11c) originating from Fe $2p_{1/2}$ and $2p_{3/2}$. These peaks correspond to the presence of metallic Fe (720.1 and 706.8 eV), FeOOH (724.2 eV), and Fe_2O_3 (710.6 eV) (Bastidas et al., 2002; Joyner et al., 1980; Tan et al., 1990). The peak at the lower binding energy corresponds to Fe $2p_{3/2}$ which was not identified in 0 (Figure 8-11 a) and 0.2 g L^{-1}

(Figure 8-11 b) HSA solutions. The detection of the metallic-state elements in the substrate indicates the formation of a very thin oxide layer. The peak intensities of Fe_2O_3 and FeOOH also decreased significantly in 4 g L^{-1} HSA solutions. Therefore, the 316L passive layer formed in the 4 g L^{-1} HSA is thinner than that developed in 0 and 0.2 g L^{-1} HSA solutions. The ICP results also showed that the release of Fe from the 316L samples incubated in the 4 g L^{-1} HSA solution increased after 22 weeks. As a result, Fe_2O_3 and FeOOH leached out in high HSA solutions. The interaction of negatively-charged carboxylate groups of the proteins with Fe and the formation of protein-Fe compounds (Adams & Berman, 1980; Karimi & Alfantazi, 2013; Omanovic & Roscoe, 1999) can decrease the oxide layer thickness in high HSA solutions.

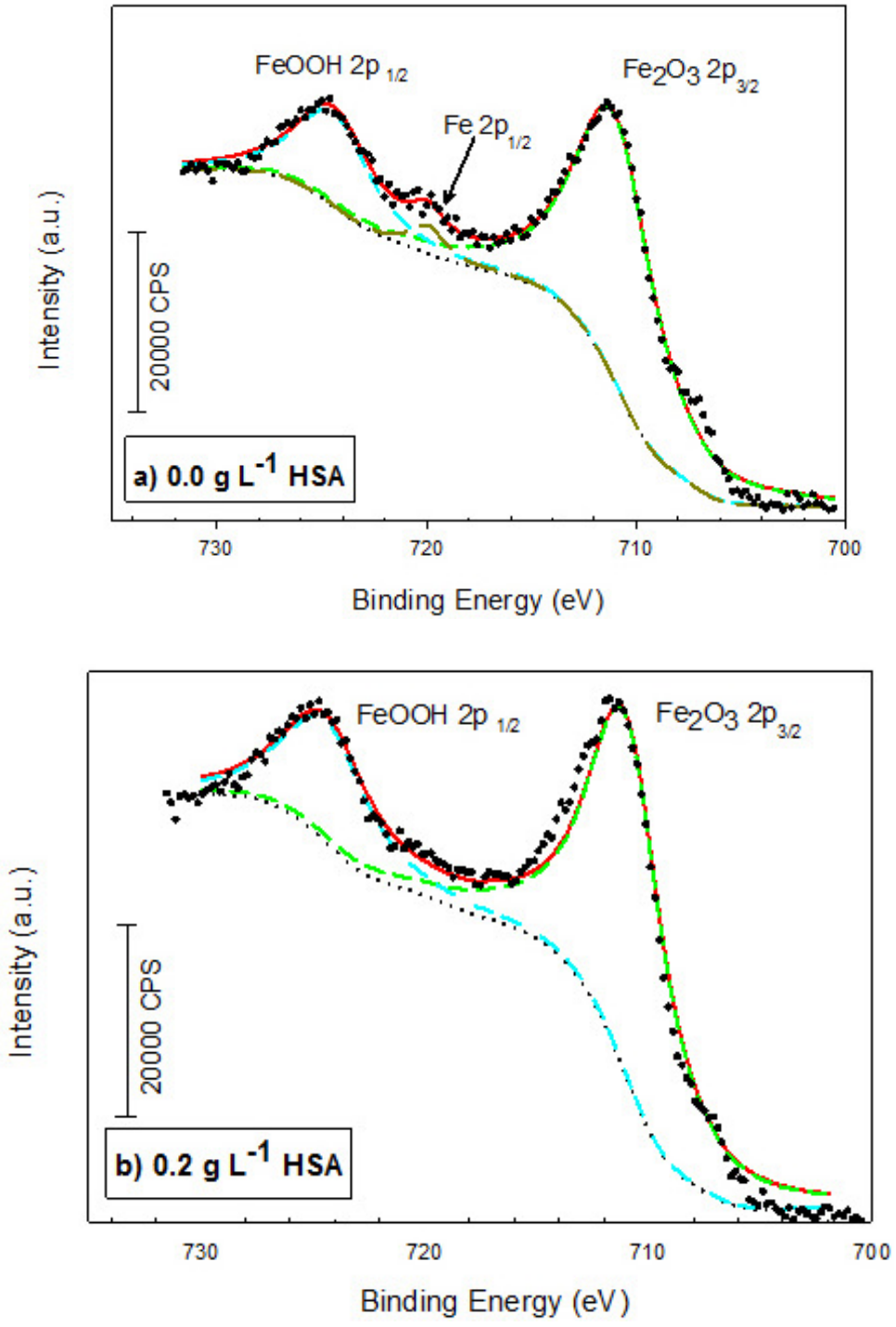

Figure 8-11 : Measured high resolution spectra of Fe 2p of the 316L after 22 weeks of exposure in PBS solutions with a) 0.0, b) 0.2, and c) 4.0 g L^{-1} HSA concentration at 37 °C along with the peak doublets

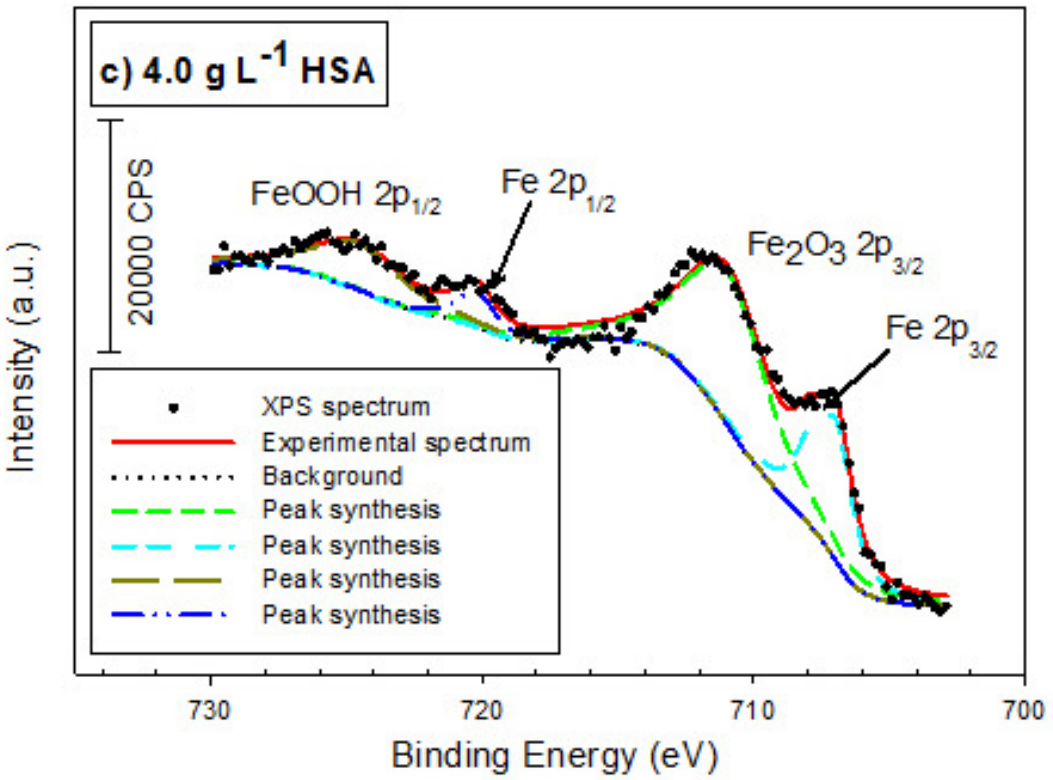

Figure 8-11: (Cont'd) Measured high resolution spectra of Fe 2p of the 316L after 22 weeks of exposure in PBS solutions with a) 0.0, b) 0.2, and c) 4.0 g L^{-1} HSA concentration at 37 °C along with the peak doublets

They were not detected in the oxide layer of 316L incubated in PBS-BSA solutions (Karimi et al., 2012). It seems that HSA could prompt Na adsorption and Na could provide active sites for Mo adsorption. The narrow scan of 316L near Mo electron-binding energy revealed the existence of three species of Mo at binding energies of 227.8, 231.5, and 235.1 eV corresponding to metallic Mo (Mo^0 $3d_{5/2}$) and oxidized Mo (MoO_2 and MoO_3) (Cimino & De Angelis, 1975; Okazaki & Gotoh, 2005; Tateishi et al., 1997). The deconvolution of the Mo spectra to these sub-peaks is depicted in Figure 8-12.

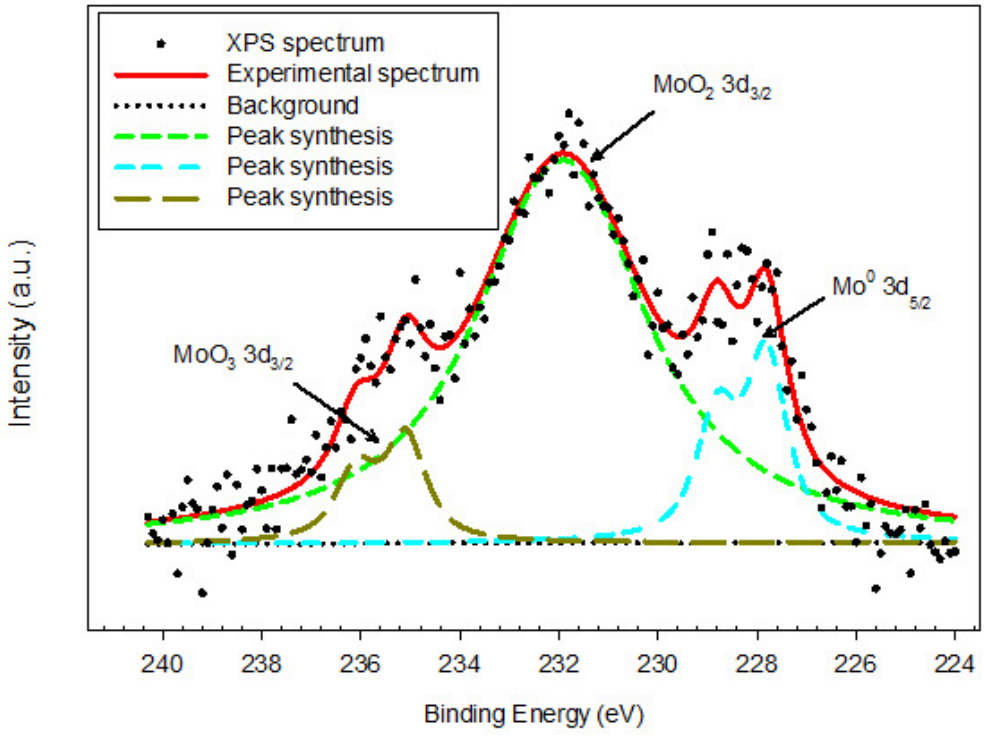

Figure 8-12 : Measured high resolution spectra of Mo 3d of the 316L after 22 weeks of exposure in PBS solutions with 4.0 g L^{-1} HSA concentration at 37 °C along with the peak doublets

Metallic Ni $2p_{3/2}$ was also identified at a binding energy of 852.8 eV in the XPS analysis of 316L immersed in PBS-HSA solutions (Figure 8-13). The presence of metallic Ni $2p_{3/2}$ with this level of energy was shown (Bianchi et al., 1993). Similar to Na and Mo, Ni did not appear in the XPS analysis of 316L in the PBS-BSA solutions. In our previous electrochemical impedance spectroscopy studies of 316L in similar environments, one time constant in the presence of BSA (Karimi et al., 2011) and a two-time constant in HSA solutions (Karimi & Alfantazi, 2013) were detected. The presence of Fe_2O_3, MoO_2, MoO_3, and Ni in the passive

layer of 316L formed in the HSA solutions could describe the appearance of two time constants.

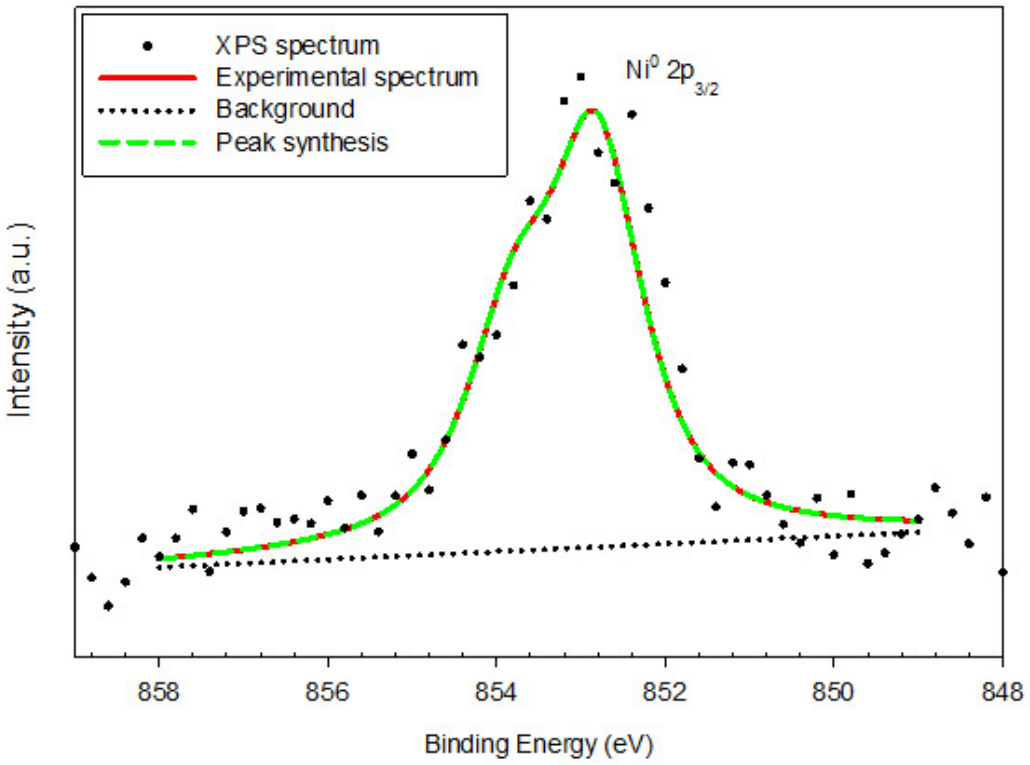

Figure 8-13 : Measured high resolution spectra of Ni 3d of the 316L after 22 weeks of exposure in PBS solutions with 4.0 g L^{-1} HSA concentration at 37 °C along with the peak doublets

The Cr concentration of Co-28Cr-6Mo oxide layer did not change considerably in the presence of 0 and 0.2 g L^{-1} HSA. However, it reduced when the HSA concentration was increased to 4 g L^{-1} (Table 8-2). Co released into the PBS-HSA solutions from Co-28Cr-6Mo alloy. The CoCrMo oxide layer did not contain Co when the samples were immersed in only PBS solution (Figure 8-8). Co appeared when the CoCrMo samples were incubated in the 0.2 g L^{-1} HSA solutions. However, the increase in the HSA concentration reduced the Co

concentration of the oxide layer. Not only the Co and Cr but also the Mo concentration of the CoCrMo oxide layer was decreased by increasing the HSA concentrations. This evidence showed that HSA can block the Co-28Cr-6Mo oxide layer from the solutions to prevent or slow down the growth of the oxide layer in the 4 g L^{-1} HSA solutions. It is proposed that negatively-charged albumin can interact with positively-charged ions and form an adsorbed film of protein (Valero Vidal & Muñoz, 2008) or produce metal/protein/hydroxylated compounds (Khan et al., 1999). In low HSA solutions, the rate of the formation of the metal-protein compound is faster than the growth of the adsorbed protein layer. However, the formation of the adsorb layer blocked the growth of the oxide layer in the high HSA concentration solutions. This observation can be confirmed by the reduction of oxygen content of the oxide layer as HSA was increased. Moreover, the nitrogen content of Co-28Cr-6Mo showed that the protein adsorption was expressively enriched by the addition and increase of HSA (Table 8-2).

The high resolution spectra of the Cr peak collected from Co-28Cr-6Mo showed a similar trend as the Cr spectra measured for 316L (Figure 8-10). In Figure 8-14, the XPS spectra of Co formed in the 4 g L^{-1} HSA solution was decomposed into three peaks of metallic Co $2p_{3/2}$ and $2p_{1/2}$ and oxidized CoO $2p_{3/2}$ with the binding energies of 778, 793.3, and 780.9 eV, respectively (Bonnelle et al., 1975; McIntyre & Cook, 1975; Oku & Hirokawa, 1976). In the BSA solution, the metallic Co at 793.3 eV was not detected (Figure 6-13) (Karimi et al., 2012). The formation of two metallic Co compounds could indicate that the oxide layer of the Co-28Cr-6Mo alloy is thinner in the HSA solutions than in the BSA solutions.

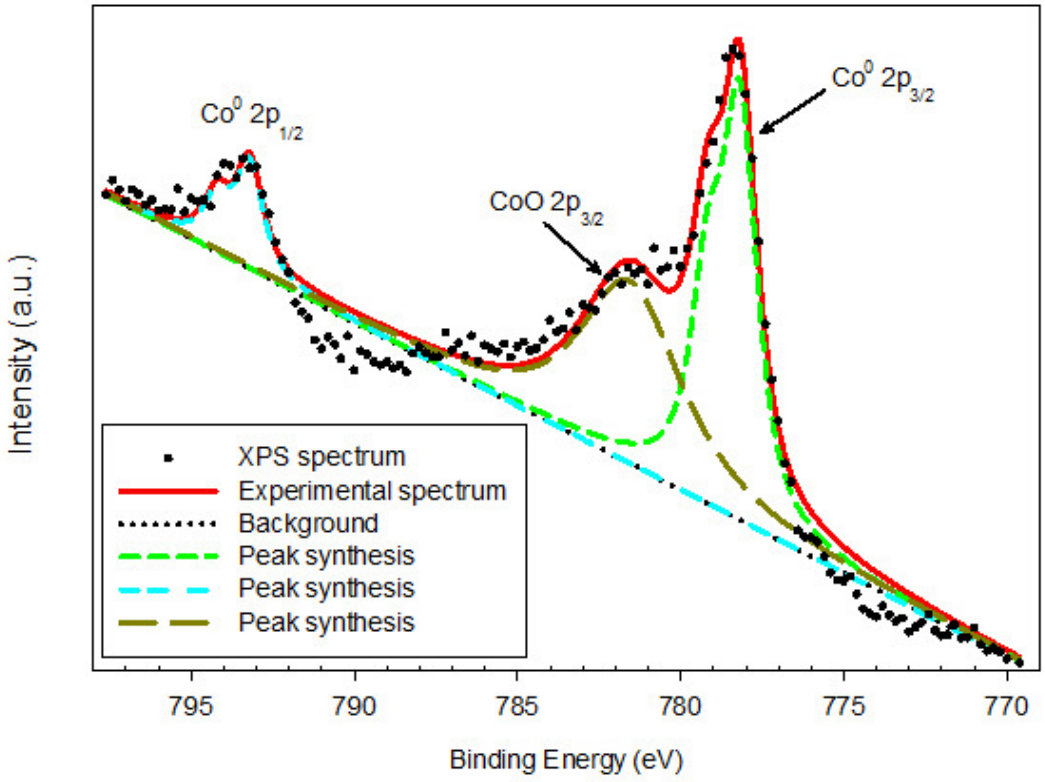

Figure 8-14 : Measured high resolution spectra of Co 2p of the Co-28Cr-6Mo sample after 22 weeks of exposure in PBS solutions with 4.0 g L^{-1} HSA concentration at 37 °C along with the peak doublets

Figure 8-15 represents the measured and experimental XPS spectrum of Mo in 4 g L^{-1} BSA and HSA along with the Mo deconvoluted peaks of Co-28Cr-6Mo alloy. In the BSA solutions, the Mo sub-peaks were determined at 231.2 and 235.5 eV (Karimi et al., 2012). In the HSA solutions, these deconvoluted peaks shifted to 231.5 and 234.7 eV, respectively. The sub-peak at the 231.5 eV corresponds to MoO_2 (Cimino & De Angelis, 1975) and the one at the binding energy of 234.7 eV corresponds to $(N\ (C_4H_9)_4)_3\ P\ Mo_{12}\ O_{38}$ (Kawafune & Matsubayashi, 1991) resulted from the interaction of HSA with Mo. This can confirm the adsorption of HSA on the oxide layer of the CoCrMo alloy which would slow down the growth

of the oxide layer in the high HSA concentration solutions. Phosphorous was not detected in the XPS analysis of the CoCrMo alloy immersed in the BSA solutions. Furthermore, the binding energy of the deconvoluted peak of Mo was at 235.5 eV, denoted to MoO_3 (Karimi et al., 2012). These observations indicated the effect of the protein type on chemical composition of the Co-28Cr-6Mo alloy.

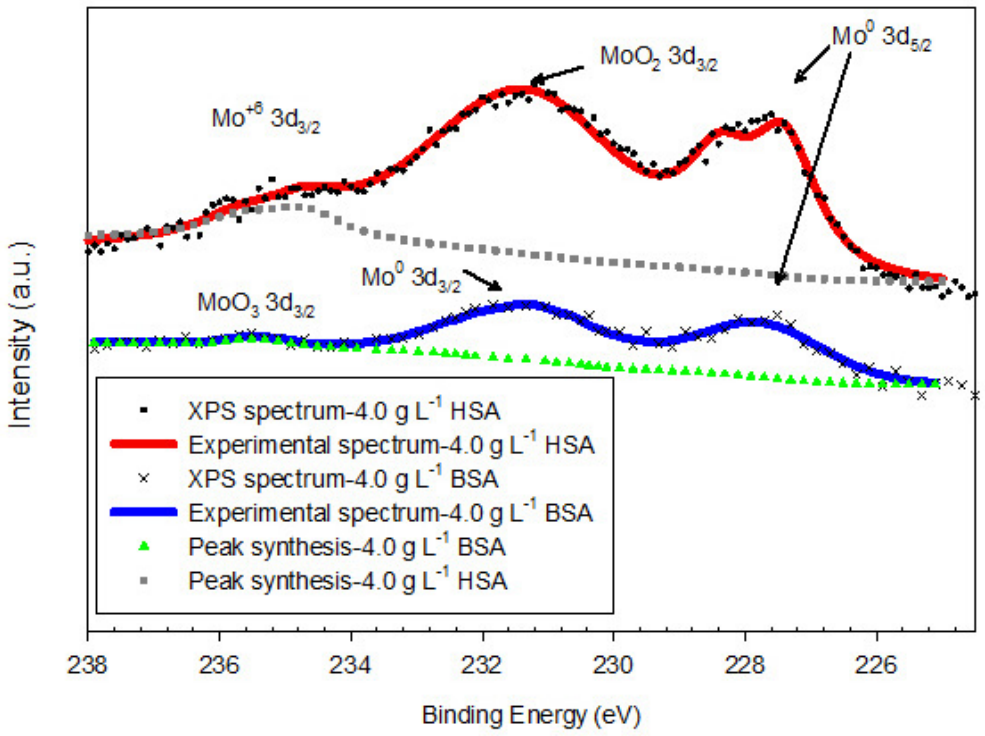

Figure 8-15 : Measured high resolution spectra of Mo 2p of the Co-28Cr-6Mo sample after 22 weeks of exposure in PBS solutions with 4.0 g L^{-1} HSA and BSA concentration at 37 °C along with the peak doublets

The oxygen and Ti concentration of Ti-6Al-4V dropped in the PBS solution with 0.2 g L^{-1} HSA (Figure 8-9 and Table8-2). This indicates that the interaction of HSA and titanium could

release the titanium oxides into the PBS solution. The increase of the HSA concentration to 4 g L^{-1} elevated the concentrations of these species. The adsorption of HSA was diminished in the solution with high protein concentration rather than that with low protein concentration which had been discussed in our previous studies (Karimi et al., 2012; Karimi & Alfantazi, 2013). The decrease of the nitrogen content of Ti-6Al-4V in 4 g L^{-1} HSA was also determined (Table 8-2) which is indicative of the lower HSA adsorption in the high HSA solutions. In addition to the presence of some cations such as Na^{+}, the number of surface hydroxyl groups (acidic or basic) can influence the reactivity of Ti with proteins (Feng et al., 2002). The chemisorption of proteins onto the Ti surface can be accomplished through the interaction of these surface hydroxyl groups and the carbon and oxygen components of proteins (Feng et al., 2002; Klinger et al., 1997). Therefore, the increase of the hydroxyl group could enhance the protein adsorption and block the interface of the oxide layer and solution. The blockage of the surface could stop further dissolution of Ti. The ICP results confirmed the dissolution and precipitation of Ti in 0.2 and 4 g L^{-1} HSA after 22 weeks of immersion, respectively.

The existence of metallic and organic bonds with oxygen on the Ti-6Al-4V surface was present in our previous study (Figure 6-10) (Karimi et al., 2012). The result of peak fitting for the Ti-6Al-4V alloy for the Ti 2p doublet immersed in HSA solution was similar to one found for this alloy incubated in BSA solution (Karimi et al., 2012). Sodium peaks also appeared in the survey scan of the Ti-6Al-4V alloy (Figure 8-9). The major Na peak (Figure 8-16b) at 1072.2 eV for Ti-6Al-4V sample immersed in 4 g L^{-1} HSA could correspond to sodium (2-methyl-propenoate) or $Na(OC(O)C(CH_3)CH_2)$ (Hammond et al., 1981). This peak

was shifted to a lower binding energy (1071.2 eV) when the Ti-6Al-4V alloy was immersed in the BSA solution (Figure 8-16a).

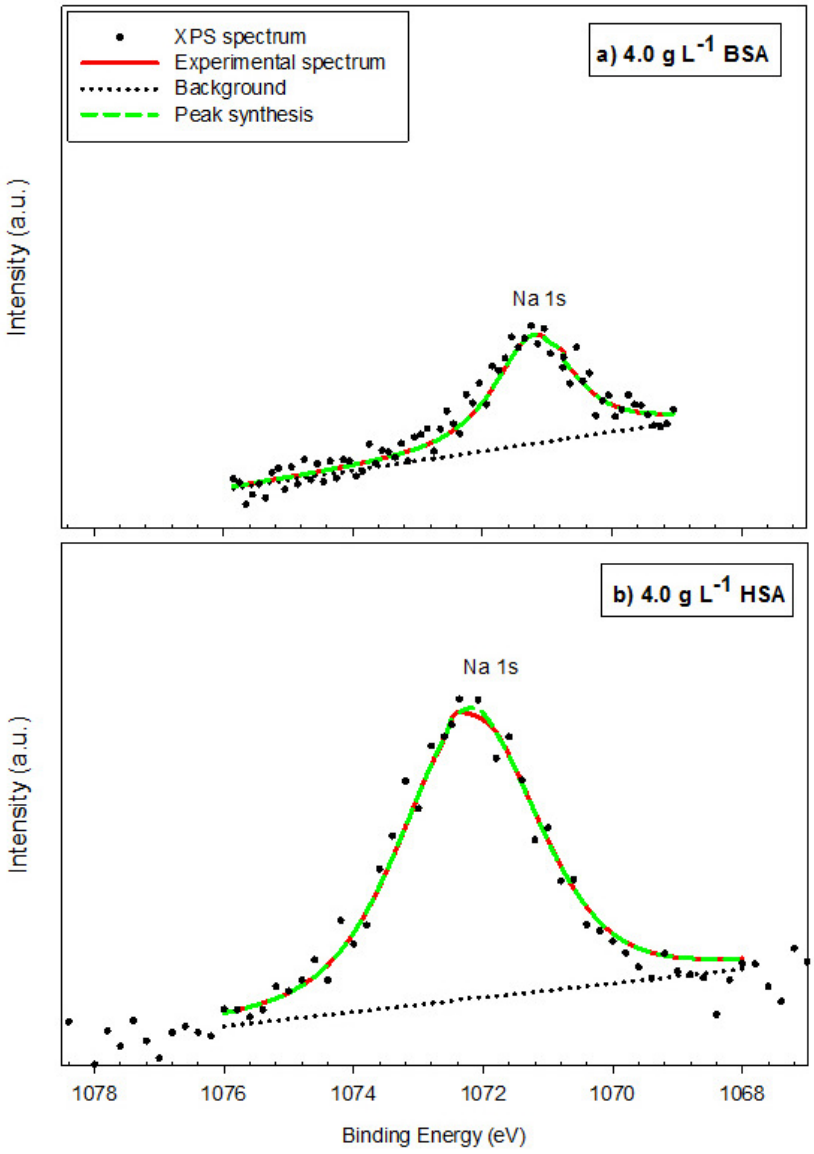

Figure 8-16 : Measured high resolution spectra of Na 1s of the Ti-6Al-4V sample after 22 weeks of exposure to PBS solutions with a) 4.0 g L^{-1} BSA and b) 4.0 g L^{-1} HSA concentration at 37 °C along with the peak doublets

In addition, the survey scan of Ti-6Al-4V oxide layer revealed the presence of not only sodium but also sulphur (Karimi et al., 2012). Hence, the peak at 1071.2 eV could be sodium mercaptoacetate (Na ($HSCH_2COO$)) (Wagner et al., 1992). This means that sodium acts as a bridge to bind the sulfhydryl group of BSA to titanium whereas sodium could bridge the carboxyl group of HSA to the Ti-6Al-4V surface.

8.4 Summary

The experimental results of weight loss, ion release, and surface characterization of three commonly used biomaterials (316L, Co-28Cr-6Mo, and Ti-6Al-4V) in the PBS solutions with five different HSA concentrations revealed the following conclusions:

- The selected bio-metallic alloys gained weight after 14 weeks of immersion. This can be addressed by precipitation of Fe and Co on 316L and Co-28Cr-6Mo alloys, respectively. Precipitations of phosphate impeded Ti release from the Ti-6Al-4V alloy.
- The weight loss measurements were used to calculate corrosion rates. The corrosion rates obtained from static immersion experiments were consistent with those calculated from polarization resistance determined by EIS measurements.
- Presence of HSA increased Fe and Ni dissolution from 316L, Co, Cr, and Mo from Co-28Cr-6Mo, and Ti from Ti-6Al-4V alloys. The XPS results indicated the thinning of the 316L and Co-28Cr-6Mo oxide layer in HSA solutions. The phosphates

leaching from Ti-6Al-4V passive layer into HSA solutions increased the Ti release rate.

- The XPS analysis of CoCrMo alloy revealed that the interaction of HSA and Mo produced organo-metallic compounds of $(N\ (C_4H_9)_4)_3\ P\ Mo_{12}\ O_{38}$ while the MoO_3 was detected in the oxide layer of CoCrMo alloy immersed in BSA solution.
- The adsorption of Na into the Ti-6Al-4V oxide layer depends on the type of protein. In the presence of HSA, sodium (2-methyl-propenoate) was detected whereas Na bounded to the sulfhydryl group of BSA and formed sodium mercaptoacetate.

9 Conclusions

Many implants placed in the body perform their functions without problems, however, a percentage of implants fail and have to be removed from the body by surgery. Implant failure significantly impacts the physical and mental health of the recipient. Not only the revision surgeries are painful but also the cost of revision surgery is not economical. Failure of metallic implant could result from corrosion and high dissolution rate of ions which are the consequences of the interaction of body fluid with the metal-oxide surface. The released ions disturb cell behavior as well as cellular metabolism leading to fatal tumorous diseases and cancers. The corrosion and ion release of metallic biomaterials is an approach to address the failure of metallic implants and to propose solutions. Studying the corrosion behavior of metallic biomaterials in vitro requires a real body environment simulation with the presence of species in the human body fluids. One of these species is protein. In this thesis, the influence of bovine and human serum albumin was investigated on the corrosion behavior of 316L, Co-28Cr-6Mo, and Ti-6Al-4V in aerated solutions of PBS. The following conclusions are drawn by conducting electrochemical corrosion experiments:

- OCP values of all the samples shifted towards more cathodic potentials by increasing BSA and HSA concentrations. The decrease in OCP values were observed at low BSA concentrations for Co-28Cr-6Mo alloy and at high BSA concentrations for the Ti-6Al-4V alloy.

- The passive behavior of the specimens obtained from potentiodynamic polarization experiments revealed that the presence of both BSA and HSA increased the stability of the 316L and Co-28Cr-6Mo passive film by the blocking of ions dissolution. However, the barrier layer stability of the Ti-6Al-4V samples depends on the BSA and HSA concentrations. This means the blocking action of BSA and HSA and, as a result, the surface coverage of these proteins on Ti-6Al-4V alloys is a function of concentration. Although the passive behavior of 316L and Co-28Cr-6Mo alloys in solutions of HSA and BSA were similar, BSA was a stronger cathodic inhibitor than HSA for 316L and Co-28Cr-6Mo alloys.
- The anodic current peak of 316L and Co-28Cr-6Mo in PBS solutions was similar to those in the presence of BSA and HSA. The anodic peaks indicated the oxidation of iron from 316L, cobalt from Co-28Cr-6Mo, and adsorbed hydrogen from Ti-6Al-4V alloys. The value of the anodic peak for 316L and Co-28Cr-6Mo was diminished upon addition of BSA and HSA, whereas the anodic peak increased for the Ti-6Al-4V alloy in the same solutions. This observation explained the blockage of BSA and HSA on 316L and Co-28Cr-6Mo alloys from iron and cobalt release. Since the lowest resulting current was found in BSA solutions for 316L and CoCrMo alloys, the dissolution of iron and cobalt in HSA solutions is faster than that in BSA solutions. The higher rate of the oxidation of adsorbed hydrogen on the Ti-6Al-4V alloy in BSA refers to the acceleration of protein adsorption through the amino groups. Overall, the

adsorptions of BSA and HSA onto 316l, CoCrMo, and Ti-6Al-4V alloys are not similar because of the different value of the i_{pa} obtained in PBS-HSA and PBS-BSA solutions.

- The impedance of the alloys in PBS-BSA solutions were characterized by a large semicircle capacitive loop and a simple Randles equivalent circuit (R_S ($R_{p\text{-}EIS}$ Q)). However, two time constants were detected for these alloys in PBS-HSA solutions which were modelled to the bilayer passive layer at the alloys-solution interface. The interaction of HSA with the released iron and cobalt and formation of ion-protein complexes can contribute to the appearance of the second time constant. The XPS analysis of 316L oxide layer in BSA and HSA showed that 316L oxide layer contained Fe_2O_3, MoO_2, MoO_3, and Ni in HSA solutions which was not detected in the oxide layer composition of 316L immersed in BSA solutions. The XPS analysis of the CoCrMo alloy revealed that that the oxide layer of Co-28Cr-6Mo alloys is thinner in HSA solutions than in BSA solutions because of the dissolution of cobalt. In addition, organometallic compounds of $(N(C_4H_9)_4)_3 P Mo_{12} O_{38}$ were found in the HSA solution while the oxide layer of the CoCrMo alloy immersed in the BSA solution contained MoO_3. The adsorption of BSA and HSA to Ti-6Al-4V alloys was different referring to the detected sodium in the oxide composition of this alloy. In the BSA solution, sodium acted as a bridge to bind the sulfhydryl group of BSA to titanium and form sodium mercaptoacetate ($Na(HSCH_2COO)$) whereas sodium could bridge the carboxyl group of HSA to the Ti-6Al-4V surface and produces sodium (2-methyl-propenoate) or $Na(OC(O)C(CH_3)CH_2)$.

- No distinct function was found between the protein concentration and the corrosion rate of the 316L, Co-28Cr-6Mo, or Ti-6Al-4V alloy. However, the difference in the corrosion rates calculated from the EIS, LPR, and immersion results were in one order of magnitude.

- Weight loss of the specimens was observed up to 14 weeks exposure in the solution. However, the weight of the samples increased slightly after 14 weeks due to the precipitation of dissolved ions. This was confirmed by ICP-OES results in which the iron and cobalt dissolution of the 316L and CoCrMo alloys were decreased within 14 to 22 weeks immersion in PBS-BSA and PBS-HSA solutions. The precipitations of Fe and Co on 316L and Co-28Cr-6Mo alloys, respectively, were determined by XPS analysis.
- Vanadium release from Ti-6Al-4V alloy is dependent on time and, although it has lower content than Ti, its dissolution rate is faster. The addition of HSA decreased the rate of vanadium release from Ti-6Al-4V alloy. Therefore, this could reduce release of toxic vanadium and could improve performance of Ti-6Al-4V implant in human body.

Therefore, to successfully simulate the body environment, one needs to consider the presence of protein in corrosion studies as well as using human serum albumin instead of animal serum albumin.

10 Future works

The electrochemical corrosion techniques were used to evaluate the stability of the metallic samples by one-hour OCP measurements in PBS solutions containing BSA and HSA concentrations of 0, 0.2, 0.4, 1.2, 2, and 4 g L^{-1}. The electrochemical corrosion behavior of the specimens then followed by PDP, EIS, and LPR measurements. In addition to studying the variation of protein concentration, pH variation at the metal tissue interface can be studied. Human body pH varies from 6.8 to 7.78, depending on the function of tissue and the response of the body to metallic implants. For instance, the body's pH drops to 5.4 as a result of infection. The detailed description of this is presented in the "Body environment and metal-tissue interface" section of the thesis. Based on these understandings, the effect of pH on electrochemical corrosion behavior of the metallic biomaterials could be investigated in the presence of various HSA concentrations (0, 0.2, 0.4, 1.2, 2, and 4 g L^{-1}) by electrochemical techniques of PDP, EIS, and LPR.

The attempt of simulating a real body environment will be continued by repeating electrochemical corrosion techniques (OCP, PDP, EIS, and LPR) in de-aerated PBS and HSA solutions. Partial pressure of the oxygen in the human body fluid (28-78 mmHg) is much less than that of aerated solutions. The oxygen contents of various biofluids are summarized in Table 2-6. The solubility of oxygen in saline solution at 37°C is almost 7 ppm. Fresh solutions of PBS will be prepared and it will be purged for 1 hour with argon gas for 1 hour. The HSA will be added to the PBS solution right after one hour of purging to avoid the foaming of the

solution. The oxygen content of the solutions can be monitored during the experiments by a dissolved oxygen (DO) meter.

The galvanic corrosion of metallic biomaterials in various HSA concentrations would be another future plan for this study since some metallic implants are made of different alloys. For example, hip implants have a Ti alloy stem and CoCrMo ball and socket parts.

Some metallic biomaterials are subjected to mechanical forces such as hip and knee implants. The passive layer of these implants is removed by the slide motion of two parts of the implants (e.g. a femoral head and acetabular cup of a hip implant). It is interesting to study the growth of oxide layers after they are removed in the de-aerated PBS and HSA solutions. The samples of 316L, Co-28Cr-6Mo, and Ti-6Al-4V will be ground while they are immersed in the PBS and BSA solutions. The polishing apparatus could consist of a plastic disk adhered by a 1200 SiC emery paper and a plastic handle. The handle will be connected to a rotor which can rotate at 500 rpm. The working electrodes will be polished while the electrode is potentiostatically conditioned at −1.0 V vs. Ag/AgCl. We will ensure that the samples' surfaces are free of any previously-formed oxides by the in-vitro conditioning of the samples. This can be confirmed by measuring the current density versus time. After removing the oxide surface, PDP and EIS measurements will be conducted to study anodic and cathodic behavior, passivity, and oxide growth on the 316L, Co-28Cr-6Mo, and Ti-6Al-4V alloys.

References

Adams, P. A., & Berman, M. C. (1980). Kinetics and mechanism of the interaction between human serum albumin and monomeric haemin. *Biochem. J., 191*(1), 95-102.

Agins, H., Alcock, N., Bansal, M., Salvati, E., Wilson, P., Pellicci, P., & Bullough, P. (1988). Metallic wear in failed titanium-alloy total hip replacements. A histological and quantitative analysis. *J. Bone Joint Surg. Am., 70*(3), 347-356.

Albrektsson, T., Brånemark, P., Hansson, H., Kasemo, B., Larsson, K., Lundström, I., McQueen, D. H., & Skalak, R. (1983). The interface zone of inorganic implants *In vivo:* Titanium implants in bone. *Ann. Biomed. Eng., 11*(1), 1-27.

Al-Hity, R. R., Kappert, H. F., Viennot, S., Dalard, F., & Grosgogeat, B. (2007). Corrosion resistance measurements of dental alloys, are they correlated? *Dent. Mater., 23*(6), 679-687.

Alves, V. A., Reis, R. Q., Santos, I. C. B., Souza, D. G., Goncalves, T. de F., Pereira-da-Silva, M. A., & da-Silva, L. A. (2009). *In situ* impedance spectroscopy study of the electrochemical corrosion of Ti and Ti–6Al–4V in simulated body fluid at 25° C and 37° C. *Corros. Sci., 51*(10), 2473-2482.

Amel-Farzad, H., Peivandi, M. T., & Yusof-Sani, S. M. R. (2007). In-body corrosion fatigue failure of a stainless steel orthopaedic implant with a rare collection of different damage mechanisms. *Eng. Fail. Anal., 14*(7), 1205-1217.

Antunes, R. A., & de Oliveira, M. C. (2012). Corrosion fatigue of biomedical metallic alloys: Mechanisms and mitigation. *Acta Biomater., 8*(3), 937-962.

Ask, M., Lausmaa, J., & Kasemo, B. (1989). Preparation and surface spectroscopic characterization of oxide films on Ti6Al4V. *Appl. Surf. Sci., 35*(3), 283-301.

ASTM Standard, G31-72. (2004). Standard practice for laboratory immersion corrosion testing of metals. West Conshohocken, PA.

Azevedo, C., & Hippert Jr, E. (2002). Failure analysis of surgical implants in brazil. Engineering Failure Analysis, 9(6), 621-633.

Aziz-Kerrzo, M., Conroy, K. G., Fenelon, A. M., Farrell, S. T., & Breslin, C. B. (2001). Electrochemical studies on the stability and corrosion resistance of titanium-based implant materials. *Biomaterials, 22*(12), 1531-1539.

Bal, W., Christodoulou, J., Sadler, P. J., & Tucker, A. (1998). Multi-metal binding site of serum albumin. J. Inorg. Biochem., 70(1), 33-39.

Balamurugan, A., Rajeswari, S., Balossier, G., Rebelo, A. H. S., & Ferreira, J. M. F. (2008). Corrosion aspects of metallic implants-An overview. *Mater. Corros., 59*(11), 855-869.

Bar-Or, D., Rael, L. T., Bar-Or, R., Slone, D. S., Mains, C. W., Rao, N. K. R., & Curtis, C. G. (2008). The cobalt-albumin binding assay: Insights into its mode of action. *Clin. Chim. Acta, 387*(1-2), 120-127.

Basketter, D., Briatico-Vangosa, G., Kaestner, W., Lally, C., & Bontinck, W. (1993). Nickel, cobalt and chromium in consumer products: A role in allergic contact dermatitis? *Contact Dermatitis, 28*(1), 15-25.

Bastidas, J. M., Torres, C. L., Cano, E., & Polo, J. L. (2002). Influence of molybdenum on passivation of polarised stainless steels in a chloride environment. *Corros. Sci., 44*(3), 625-633.

Bell, K. L., & Brenner, H. C. (1982). Phosphorescence and optically detected magnetic resonance study of the tryptophan residue in human serum albumin. *Biochem., 21*(4), 799-804.

Bianchi, C. L., Cattania, M. G., & Villa, P. (1993). XPS characterization of Ni and Mo oxides before and after "in situ" treatments. *Appl. Surf. Sci., 70*, 211-216.

Bianco, P. D., Ducheyne, P., & Cuckler, J. M. (1997). Systemic titanium levels in rabbits with a titanium implant in the absence of wear. *J. Mater. Sci. – Mater. Med.*, *8*(9), 525-529.

Black, J. (1984). Systemic effects of biomaterials. *Biomaterials, 5*(1), 11-18.

Black, J. (1992). *Biological performance of materials.* New York, NY: Marcel Dekker.

Black, J., Maitin, E. C., Gelman, H., & Morris, D. M. (1983). Serum concentrations of chromium, cobalt and nickel after total hip replacement: A six month study. *Biomaterials, 4*(3), 160-164.

Boehm, H. P. (1971). Acidic and basic properties of hydroxylated metal oxide surfaces. *Spec. Discuss. Faraday Soc. Special, 52*, 264-275.

Bonilla, S. H., & Zinola, C. F. (1998). Changes in the voltammetric response of titanium electrodes caused by potential programmes and illumination. *Electrochim. Acta, 43*(3), 423-426.

Bonnelle, J. P., Grimblot, J., & D'huysser, A. (1975). Influence de la polarisation des liaisons sur les spectres esca des oxydes de cobalt. *J. Electron. Spectrosc. Relat. Phenom., 7*(2), 151-162.

Brodner, W., Bitzan, P., Meisinger, V., Kaider, A., Gottsauner-Wolf, F., & Kotz, R. (2003). Serum cobalt levels after metal-on-metal total hip arthroplasty. *J. Bone Joint Surg. Am., 85*(11), 2168-2173.

Brown, J. R. (1975). Structure of bovine serum albumin. *Fed. Proc., 34,* 591.

Bundy, K. J. (2008). Biomaterials and the chemical environment of the body. In P. A. Revell (Ed.), *Joint replacement technology* (pp. 56-80) USA: CRC Press.

Bundy, K. J. (1994). Corrosion and other electrochemical aspects of biomaterials. *Crit. Rev. Biomed. Eng., 22*(3-4), 139-251.

Burstein, G. T., & Liu, C. (2007). Nucleation of corrosion pits in ringer's solution containing bovine serum. *Corros. Sci., 49*(11), 4296-4306.

Cahoon, J. R., & Paxton, H. W. (2004). Metallurgical analyses of failed orthopedic implants. *J. Biomed. Mater. Res., 2*(1), 1-22.

Cao, B., Xi, T., Zheng, Y., & Hui, D. (2011). Corrosion behavior of copper in the presence of proteins. *Metalurgija, 17*(3), 111-117.

Carter, D. C., Chang, B., Ho, J. X., Keeling, K., & Krishnasami, Z. (1994). Preliminary crystallographic studies of four crystal forms of serum albumin. *Europ. J. Biochem., 226*(3), 1049-1052.

Carter, D. C., & Ho, J. X. (1994). Structure of serum albumin. In V. N. Schumaker (Ed.), *Advances in protein chemistry* (pp. 153-203) New York, NY: Academic Press.

Casabán Julián, L., & Igual Muñoz, A. (2011). Influence of microstructure of HC CoCrMo biomedical alloys on the corrosion and wear behaviour in simulated body fluids. *Tribol. Int., 44*(3), 318-329.

Cheng, X., & Roscoe, S. G. (2005). Corrosion behavior of titanium in the presence of calcium phosphate and serum proteins. *Biomaterials, 26*(35), 7350-7356.

Cimino, A., & De Angelis, B. A. (1975). The application of X-ray photoelectron spectroscopy to the study of molybdenum oxides and supported molybdenum oxide catalysts. *J. Catal., 36*(1), 11-22.

Clark, G., & Williams, D. (2004). The effects of proteins on metallic corrosion. *J. Biomed. Mater. Res., 16*(2), 125-134.

Clayton, C., & Lu, Y. (1986). A bipolar model of the passivity of stainless steel: The role of Mo addition. *J. Electrochem. Soci., 133*(12), 2465.

Cobb, A. G., & Schmalzreid, T. P. (2006). The clinical significance of metal ion release from cobalt-chromium metal-on-metal hip joint arthroplasty. *Proc. Inst. Mech. Eng. H: J. Eng. Med., 220*(2), 385-398.

Contu, F., Elsener, B., & Böhni, H. (2002). Characterization of implant materials in fetal bovine serum and sodium sulfate by electrochemical impedance spectroscopy. I. Mechanically polished samples. *J. Biomed. Mater. Res. A, 62*(3), 412-421.

Contu, F., Elsener, B., & Böhni, H. (2004). Serum effect on the electrochemical behaviour of titanium, Ti6Al4V and Ti6Al7Nb alloys in sulphuric acid and sodium hydroxide. *Corros. Sci., 46*(9), 2241-2254.

Contu, F., Elsener, B., & Böhni, H. (2003). Characterization of implant materials in fetal bovine serum and sodium sulfate by electrochemical impedance spectroscopy. II. Coarsely sandblasted samples. *J. Biomed. Mater. Res. A, 67*(1), 246-254.

Contu, F., Elsener, B., & Böhni, H. (2005). Corrosion behaviour of CoCrMo implant alloy during fretting in bovine serum. *Corros. Sci., 47*(8), 1863-1875.

Cosman, N. P., Fatih, K., & Roscoe, S. G. (2005). Electrochemical impedance spectroscopy study of the adsorption behaviour of [alpha]-lactalbumin and [beta]-casein at stainless steel. *J. Electroanal. Chem., 574*(2), 261-271.

Dauphas, N., Pourmand, A., & Teng, F. Z. (2009). Routine isotopic analysis of iron by HR-MC-ICPMS: How precise and how accurate? *Chem. Geol., 267*(3-4), 175-184.

Desroches, M. J., Chaudhary, N., & Omanovic, S. (2007). PM-IRRAS investigation of the interaction of serum albumin and fibrinogen with a biomedical-grade stainless steel 316LVM surface. *Biomacromolecules, 8*(9), 2836-2844.

Dimah, M. K., Devesa Albeza, F., Amigó Borrás, V., & Igual Muñoz, A. (2012). Study of the biotribocorrosion behaviour of titanium biomedical alloys in simulated body fluids by electrochemical techniques. *Wear, 294*, 409-418.

Dobbs, H. S., & Scales, J. T. (1983). Behavior of commercially pure titanium and Ti-318 (Ti-6AI-4V) in orthopedic implants. *Titanium alloys in surgical implants - STP 796* (pp. 173-186) ASTM International.

Ducheyne, P., Radin, S., & Ishikawa, K. (1992). The rate of calcium phosphate precipitation on metal and ceramics, and the relationship to bioactivity. In P. Ducheyne, T. Kokubo & C. A. van Blitterswijk (Eds.), *Bone-bonding biomaterials* (pp. 62-65).

Ellingsen, J. E. (1991). A study on the mechanism of protein adsorption to TiO2. *Biomaterials, 12*(6), 593-596.

Ellman, M. B., & Levine, B. R. (2011). Fracture of the modular femoral neck component in total hip arthroplasty. *J. Arthroplasty, 28*(1), 196e1-5.

Fasano, M., Curry, S., Terreno, E., Galliano, M., Fanali, G., Narciso, P., Notari, P., & Ascenzi, P. (2005). The extraordinary ligand binding properties of human serum albumin. *IUBMB Life, 57*(12), 787-796.

Feng, B., Weng, J., Yang, B. C., Chen, J. Y., Zhao, J. Z., He, L., Qi, S. K., & Zhang, X. D. (2002). Surface characterization of titanium and adsorption of bovine serum albumin. *Mater. Charact., 49*(2), 129-137.

Fiset, M., Mantovani, D., Dubé, D., Hermawan, H., & Moravej, M. (2007). Degradation behaviour of metallic biomaterials for degradable stents. *Adv. Mater. Res., 15*, 113-118.

Fraitzl, C. R., Moya, L. E., Castellani, L., Wright, T. M., & Buly, R. L. (2011). Corrosion at the stem-sleeve interface of a modular titanium alloy femoral component as a reason for impaired disengagement. *J. Arthroplasty, 26*(1), 113-119. e1.

Fraker, A. C. (1987). Corrosion of metallic implants and prosthetic devices. *Corrosion.* (pp. 1324-1335) Metals Handbook, ASM International.

Fraker, A. (1995). Medical and dental. In R. Baboian (Ed.), *Corrosion tests and standards: Application and interpretation* (pp. 705-715) American Society for Testing and Materials.

Frateur, I., Lartundo-Rojas, L., Méthivier, C., Galtayries, A., & Marcus, P. (2006). Influence of bovine serum albumin in sulphuric acid aqueous solution on the corrosion and the passivation of an iron-chromium alloy. *Electrochim. Acta, 51*(8-9), 1550-1557.

Frederix, F., Bonroy, K., Laureyn, W., Reekmans, G., Campitelli, A., Dehaen, W., & Maes, G. (2003). Enhanced performance of an affinity biosensor interface based on mixed self-assembled monolayers of thiols on gold. *Langmuir, 19*(10), 4351-4357.

Fukuzaki, S., Urano, H., & Nagata, K. (1995). Adsorption of protein onto stainless-steel surfaces. *J. Ferment. Bioeng.g, 80*(1), 6-11.

Galante, J. O., Rostoker, W., & Doyle, J. (1975). Failed femoral stems in total hip prostheses. A report of six cases. *J. Bone Joint Surg. Am., 57*(2), 230-236.

Gettens, R. T. T., & Gilbert, J. L. (2008). Fibrinogen adsorption onto 316L stainless steel under polarized conditions. *J. Biomed. Mater. Res. A, 85*(1), 176-187.

Gilbert, J. L., Buckley, C. A., & Jacobs, J. J. (1993). In vivo corrosion of modular hip prosthesis components in mixed and similar metal combinations. the effect of crevice, stress, motion, and alloy coupling. *J. Biomed. Mater. Res., 27*(12), 1533-1544.

Gilbert, J. L., & Mali, S. A. (2012). Medical implant corrosion: Electrochemistry at metallic biomaterial surfaces. *Degradation of implant materials* (pp. 1-28) Springer.

Granchi, D., Ciapetti, G., Filippini, F., Stea, S., Cenni, E., Pizzoferrato, A., & Toni, A. (2000). In vitro cytokine production by mononuclear cells exposed to bone cement extracts. *Biomaterials, 21*(17), 1789-1795.

Grebner, T., & Hansen, D. C. (2008). The effect of galvanic coupling between modern fracture fixation constructs in physiologically relevant solutions: The role of serum proteins on the corrosion of Ti6Al4V and 316L alloys. *ECS Transactions, 11*(21), 13-27.

Gurappa, I. (2002). Characterization of different materials for corrosion resistance under simulated body fluid conditions. *Mater. Charact., 49*(1), 73-79.

Hallab, N. J., Skipor, A., & Jacobs, J. J. (2003). Interfacial kinetics of titanium-and cobalt-based implant alloys in human serum: Metal release and biofilm formation. *J. Biomed. Mater. Res. A, 65*(3), 311-318.

Hallab, N. J., Jacobs, J. J., & Katz, J. L. (2004). Orthopedic applications. In B. D. Ratner, A. S. Hoffman, F. J. Schoen & J. E. Lemons (Eds.), *Biomaterials science: An introduction to materials in medicine* (2nd ed., pp. 526) Elsevier.

Hamdani, S., Joly, D., Carpentier, R., & Tajmir-Riahi, H. (2009). The effect of methylamine on the solution structures of human and bovine serum albumins. *J. Mol. Struct., 936*(1), 80-86.

Hammond, J., Holubka, J., DeVries, J., & Dickie, R. (1981). The application of x-ray photo-electron spectroscopy to a study of interfacial composition in corrosion-induced paint de-adhesion. *Corros. Sci., 21*(3), 239-253.

Hanawa, T. (2004). Metal ion release from metal implants. *Mater. Sci. Eng. C, 24*(6-8), 745-752.

Hanawa, T., Hiromoto, S., & Asami, K. (2001). Characterization of the surface oxide film of a co-cr-mo alloy after being located in quasi-biological environments using XPS. *Appl. Surf. Sci., 183*(1-2), 68-75.

Hanawa, T., Hiromoto, S., Yamamoto, A., Kuroda, D., & Asami, K. (2002). XPS characterization of the surface oxide film of 316L stainless steel samples that were located in quasi-biological environments. *Mater. Trans., 43*(12), 3088-3092.

Hanawa, T. (2004). Metal ion release from metal implants. *Mater. Sci. Eng. C, 24*(6-8), 745-752.

Hang, R., Ma, S., Ji, V., & Chu, P. K. (2010). Corrosion behavior of NiTi alloy in fetal bovine serum. *Electrochim. Acta, 55*(20), 5551-5560.

Hansen, D. C., Luther, G. W., & Waite, J. H. (1994). The adsorption of the adhesive protein of the blue mussel mytilus edulis L onto type 304L stainless steel. *J. Colloid Interface Sci., 168*(1), 206-216.

Haudrech, P., Foussereau, J., Mantout, B., & Baroux, B. (1994). Nickel release from nickel-plated metals and stainless steels. *Contact Dermatitis, 31*(4), 249-255.

He, X. M., & Carter, D. C. (1992). Atomic structure and chemistry of human serum albumin. *Nature, 358,* 209-215.

Healy, K. E., & Ducheyne, P. (1992). Hydration and preferential molecular adsorption on titanium in vitro. *Biomaterials, 13*(8), 553-561.

Healy, K., & Ducheyne, P. (1996). Passive dissolution of titanium in biological environments. *ASTM Special Technical Publication, 1272*, 179-187.

Herve, F., Urien, S., Albengres, E., Duche, J., & Tillement, J. (1994). Drug binding in plasma. A summary of recent trends in the study of drug and hormone binding. *Clinical Pharmacokinetics, 26*(1), 44.

Hirayama, K., Akashi, S., Furuya, M., & Fukuhara, K. (1990). Rapid confirmation and revision of the primary structure of bovine serum albumin by ESIMS and frit-FAB LC/MS. *Biochem. Biophys. Res. Commun., 173*(2), 639-646.

Hiromoto, S., Hanawa, T., & Asami, K. (2004). Composition of surface oxide film of titanium with culturing murine fibroblasts L929. *Biomaterials, 25*(6), 979-986.

Hiromoto, S., Onodera, E., Chiba, A., Asami, K., & Hanawa, T. (2005). Microstructure and corrosion behaviour in biological environments of the new forged low-Ni Co-Cr-Mo alloys. *Biomaterials, 26*(24), 4912-4923.

Hodgson, A. W. E., Mueller, Y., Forster, D., & Virtanen, S. (2002). Electrochemical characterisation of passive films on Ti alloys under simulated biological conditions. *Electrochim. Acta, 47*(12), 1913-1923.

Hodgson, A., Kurz, S., Virtanen, S., Fervel, V., Olsson, C. O. A., & Mischler, S. (2004). Passive and transpassive behaviour of CoCrMo in simulated biological solutions. *Electrochim. Acta, 49*(13), 2167-2178.

Howie, D. W., Rogers, S. D., McGee, M. A., & Haynes, D. R. (1996). Biologic effects of cobalt chrome in cell and animal models. *Clin. Orthop. Relat. Res., 329*, 217-232.

Huang, H. H., Chiu, Y. H., Lee, T. H., Wu, S. C., Yang, H. W., Su, K. H., & Hsu, C. C. (2003). Ion release from NiTi orthodontic wires in artificial saliva with various acidities. *Biomaterials, 24*(20), 3585-3592.

Huang, H. (2003). Effect of fluoride and albumin concentration on the corrosion behavior of Ti–6Al–4V alloy. *Biomaterials, 24*(2), 275-282.

Huot Carlson, J. C., Van Citters, D. W., Currier, J. H., Bryant, A. M., Mayor, M. B., & Collier, J. P. (2012). Femoral stem fracture and in vivo corrosion of retrieved modular femoral hips. *J. Arthroplasty, 27*(7), 1389-1396.e1.

Igual Muñoz, A., & Casabán Julián, L. (2010). Influence of electrochemical potential on the tribocorrosion behaviour of high carbon CoCrMo biomedical alloy in simulated body fluids by electrochemical impedance spectroscopy. *Electrochim. Acta, 55*(19), 5428-5439.

Ionitaa, D., Popescua, R., Titea, T., & Demetrescua, I. (2008). The behaviour of pure titanium in albumin solution. *Molecular Crystals and Liquid Crystals, 486*(1), 166-174.

Jackson, D. R., Omanovic, S., & Roscoe, S. G. (2000). Electrochemical studies of the adsorption behavior of serum proteins on titanium. *Langmuir, 16*(12), 5449-5457.

Joyner, D. J., Johnson, O., & Hercules, D. M. (1980). A study of the iron borides. 1. electron spectroscopyJ. Am. Chem. Soc*., 102*(6), 1910-1917.

Kanerva, L., Sipiläinen-Malm, T., Estlander, T., Zitting, A., Jolanki, R., & Tarvainen, K. (1994). Nickel release from metals, and a case of allergic contact dermatitis from stainless steel. *Contact Dermatitis, 31*(5), 299-303.

Kannan, S., Balamurugan, A., Rajeswari, S., & Subbaiyan, M. (2002). Metallic implants: An approach for long term applications in bone related defects. *Corros. Rev., 20*(4-5), 339-358.

Karimi, S., & Alfantazi, A. (2013). Electrochemical corrosion behavior of orthopedic biomaterials in presence of human serum albumin. *J. Electrochem. Soci., 160*(6), C206-C214.

Karimi, S., Nickchi, T., & Alfantazi, A. (2011). Effects of bovine serum albumin on the corrosion behaviour of AISI 316L, Co–28Cr–6Mo, and Ti–6Al–4V alloys in phosphate buffered saline solutions. *Corros. Sci., 53*(10), 3262-3272.

Karimi, S., Nickchi, T., & Alfantazi, A. M. (2012). Long-term corrosion investigation of AISI 316L, Co–28Cr–6Mo, and Ti–6Al–4V alloys in simulated body solutions. *Appl. Surf. Sci., 258*(16), 6087-6096.

Kasemo, B., & Gold, J. (1999). Implant surfaces and interface processes. *Adv. Dental Res., 13*(1), 18-20.

Kasemo, B., & Lausmaa, J. (1986). Surface science aspects on inorganic biomaterials. *CRC Crit. Rev. Clin. Neurobiol., 2,* 335-380.

Kasemo, B., & Lausmaa, J. (1994). Material-tissue interfaces: The role of surface properties and processes. *Environ. Health Perspect., 102*(Suppl 5), 41-45.

Kawafune, I., & Matsubayashi, G. (1991). Isolation and characterization of oxygen-deficient reduced forms of the dodecamolybdophosphate anion salt. *Inorg. Chim. Acta, 188*(1), 33-39.

Khan, M., Williams, R., & Williams, D. (1996). In-vitro corrosion and wear of titanium alloys in the biological environment. *Biomaterials, 17*(22), 2117-2126.

Khan, M., Williams, R., & Williams, D. (1999). The corrosion behaviour of ti-6Al-4V, Ti-6Al-7Nb and Ti-13Nb-13Zr in protein solutions. *Biomaterials, 20*(7), 631-637.

Klarstrom, D., Crook, P., & Wu, J. (2004). Metallography and microstructures of cobalt and cobalt alloys. In G. F. Vander Voort (Ed.), *ASM handbook: Metallography and microstructures* (pp. 764-774) ASM International, Materials Park, OH, USA.

Klinger, A., Steinberg, D., Kohavi, D., & Sela, M. (1997). Mechanism of adsorption of human albumin to titanium in vitro. *J. Biomed. Mater. Res., 36*(3), 387-392.

Kocijan, A., Donik, C., & Jenko, M. (2007). Electrochemical and XPS studies of the passive film formed on stainless steels in borate buffer and chloride solutions. *Corros. Sci., 49*(5), 2083-2098.

Koike, M., & Fujii, H. (2001). The corrosion resistance of pure titanium in organic acids. *Biomaterials, 22*(21), 2931-2936.

Konttinen, Y. T., Takagi, M., Mandelin, J., Lassus, J., Salo, J., Ainola, M., Li, T. F., Virtanen, I., Liljestrom, M., Sakai, H., Kobayashi, Y., Sorsa, T., Lappalainen, R., Demulder, A., & Santavirta, S. (2001). Acid attack and cathepsin K in bone resorption around total hip replacement prosthesis. *J. Bone Miner. Res., 16*(10), 1780-1786.

Kop, A. M., & Swarts, E. (2009). Corrosion of a hip stem with a modular neck taper junction: A retrieval study of 16 cases. *J. Arthroplasty, 24*(7), 1019-1023.

Korovessis, P., Petsinis, G., Repanti, M., & Repantis, T. (2006). Metallosis after contemporary metal-on-metal total hip arthroplastyFive to nine-year follow-up. *J. Bone Joint Surg., 88*(6), 1183-1191.

Kragh-Hansen, U., Chuang, V. T. G., & Otagiri, M. (2002a). Practical aspects of the ligand-binding and enzymatic properties of human serum albumin. *Biol. Pharm. Bull, 25*(6), 695-704.

Kruger, J. (1979). Fundamental aspects of the corrosion of metallic implants. In B. Syrett, & A. Acharya (Eds.), *Corrosion and degradation of implant materials, ASTM STP 684* (pp. 107-127) ASTM International.

Kuhn, A. T., Neufeld, P., & Rae, T. (1986). Synthetic environments for the testing of metallic biomaterials. In V. E. Francis, & T. S. Lee (Eds.), *The use of synthetic environments for corrosion testing* (pp. 79-97) American Society for Testing and Materials.

Laing, P. G., Ferguson, A. B., & Hodge, E. S. (1967). Tissue reaction in rabbit muscle exposed to metallic implants. *J. Biomed. Mater. Res., 1*(1), 135-149.

Lalor, P., Revell, P., Gray, A., Wright, S., Railton, G., & Freeman, M. (1991). Sensitivity to titanium. A cause of implant failure? *J. Bone Joint Surg., 73*(1), 25-28.

Laurell, C. B., & Jeppsson, J., (1975). Protease inhibitors in plasma: In Putnam, F. (Ed.), *The plasma proteins: structure, function, and genetic control* (pp. 229-264). New York, San Francisco, London: Academic Press.

Laussac, J. P., & Sarker, B. (1984). Characterization of the copper (II) and nickel (II) transport site of human serum albumin. studies of copper (II) and nickel (II) binding to peptide 1-24 of human serum albumin by carbon-13 and proton NMR spectroscopy. *Biochemistry, 23*(12), 2832-2838.

Lee, S. H., & Ruckenstein, E. (1988). Adsorption of proteins onto polymeric surfaces of different hydrophilicities—a case study with bovine serum albumin. J. Colloid Interface Sci., 125(2), 365-379.

Lewis, A. C., Kilburn, M., Heard, P. J., Scott, T. B., Hallam, K., Allen, G. C., & Learmonth, I. (2006). The entrapment of corrosion products from CoCr implant alloys in the deposits of calcium phosphate: A comparison of serum, synovial fluid, albumin, EDTA, and water. *J. Orthopaedic Res., 24*(8), 1587-1596.

Lewis, A., Kilburn, M., Papageorgiou, I., Allen, G., & Case, C. (2005). Effect of synovial fluid, phosphate-buffered saline solution, and water on the dissolution and corrosion properties of CoCrMo alloys as used in orthopedic implants. *J. Biomed. Mater. Res. A, 73*(4), 456-467.

Lhotka, C., Szekeres, T., Steffan, I., Zhuber, K., & Zweymüller, K. (2003). Four-year study of cobalt and chromium blood levels in patients managed with two different metal-on-metal total hip replacements. *J. Orthopaedic Res., 21*(2), 189-195.

Liang, H., Huang, J., Tu, C. Q., Zhang, M., Zhou, Y. Q., & Shen, P. W. (2001). The subsequent effect of interaction between co< sup> 2 </sup> and human serum albumin or bovine serum albumin. *J. Inorg. Biochem., 85*(2), 167-171.

Lima, J., Sousa, S., Ferreira, A., & Barbosa, M. (2001). Interactions between calcium, phosphate, and albumin on the surface of titanium. *J. Biomed. Mater. Res., 55*(1), 45-53.

Lin, H. Y., & Bumgardner, J. D. (2004). Changes in surface composition of the Ti-6Al-4V implant alloy by cultured macrophage cells. *Appl. Surf. Sci., 225*(1-4), 21-28.

Lin, H. Y., & Bumgardner, J. D. (2004). Changes in the surface oxide composition of Co-Cr-Mo implant alloy by macrophage cells and their released reactive chemical species. *Biomaterials, 25*(7-8), 1233-1238.

Lin, H. Y., & Bumgardner, J. D. (2004). In vitro biocorrosion of Co-Cr-Mo implant alloy by macrophage cells. *J. Orthopaedic Res., 22*(6), 1231-1236.

Liu, B., & Zheng, Y. (2011). Effects of alloying elements (Mn, Co, Al, W, Sn, B, C and S) on biodegradability and in vitro biocompatibility of pure iron. *Acta Biomaterialia, 7*(3), 1407-1420.

Liu, C., Wang, Y., Wang, M., Huang, W., & Chu, P. (2012). Electrochemical behaviour of TiO 2 nanotube on titanium in artificial saliva containing bovine serum albumin. *Corros. Eng. Sci. Tech., 47*(3), 167-169.

López, D. A., Duran, A., & Ceré, S. M. (2008). Electrochemical characterization of AISI 316L stainless steel in contact with simulated body fluid under infection conditions. *J. Mater. Sci.: Mater. Med., 19*(5), 2137-2144.

Lopez, M., Jimenez, J., & Gutierrez, A. (2003). Corrosion study of surface-modified vanadium-free titanium alloys. *Electrochim. Acta, 48*(10), 1395-1402.

Lori, J., & Hanawa, T. (2001). Characterization of adsorption of glycine on gold and titanium electrodes using electrochemical quartz crystal microbalance. *Corros. Sci., 43*(11), 2111-2120.

Lowenberg, B., Lugowski, S., Chirman, M., & Davies, J. (1994). ASTM-F86 passivation increases trace element release from Ti6AI4V into culture medium. *J. Mater. Sci.: Mater. Med., 5*(6-7), 467-472.

Lundin, M., Hedberg, Y., Jiang, T., Herting, G., Wang, X., Thormann, E., Blomberg, E., & Wallinder, I. O. (2011). Adsorption and protein-induced metal release from chromium metal and stainless steel. *J. Colloid Interface Sci., 366*(1), 155-164.

M.R. Louthan, J. (1986). Optical metallography. *Metals handbook* (9th Edition ed., pp. 305-307) ASM International.

Marcus, P., & Maurice, V. (2006). XPS characterization of BSA adsorption on stainless steel. *Passivation of Metals and Semiconductors, and Properties of Thin Oxide Layers: A Selection of Papers from the 9th International Symposium, Paris, France, 27 June-1 July 2005,* 365.

Marie de Ficquelmont-Loïzos, M., Takenouti, H., & Kante, W. (1997). Long-time and short-time investigation of the electrode interface through electrochemical impedance measurements. application to adsorption of human serum albumin onto glassy carbon rotating disc electrode. *J. Electroanal. Chem., 428*(1), 129-140.

Martin, E. J., Pourzal, R., Mathew, M. T., & Shull, K. R. (2013). Dominant role of molybdenum in the electrochemical deposition of biological macromolecules on metallic surfaces. *Langmuir, 29*(15), 4813-4822.

McIntyre, N., & Cook, M. (1975). X-ray photoelectron studies on some oxides and hydroxides of cobalt, nickel, and copper. *Anal. Chem., 47*(13), 2208-2213.

Merritt, K., & Brown, S. A. (2004). Effect of proteins and pH on fretting corrosion and metal ion release. *J. Biomed. Mater. Res., 22*(2), 111-120.

Merritt, K., & Rodrigo, J. J. (1996). Immune response to synthetic materials: Sensitization of patients receiving orthopaedic implants. *Clin. Orthop. Relat. Res., 326*, 71-9.

Merritt, K., Wortman, R., Millard, M., & Brown, S. (1983). XPS analysis of 316 LVM corroded in serum and saline. *Artificial Cells, Blood Substitutes and Biotechnology, 11*(1), 115-124.

Metikos-Hukovic, M., Kwokal, A., & Piljac, J. (2003). The influence of niobium and vanadium on passivity of titanium-based implants in physiological solution. *Biomaterials, 24*(21), 3765-3775.

Miloev, I., Metiko-Hukovi, M., & Strehblow, H. H. (2000). Passive film on orthopaedic TiAlV alloy formed in physiological solution investigated by X-ray photoelectron spectroscopy. *Biomaterials, 21*(20), 2103-2113.

Miloev, I., & Strehblow, H. H. (2003). The composition of the surface passive film formed on CoCrMo alloy in simulated physiological solution. *Electrochim. Acta, 48*(19), 2767-2774.

Milošev, I., & Strehblow, H. H. (2000). The behavior of stainless steels in physiological solution containing complexing agent studied by X-ray photoelectron spectroscopy. *J. Biomed. Mater. Res. A, 52*(2), 404-412.

Milošev, I., Pišot, V., & Campbell, P. (2005). Serum levels of cobalt and chromium in patients with sikomet metal–metal total hip replacements. *J. Orthopaedic Res., 23*(3), 526-535.

Milošev, I., Trebše, R., Kovač, S., Cör, A., & Pišot, V. (2006). Survivorship and retrieval analysis of sikomet metal-on-metal total hip replacements at a mean of seven years. *J. Bone Joint Surg., 88*(6), 1173-1182.

Mineta, S., Namba, S., Yoneda, T., Ueda, K., & Narushima, T. (2010). Carbide formation and dissolution in biomedical co-cr-mo alloys with different carbon contents during solution treatment. *Metall. Mater. Trans. A,* 41(8), 2129-2138.

Morita, M., Sasada, T., Nomura, I., Wei, Y. Q., & Tsukamoto, Y. (1992). Influence of low dissolved oxygen concentration in body fluid on corrosion fatigue behaviors of implant metals. *Ann. Biomed. Eng., 20*(5), 505-516.

Moriyama, Y., Ohta, D., Hachiya, K., Mitsui, Y., & Takeda, K. (1996). Fluorescence behavior of tryptophan residues of bovine and human serum albumins in ionic surfactant solutions: A comparative study of the two and one tryptophan (s) of bovine and human albumins. *J. Protein Chem., 15*(3), 265-272.

Mothes, E., & Faller, P. (2007). Evidence that the principal CoII-binding site in human serum albumin is not at the N-terminus: Implication on the albumin cobalt binding test for detecting myocardial ischemia. *Biochemistry, 46*(8), 2267-2274.

Muñoz, A. I., & Mischler, S. (2007). Interactive effects of albumin and phosphate ions on the corrosion of CoCrMo implant alloy. *J. Electrochem. Soci., 154*, C562.

Nadrich, J. (2013). Johnson & Johnson study predicts 37% failure rate of metal hips; attorney jeff nadrich responds. Retrieved Nov/15, 2013, from http://www.prweb.com/releases/depuy-hip/attorney/prweb10377158.htm.

Nechay, B. R., Nanninga, L. B., & Nechay, P. S. (1986). Vanadyl (IV) and vanadate (V) binding to selected endogenous phosphate, carboxyl, and amino ligands; calculations of cellular vanadium species distribution. *Arch. Biochem. Biophys., 251*(1), 128-138.

Nilner, K., & Holland, R. O. Y. I. (1985). Electrochemical potentials of amalgam restorations in vivo. *Europ. J. Oral Sci., 93*(4), 357-359.

Nyrén, O., McLaughlin, J. K., Gridley, G., Ekbom, A., Johnell, O., Fraumeni, J. F., & Adami, H. O. (1995). Cancer risk after hip replacement with metal implants: A population-based cohort study in sweden. *J. National Cancer Inst., 87*(1), 28-33.

Okazaki, Y., & Gotoh, E. (2005). Comparison of metal release from various metallic biomaterials in vitro. *Biomaterials, 26*(1), 11-21.

Okazaki, Y., & Gotoh, E. (2008). Metal release from stainless steel, Co–Cr–Mo–Ni–Fe and Ni–Ti alloys in vascular implants. *Corros. Sci., 50*(12), 3429-3438.

Oku, M., & Hirokawa, K. (1976). X-ray photoelectron spectroscopy of Co_3O_4, Fe_3O_4, Mn_3O_4, and related compounds. *J. Electron. Spectrosc. Relat. Phenom., 8*(5), 475-481.

Oliva, F. Y., Avalle, L. B., Cámara, O. R., & De Pauli, C. P. (2003). Adsorption of human serum albumin (HSA) onto colloidal TiO2 particles, part I. *J. Colloid Interface Sci., 261*(2), 299-311.

Olsson, C. O. A., & Landolt, D. (2003). Passive films on stainless steels-chemistry, structure and growth. *Electrochim. Acta, 48*(9), 1093-1104.

Omanovic, S., & Roscoe, S. G. (1999). Electrochemical studies of the adsorption behavior of bovine serum albumin on stainless steel. *Langmuir, 15*(23), 8315-8321.

Oshida, Y. (2006). *Bioscience and bioengineering of titanium materials.* Burlington, MA: Elsevier Science.

Ouerd, A., Alemany-Dumont, C., Normand, B., & Szunerits, S. (2008). Reactivity of CoCrMo alloy in physiological medium: Electrochemical characterization of the metal/protein interface. *Electrochim. Acta, 53*(13), 4461-4469.

Ouerd, A., Alemany-Dumont, C., Berthomé, G., Normand, B., & Szunerits, S. (2007). Reactivity of titanium in physiological medium I. electrochemical characterization of the metal/protein interface. *J. Electrochem. Soci., 154*(10), C593-C601.

Paliwal, M., Gordon Allan, D., & Filip, P. (2010). Failure analysis of three uncemented titanium-alloy modular total hip stems. *Eng. Fail. Anal., 17*(5), 1230-1238.

Penido, M. G. M., & Alon, U. S. (2012). Phosphate homeostasis and its role in bone health. *Pediatric Nephrology, 27*(11), 2039-2048.

Peterman, B., & Laidler, K. J. (1980). Study of reactivity of tryptophan residues in serum albumins and lysozyme by N-bromosuccinamide fluorescence quenching. *Arch. Biochem. Biophys., 199*(1), 158-164.

Popa, M., Vasilescu, E., Drob, P., Demetrescu, I., Popescu, B., Ionescu, D., & Vasilescu, C. (2003). In vitro assessment and monitoring of the implant titanium materials–physiological environment interactions. *Mater. Corros., 54*(4), 215-221.

Porath, J., & Olin, B. (1983). Immobilized metal affinity adsorption and immobilized metal affinity chromatography of biomaterials. Serum protein affinities for gel-immobilized iron and nickel ions. *Biochemistry, 22*(7), 1621-1630.

Pourbaix, M. (1984). Electrochemical corrosion of metallic biomaterials. *Biomaterials, 5*(3), 122-134.

Pradier, C., Kármán, F., Telegdi, J., Kálmán, E., & Marcus, P. (2003). Adsorption of bovine serum albumin on chromium and molybdenum surfaces investigated by fourier-transform infrared reflection-absorption spectroscopy (FT-IRRAS) and X-ray photoelectron spectroscopy. *The J. Phys. Chem. B, 107*(28), 6766-6773.

Purcell, M., Neault, J., Malonga, H., Arakawa, H., & Tajmir-Riahi, H. (2001). Interaction of human serum albumin with oxovanadium ions studied by FT-IR spectroscopy and gel and capillary electrophoresis. *Can. J. Chem., 79*(10), 1415-1421.

Rae, T. (1981). The toxicity of metals used in orthopaedic prostheses. An experimental study using cultured human synovial fibroblasts. *J. Bone Joint Surg., 63*(3), 435-440.

Ramasubramanian, N., Preocanin, N., & Davidson, R. (1985). Analysis of passive films on stainless steel by cyclic voltammetry and auger spectroscopy. *J. Electrochem. Soci., 132*(4), 793-798.

Ronald N. Caron, Olin Corporation, & James T. Staley. (1997). Effects of composition, processing, and structure on properties of nonferrous alloys. *ASM handbook* (pp. 383-415).

Rondelli, G., Torricelli, P., Fini, M., & Giardino, R. (2005). In vitro corrosion study by EIS of a nickel-free stainless steel for orthopaedic applications. *Biomaterials, 26*(7), 739-744.

Rudee, M., & Price, T. M. (1985). The initial stages of adsorption of plasma derived proteins on artificial surfaces in a controlled flow environment. *J. Biomed. Mater. Res., 19*(1), 57-66.

Sakiyama, T., Tomura, J., Imamura, K., & Nakanishi, K. (2004). Adsorption characteristics of bovine serum albumin and its peptide fragments on a stainless steel surface. *Colloids and Surfaces B: Biointerfaces, 33*(2), 77-84.

Samelko, L., Caicedo, M. S., Lim, S., Della-Valle, C., Jacobs, J., & Hallab, N. J. (2013). Cobalt-alloy implant debris induce HIF-1α hypoxia associated responses: A mechanism for metal-specific orthopedic implant failure. *PloS One, 8*(6), e67127.

Sargeant, A., & Goswami, T. (2007). Hip implants-paper VI-ion concentrations. *Materials & Design, 28*(1), 155-171.

Sato, N., Kudo, K., & Noda, T. (1970). Single layer of the passive film on Fe. *Corros. Sci., 10*(11), 785-794.

Savarino, L., Granchi, D., Ciapetti, G., Cenni, E., Greco, M., Rotini, R., Veronesi, C. A., Baldini, N., & Giunti, A. (2003). Ion release in stable hip arthroplasties using metal-on-metal articulating surfaces: A comparison between short-and medium-term results. *J. Biomed. Mater. Res. A,, 66*(3), 450-456.

Scales, J. T., Winter, G., & Shirley, H. (1961). Corrosion of orthopaedic implants. *British Med. J., 2*(5250), 478.

Schaffer, A. W., Schaffer, A., Pilger, A., Engelhardt, C., Zweymueller, K., & Ruediger, H. W. (1999). Increased blood cobalt and chromium after total hip replacement. *Clin. Toxicol., 37*(7), 839-844.

Shadanbaz, S., Walker, J., Staiger, M. P., Dias, G. J., & Pietak, A. (2013). Growth of calcium phosphates on magnesium substrates for corrosion control in biomedical applications via immersion techniques. *J. Biomed. Mater. Res. B: Appl. Biomater., 101*(1), 162-172.

Sharma, C., & Sunny, M. (1986). Titanium oxide layer thickness and protein interaction at the interface. *Trans. Biomater. Artif. Organ, 6*(1), 89-98.

Shih, C. C., Shih, C. M., Su, Y. Y., Su, L. H. J., Chang, M. S., & Lin, S. J. (2004). Effect of surface oxide properties on corrosion resistance of 316L stainless steel for biomedical applications. *Corros. Sci., 46*(2), 427-441.

Singh, A. K., Pradhan, S., Bhalla, R., & Unnikumar, K. (2009). Proteins: Structure, function and biotechnology aspects. (pp. 135) IK International Pvt Ltd.

Sivakumar, M., Kumar Dhanadurai, K. S., Rajeswari, S., & Thulasiraman, V. (1995). Failures in stainless steel orthopaedic implant devices: A survey. *J. Mater. Sci. Lett., 14*(5), 351-354.

Sleigh, C., Pijpers, A., Jaspers, A., Coussens, B., & Meier, R. J. (1996). On the determination of atomic charge via ESCA including application to organometallics. *J. Electron. Spectrosc. Relat. Phenom., 77*(1), 41-57.

Sodhi, R., Weninger, A., Davies, J., & Sreenivas, K. (1991). X-ray photoelectron spectroscopic comparison of sputtered Ti, Ti6Al4V, and passivated bulk metals for use in cell culture techniques. *J. Vacu. Sci. Tech. A: Vacuum, Surfaces, and Films, 9*(3), 1329-1333.

Sokołowska, M., Wszelaka-Rylik, M., Poznański, J., & Bal, W. (2009). Spectroscopic and thermodynamic determination of three distinct binding sites for Co(II) ions in human serum albumin. *J. Inorg. Biochem., 103*(7), 1005-1013.

Solar, R. J., Pollack, S. R., & Korostoff, E. (2004). In vitro corrosion testing of titanium surgical implant alloys: An approach to understanding titanium release from implants. *J. Biomed. Mater. Res., 13*(2), 217-250.

Sotereanos, N. G., Sauber, T. J., & Tupis, T. T. (2013). Modular femoral neck fracture after primary total hip arthroplasty. *J. Arthroplasty, 28*(1), 196. e7-9.

Sousa, S., & Barbosa, M. (1991). Electrochemistry of AISI 316L stainless steel in calcium phosphate and protein solutions. *J. Mater. Sci.: Mater. Med., 2*(1), 19-26.

Sousa, S., & Barbosa, M. (1993). Corrosion resistance of titanium CP in saline physiological solutions with calcium phosphate and proteins. *Clinic. Mater., 14*(4), 287-294.

Souza, M. E. P., Lima, L., Lima, C. R. P., Zavaglia, C. A. C., & Freire, C. M. A. (2009). Effects of pH on the electrochemical behaviour of titanium alloys for implant applications. *J. Mater. Sci.: Mater. Med., 20*(2), 549-552.

Speight, J. G. (2005). *Lange's handbook of chemistry,* New York, NY: McGraw-Hill.

Stankovich, M. T., & Bard, A. J. (1978). The electrochemistry of proteins and related substances part III. bovine serum albumin. *J. Electroanal. Chem., 86*(1), 189-199.

Stansbury, E. E., & Buchanan, R. A. (2000). Electrochemical corrosion rate measurements. *Fundamentals of electrochemical corrosion* (pp. 253-255) ASM International.

Sudhakar, K. (2005). Investigation of failure mechanism in vitallium 2000 implant. *Eng. Fail. Anal., 12*(2), 257-262.

Sunny, M., & Sharma, C. P. (1991). Titanium-protein interaction: Changes with oxide layer thickness. *J. Biomater. Appl., 6*(1), 89.

Svare, C., Belton, G., & Korostoff, E. (1970). The role of organics in metallic passivation. *J. Biomed. Mater. Res., 4*(3), 457-467.

Takemoto, S., Hattori, M., Yoshinari, M., Kawada, E., & Oda, Y. (2005). Corrosion behavior and surface characterization of titanium in solution containing fluoride and albumin. *Biomaterials, 26*(8), 829-837.

Tan, B. J., Klabunde, K. J., & Sherwood, P. M. (1990). X-ray photoelectron spectroscopy studies of solvated metal atom dispersed catalysts. nonometallic iron and bimetallic iron-cobalt particles on alumina. *Chem. Mater., 2*(2), 186-191.

Tang, Y. C., Katsuma, S., Fujimoto, S., & Hiromoto, S. (2006). Electrochemical study of type 304 and 316L stainless steels in simulated body fluids and cell cultures. *Acta Biomaterialia, 2*(6), 709-715.

Tang, J., De Poortere, E. P., Klare, J. E., Nuckolls, C., & Wind, S. J. (2006). Single-molecule transistor fabrication by self-aligned lithography and in situ molecular assembly. *Microelec. Eng., 83*(4-9), 1706-1709.

Tateishi, T., Ito, Y., & Okazaki, Y. (1997). Corrosion resistance of implant alloys in pseudo physiological solution and role of alloying elements in passive film. *Mater.Trans.JIM, 38*(1), 78-84.

Torres Bautista, B. E., Carvalho, M. L., Seyeux, A., Zanna, S., Cristiani, P., Tribollet, B., Marcus, P.,& Frateur, I. (2013). Effect of protein adsorption on the corrosion behaviour of 70Cu-30Ni alloy in artificial seawater. *Bioelectrochem. 97,* 34-42.

Valero Vidal, C., & Muñoz, I. (2008). Electrochemical characterization of biomedical alloys for surgical implants in simulated body fluids. *Corros. Sci., 50*(7), 1954-1961.

Valero Vidal, C., Olmo Juan, A., & Igual Muñoz, A. (2010). Adsorption of bovine serum albumin on CoCrMo surface: Effect of temperature and protein concentration. *Colloids and Surfaces B: Biointerfaces, 80*(1), 1-11.

Vasilescu, C., Drob, P., Vasilescu, E., Demetrescu, I., Ionita, D., Prodana, M., & Drob, S. (2011). Characterization and corrosion resistance of the electrodeposited hydroxyapatite and bovine serum albumin/hydroxyapatite films on Ti–6Al–4V–1Zr alloy surface. *Corros. Sci., 53*(3), 992-999.

Vidal, C. V., & Muñoz, A. I. (2010). Study of the adsorption process of bovine serum albumin on passivated surfaces of CoCrMo biomedical alloy. *Electrochim. Acta, 55*(28), 8445-8452.

Virtanen, S., Milošev, I., Gomez-Barrena, E., Trebše, R., Salo, J., & Konttinen, Y. T. (2008). Special modes of corrosion under physiological and simulated physiological conditions. *Acta Biomaterialia, 4*(3), 468-476.

Wagner, C., Riggs, W., Davis, L., Moulder, J., & Muilenberg, G. (1992). Handbook of X-ray photoelectron spectroscopy. Eden prairie, MN: Perkin-Elmer.

Walter, L. R., Marel, E., Harbury, R., & Wearne, J. (2008). Distribution of chromium and cobalt ions in various blood fractions after resurfacing hip arthroplasty. *J. Arthroplasty, 23*(6), 814-821.

Wan, P., Lin, X., Tan, L., Li, L., Li, W., & Yang, K. (2013). Influence of albumin and inorganic ions on electrochemical corrosion behavior of plasma electrolytic oxidation coated magnesium for surgical implants. *Appl. Surf. Sci., 282,* 186-194.

Wang, W., & Alfantazi, A. (2013). Effect of microstructure and temperature on electrochemical behavior of niobium in phosphate-buffered saline solutions. *J. Electrochem. Soci., 160*(1), C1-C11.

Wang, W., Mohammadi, F., & Alfantazi, A. (2012). Corrosion behaviour of niobium in phosphate buffered saline solutions with different concentrations of bovine serum albumin. *Corros. Sci., 57*, 11-21.

Wassell, D. T. H., & Embery, G. (1996). Adsorption of bovine serum albumin on to titanium powder. *Biomater. 17*(9), 859-864.

Weijers, R. (1977). Amino acid sequence in bovine serum albumin. *Clinic. Chem., 23*(7), 1361.

Williams, D. (1989). A model for biocompatibility and its evaluation. *J. Biomed. Eng., 11*(3), 185-191.

Williams, D. (1999). *Dictionary of biomaterials* Liverpool, Liverpool: University Press.

Williams, R. L., Brown, S. A., & Merritt, K. (1988). Electrochemical studies on the influence of proteins on the corrosion of implant alloys. *Biomater. 9*(2), 181-186.

Winter, G. D. (1974). Tissue reaction to metallic wear and corrosion products in human patients. *J. Biomed. Mater. Res., 8*(3), 11-26.

Woodman, J., Black, J., & Jiminez, S. (1984). Isolation of serum protein organometallic corrosion products from 316LSS and HS-21 in vitro and in vivo. *J. Biomed. Mater. Res., 18*(1), 99-114.

Yan, Y., Neville, A., & Dowson, D. (2007). Biotribocorrosion of CoCrMo orthopaedic implant materials--assessing the formation and effect of the biofilm. *Tribol. Int., 40*(10-12), 1492-1499.

Yang, J., & Black, J. (1994). Competitive binding of chromium, cobalt and nickel to serum proteins. *Biomater, 15*(4), 262-268.

Zanna, S., Compere, C., & Marcus, P. (2006). XPS characterisation of BSA adsorption on stainless steel. In P. Marcus, & V. Maurice (Eds.), *Passivation of metals and semiconductors, and properties of thin oxide layers: A selection of papers from the 9th international symposium, Paris, France, 27 June-1 July 2005* (pp. 365) Elsevier Science Ltd.

Zhang, G. C., Xu, J. Y., & Wang, Y. Q. (2011). Studies on the interaction between chromium (VI) and human serum albumin: Spectroscopic approach. *Spectrochim. Acta A, 86*, 381-386.

Zhao, J., Zheng, X., Xing, W., Huang, J., & Li, G. (2007). Electrochemical studies of camptothecin and its interaction with human serum albumin. *Int. J. Mol. Sci., 8*(1), 42-50.